nagra.

Arbeitsbericht NAB 20-09

TBO Trüllikon-1-1: Data Report

Dossier VIII
Rock Properties, Porewater Characterisation and Natural Tracer Profiles

June 2021

L. Aschwanden, L. Camesi, T. Gimmi,
A. Jenni, M. Kiczka, U. Mäder,M. Mazurek,
D. Rufer, H.N. Waber, P. Wersin,
C. Zwahlen & D. Traber

National Cooperative
for the Disposal of
Radioactive Waste

Hardstrasse 73
P.O. Box 280
5430 Wettingen
Switzerland
Tel. +41 56 437 11 11

www.nagra.ch

nagra.

Arbeitsbericht NAB 20-09

TBO Trüllikon-1-1: Data Report

Dossier VIII
Rock Properties, Porewater Characterisation and Natural Tracer Profiles

June 2021

L. Aschwanden[1], L. Camesi[1], T. Gimmi[1], A. Jenni[1], M. Kiczka[1], U. Mäder[1], M. Mazurek[1], D. Rufer[1], H.N. Waber[1], P. Wersin[1], C. Zwahlen[1] & D. Traber[2]

[1] Rock-Water Interaction, Institute of Geological Sciences, University of Bern

[2] Nagra

Keywords:
TRU1-1, Zürich Nordost, TBO, deep drilling campaign, rock properties, petrophysical parameters, water content, porosity, mineralogy, clay content, clay mineral composition, sulphate minerals, porewater chemistry, natural tracer profiles

National Cooperative for the Disposal of Radioactive Waste

Hardstrasse 73
P.O. Box 280
5430 Wettingen
Switzerland
Tel. +41 56 437 11 11

www.nagra.ch

Nagra Arbeitsberichte ("Working Reports") present the results of work in progress that have not necessarily been subject to a comprehensive review. They are intended to provide rapid dissemination of current information.

This NAB aims at reporting drilling results at an early stage. Additional borehole-specific data will be published elsewhere.

In the event of inconsistencies between dossiers of this NAB, the dossier addressing the specific topic takes priority. In the event of discrepancies between Nagra reports, the chronologically later report is generally considered to be correct. Data sets and interpretations laid out in this NAB may be revised in subsequent reports. The reasoning leading to these revisions will be detailed there.

This Dossier was prepared by the Rock-Water Interaction Group of the University of Bern (authors are listed in the individual chapters). D. Traber was the responsible Nagra project manager.

The authors warmly acknowledge the laboratory work of:
P. Bähler, C. Pichler and P. Wanner efficiently produced a substantial part of the data presented in this report.
U. Eggenberger, J. Krbanjevic, M. Wolffers and J.W. Zucha provided data for mineralogical and BET analyses as well as evaluation tools.
T. Oyama (CRIEPI, Japan) kindly collaborated in the context of porewater squeezing.

We also acknowledge the experimental and analytical work performed at Hydroisotop GmbH and at the French Geological Survey (BRGM) who conducted a large number of isotope diffusive-exchange and aqueous leaching experiments, respectively.

We are also grateful for the excellent work of the drill-site team who successfully provided sealed core samples according to our specifications.

We thank P. Blaser and M. Unger for editorial work.

The comments and suggestions of Andreas Gautschi on an earlier version of the manuscript are gratefully acknowledged.

"Copyright © 2021 by Nagra, Wettingen (Switzerland) / All rights reserved.
All parts of this work are protected by copyright. Any utilisation outwith the remit of the copyright law is unlawful and liable to prosecution. This applies in particular to translations, storage and processing in electronic systems and programs, microfilms, reproductions, etc."

Table of Contents

List of Tables

List of Figures

Electronic Appendices

App. A Comprehensive data base with results of laboratory analyses (xls format)

App. B Results of aqueous-extraction tests at different solid/liquid ratios (xls format)

App. C BRGM data report (pdf format)

App. D Detailed documentation of advective displacement experiments (xls format)

App. E Hydroisotop GmbH data report (pdf format)

Note: The Appendices C and E are only included in the digital version of this report and can be found under the paper clip symbol. The Appendices A, B and D are available upon request.

1 Introduction

1.1 Context

To provide input for site selection and the safety case for deep geological repositories for radioactive waste, Nagra has drilled a series of deep boreholes in Northern Switzerland. The aim of the drilling campaign is to characterise the deep underground of the three remaining siting regions located at the edge of the Northern Alpine Molasse Basin (Fig. 1-1).

In this report, we present the results from the Trüllikon-1-1 borehole.

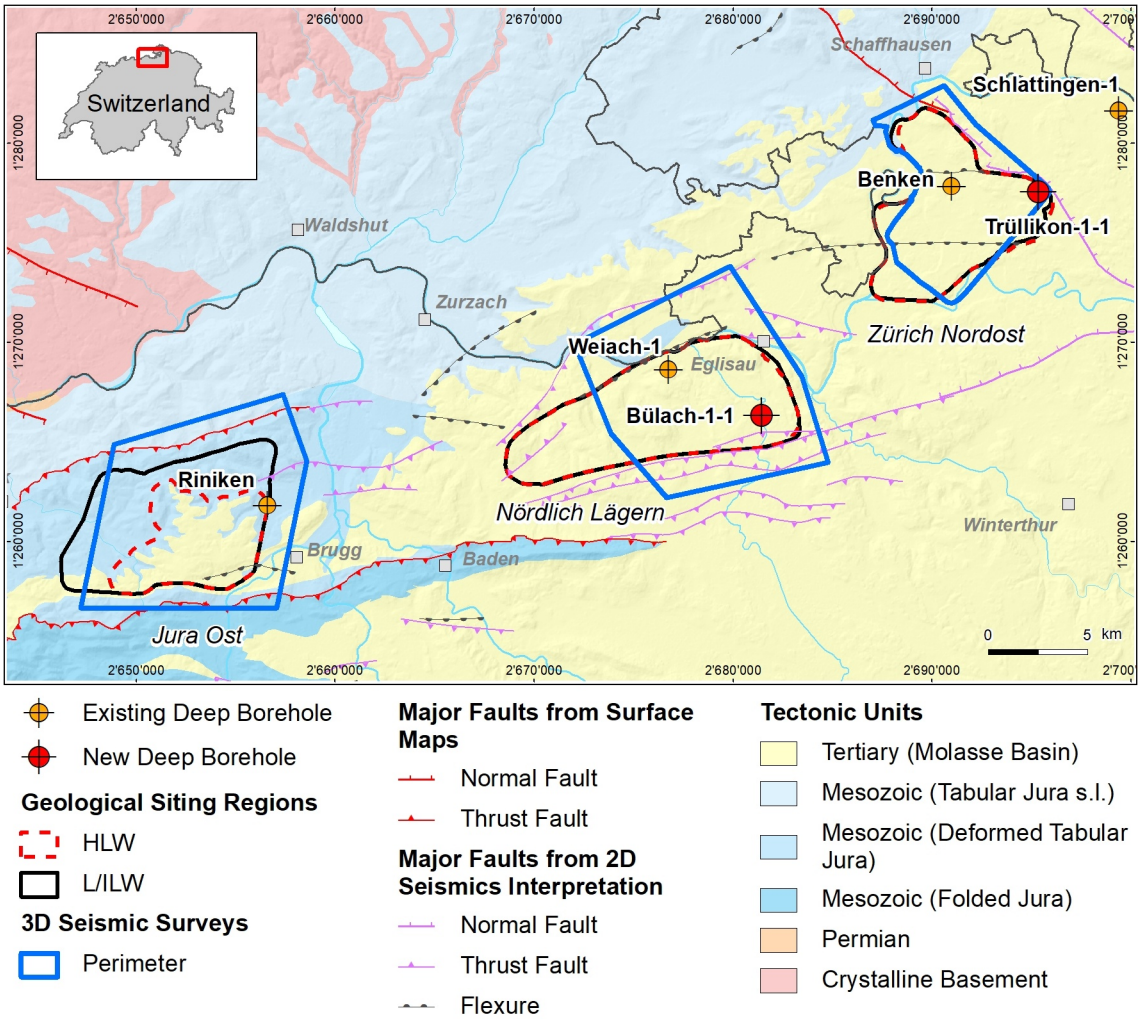

Fig. 1-1: Tectonic overview map with the three siting regions under investigation

1.2 Location and specifications of the borehole

The Trüllikon-1-1 (TRU1-1) exploratory borehole is the second borehole drilled within the framework of the TBO project. The drill site is located in the eastern part of the Zürich Nordost siting region (Fig. 1-2). The vertical borehole reached a final depth of 1'310 m (MD)[1]. The borehole specifications are provided in Tab. 1-1.

Tab. 1-1: General information about the TRU1-1 borehole

Siting region	Zürich Nordost
Municipality	Trüllikon (Canton Zürich / ZH), Switzerland
Drill site	Trüllikon-1 (TRU1)
Borehole	Trüllikon-1-1 (TRU1-1)
Coordinates	LV95: 2'695'372.648 / 1'277'548.076
Elevation	Ground level = top of rig cellar: 475.07 m above sea level (asl)
Borehole depth	1'310.0 m measured depth (MD) below ground level (bgl)
Drilling period	15. August 2019 – 5. April 2020 (spud date to end of rig release)
Drilling company	PR Marriott Drilling Ltd.
Drilling rig	Rig-16 Drillmec HH102
Drilling fluid	Water-based mud with various amounts of different components such as[2]: 46 – 712 m: Pure-Bore® 712 – 1'161 m: Potassium silicate 1'161 – 1'310 m: Sodium chloride & polymers

The lithostratigraphic profile and the casing scheme are shown in Fig. 1-3. The comparison of the core versus log depth[3] of the main lithostratigraphic boundaries in the TRU1-1 borehole is shown in Tab. 1-2.

[1] Measured depth (MD) refers to the position along the borehole trajectory, starting at ground level, which for this borehole is the top of the rig cellar. For a perfectly vertical borehole, MD below ground level (bgl) and true vertical depth (TVD) are the same. In all Dossiers depth refers to MD unless stated otherwise.

[2] For detailed information see Dossier I.

[3] Core depth refers to the depth marked on the drill cores. Log depth results from the depth observed during geophysical wireline logging. Note that the petrophysical logs have not been shifted to core depth, hence log depth differs from core depth.

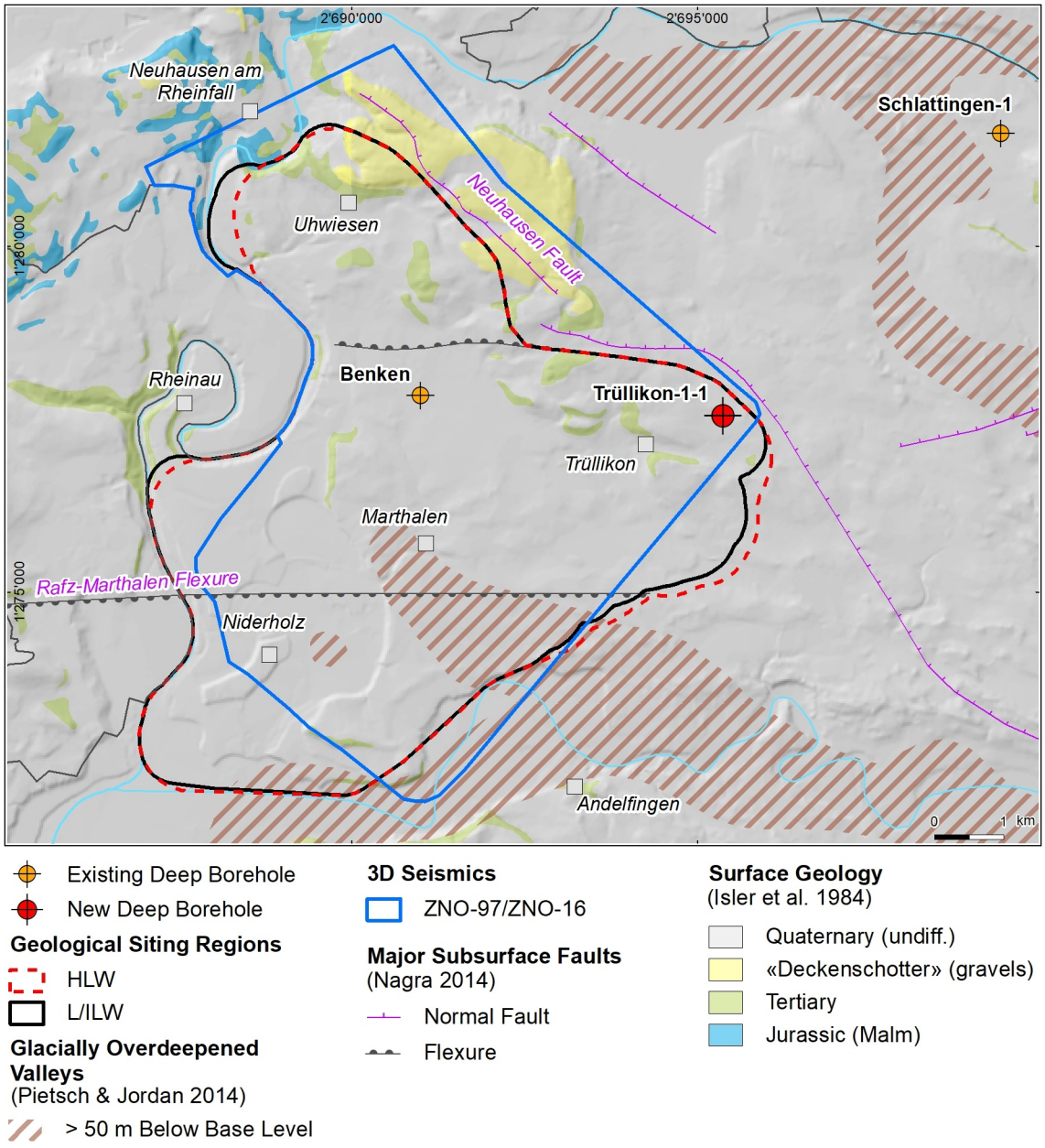

Fig. 1-2: Overview map of the investigation area in the Zürich Nordost siting region with the location of the TRU1-1 borehole in relation to the boreholes Benken and Schlattingen

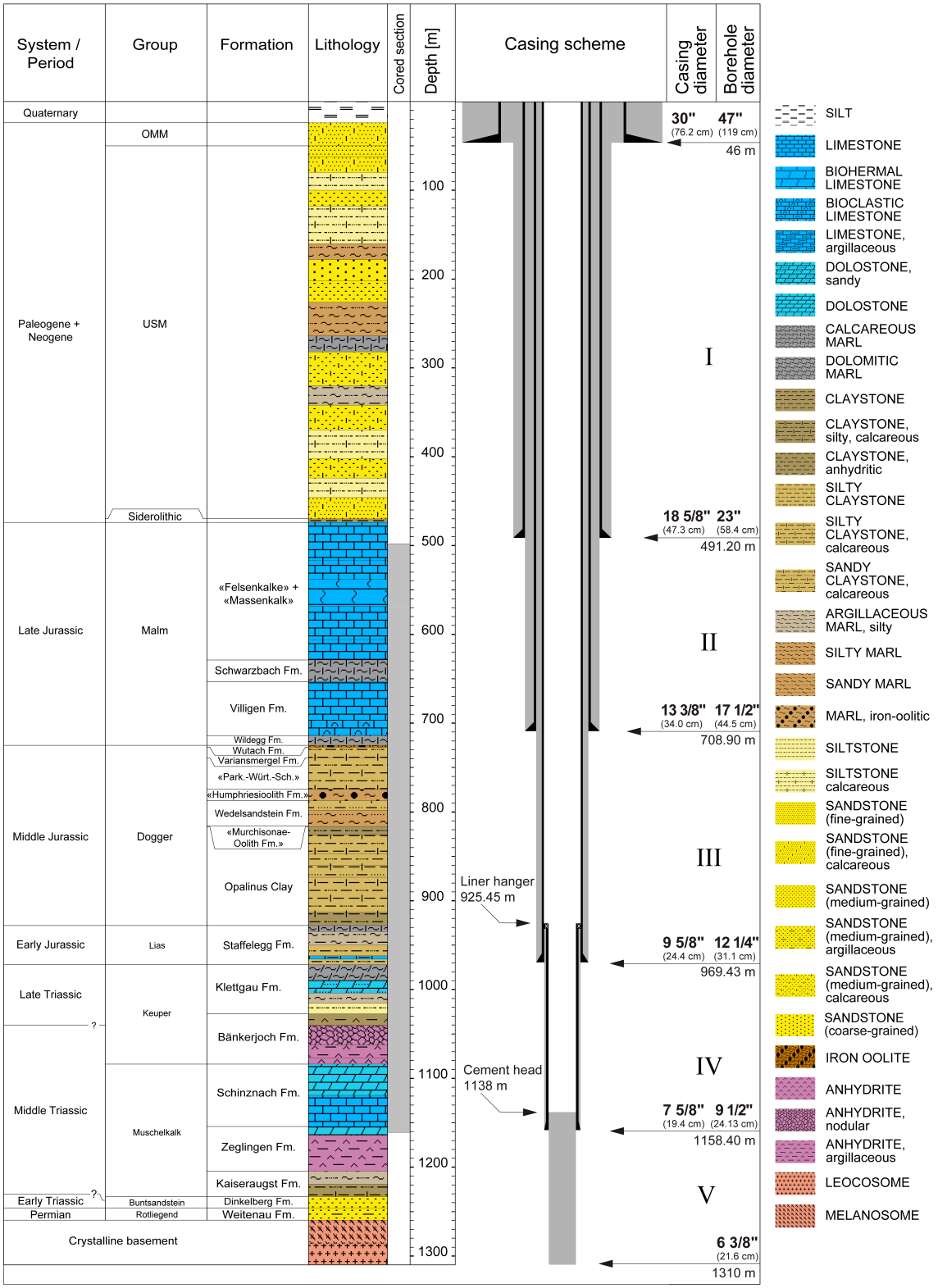

Fig. 1-3: Lithostratigraphic profile and casing scheme for the TRU1-1 borehole[4]

[4] For detailed information see Dossier I and III.

Tab. 1-2: Core and log depth for the main lithostratigraphic boundaries in the TRU1-1 borehole[5]

System / Period	Group	Formation	Core depth in m (MD)	Log depth in m (MD)	
Quaternary				**24.0**	—
Paleogene + Neogene	OMM			50.0	—
	USM			470.0	—
	Siderolithic			**474.0**	—
Jurassic	Malm	«Felsenkalke» + «Massenkalk»	628.87	628.75	—
		Schwarzbach Formation	653.29	653.15	—
		Villigen Formation	714.00	714.00	—
		Wildegg Formation	724.85	725.03	—
	Dogger	Wutach Formation	727.13	727.27	—
		Variansmergel Formation	738.97	739.06	—
		«Parkinsoni-Württembergica-Schichten»	774.55	774.66	—
		«Humphriesioolith Formation»	787.50	787.55	—
		Wedelsandstein Formation	815.51	815.50	—
		«Murchisonae-Oolith Formation»	816.42	816.43	—
		Opalinus Clay	927.91	927.87	—
	Lias	Staffelegg Formation	**971.68**	**971.55**	—
Triassic	Keuper	Klettgau Formation	1027.22	1027.44	—
		Bänkerjoch Formation	1084.01	1084.22	—
	Muschelkalk	Schinznach Formation	1154.25	1154.43	—
		Zeglingen Formation	1204.5		—
		Kaiseraugst Formation	1233.2		—
	Buntsandstein	Dinkelberg Formation	**1246.1**		—
Permian	Rotliegend	Weitenau Formation	**1259.7**		—
		Crystalline Basement	1310.0	final depth	

[5] For details regarding lithostratigraphic boundaries see Dossier III; for details about depth shifts (core goniometry) see Dossier V.

1.3 Documentation structure for the TRU1-1 borehole

NAB 20-09 documents the majority of the investigations carried out in the TRU1-1 borehole, including laboratory investigations on core material. The NAB comprises a series of stand-alone dossiers addressing individual topics and a final dossier with a summary composite plot (Tab. 1-3).

This documentation aims at early publication of the data collected in the TRU1-1 borehole. It includes most of the data available approximately one year after completion of the borehole. Some analyses are still ongoing (e.g. diffusion experiments, analysis of veins, hydrochemical interpretation of water samples) and results will be published in separate reports.

The current borehole report will provide an important basis for the integration of data sets from different boreholes. The integration and interpretation of the results in the wider geological context will be documented later in separate geoscientific reports.

Tab. 1-3: List of dossiers included in NAB 20-09

Black indicates the dossier at hand.

Dossier	Title	Authors
I	TBO Trüllikon-1-1: Drilling	M. Ammen & P.-J. Palten
II	TBO Trüllikon-1-1: Core Photography	D. Kaehr & M. Gysi
III	TBO Trüllikon-1-1: Lithostratigraphy	M. Schwarz, P. Jordan, P. Schürch, H. Naef, T. Ibele, R. Felber & M. Gysi
IV	TBO Trüllikon-1-1: Microfacies, Bio- and Chemostratigraphic Analyses	S. Wohlwend, H.R. Bläsi, S. Feist-Burkhardt, B. Hostettler, U. Menkveld-Gfeller, V. Dietze & G. Deplazes
V	TBO Trüllikon-1-1: Structural Geology	A. Ebert, S. Cioldi, L. Gregorczyk, S. Rust, D. Böhni & M. Gysi
VI	TBO Trüllikon-1-1: Wireline Logging and Microhydraulic Fracturing	J. Gonus, E. Bailey, J. Desroches & R. Garrard
VII	TBO Trüllikon-1-1: Hydraulic Packer Testing	R. Schwarz, L. Schlickenrieder, H.R. Müller, S. Köhler, A. Pechstein & T. Vogt
VIII	TBO Trüllikon-1-1: Rock Properties, Porewater Characterisation and Natural Tracer Profiles	L. Aschwanden, L. Camesi, T. Gimmi, A. Jenni, M. Kiczka, U. Mäder, M. Mazurek, D. Rufer, H.N. Waber, P. Wersin, C. Zwahlen & D. Traber
IX	TBO Trüllikon-1-1: Rock-mechanical and Geomechanical Laboratory Testing	E. Crisci, L. Laloui & S. Giger
X	TBO Trüllikon-1-1: Petrophysical Log Analysis	S. Marnat & J.K. Becker
	TBO Trüllikon-1-1: Summary Plot	Nagra

1.4 Scope and objectives of this dossier

Dossier VIII summarises the laboratory work of the Rock-Water Interaction Group (RWI) of the University of Bern, the French Geological Survey (BRGM) and Hydroisotop GmbH dedicated to rock and porewater characterisation of core materials obtained from the TRU1-1 borehole. The level of ambition is to document observations and measurements and to provide a quality-assured data set. The obtained data are evaluated and discussed to some degree, including consistency and plausibility checks. On the other hand, an in-depth discussion, sophisticated modelling efforts and regional comparisons with data from other sites are beyond the scope of the report. Data obtained by other groups (e.g. hydraulic tests, groundwater sampling, geophysical borehole and core logging, structural logging) are considered in several cases but not in a comprehensive way. Given the fact that those data were not available in complete and final form at the time when this report was written, an integrated interpretation of all available data needs to be deferred to later stages of the TBO programme.

Throughout this report, rock samples used for analysis are identified by their mid-sample depth in m. Note that the term «Brauner Dogger» is used for the Dogger units overlying the Opalinus Clay. In the Sectoral Plan Stage 1 and 2, «Brauner Dogger» is referred to clay-rich rocks only (Nagra 2008).

2 Geoscientific data available for the TRU1-1 borehole

Lukas Aschwanden

2.1 Geological information

As illustrated in Fig. 1-2, the TRU1-1 borehole is located in the eastern part of the Zürich Nordost area, which, tectonically, belongs to the autochthonous eastern Tabular Jura. The major tectonic structures in the area are the Neuhausen Fault and the Rafz – Marthalen Flexure. The first constitutes the northeastern border of the Zürich Nordost area and is located approximately 1 km east of the TRU1-1 borehole. The fault strikes NW-SE and runs parallel to the Bonndorf – Hegau – Bodensee Graben, slicing through the entire Mesozoic sediment stack. The Rafz – Marthalen Flexure is a W-E striking structure in the southern part of the area. Potentially it is associated with the northern margin of a Permo-Carboniferous Trough.

2.2 Hydrogeological conditions

Tab. 2-1 gives a summary of the hydraulic tests performed. The results of the hydraulic packer tests in the TRU1-1 borehole and of the fluid logging in the Malm aquifer are documented in Dossier VII.

Fluid logging in the Malm was from 491 to 712 m depth. The hydraulic packer test and the water sampling in the Malm were performed in the most transmissive zone indicated by fluid logging (ca. 592 – 594 m). A minor inflow zone was observed from 531 to 537 m depth.

Tab. 2-1: Results of hydraulic packer tests in borehole Trüllikon-1-1

The best estimates for transmissivity T, hydraulic conductivity K and hydraulic head are indicated. Hydraulic heads in the clay-rich formations are believed to be affected by transient hydromechanical processes. See Dossier VII for further details.

Top [m MD]	**Bottom** [m MD]	**Length** [m]	**Geological units**	**T** [m^2/s]	**K** [m/s]	**(Apparent) Head** [m asl]
589.0	600.4	11.4	«Massenkalk» (Malm aquifer)	5E-7	4E-8	415
782.3	805.3	23.0	«Brauner Dogger»	5E-12	2E-13	497
806.5	822.2	15.7	«Brauner Dogger» and Opalinus Clay	3E-11	2E-12	446
829.0	854.0	25.0	Opalinus Clay	8E-13	3E-14	929
868.5	887.5	19.0	Opalinus Clay	8E-13	4E-14	784
923.7	944.5	20.8	Staffelegg Fm.	5E-13	2E-14	870
944.5	965.3	20.8	Staffelegg Fm.	3E-12	1E-13	668
990.7	1'035.0	44.3	Klettgau Fm. – Bänkerjoch Fm. (Keuper aquifer)	6E-5	2E-6	398
1'085.3	1'110.3	25.0	Schinznach Fm. (Muschelkalk aquifer)	1E-6	5E-8	423

2.3 Groundwater samples

Groundwater samples with variable degrees of drilling-fluid contamination were obtained from the Malm, Keuper and Muschelkalk aquifers. For the present report, values for the chemically conservative parameters Cl and Br and the water-isotope ratios $\delta^{18}O$ and $\delta^{2}H$ are of interest, as these serve as boundary conditions for the porewater data. These values were corrected by Lorenz (2020) for drilling-fluid contamination and are reproduced in Tab. 2-2 along with information on the chemical water type and mineralisation of the groundwaters.

Tab. 2-2: Conservative parameters for waters from the Malm, Keuper and Muschelkalk aquifers corrected for drilling-fluid contamination

From Lorenz (2020).

Parameter	Unit	Malm aquifer	Keuper aquifer	Muschelkalk aquifer
Chemical type		**Na-Cl**	**Na-SO_4**-(Cl)	**Ca-Mg-SO_4**
Mineralisation	[g/L]	6.9	8.8	2.5
Chloride (Cl^-)	[mg/L]	4190	458	26.8 *
Bromide (Br^-)	[mg/L]	13.1	0.89	< 0.1 *
$\delta^{18}O$ of water	[‰$_{VSMOW}$]	−1.88	−10.08	−12.40
$\delta^{2}H$ of water	[‰$_{VSMOW}$]	−56.8	−65.6	−89.3

* Values represent analytical results of groundwater sampled towards the end of the pumping test.
Extrapolation to in situ values failed owing to a small contamination with drilling fluid (< 0.31%; based on uranine).

2.4 Structural logging

The results of structural core logging are documented in Dossier V, where the following types are distinguished:

- fault planes and fault zones (shear structures, mostly compressional)
- brittle extensional fractures (structures without shear or slip indications, e.g. joints, veins, tension gashes)
- stylolites

The large majority of all structures are found in the Malm and in the Triassic. A number of larger fault zones were defined and are listed in Tab. 2-3. In particular, 2 major fault zones were identified in the Klettgau Formation at 983.20 – 987.57 m MD and 1'004.67 – 1'006.15 m MD, respectively.

Tab. 2-3: Fault zones in the cored section of the TRU1-1 borehole

From Dossier V.

Top [m a.h.]	**Bottom** [m a.h.]	**Thickness** [m a.h.]	**Unit**
505.45	505.60	0.15	«Felsenkalke» + «Massenkalk»
516.00	516.13	0.13	«Felsenkalke» + «Massenkalk»
593.30	593.46	0.16	«Felsenkalke» + «Massenkalk»
677.17	678.47	1.30	Villigen Formation
830.91	830.94	0.03	Opalinus Clay
842.00	842.50	0.50	Opalinus Clay
983.20	987.57	4.37	Klettgau Formation
987.90	988.10	0.20	Klettgau Formation
1'004.67	1'006.15	1.48	Klettgau Formation
1'007.90	1'008.20	0.30	Klettgau Formation
1'018.00	1'018.08	0.08	Klettgau Formation
1'020.40	1'020.62	0.22	Klettgau Formation
1'020.85	1'021.07	0.22	Klettgau Formation
1'022.79	1'023.06	0.27	Klettgau Formation
1'025.50	1'025.70	0.20	Klettgau Formation
1'029.75	1'029.89	0.14	Bänkerjoch Formation
1'059.80	1'059.85	0.05	Bänkerjoch Formation

3 Sampling and applied methods

3.1 Sampling strategy

Lukas Aschwanden

A suite of 6 different sample types were investigated (Tab. 3-1). Sample types and the general procedures of core sampling, sample conditioning and storage are described by Rufer (2019).

Tab. 3-1: Sample types and sampling strategy

Sample type	**Main study targets**	**Sampling (by on-site team)**
PW (porewater chemistry), RP (various rock properties)	Characterisation of rock and porewater chemistry	Sample lithology representative of the current lithofacies and the sampled core section (usually 3 m). Sampling with a regular spacing in order to obtain a representative data set
SQ (squeezing)	Characterisation of porewater chemistry	Focussed on clay-rich lithologies due to methodological constraints
AD (advective displacement)	Characterisation of porewater chemistry	Focussed on clay-rich lithologies due to methodological constraints
DI (diffusion experiments)	Diffusion coefficients (at PSI)	Coverage of a wide range of lithologies (in particular clay-mineral contents)
NG (noble gas analysis)	Concentrations and isotopic compositions of dissolved noble and reactive gases	Sampling with a regular spacing, with situational tightening of the sampling interval close to potentially water-conducting features
GM (geomechanics)	Mineralogy and grain density of samples studied for their geomechanical properties by other laboratories	Representative sampling of the most relevant lithologies within the Opalinus Clay and the overlying Wedelsandstein Fm.

3.2 Laboratory programme

Lukas Aschwanden

In total, 216 samples were investigated, and Tab. 3-2 provides an overview. The majority of PW and RP samples were investigated by the French Geological Survey (BRGM) and Hydroisotop GmbH (HI). One third of all PW samples were investigated by RWI for inter-laboratory comparison. Samples of types SQ, AD, DI, NG and GM were all investigated by RWI (main studies of DI and GM samples were performed by other laboratories; see Tab. 3-1). In Tab. 3-3, the analytical programme for the various sample types and the different laboratories is shown in more detail.

Tab. 3-2: Numbers of samples analysed for the different geological units

In the case of the NG samples, the number refers to the total number of samples collected (RWI: Rock-Water Interaction Group of the University of Bern, BRGM: French Geological Survey, HI: Hydroisotop GmbH).

Unit	**PW**		**RP**		**SQ**	**AD**	**DI**	**NG**	**GM**	**Total**
	RWI	BRGM	RWI	HI	RWI	RWI	RWI	RWI	RWI	
Malm	6	12	1	11			5	9		44
«Brauner Dogger»	3	10		11	2	1	14	8	2	51
Opalinus Clay	5	13		13	2	2	9	6	17	67
Staffelegg Fm.	2	5		6	2		6	3		24
Klettgau Fm.	2	6		5			2	5		20
Bänkerjoch Fm.	4							3		7
Schinznach Fm.								3		3
Zeglingen Fm.										
All	**22**	**46**	**1**	**46**	**6**	**3**	**36**	**37**	**19**	**216**

Tab. 3-3: Analytical programme performed for the different sample types

×× = standard programme, × = selected samples only, calc. = calculated.

Method	**PW, RP** (RWI)	**PW** (BRGM)	**RP** (HI)	**SQ**	**AD**	**DI**	**NG**	**GM**
Bulk mineralogical composition incl. CNS analysis	×	×**		××	××	××		××
Clay mineralogy	×				××	××		
Bulk wet density	××	××			calc.		calc.	
Grain density	××	××			calc.	××		××
Water content	××	××	××	××	××	××	xx	
BET surface area						××		
Cation-exchange properties	×*				××	×*		
Sorption measurements						×*		
Aqueous extraction	××	××		××	××			
Porewater squeezing				××				
Advective displacement of porewater					××			
Water isotopes	××		××	××	××			
Dissolved noble gases							×	
Dissolved reactive gases							×	

* Subsamples collected during sample preparation, re-packed and sent to PSI for analysis

** Analyses performed by RWI on remaining rock material from experiments of BRGM

3.3 Analytical methods and methods of raw-data processing

Lukas Aschwanden

Experimental procedures of RWI and associated analytical methods, formalisms to process measured data and quantification of propagated errors are documented in Waber (ed.) (2020) and are not repeated here. Moreover, Mazurek et al. (2021) provide additional information for situations where the current practice is not documented or deviates from that described in Waber (ed.) (2020).

Water contents (gravimetry and isotope mass balance) and isotope data from diffusive-exchange experiments by Hydroisotop GmbH were obtained using the same protocol as that applied by the University of Bern, documented in Waber (ed.) (2020). On the other hand, BRGM used different protocols for sample preparation and for the quantification of petrophysical parameters, which are presented in Section 3.4 and in their data report provided in the electronic Appendix.

3.4 Petrophysical parameters studied by BRGM

Martin Mazurek & Thomas Gimmi

Sample preparation

The samples were cut open from the Al/plastic seals in a glovebox under N_2 atmosphere. All preparation using hammer and chisel was performed in the glovebox. The drying oven to measure water content was also placed within the glovebox, meaning that rock oxidation during drying could be completely suppressed.

Bulk wet density and water content $WC_{2\,d}$

An aliquot of the sample was weighed as received (wet mass, $m_{init\ 1}$), then immersed in kerosene until bubbles disappeared at the surface. Then the immersed material was taken out of the kerosene, wiping the excess petroleum residue on the surface with a tissue. The water- and kerosene-saturated aliquot was weighed again ($m_{init\ 2}$). Subsequently, the aliquot was immersed into kerosene again and weighed according to Archimedes' principle ($m_{in\ kerosene}$; Monnier et al. 1973, Charpentier et al. 2003, Gaboreau et al. 2011). Together with the known density of liquid kerosene ($\rho_{kerosene}$), the bulk volume ($V_{bulk} = [m_{init\ 2} - m_{in\ kerosene}]/\rho_{kerosene}$) of the aliquot and therefore bulk wet density of the aliquot ($\rho_{bulk\ wet} = m_{init\ 1}/V_{bulk}$) were obtained. Note that according to this definition the obtained bulk wet density refers to that of the sample prior to immersion in kerosene. If some degree of evaporation occurred during sample preparation, bulk wet density is slightly underestimated. Finally, the aliquot was dried in an oven at 105 °C for 48 h (2 d), which was expected to remove both porewater and kerosene, so that the dry rock mass (m_{dry}) was obtained by subsequent weighing. From this, the water content $WC_{wet,\ 2\ d} = (m_{init\ 1} - m_{dry})/\ m_{init\ 1}$ was calculated.

Water content $WC_{28\,d}$

Another aliquot of the sample (150 – 270 g) was weighed and then dried for 28 d at 105 °C. Sample mass was measured recurrently, and all samples reached a mass plateau that did not further change over time. This is a minor difference to the experience made by the University of

Bern where sample mass reaches a minimum and then increases weakly (typically < 0.02% over 1 – 2 weeks) due to ongoing oxidation. This latter process was minimised in BRGM's campaign because drying was performed under oxygen-free conditions in the glovebox.

Comparison of water contents $WC_{2\,d}$ and $WC_{28\,d}$

The data are compared in Fig. 3.4-1, which shows that on average $WC_{28\,d}$ exceeds $WC_{2\,d}$ except for samples with very low water contents, indicating that the drying process is not complete after 2 d. In that sense, $WC_{28\,d}$ is probably more appropriate.

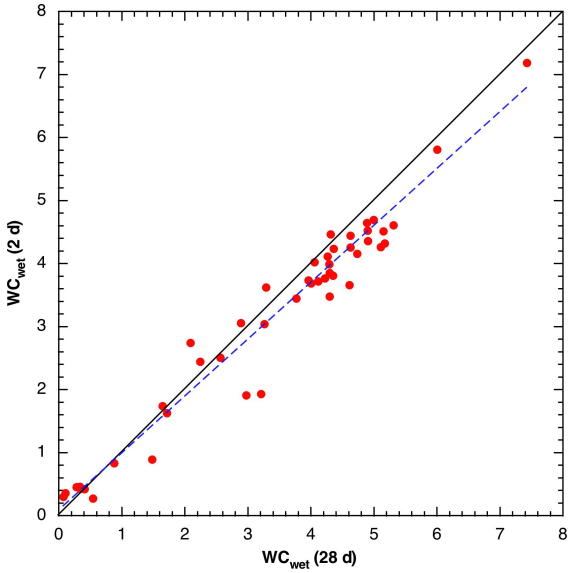

Fig. 3.4-1: Comparison of water contents obtained by BRGM by drying at 105 °C over 2 and 28 d

Stippled blue line is a linear regression of the data.

Aqueous extraction

Aqueous extracts at S/L ≈ 1 were prepared from yet another aliquot of the sample, applying the same protocols as described in Waber (ed.) (2020). Samples were extracted as received, i.e. they were not dried before extraction. Cl and SO_4 were quantified by ion chromatography, while ICP-MS was used for Br. Cations were not investigated. All manipulations were performed in a glove-box under N_2 atmosphere.

Partial desaturation during sample processing

Formally, the ratio between water-loss porosity and pycnometer porosity corresponds to the water saturation S_w of the sample. The error of such saturation values is typically very large, possibly affected by (unknown) heterogeneity between two aliquots, which is not represented in the propagated error. Thus, absolute numbers of this ratio have to be interpreted with care.

When comparing porosity obtained from water content with pycnometer porosity, indeed minor to major discrepancies were identified (Fig. 3.4-2). In the BRGM data set, water-loss porosities tend to be smaller than pycnometer porosities, in many cases substantially so, in particular in low-porosity (i.e. clay-poor) samples. Such behaviour is not observed in the data produced by the University of Bern. There, some scatter exists as well, but the ratio of the two types of porosities is centred around 1, which is not the case for samples investigated by BRGM. For samples with a small porosity, the deviations from 1 may be substantial in the data of the University of Bern as well, and they may be due to the fact that the aliquots used for the two methods were not identical and heterogeneity becomes particularly important in such cases. Fig. 3.4-2 (right) illustrates these findings.

It must therefore be concluded that, unlike the samples examined by the University of Bern, the BRGM samples are affected by partial desaturation. The likely reason lies in the fact that all sample processing at BRGM was performed in a glovebox, while this step was performed under atmospheric conditions at the University of Bern. The N_2 atmosphere in the glovebox is extremely dry, so porewater evaporation is more rapid than outside the glovebox. In addition, sample preparation and processing within the glovebox inevitably takes longer than outside, which leads to longer exposure times. Thus, while working in a glovebox is certainly the ideal procedure to suppress oxidation, it also has some disadvantages.

Partial desaturation of the aliquots also means that all quantities that refer to the wet mass are somewhat biased compared to a saturated sample. For instance, the measured bulk wet density is slightly underestimated. However, the calculated bulk dry density is independent of the degree of saturation (unless sample shrinkage occurred due to partial desaturation). The following equations document the formalism to derive the degree of water saturation from measured data:

$$V_{bulk} = (m_{init\ 2} - m_{in\ kerosene})/\rho_{kerosene} \quad (1)$$

$$V_{water} = (m_{init\ 1} - m_{dry})/\ \rho_{water} \quad (2)$$

$$V_{solid} = m_{dry}/\rho_{grain} \quad (3)$$

$$V_{pores} = V_{bulk} - V_{solid} \quad (4)$$

$$S_w = V_{water}/V_{pores} \quad (5)$$

$$\phi_{pyc} = V_{pores}/V_{bulk} \quad (6)$$

It can be shown that formally:

$$S_w = \phi_{WL}/\phi_{pyc} \quad (7)$$

With:

V_{bulk} = bulk volume of aliquot
V_{water} = volume of water
V_{solid} = volume of solids
$m_{init\ 1}$ = mass of aliquot (under air) prior to saturation with kerosene
$m_{init\ 2}$ = mass of aliquot (under air) after saturation with kerosene
$m_{in\ kerosene}$ = mass of aliquot immersed in kerosene
m_{dry} = mass of aliquot after drying at 105 °C

$\rho_{kerosene}$ = density of kerosene
ρ_{water} = density of water
ρ_{grain} = grain density
S_w = degree of water saturation
ϕ_{pyc} = pycnometer porosity
ϕ_{WL} = water-loss porosity

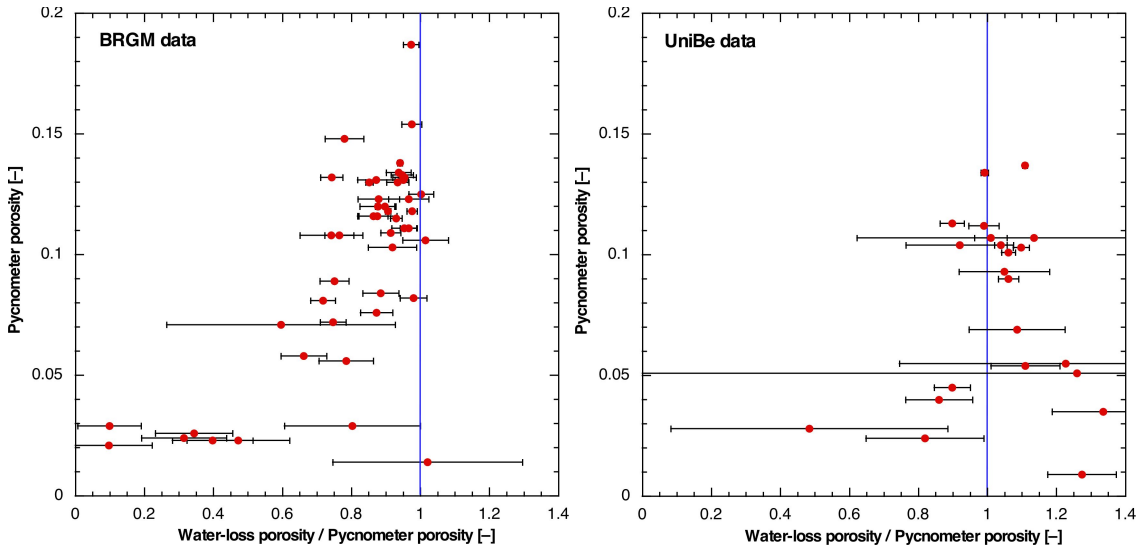

Fig. 3.4-2: Ratio of water-loss porosity (calculated from $WC_{28\ d}$ in the case of BRGM) and pycnometer porosity obtained from measurements at BRGM and at the University of Bern

Recalculation of Cl concentrations in aqueous extracts to porewater concentrations

In order to recalculate ion concentrations in aqueous extracts to porewater concentrations, a water content of the sample is needed. Given the fact that both sets of water-content measurements at BRGM ($WC_{2\ d}$ and $WC_{28\ d}$) are affected by partial desaturation, a correction considering S_w is required, as specified in Equation 6-1 in Waber (ed.) (2020). Alternatively, it follows from (7) that the recalculation can also be performed using the water content WC_{dry} derived from pycnometer porosity ϕ_{pyc} and setting $S_w = 1$:

$$WC_{dry} = \phi_{pyc}\ \rho_{water}/\rho_{bulk\ dry}\ . \qquad (8)$$

4 Results

4.1 Documentation of measured and calculated data

Martin Mazurek & Lukas Aschwanden

Raw data collected by the three different laboratories in the frame of the analytical programme of the TRU1-1 borehole, are organised in a FileMaker data base, including raw-data files, graphics and photographs. The main purpose of this data base is to ensure the full documentation and traceability of original and derived data presented in this report. From this data base, the relevant data were exported into a comprehensive Excel sheet, which is attached in Appendix A (the full data set of Hydroisotop GmbH and BRGM is provided in their data reports in the electronic Appendices C and E, respectively). The objective of this Excel sheet is not to fully document all analyses made but, per parameter and sample, to indicate the "best" or most representative value in case multiple measurements were made, and to list parameters calculated from the original measurements. For example, only one composition is given for squeezed and advectively displaced porewaters in a sample, even though multiple aliquots were collected and analysed. Explanatory notes to this sheet follow here.

Bulk mineralogy (X-ray diffraction and CNS analysis)

- Contents of minerals not detected by X-ray diffraction are set to 0, as the actual detection limits are difficult to quantify. "tr" = present in trace amounts.
- Clay-mineral content is not measured directly but is calculated by difference to 100%.
- Pyrite content is calculated from the measured S content, assuming that pyrite is the main S reservoir in the rock. This is not the case in anhydrite-bearing rocks, which are typically free of pyrite. Here, the S is used to calculate the content of anhydrite.
- Column "Füchtbauer name" refers to the nomenclature of clastic rocks as defined in Naef et al. (2019). Names are listed only for rock compositions that have < 10 wt.-% minerals not represented in the Füchtbauer triangle (i.e. minerals other than clays, calcite, dolomite/ ankerite, siderite, quartz, K-feldspar, plagioclase). In particular, this means that evaporitic rocks are not given a Füchtbauer name. If a rock contains ≥ 90 wt.-% minerals represented in the Füchtbauer triangle but also contains anhydrite, this is stated in brackets.
- The Füchtbauer triangle does not distinguish between limestones and dolostones. In cases when the contents of calcite exceed those of dolomite/ankerite, the terms "limestone" or "calcareous" are used in this report, and "dolostone" or "dolomitic" are used if the opposite applies.

Clay mineral groups

- All data refer to wt.-% of the total rock.
- Illite/smectite ML (85-90) refers to a mixed-layer phase with 85 – 90% illite layers, Chl/Sm ML (85-95) designates a chlorite-smectite mixed-layer phase with 85 – 95% chlorite (analogous for the other listed mixed-layer phases).

End-member clays

- All data refer to wt.-% of the total rock.
- Illite, smectite and chlorite partially occur in mixed-layer phases. Here, the respective total contents of the end-members are calculated. For example, if a sample contains 10 wt.-% illite and 8 wt.-% illite/smectite mixed layers containing 75% illite, the end-member illite content would be 16 wt.-%.

Petrophysical parameters

- Bulk wet density was measured, and bulk dry density was calculated using Equation 5-14 in Waber (ed.) (2020).
- Pycnometer porosity was calculated from densities using Equation 5-16 in Waber (ed.) (2020).
- Water content (dry) was calculated from water content (wet) using $w_d = w_w/(1-w_w)$.
- Water-loss porosity was calculated using bulk wet density (Equation 5-9 in Waber ed. 2020) or grain density (Equation 5-7 in Waber ed. 2020).
- The formalisms to calculate water content from isotope diffusive exchange experiments are detailed in Mazurek et al. (2021).

Cl^- and Br^- from aqueous extracts recalculated to porewater concentrations using water content

- Concentrations are given relative to bulk porewater as well as relative to various assumptions regarding anion accessibility in the pore space. The calculation is made using Equation 6-1 in Waber (ed.) (2020). In case of the BRGM data a correction for the partial desaturation of the sample material is applied (see Section 3.4, eq. 8). The variants pertaining to the dependence of anion accessibility on clay-mineral content are discussed in Chapter 5.

Errors

- The error columns refer to analytical uncertainty or instrument precision for measured parameters and to propagated errors for calculated parameters, following the formalisms documented in Waber (ed.) (2020) and Appendices A and B.

4.2 Mineralogical composition

Martin Mazurek

4.2.1 Whole rock

A total of 125 mineralogical analyses were performed in the section Malm – Keuper. The full data set is documented in Appendix A, and Tab. 4.2-1 provides formation-specific summaries. The depth trends for the most relevant minerals are shown graphically in Fig. 4.2-1, and a representation in the Füchtbauer triangle is given in Fig. 4.2-2. Clay-mineral contents are low in the Malm but become substantially larger in the underlying Dogger. Whereas the lithological heterogeneity is marked in the Wedelsandstein Formation, the Opalinus Clay is more homogeneous. Again, more heterogeneity characterises the Staffelegg Formation and the underlying Triassic.

Tab. 4.2-1: Bulk-rock mineralogy: formation-specific means, medians, standard devations and ranges

For the calculation of statistical parameters, values below detection were set to 0. In several cases, systematic depth trends of mineral contents are observed (see below). This means that in these cases the data do not follow a Gaussian distribution, which is a pre-requisite for the calculation of meaningful standard deviations. In such cases, the ranges (also listed) are more meaningful.

Formation (number of analyses)	**Member**		**S** [wt.-%]	**C(inorg)** [wt.-%]	**C(org)** [wt.-%]	**Quartz** [wt.-%]	**K-feldspar** [wt.-%]	**Plagioclase** [wt.-%]	**Calcite** [wt.-%]	**Dolomit/Ank.** [wt.-%]	**Siderite** [wt.-%]	**Anhydrite** [wt.-%]	**Celestite** [wt.-%]	**Pyrite** [wt.-%]	**Clay minerals** [wt.-%]
«Felsenkalke» + «Massenkalk» (6)		Mean	0.01	11.49	0.18	0.8	0.2	0.0	95.4	0.5	0.0	0.0	0.0	0.0	3.0
		Median	0.00	11.74	0.18	0.3	0.0	0.0	97.8	0.0	0.0	0.0	0.0	0.0	1.9
		Stdev	0.02	0.64	0.12	1.2	0.5	0.0	6.5	1.1	0.0	0.0	0.0	0.0	3.7
		Min	0.00	10.24	0.00	0.0	0.0	0.0	82.3	0.0	0.0	0.0	0.0	0.0	0.4
		Max	0.05	11.94	0.35	3.1	1.2	0.0	99.5	2.8	0.0	0.0	0.0	0.1	10.3
Schwarzbach Fm. (1)		Mean	0.04	9.03	0.32	4.9	2.2	0.0	73.0	2.0	0.0	0.0	0.0	0.1	17.5
Villigen Fm. (4)		Mean	0.03	11.38	0.21	0.9	0.0	0.0	94.1	0.5	0.0	0.0	0.0	0.1	4.3
		Median	0.03	11.43	0.21	0.8	0.0	0.0	93.8	0.0	0.0	0.0	0.0	0.1	4.0
		Stdev	0.04	0.25	0.04	1.0	0.0	0.0	2.1	1.0	0.0	0.0	0.0	0.1	1.7
		Min	0.00	11.03	0.15	0.0	0.0	0.0	91.9	0.0	0.0	0.0	0.0	0.0	2.8
		Max	0.08	11.61	0.25	2.0	0.0	0.0	96.8	1.9	0.0	0.0	0.0	0.1	6.4
Wildegg Fm. (1)		Mean	0.00	10.09	0.24	2.7	2.0	0.0	82.0	1.9	0.0	0.0	0.0	0.0	11.1
Variansmergel Fm. (5)		Mean	0.57	3.90	0.58	23.1	4.7	1.4	31.4	0.6	0.4	0.0	0.0	1.1	36.7
		Median	0.67	3.80	0.64	24.4	5.3	1.7	31.7	0.0	0.0	0.0	0.0	1.3	37.3
		Stdev	0.22	1.34	0.11	3.8	2.7	0.9	12.0	1.4	0.6	0.0	0.0	0.4	12.4
		Min	0.23	2.52	0.40	19.2	0.0	0.0	17.5	0.0	0.0	0.0	0.0	0.4	19.7
		Max	0.77	5.89	0.66	28.1	6.8	2.3	48.0	3.2	1.3	0.0	0.0	1.4	49.3
«Parkinsoni-Württembergica-Sch.» (13)		Mean	0.62	3.61	0.72	19.2	5.2	2.0	28.0	1.8	0.2	0.0	0.0	1.2	41.9
		Median	0.68	2.92	0.69	19.0	5.3	2.0	24.3	1.9	0.0	0.0	0.0	1.3	43.5
		Stdev	0.39	1.43	0.17	3.5	1.1	0.9	11.8	1.4	0.4	0.0	0.0	0.7	9.4
		Min	0.00	1.99	0.44	14.3	3.0	0.0	13.5	0.0	0.0	0.0	0.0	0.0	24.0
		Max	1.32	6.64	1.01	26.2	6.7	3.3	53.2	4.4	1.3	0.0	0.0	2.5	55.7

Tab. 4.2-1: continued

Formation (number of analyses)	**Member**		**S** [wt.-%]	**C(inorg)** [wt.-%]	**C(org)** [wt.-%]	**Quartz** [wt.-%]	**K-feldspar** [wt.-%]	**Plagioclase** [wt.-%]	**Calcite** [wt.-%]	**Dolomit/Ank.** [wt.-%]	**Siderite** [wt.-%]	**Anhydrite** [wt.-%]	**Celestite** [wt.-%]	**Pyrite** [wt.-%]	**Clay minerals** [wt.-%]
«Humphriesi-oolith Fm.» (3)		Mean	0.32	4.97	0.51	23.1	3.7	1.4	38.8	2.1	0.3	0.0	0.0	0.6	29.5
		Median	0.41	3.25	0.58	28.0	3.0	2.0	26.3	1.2	0.0	0.0	0.0	0.8	38.2
		Stdev	0.29	3.61	0.25	11.2	1.7	1.2	27.3	2.8	0.5	0.0	0.0	0.5	15.5
		Min	0.00	2.54	0.23	10.3	2.5	0.0	19.9	0.0	0.0	0.0	0.0	0.0	11.6
		Max	0.56	9.12	0.73	31.0	5.6	2.1	70.1	5.2	0.9	0.0	0.0	1.0	38.7
Wedelsandstein Fm. (13)		Mean	0.36	2.40	0.54	38.7	6.0	3.2	19.1	0.5	0.0	0.0	0.0	0.7	31.3
		Median	0.39	2.24	0.50	40.3	5.9	3.4	17.5	0.0	0.0	0.0	0.0	0.7	27.9
		Stdev	0.19	1.02	0.15	10.7	1.0	1.1	8.6	0.9	0.0	0.0	0.0	0.4	16.5
		Min	0.04	0.66	0.33	20.0	4.0	0.0	5.3	0.0	0.0	0.0	0.0	0.1	13.2
		Max	0.69	4.72	0.79	56.3	7.7	4.6	39.3	2.8	0.0	0.0	0.0	1.3	67.8
Opalinus Clay (49)	All	Mean	0.35	1.31	1.02	22.4	5.2	3.1	8.0	0.0	3.4	0.0	0.0	0.7	56.3
		Median	0.28	1.29	1.02	23.1	5.3	3.2	7.3	0.0	3.7	0.0	0.0	0.5	55.5
		Stdev	0.29	0.34	0.12	3.8	0.9	0.7	2.8	0.1	1.7	0.0	0.0	0.5	5.4
		Min	0.07	0.83	0.76	11.2	3.0	0.0	3.9	0.0	0.0	0.0	0.0	0.1	40.9
		Max	1.71	2.82	1.39	30.9	7.2	4.1	21.7	0.4	6.5	0.0	0.0	3.2	67.9
Opalinus Clay (11)	Sub-unit with silty calcareous beds	Mean	0.60	1.06	1.08	23.3	5.3	3.0	6.7	0.0	2.5	0.0	0.0	1.1	57.0
		Median	0.42	1.08	1.03	23.6	5.4	3.4	6.1	0.0	3.0	0.0	0.0	0.8	54.9
		Stdev	0.48	0.14	0.16	3.6	1.2	1.1	2.0	0.0	1.4	0.0	0.0	0.9	5.0
		Min	0.11	0.87	0.93	17.6	3.0	0.0	3.9	0.0	0.0	0.0	0.0	0.2	51.4
		Max	1.71	1.22	1.39	29.9	6.9	3.8	10.1	0.0	3.9	0.0	0.0	3.2	67.9
Opalinus Clay (6)	Upper silty sub-unit	Mean	0.39	1.23	1.04	24.3	5.6	3.3	7.5	0.0	3.2	0.0	0.0	0.7	54.3
		Median	0.38	1.26	1.05	23.9	5.6	3.5	6.7	0.0	3.6	0.0	0.0	0.7	54.9
		Stdev	0.15	0.17	0.09	1.8	0.8	0.4	2.1	0.0	1.7	0.0	0.0	0.3	3.0
		Min	0.22	0.99	0.89	22.1	4.4	2.7	5.3	0.0	0.0	0.0	0.0	0.4	50.1
		Max	0.64	1.44	1.17	27.0	6.8	3.7	11.0	0.0	5.2	0.0	0.0	1.2	57.0
Opalinus Clay (25)	Mixed clay-silt-carbonate sub-unit	Mean	0.22	1.45	1.02	23.6	5.1	3.1	8.7	0.0	3.9	0.0	0.0	0.4	54.1
		Median	0.16	1.41	1.03	23.1	5.1	3.2	7.7	0.0	4.5	0.0	0.0	0.3	54.8
		Stdev	0.15	0.39	0.09	2.0	0.8	0.5	3.3	0.1	1.8	0.0	0.0	0.3	4.3
		Min	0.07	0.83	0.87	21.5	3.0	2.0	5.0	0.0	0.0	0.0	0.0	0.1	40.9
		Max	0.67	2.82	1.26	30.9	7.2	4.1	21.7	0.4	6.5	0.0	0.0	1.3	60.4
Opalinus Clay (7)	Clay-rich sub-unit	Mean	0.38	1.26	0.91	15.2	4.7	3.2	7.8	0.0	3.1	0.0	0.0	0.7	64.4
		Median	0.38	1.27	0.96	15.3	4.8	3.2	7.4	0.0	3.0	0.0	0.0	0.7	64.9
		Stdev	0.10	0.23	0.10	2.1	0.5	0.2	2.1	0.0	0.6	0.0	0.0	0.2	1.7
		Min	0.26	1.00	0.76	11.2	4.0	2.9	6.0	0.0	2.2	0.0	0.0	0.5	61.6
		Max	0.58	1.69	1.01	18.3	5.3	3.4	12.2	0.0	4.1	0.0	0.0	1.1	66.4
Staffelegg Fm. (15)		Mean	0.93	2.76	2.60	18.4	4.0	2.4	21.1	1.1	0.6	0.0	0.0	1.7	48.0
		Median	0.54	1.29	0.94	15.3	4.2	2.3	10.2	1.0	0.0	0.0	0.0	1.0	43.4
		Stdev	0.95	2.31	2.49	11.2	1.4	0.8	19.2	1.1	1.0	0.0	0.0	1.8	14.4
		Min	0.03	0.36	0.38	2.0	2.0	1.1	0.9	0.0	0.0	0.0	0.0	0.1	26.9
		Max	3.30	7.49	7.84	40.9	6.2	3.8	58.1	3.2	2.8	0.0	0.0	6.2	81.1

Tab. 4.2-1: continued

Formation (number of analyses)	**Member**		**S** [wt.-%]	**C(inorg)** [wt.-%]	**C(org)** [wt.-%]	**Quartz** [wt.-%]	**K-feldspar** [wt.-%]	**Plagioclase** [wt.-%]	**Calcite** [wt.-%]	**Dolomit/Ank.** [wt.-%]	**Siderite** [wt.-%]	**Anhydrite** [wt.-%]	**Celestite** [wt.-%]	**Pyrite** [wt.-%]	**Clay minerals** [wt.-%]
Klettgau Fm.		Mean	0.11	3.91	0.22	17.7	7.7	3.4	2.6	27.5	0.0	0.0	0.0	0.2	40.6
(11)		Median	0.00	4.22	0.18	8.9	8.3	3.4	1.2	28.4	0.0	0.0	0.0	0.0	44.1
		Stdev	0.17	3.86	0.13	20.5	3.9	2.1	5.3	28.6	0.0	0.0	0.0	0.3	19.0
		Min	0.00	0.00	0.06	1.0	0.0	0.0	0.0	0.0	0.0	0.0	0.0	0.0	3.5
		Max	0.50	12.37	0.54	71.4	13.9	7.2	18.1	93.6	0.0	0.0	0.0	0.9	72.8
Bänkerjoch Fm.		Mean	7.48	4.55	0.13	5.9	4.9	0.7	0.4	34.5	0.0	31.7	0.0	0.0	21.7
(4)		Median	8.95	5.12	0.14	4.5	4.7	0.6	0.0	39.3	0.0	38.0	0.0	0.0	23.1
		Stdev	5.45	3.26	0.03	5.4	2.8	0.9	0.9	25.8	0.0	23.1	0.0	0.0	14.2
		Min	0.00	0.25	0.10	1.2	1.9	0.0	0.0	0.0	0.0	0.0	0.0	0.0	5.0
		Max	12.00	7.73	0.17	13.3	8.3	1.7	1.8	59.3	0.0	51.0	0.0	0.0	35.8

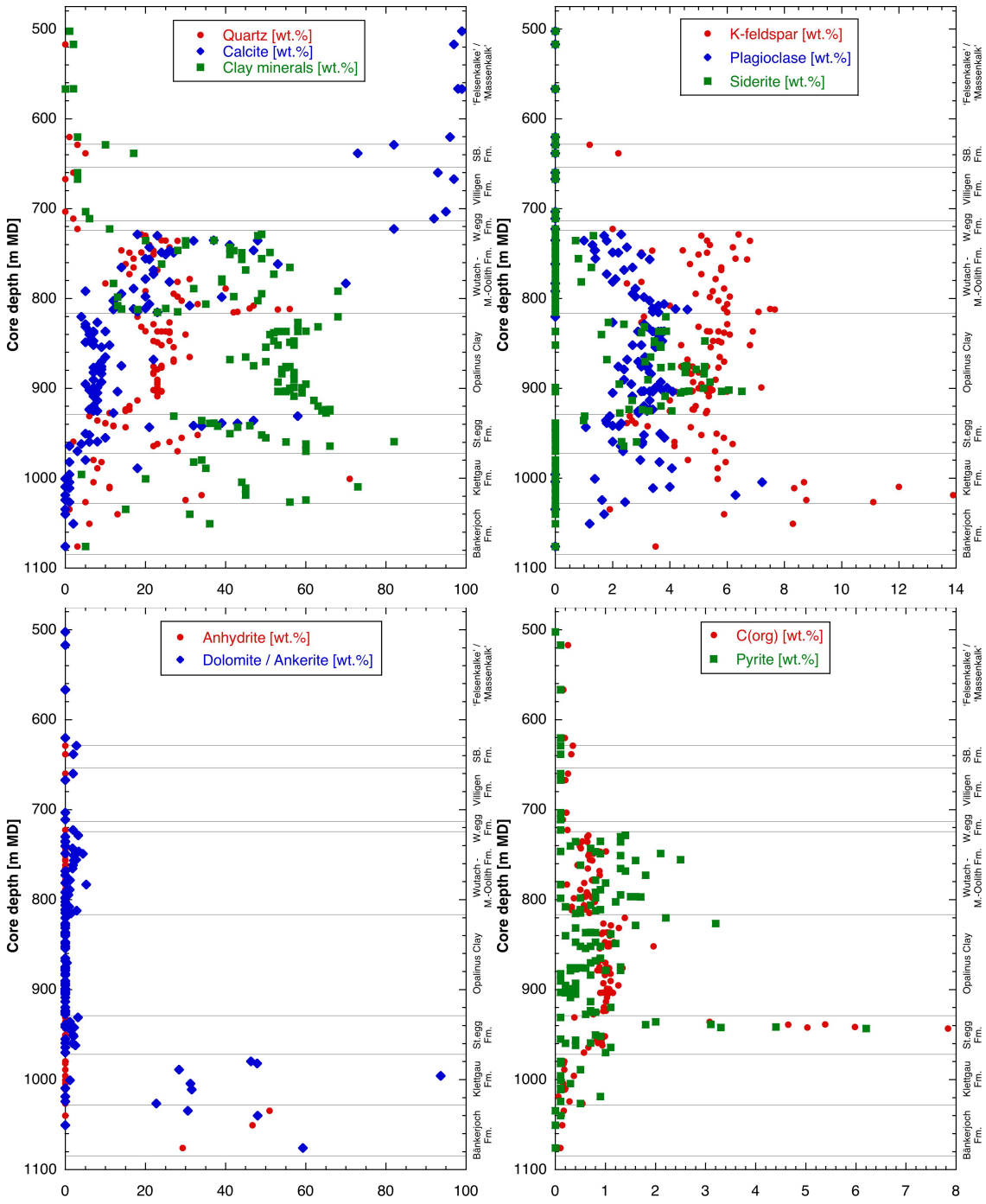

Fig. 4.2-1: Mineral contents in the bulk rock as a function of depth

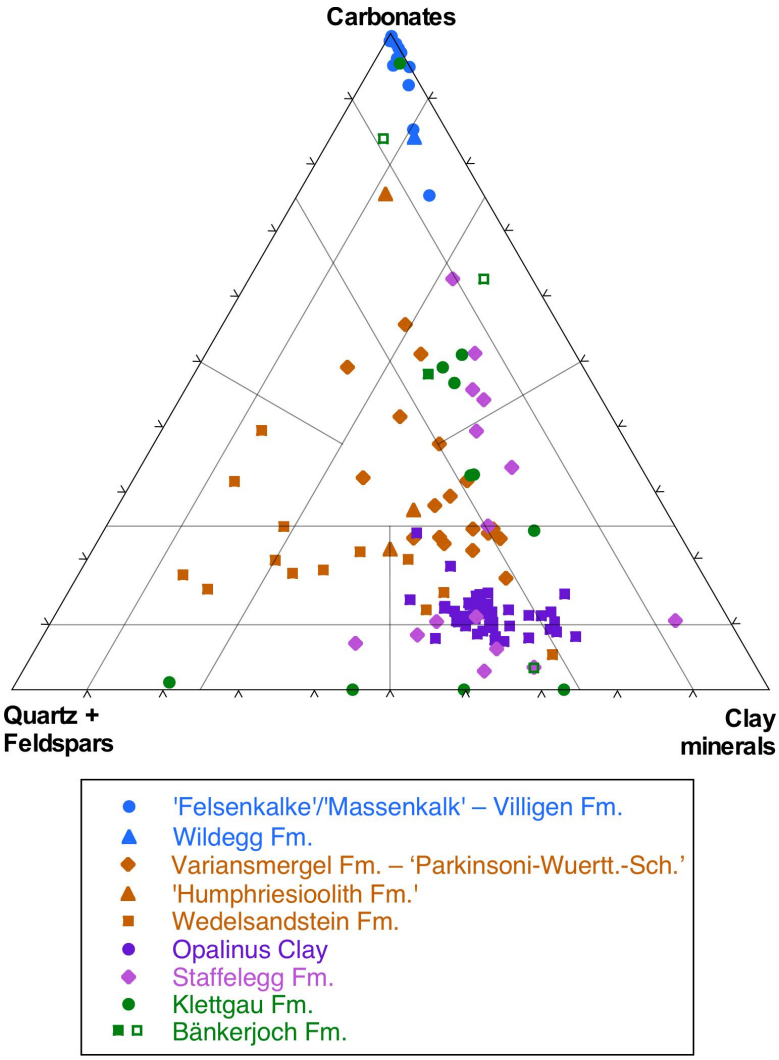

Fig. 4.2-2: Mineralogical composition of studied samples in the Füchtbauer triangle

Open symbols in the Bänkerjoch Formation indicate samples containing > 10 wt.-% minerals other than those represented by the Füchtbauer triangle (i.e. clays, calcite, dolomite/ankerite, siderite, quartz, K-feldspar, plagioclase). In all cases, anhydrite is the main additional phase.

A closer look at the clay-rich section Staffelegg Formation – Opalinus Clay – «Brauner Dogger»

The graphics shown in Fig. 4.2-3 indicate systematic depth trends in particular of quartz, clay-mineral and calcite contents, whereas most other minerals show less systematic variability.

Staffelegg Formation

- Clay-mineral contents decrease substantially upwards. In contrast, quartz and plagioclase increase upwards systematically in the lower part (Schambelen Member – Frick Member), and this trend is reversed for quartz (at lower contents) in the upper part (Rietheim Member – Gross Wolf Member). The differentiation of two cycles is also supported by calcite contents, which are low and increase slightly in the lower part but then increase more strongly in the upper part. The existence of two cycles is also seen in the depth profile of the quartz / clay ratio.
- The Rietheim Member is characterised by a strong positive excursion of the contents of C(org) and pyrite, pointing to highly reducing conditions during deposition.

Opalinus Clay

Informal sub-units within the Opalinus Clay were defined by Mazurek & Aschwanden (2020) on a regional basis. In Dossier III this scheme is successfully applied to the Trüllikon-1-1 core, and the sub-unit boundaries are included in Fig. 4.2-3.

- The base of the Opalinus Clay correlates with the onset of more homogeneous mineral contents, in contrast to a substantial scatter in the underlying Staffelegg Formation. In the clay-rich sub-unit at the base of the Opalinus Clay, quartz contents increase and clay-mineral contents decrease upwards.
- In the overlying mixed clay-silt-carbonate sub-unit, quartz contents first stay constant and then increase upwards in the uppermost part. Clay-mineral contents decrease with a similar slope as in the clay-rich sub-unit, but the decrease becomes more pronounced in the uppermost part where quartz contents increase. This means that, from a mineralogical point of view, a boundary exists at about 873 m where the trends change, likely in response to a change of sedimentary facies. Note that, based on lithostratigraphic logging, the mixed clay-silt-carbonate sub-unit can also be subdivided into two parts, with a boundary at 873.45 m (Dossier III).
- The boundary between the mixed clay-silt-carbonate and the overlying upper silty sub-unit corresponds to a major mineralogical discontinuity and a trend reversal of both quartz and clay-mineral contents.
- The upward trends of increasing clay-mineral and decreasing quartz and calcite contents remain constant over the upper silty sub-unit and the overlying sub-unit with silty calcareous beds, i.e. these sub-units cannot be distinguished on the basis of discontinuities in the mineralogical composition.
- The top of the Opalinus Clay correlates with a major discontinuity of clay-mineral, quartz and calcite contents.

Wedelsandstein Formation

- Mineralogical heterogeneity is substantial and mostly unsystematic. A general upward decrease of quartz and plagioclase contents can be identified.

«Humphriesioolith Formation»

- No obvious trends are seen in this somewhat heterogeneous unit.

«Parkinsoni-Württembergica-Schichten»

- Apart from a weak general increase of quartz contents, no obvious trends are seen in this somewhat heterogeneous unit.

Variansmergel Formation

- Even though defined by a limited number of data points, quartz and calcite appear to substantially decrease upwards, while clay minerals increase. The ratio quartz/clay minerals, thus, shows a well-expressed decrease.

Conclusion

A number of mineralogical discontinuities and changes in depth trends were identified and correlate well with the lithostratigraphic subdivision in Dossier III. Within the mixed clay-silt-carbonate sub-unit of the Opalinus Clay, a further subdivision can be made both based on bulk mineralogy and lithostratigraphic logging.

Quartz and clay-mineral contents show the most pronounced trends and discontinuities in their depth profiles, whereas for calcite this is the case only in the Staffelegg Formation and the Variansmergel Formation. As the contents of quartz and clay minerals often show inverse depth trends, the ratio quartz/clay minerals most clearly highlights the depositional cycles that govern the mineralogical composition, as shown in Fig. 4.2-3d. Last, let us note that the sub-units of the Opalinus Clay as defined by Mazurek & Aschwanden (2020) are not zones with constant properties but rather zones with constant trends, i.e. depositional cycles.

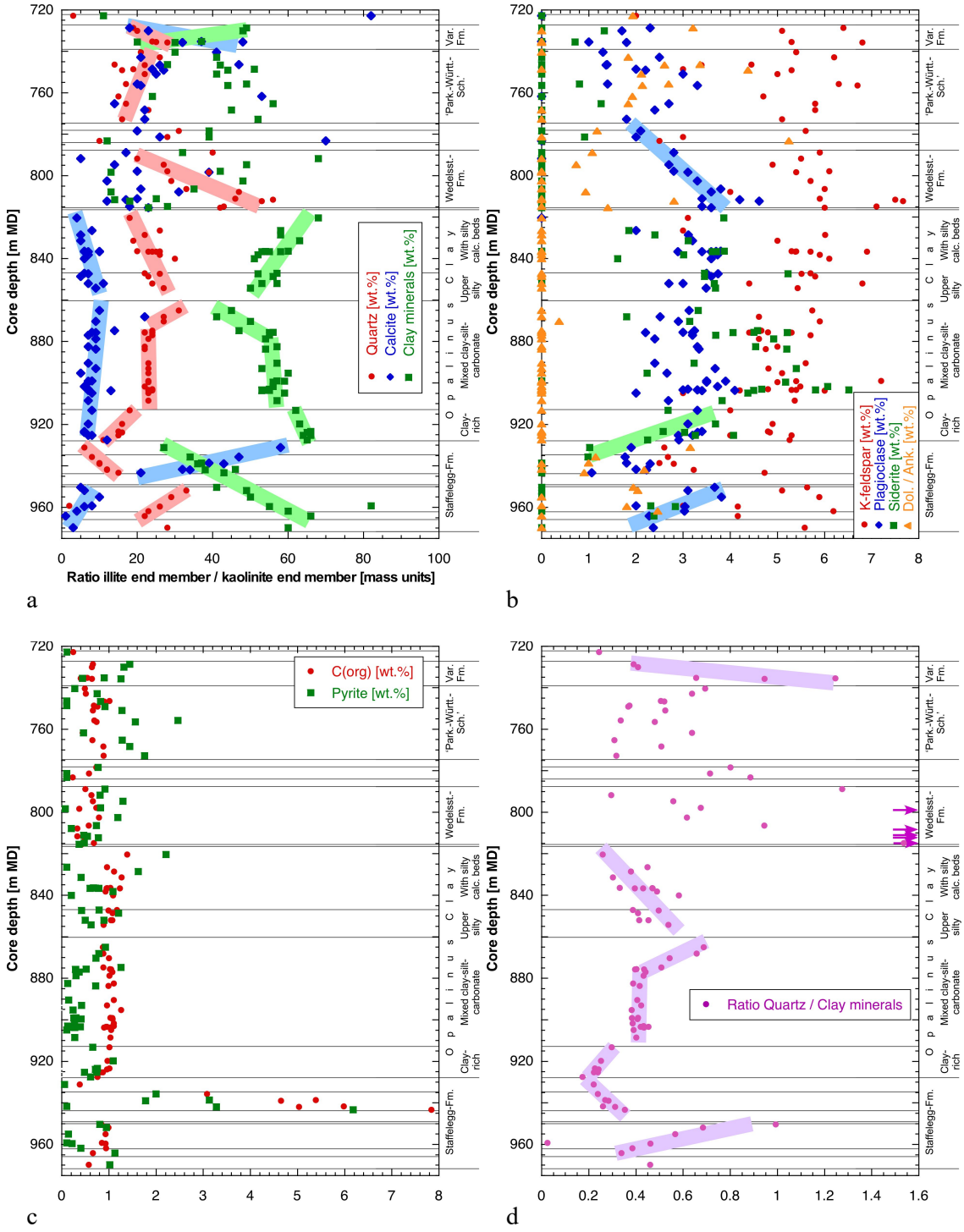

Fig. 4.2-3: Depth trends of mineral contents in the bulk rock of the Lias – Dogger interval

Coloured bars highlight systematic trends. Detailed lithostratigraphic subdivision according to Dossier III. Pink arrows in graphic d indicate high values that are outside the plotted range.

4.2.2 Clay minerals

A total of 50 mineralogical analyses of the clay fraction were performed in the section Malm – Keuper. The full data set is documented in Appendix A, and Tab. 4.2-2 provides formation-specific summaries, normalising the contents of individual clay phases to the sum of all clay minerals.

The identified clay-mineral species include illite, smectite, illite/smectite mixed layers, kaolinite, chlorite and chlorite/smectite mixed layers. The identification of chlorite/smectite mixed layers in all samples is in contrast with previous data from northern Switzerland where this mineral was rarely identified (Mazurek 2017). However, this is not a real difference but due to the improved methodology of the evaluation of X-ray patterns that was applied for the TBO campaign (details in Waber ed. 2020). Because the chlorite/smectite mixed-layer phase contains 85 – 95% chlorite layers, its XRD reflections are close to those of pure chlorite. The new methodology also allows to better resolve the fraction of smectite layers in the illite/smectite mixed-layer phase. As seen in Tab. 4.2-2, illite-rich mixed layers dominate, but minor amounts of illite-poorer mixed layers also occur. Given the fact that the contents of mixed-layer phases and the smectite fractions in these are known, the end-member compositions of illite, smectite, chlorite and kaolinite (whether in mixed layers or as a discrete phase) can be calculated and are also listed in Tab. 4.2-2.

Depth trends are shown graphically in Fig. 4.2-4 for individual clay phases (a) and end-member clays (b). The depth plot of the latter is less noisy than that of the individual clay minerals. In the interval Klettgau Formation – Staffelegg Formation, the contents of kaolinite increase upwards at the expense of the illite end-member. In the Opalinus Clay, all end-member phases occur in remarkably constant ratios. Illite end-member contents are the lowest and those of kaolinite are the highest in the whole drilled profile (except for an outlier in the Klettgau Formation). The base of the Wedelsandstein Formation correlates with a major discontinuity, in that the contents of the illite end-member increase sharply at the expense of kaolinite. The ratio kaolinite/illite end-member decreases markedly from the top of the Wedelsandstein Formation towards the Malm.

Tab. 4.2-2: Mineralogical composition of the clay fraction: formation-specific means, medians, standard deviations and ranges

In some cases, systematic depth trends of clay-mineral contents are observed. This means that in these cases the data do not follow a Gaussian distribution, which is a pre-requisite for the calculation of meaningful standard deviations. In such cases, the ranges (also listed) are more meaningful.

Formation (number of analyses)	**Member**		**Individual clay phases** [wt.-% of clay fraction]										**End-member clays** [wt.-% of clay fraction]			
			Illite	**Ill/Sm ML (85-90)**	**Ill/Sm ML (75-80)**	**Ill/Sm ML (50-70)**	**Ill/Sm ML (20-40)**	**Total Ill/Sm**	**Smectite**	**Kaolinite**	**Chlorite**	**Chl/Sm ML (85-95)**	**Illite**	**Smectite**	**Kaolinite**	**Chlorite**
Schwarzbach Fm. (1)		Mean	54.0	18.0	15.0	2.0	0.0	35.0	0.0	6.0	4.0	2.0	82.0	7.0	6.0	6.0
Villigen Fm. (2)		Mean	38.5	27.5	4.5	2.5	0.5	35.0	0.0	18.0	4.5	4.0	68.0	6.5	18.0	7.5
		Median	38.5	27.5	4.5	2.5	0.5	35.0	0.0	18.0	4.5	4.0	68.0	6.5	18.0	7.5
		Stdev	10.6	23.3	6.4	3.5	0.7	14.1	0.0	1.4	2.1	4.2	4.2	0.7	1.4	2.1
		Min	31.0	11.0	0.0	0.0	0.0	25.0	0.0	17.0	3.0	1.0	65.0	6.0	17.0	6.0
		Max	46.0	44.0	9.0	5.0	1.0	45.0	0.0	19.0	6.0	7.0	71.0	7.0	19.0	9.0
Wildegg Fm. (1)		Mean	44.0	17.0	11.0	3.0	0.0	31.0	0.0	17.0	3.0	5.0	69.0	6.0	17.0	8.0
Variansm. Fm. (3)		Mean	41.0	18.0	3.0	2.3	0.0	23.3	0.0	25.3	4.3	5.7	60.0	5.0	25.3	9.0
		Median	40.0	17.0	0.0	2.0	0.0	25.0	0.0	26.0	3.0	6.0	60.0	5.0	26.0	9.0
		Stdev	5.6	4.6	5.2	1.5	0.0	4.7	0.0	1.2	2.3	2.5	2.0	2.0	1.2	1.0
		Min	36.0	14.0	0.0	1.0	0.0	18.0	0.0	24.0	3.0	3.0	58.0	3.0	24.0	8.0
		Max	47.0	23.0	9.0	4.0	0.0	27.0	0.0	26.0	7.0	8.0	62.0	7.0	26.0	10.0
«Parkinsoni-Württembergica-Sch.» (6)		Mean	39.2	13.8	9.3	2.2	0.2	25.5	0.0	26.2	4.0	5.3	59.8	5.3	26.2	8.5
		Median	39.0	16.0	4.5	2.0	0.0	25.5	0.0	27.0	3.5	6.0	59.0	5.0	27.0	8.0
		Stdev	2.6	10.1	11.6	0.8	0.4	2.9	0.0	2.2	1.3	1.0	2.6	1.0	2.2	0.8
		Min	36.0	0.0	0.0	1.0	0.0	21.0	0.0	23.0	3.0	4.0	57.0	4.0	23.0	8.0
		Max	42.0	25.0	25.0	3.0	1.0	29.0	0.0	29.0	6.0	6.0	63.0	7.0	29.0	10.0
«Humphriesioolith Fm.» (1)		Mean	34.0	12.0	12.0	2.0	0.0	26.0	0.0	26.0	6.0	7.0	55.0	6.0	26.0	12.0
Wedelsandstein Fm. (8)		Mean	35.9	9.4	24.1	3.2	0.4	37.0	0.0	15.3	6.4	5.2	65.3	8.4	15.4	11.2
		Median	38.5	6.5	25.5	3.2	0.0	29.5	0.0	17.0	6.2	5.0	64.0	7.5	17.0	11.3
		Stdev	8.4	9.5	7.1	2.4	0.7	12.4	0.0	6.4	2.0	2.0	5.6	2.3	6.4	2.1
		Min	16.0	0.0	12.0	0.0	0.0	27.0	0.0	5.0	4.0	2.0	59.0	6.0	5.0	7.0
		Max	42.0	31.0	34.0	8.0	2.0	60.0	0.0	23.0	10.0	8.0	77.0	12.0	23.0	14.0
Opalinus Clay (15)		Mean	30.4	12.0	9.3	2.3	0.1	23.7	0.0	33.9	4.5	7.3	49.6	5.5	33.9	11.0
		Median	30.0	11.0	11.0	2.0	0.0	24.0	0.0	34.0	4.0	7.0	50.0	5.0	34.0	11.0
		Stdev	2.0	4.0	5.2	1.1	0.3	2.0	0.0	1.8	1.2	1.3	1.3	0.5	1.9	1.1
		Min	28.0	7.0	0.0	1.0	0.0	21.0	0.0	31.0	2.2	5.0	47.0	5.0	31.0	9.0
		Max	34.0	20.0	16.0	4.0	1.0	28.0	0.0	37.0	7.0	10.0	51.8	6.0	37.0	13.0

Tab. 4.2-2 continued

Formation (number of analyses)	**Member**		**Individual clay phases** [wt.-% of clay fraction]										**End-member clays** [wt.-% of clay fraction]			
			Illite	**Ill/Sm ML (85-90)**	**Ill/Sm ML (75-80)**	**Ill/Sm ML (50-70)**	**Ill/Sm ML (20-40)**	**Total Ill/Sm**	**Smectite**	**Kaolinite**	**Chlorite**	**Chl/Sm ML (85-95)**	**Illite**	**Smectite**	**Kaolinite**	**Chlorite**
Opalinus Clay (3)	With silty calc. beds	Mean	31.7	8.3	12.0	2.0	0.0	22.3	0.0	34.0	4.3	7.3	50.0	5.3	34.0	10.7
		Median	32.0	8.0	11.0	2.0	0.0	21.0	0.0	33.0	4.0	7.0	50.0	5.0	33.0	10.0
		Stdev	1.5	0.6	2.6	1.0	0.0	2.3	0.0	1.7	1.5	0.6	1.0	0.6	1.7	1.2
		Min	30.0	8.0	10.0	1.0	0.0	21.0	0.0	33.0	3.0	7.0	49.0	5.0	33.0	10.0
		Max	33.0	9.0	15.0	3.0	0.0	25.0	0.0	36.0	6.0	8.0	51.0	6.0	36.0	12.0
Opalinus Clay (2)	Upper silty	Mean	31.5	12.0	9.0	2.5	0.0	23.5	0.0	33.5	5.5	7.0	50.0	5.5	33.5	11.5
		Median	31.5	12.0	9.0	2.5	0.0	23.5	0.0	33.5	5.5	7.0	50.0	5.5	33.5	11.5
		Stdev	2.1	2.8	5.7	0.7	0.0	2.1	0.0	0.7	0.7	0.0	0.0	0.7	0.7	0.7
		Min	30.0	10.0	5.0	2.0	0.0	22.0	0.0	33.0	5.0	7.0	50.0	5.0	33.0	11.0
		Max	33.0	14.0	13.0	3.0	0.0	25.0	0.0	34.0	6.0	7.0	50.0	6.0	34.0	12.0
Opalinus Clay (7)	Mixed clay-silt-carbo-nate	Mean	29.5	12.8	9.9	2.1	0.1	25.0	0.0	34.0	4.5	7.0	49.7	5.6	34.0	10.5
		Median	29.0	11.0	11.0	2.0	0.0	24.9	0.0	34.0	4.0	7.0	49.0	6.0	34.0	10.5
		Stdev	1.7	4.6	5.7	1.3	0.4	1.6	0.0	2.1	1.5	1.5	1.5	0.5	2.1	1.0
		Min	28.0	7.0	0.0	1.0	0.0	23.0	0.0	31.8	2.2	5.0	48.0	5.0	31.8	9.0
		Max	32.0	20.0	16.0	4.0	1.0	28.0	0.0	37.0	7.0	9.0	51.8	6.0	37.0	12.0
Opalinus Clay (3)	Clay-rich	Mean	30.7	14.0	5.3	3.0	0.0	22.3	0.0	34.0	4.3	8.3	48.7	5.3	34.0	12.0
		Median	29.0	16.0	5.0	3.0	0.0	22.0	0.0	35.0	4.0	8.0	49.0	5.0	35.0	12.0
		Stdev	2.9	4.4	5.5	1.0	0.0	1.5	0.0	2.6	0.6	1.5	1.5	0.6	2.6	1.0
		Min	29.0	9.0	0.0	2.0	0.0	21.0	0.0	31.0	4.0	7.0	47.0	5.0	31.0	11.0
		Max	34.0	17.0	11.0	4.0	0.0	24.0	0.0	36.0	5.0	10.0	50.0	6.0	36.0	13.0
Staffelegg Fm. (8)		Mean	39.7	19.7	9.2	2.8	0.4	32.0	0.1	17.4	4.3	6.4	65.6	6.9	17.4	10.1
		Median	38.0	22.0	0.9	3.0	0.0	29.0	0.0	14.0	4.0	6.5	69.0	6.0	14.0	9.8
		Stdev	6.5	12.2	13.5	0.9	0.7	7.6	0.2	9.1	1.0	1.4	8.4	1.7	9.1	1.1
		Min	32.0	0.0	0.0	1.0	0.0	25.0	0.0	5.0	3.0	5.0	55.0	5.0	5.0	9.0
		Max	49.0	40.3	36.0	4.0	2.0	46.3	0.5	30.0	6.0	9.0	77.0	9.5	30.0	12.0
Klettgau Fm. (5)		Mean	48.0	24.8	2.4	1.0	0.2	28.4	0.0	13.8	4.8	4.4	72.2	5.2	13.8	8.8
		Median	47.0	27.0	0.0	1.0	0.0	29.0	0.0	4.0	4.0	5.0	75.0	5.0	4.0	10.0
		Stdev	16.4	14.6	5.4	1.0	0.4	10.6	0.0	20.8	4.5	2.9	22.3	1.8	20.8	4.2
		Min	24.0	1.0	0.0	0.0	0.0	13.0	0.0	1.0	1.0	1.0	35.0	3.0	1.0	3.0
		Max	69.0	38.0	12.0	2.0	1.0	40.0	0.0	50.0	12.0	8.0	90.0	7.0	50.0	13.0

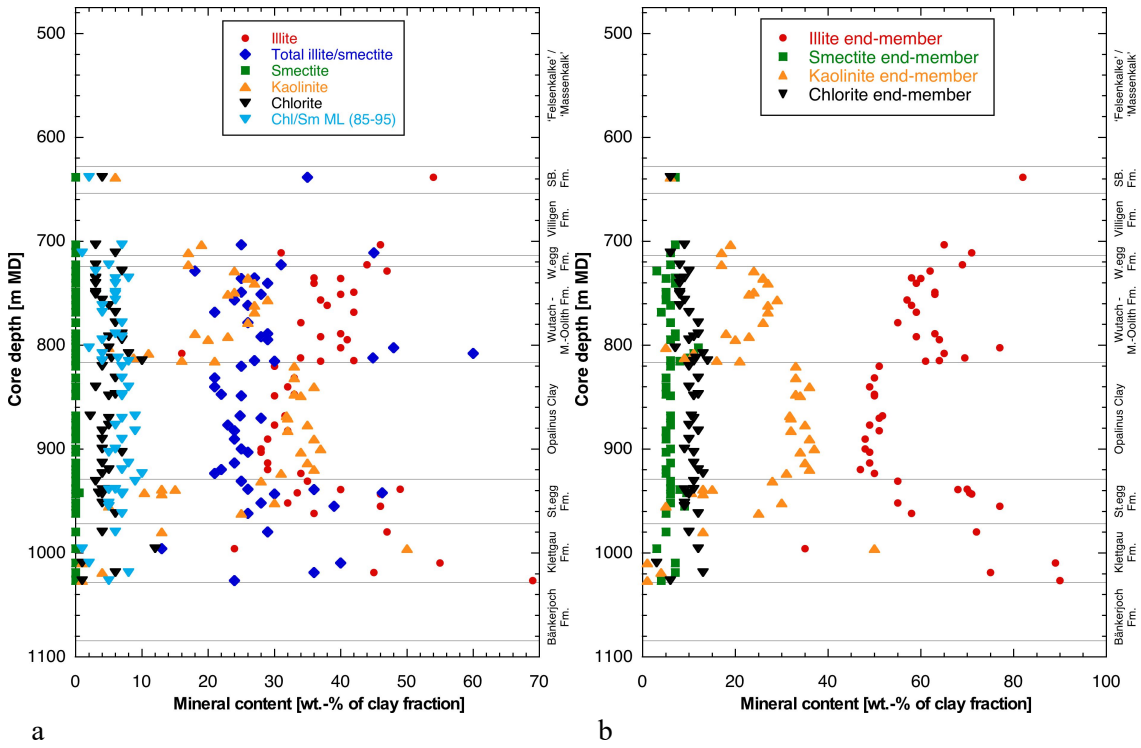

Fig. 4.2-4: Mineralogical composition of the clay fraction as a function of depth

a Individual clay minerals

b End-member clays

A closer look at the clay-rich section Staffelegg Formation – Opalinus Clay – «Brauner Dogger»

The composition of the clay fraction shows less variability with depth than that of the total clay content (Section 4.2.1) but, nevertheless, some depth trends can be identified (Fig. 4.2-5). In the Staffelegg Formation, chlorite and chlorite/illite mixed layers decrease upwards and then remain at a constant level higher up.

In the lower half of the Staffelegg Formation, the ratio kaolinite/illite end-member is heterogeneous, whereas a systematic upward increase is seen in the upper half (Fig. 4.2-6). The relative contents of end-member clays remain remarkably constant throughout the Opalinus Clay. The ratio illite / kaolinite end-member increases sharply in the Wedelsandstein Formation and becomes more heterogeneous in comparison to the Opalinus Clay.

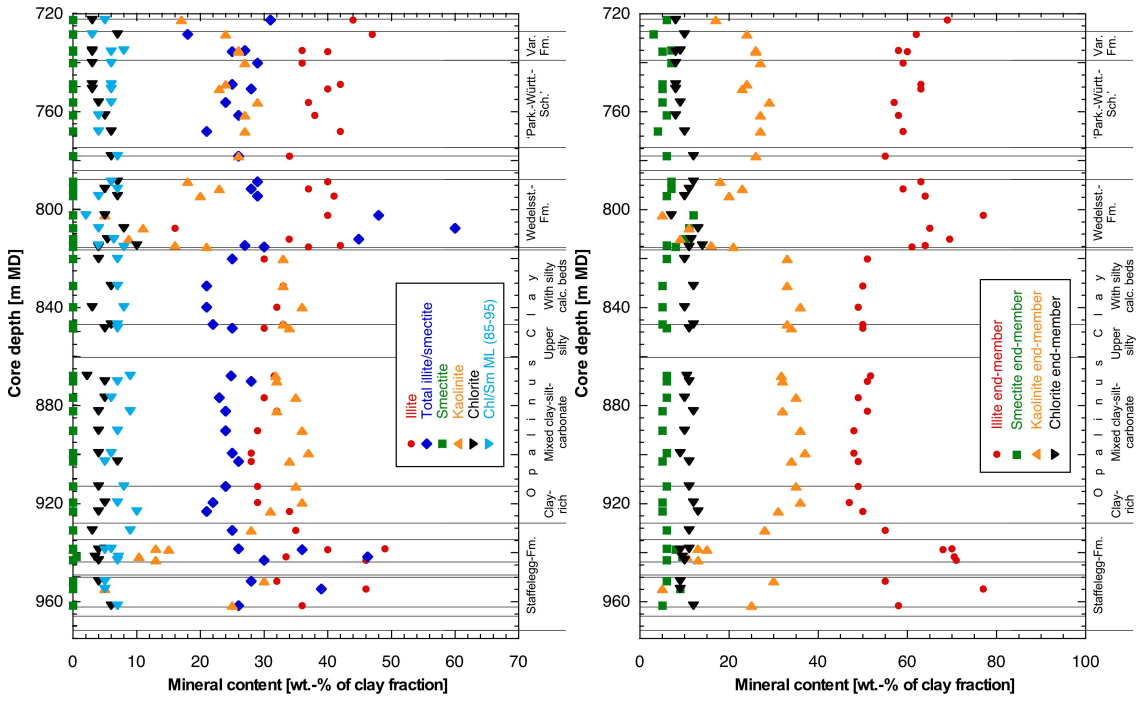

Fig. 4.2-5: Mineralogical composition of the clay fraction as a function of depth in the Lias – Dogger interval

a Individual clay minerals

b End-3member clays

Detailed lithostratigraphic subdivision according to Dossier III.

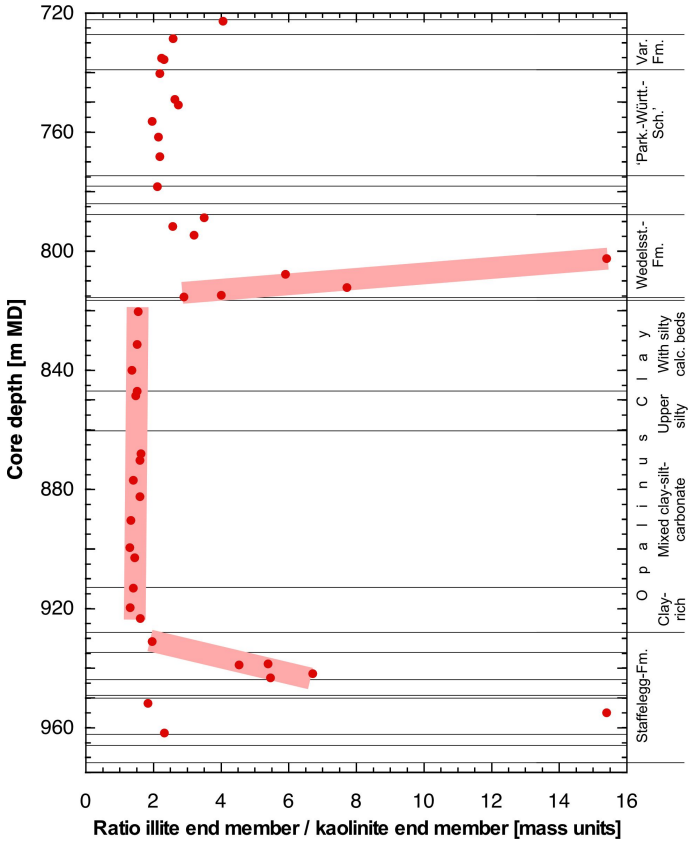

Fig. 4.2-6: Ratio of the illite to kaolinite end-member clays as a function of depth

Red bars highlight systematic trends. Detailed lithostratigraphic subdivision according to Dossier III.

4.3 Petrophysical parameters

Martin Mazurek, Lukas Aschwanden & Thomas Gimmi

Petrophysical parameters were obtained by 3 different laboratories, and the acquired parameters are listed in Tab. 4.3-1.

Tab. 4-3.1: Analytical programme for petrophysical measurements

Parameter	**University of Bern**	**BRGM**	**Hydroisotop GmbH**
Bulk wet density	26	46	
Grain density	85	46	
Gravimetric water content	22	46	46
Water content from isotope mass balance	22		44
N_2 adsorption isotherm	31		

The formalisms to calculate additional parameters from measured data (such as porosity) are detailed in Waber (ed.) (2020). Given the different analytical protocols used for the quantification of petrophysical parameters by University of Bern / Hydroisotop GmbH on the one hand and BRGM on the other hand (Section 3.4), these two data sets are treated separately. Formation-specific statistical data are summarised in Tab. 4.3-2 for University of Bern / Hydroisotop GmbH and in Tab. 4.3-3 for BRGM. The full data set is documented in Appendix A. Note that, given the absence of density data for samples studied by Hydroisotop GmbH, water-loss porosity was calculated assuming a grain density of 2.7 g/cm^3. The uncertainty related to this assumption is small.

Tab. 4-3.2: Summary of measured and calculated petrophysical data obtained by University of Bern and Hydroisotop GmbH

Listed water contents (wet) are averages of measurements performed on typically 3 sub-samples. n = number of samples per geological unit.

							Gravimetry				Isotope mass balance			
Formation	**Member**		**Bulk wet density** [g/cm³]	**Bulk dry density, calculated** [g/cm³]	**Grain density** [g/cm³]	**Pycnometer porosity** [–]	**Water content (wet) (105 °C)** [wt.-%]	**Water content (dry) (105 °C)** [wt.-%]	**Water-loss porosity using bulk wet density** [–]	**Water-loss porosity using grain density** [–]	**Water content (wet) based on isotope diff. exch.** [wt.-%]	**Porosity based on isotope diff. exch. using bulk wet density** [–]	**Porosity based on isotope diff. exch. using grain density** [–]	**External surface area (BET)** [m²/g dry rock]
«Felsenkalke» + «Massenkalk»		Mean	2.655	2.626	2.714	0.031	1.247	1.267	0.029	0.033	1.275	0.028	0.034	2.61
		Median	2.643	2.608	2.714	0.040	1.289	1.306	0.034	0.034	1.309	0.035	0.035	
		Stdev	0.038	0.054	0.006	0.020	0.643	0.664	0.016	0.016	0.686	0.013	0.018	
		Min	2.624	2.583	2.706	0.009	0.406	0.408	0.011	0.011	0.496	0.013	0.013	
		Max	2.698	2.687	2.720	0.045	2.699	2.774	0.041	0.070	2.603	0.037	0.067	
		n	3	3	6	3	10	10	3	10	7	3	7	1
Schwarzbach Fm.		Mean	2.619	2.560	2.705	0.054	2.360	2.418	0.060	0.061	2.526	0.062	0.065	
		Median					2.283	2.336		0.059	2.511		0.065	
		Stdev					0.364	0.383		0.009	0.169		0.004	
		Min					2.040	2.083		0.053	2.365		0.062	
		Max					2.757	2.835		0.071	2.702		0.070	
		n	1	1	1	1	3	3	1	3	3	1	3	0
Villigen Fm.		Mean	2.669	2.650	2.721	0.024	0.702	0.708	0.020	0.019	0.749	0.019	0.020	3.13
		Median			2.720		0.724	0.730		0.019	0.789		0.021	3.13
		Stdev			0.006		0.272	0.275		0.007	0.244		0.006	1.34
		Min			2.715		0.280	0.281		0.008	0.363		0.010	2.19
		Max			2.727		1.103	1.115		0.029	1.027		0.027	4.08
		n	1	1	4	1	8	8	1	8	5	1	5	2
Wildegg Fm.		Mean	2.666	2.619	2.714	0.035	1.756	1.787	0.047	0.046	2.256	0.060	0.059	0.00
			1	1	1	1	1	1	1	1	1	1	1	1
Variansmergel Fm.		Mean			2.706		3.839	4.004		0.097	4.147		0.104	28.72
		Median			2.703		3.544	3.674		0.090	4.147		0.104	28.72
		Stdev			0.015		1.119	1.210		0.027	1.929		0.045	9.47
		Min			2.693		2.399	2.458		0.062	2.783		0.072	22.02
		Max			2.722		5.005	5.268		0.125	5.511		0.136	35.41
		n	0	0	3	0	5	5	0	5	2	0	2	2

Tab. 4-3.2: continued

Formation	Member		Bulk wet density [g/cm³]	Bulk dry density, calculated [g/cm³]	Grain density [g/cm³]	Pycnometer porosity [–]	Gravimetry				Isotope mass balance			External surface area (BET) [m²/g dry rock]
							Water content (wet) (105 °C) [wt.-%]	Water content (dry) (105 °C) [wt.-%]	Water-loss porosity using bulk wet density [–]	Water-loss porosity using grain density [–]	Water content (wet) based on isotope diff. exch. [wt.-%]	Porosity based on isotope diff. exch. using bulk wet density [–]	Porosity based on isotope diff. exch. using grain density [–]	
«Parkinsoni-Württ.-Sch.»		Mean	2.578	2.491	2.704	0.081	4.365	4.576	0.086	0.109	4.427	0.095	0.111	30.77
		Median	2.578	2.491	2.704	0.081	4.730	4.964	0.086	0.118	5.175	0.095	0.128	30.13
		Stdev	0.025	0.041	0.009	0.017	1.091	1.173	0.016	0.026	1.333	0.011	0.032	1.95
		Min	2.560	2.462	2.687	0.069	1.631	1.658	0.075	0.043	2.080	0.087	0.054	29.22
		Max	2.595	2.521	2.716	0.093	5.190	5.474	0.098	0.129	5.535	0.102	0.137	33.62
		n	2	2	8	2	12	12	2	12	7	2	7	4
«Humphriesiool. Fm.»		Mean			2.711		5.164	5.445		0.128				31.78
		Median					5.164	5.445		0.128				
		Stdev					0.090	0.100		0.002				
		Min					5.100	5.374		0.127				
		Max					5.227	5.515		0.130				
		n	0	0	1	0	2	2	0	2	0	0	0	1
Wedelsandstein Fm.		Mean	2.473	2.339	2.688	0.133	4.113	4.301	0.134	0.103	4.799	0.176	0.119	21.25
		Median	2.473	2.339	2.687	0.133	3.841	3.995	0.134	0.097	4.230	0.176	0.107	19.04
		Stdev	0.022	0.003	0.012	0.006	1.057	1.153	0.025	0.025	1.423		0.032	9.61
		Min	2.458	2.337	2.671	0.129	2.192	2.241	0.117	0.057	3.656		0.093	9.19
		Max	2.489	2.341	2.708	0.137	6.108	6.505	0.152	0.150	7.071		0.171	34.46
		n	2	2	10	2	12	12	2	12	5	1	5	6
Opalinus Clay	All	Mean	2.524	2.414	2.690	0.106	4.332	4.531	0.110	0.109	4.841	0.128	0.121	29.29
		Median	2.529	2.422	2.690	0.104	4.310	4.504	0.109	0.108	4.837	0.123	0.121	29.19
		Stdev	0.022	0.036	0.013	0.016	0.463	0.506	0.016	0.011	0.556	0.013	0.013	3.03
		Min	2.481	2.349	2.655	0.086	3.155	3.258	0.080	0.081	3.794	0.116	0.096	25.00
		Max	2.547	2.467	2.712	0.134	5.357	5.660	0.133	0.133	5.927	0.147	0.146	33.50
		n	7	7	34	6	31	31	7	31	18	5	18	9
Opalinus Clay	With silty calc. beds	Mean	2.481	2.349	2.690	0.134	4.694	4.928	0.133	0.117	5.261	0.147	0.130	29.13
		Median			2.690		4.637	4.862		0.116	5.414		0.134	29.13
		Stdev			0.013		0.517	0.568		0.012	0.725		0.017	5.83
		Min			2.670		3.822	3.974		0.097	4.288		0.108	25.00
		Max			2.712		5.357	5.660		0.133	5.927		0.146	33.25
		n	1	1	8	1	7	7	1	7	4	1	4	2

Tab. 4-3.2: continued

Formation	Member		Bulk wet density [g/cm³]	Bulk dry density, calculated [g/cm³]	Grain density [g/cm³]	Pycnometer porosity [–]	Gravimetry				Isotope mass balance			External surface area (BET) [m²/g dry rock]
							Water content (wet) (105 °C) [wt.-%]	Water content (dry) (105 °C) [wt.-%]	Water-loss porosity using bulk wet density [–]	Water-loss porosity using grain density [–]	Water content (wet) based on isotope diff. exch. [wt.-%]	Porosity based on isotope diff. exch. using bulk wet density [–]	Porosity based on isotope diff. exch. using grain density [–]	
Opalinus Clay	Upper silty	Mean	2.518	2.409	2.691	0.107	4.129	4.307	0.109	0.104	4.499	0.120	0.113	28.86
		Median			2.690		4.115	4.292		0.104	4.499		0.113	
		Stdev			0.014		0.174	0.190		0.004	0.389		0.009	
		Min			2.678		3.962	4.125		0.100	4.224		0.106	
		Max			2.705		4.310	4.504		0.108	4.774		0.119	
		n	1	1	4	1	3	3	1	3	2	1	2	1
Opalinus Clay	Mixed clay-silt-carb.	Mean	2.536	2.438	2.688	0.097	4.077	4.251	0.098	0.103	4.565	0.119	0.114	28.16
		Median	2.532	2.424	2.690	0.101	4.216	4.402	0.107	0.106	4.638	0.119	0.116	28.54
		Stdev	0.010	0.025	0.013	0.009	0.381	0.413	0.016	0.009	0.378	0.006	0.009	2.24
		Min	2.529	2.422	2.655	0.086	3.155	3.258	0.080	0.081	3.794	0.116	0.096	25.17
		Max	2.547	2.467	2.707	0.104	4.667	4.895	0.108	0.117	4.877	0.123	0.122	30.38
		n	3	3	17	3	15	15	3	15	9	2	9	4
Opalinus Clay	Clay-rich	Mean	2.529	2.413	2.696	0.103	4.649	4.876	0.116	0.116	5.338	0.136	0.132	31.95
		Median	2.529	2.413	2.700		4.609	4.831	0.116	0.115	5.360		0.133	31.95
		Stdev	0.022	0.026	0.013		0.149	0.164	0.003	0.003	0.117		0.003	2.19
		Min	2.513	2.395	2.677		4.459	4.667	0.113	0.112	5.212		0.129	30.40
		Max	2.544	2.431	2.711		4.906	5.159	0.118	0.122	5.444		0.135	33.50
		n	2	2	5	1	6	6	2	6	3	1	3	2
Staffelegg Fm.		Mean	2.420	2.319	2.603	0.105	4.103	4.282	0.101	0.102	4.763	0.118	0.118	26.57
		Median	2.381	2.275	2.627	0.113	4.154	4.334	0.101	0.103	4.754	0.118	0.119	26.32
		Stdev	0.107	0.111	0.109	0.013	0.568	0.615	0.005	0.013	0.591	0.009	0.013	7.23
		Min	2.338	2.237	2.419	0.090	2.819	2.900	0.096	0.073	3.875	0.112	0.098	17.41
		Max	2.542	2.446	2.713	0.113	5.071	5.342	0.106	0.126	5.745	0.124	0.141	36.20
		n	3	3	8	3	16	16	3	16	8	2	8	5
Klettgau Fm.		Mean	2.570	2.467	2.761	0.108	4.519	4.804	0.103	0.112	5.356	0.138	0.131	45.50
		Median	2.570	2.467	2.755	0.108	5.094	5.367	0.103	0.129	6.212	0.138	0.153	
		Stdev	0.087	0.098	0.047	0.005	2.634	2.850	0.010	0.063	2.797	0.036	0.067	
		Min	2.508	2.398	2.700	0.104	0.042	0.042	0.096	0.001	0.301	0.113	0.008	
		Max	2.632	2.536	2.832	0.112	7.920	8.601	0.111	0.191	8.592	0.163	0.202	
		n	2	2	5	2	10	10	2	10	6	2	6	1

Tab. 4-3.2: continued

Formation	Member		Bulk wet density [g/cm³]	Bulk dry density, calculated [g/cm³]	Grain density [g/cm³]	Pycnometer porosity [–]	Gravimetry				Isotope mass balance			External surface area (BET) [m²/g dry rock]
							Water content (wet) (105 °C) [wt.-%]	Water content (dry) (105 °C) [wt.-%]	Water-loss porosity using bulk wet density [–]	Water-loss porosity using grain density [–]	Water content (wet) based on isotope diff. exch. [wt.-%]	Porosity based on isotope diff. exch. using bulk wet density [–]	Porosity based on isotope diff. exch. using grain density [–]	
Bänkerjoch Fm.		Mean	2.732	2.666	2.835	0.060	2.473	2.560	0.066	0.066	3.997	0.108	0.103	
		Median	2.754	2.688	2.838	0.053	2.383	2.441	0.066	0.065	4.794	0.129	0.124	
		Stdev	0.097	0.138	0.055	0.033	1.705	1.799	0.044	0.043	2.636	0.070	0.066	
		Min	2.606	2.485	2.782	0.028	0.482	0.484	0.014	0.014	0.285	0.008	0.008	
		Max	2.815	2.802	2.884	0.107	4.646	4.873	0.121	0.119	6.116	0.166	0.154	
		n	4	4	4	4	4	4	4	4	4	4	4	0

Tab. 4-3.3: Summary of measured and calculated petrophysical data obtained by BRGM

Water-content data (drying over 28 d) are mostly affected by some degree of partial desaturation during sample preparation and so underestimate the in situ values. The carbonate-rich lithologies of the Malm are most strongly affected. Nevertheless, all available data were considered to calculate the listed statistical parameters, but values affected by desaturation are shown in italics. Bulk wet densities are also affected by desaturation, even though this effect is minor in quantitative terms. Bulk dry densities were calculated from bulk wet densities using the water content measured on the same samples. Thus, they are adequate and do not depend on the degree of saturation. Listed water contents and bulk wet densities are averages of measurements performed on 2 aliquots of the same sample. n = number of samples per geological unit.

Formation	**Member**		**Bulk wet density** [g/cm³]	**Bulk dry density, calculated** [g/cm³]	**Grain density** [g/cm³]	**Pycnometer porosity** [–]	**Gravimetry**		
							Water content (wet) (105 °C) [wt.-%]	**Water content (dry) (105 °C)** [wt.-%]	**Water-loss porosity using bulk wet density** [–]
«Felsenkalke» + «Massenkalk»		Mean	2.610	2.583	2.697	0.042	*0.897*	*0.913*	*0.023*
		Median	2.627	2.617	2.695	0.029	*0.335*	*0.336*	*0.009*
		Stdev	0.046	0.070	0.007	0.025	*1.013*	*1.036*	*0.026*
		Min	2.539	2.477	2.691	0.021	*0.077*	*0.077*	*0.002*
		Max	2.659	2.651	2.708	0.081	*2.246*	*2.298*	*0.058*
		n	5	5	5	5	5	5	5
Schwarzbach Fm.		Mean	2.615	2.569	2.706	0.051	*1.486*	*1.512*	*0.039*
		Median	2.615	2.569	2.706	0.051	*1.486*	*1.512*	*0.039*
		Stdev	0.042	0.077	0.006	0.031	*0.854*	*0.880*	*0.022*
		Min	2.585	2.514	2.702	0.029	*0.882*	*0.890*	*0.023*
		Max	2.645	2.623	2.710	0.072	*2.090*	*2.135*	*0.054*
		n	2	2	2	2	2	2	2
Villigen Fm.		Mean	2.641	2.620	2.706	0.032	*0.830*	*0.844*	*0.022*
		Median	2.651	2.639	2.704	0.023	*0.410*	*0.412*	*0.011*
		Stdev	0.034	0.058	0.010	0.025	*0.975*	*1.004*	*0.025*
		Min	2.583	2.518	2.699	0.014	*0.281*	*0.282*	*0.007*
		Max	2.672	2.665	2.725	0.076	*2.565*	*2.632*	*0.066*
		n	5	5	5	5	5	5	5
Variansmergel Fm.		Mean	2.475	2.399	2.675	0.103	*4.159*	*4.350*	*0.103*
		Median	2.475	2.399	2.675	0.103	*4.159*	*4.350*	*0.103*
		Stdev	0.041	0.081	0.000	0.030	*1.341*	*1.460*	*0.031*
		Min	2.446	2.342	2.675	0.082	*3.211*	*3.318*	*0.080*
		Max	2.504	2.456	2.675	0.125	*5.107*	*5.382*	*0.125*
		n	2	2	2	2	2	2	2

Tab. 4-3.3: continued

Formation	Member		Bulk wet density [g/cm³]	Bulk dry density, calculated [g/cm³]	Grain density [g/cm³]	Pycnometer porosity [–]	Gravimetry		
							Water content (wet) (105 °C) [wt.-%]	Water content (dry) (105 °C) [wt.-%]	Water-loss porosity using bulk wet density [–]
«Parkinsoni-Württ.-Sch.»		Mean	2.463	2.370	2.697	0.121	*4.594*	*4.825*	*0.113*
		Median	2.458	2.348	2.701	0.131	*5.043*	*5.311*	*0.124*
		Stdev	0.026	0.055	0.018	0.025	*1.092*	*1.187*	*0.026*
		Min	2.439	2.333	2.675	0.084	*2.976*	*3.067*	*0.074*
		Max	2.498	2.450	2.712	0.138	*5.313*	*5.611*	*0.130*
		n	4	4	4	4	4	4	4
«Humphriesiool. Fm.»		Mean	2.583	2.560	2.717	0.058	*1.481*	*1.503*	*0.038*
		n	1	1	1	1	1	1	1
Wedelsandstein Fm.		Mean	2.429	2.332	2.671	0.127	*4.705*	*4.939*	*0.114*
		Median	2.433	2.323	2.682	0.130	*4.616*	*4.839*	*0.110*
		Stdev	0.033	0.031	0.019	0.008	*0.408*	*0.450*	*0.010*
		Min	2.393	2.306	2.649	0.118	*4.350*	*4.548*	*0.107*
		Max	2.460	2.367	2.684	0.134	*5.151*	*5.430*	*0.125*
		n	3	3	3	3	3	3	3
Opalinus Clay	All	Mean	2.489	2.392	2.702	0.114	*4.174*	*4.357*	*0.104*
		Median	2.488	2.384	2.705	0.115	*4.267*	*4.457*	*0.106*
		Stdev	0.018	0.023	0.011	0.008	*0.353*	*0.383*	*0.008*
		Min	2.463	2.354	2.687	0.103	*3.294*	*3.406*	*0.082*
		Max	2.513	2.426	2.722	0.131	*4.631*	*4.856*	*0.115*
		n	13	13	13	13	13	13	13
Opalinus Clay	With silty calcareous beds	Mean	2.492	2.389	2.698	0.114	*4.463*	*4.671*	*0.111*
		Median	2.492	2.389	2.698	0.114	*4.463*	*4.671*	*0.111*
		Stdev	0.022	0.025	0.016	0.004	*0.237*	*0.260*	*0.005*
		Min	2.476	2.371	2.687	0.111	*4.295*	*4.487*	*0.108*
		Max	2.507	2.407	2.709	0.118	*4.630*	*4.855*	*0.115*
		n	2	2	2	2	2	2	2
Opalinus Clay	Upper silty	Mean	2.493	2.401	2.699	0.110	*4.300*	*4.493*	*0.107*
		Median	2.493	2.401	2.699	0.110	*4.300*	*4.493*	*0.107*
		Stdev	0.019	0.025	0.010	0.006	*0.001*	*0.001*	*0.001*
		Min	2.479	2.384	2.692	0.106	*4.299*	*4.493*	*0.107*
		Max	2.506	2.419	2.706	0.115	*4.300*	*4.494*	*0.108*
		n	2	2	2	2	2	2	2

Tab. 4-3.3: continued

Formation	Member		Bulk wet density [g/cm³]	Bulk dry density, calculated [g/cm³]	Grain density [g/cm³]	Pycnometer porosity [–]	Gravimetry		
							Water content (wet) (105 °C) [wt.-%]	Water content (dry) (105 °C) [wt.-%]	Water-loss porosity using bulk wet density [–]
Opalinus Clay	Mixed clay-silt-carbonate	Mean	2.491	2.398	2.700	0.112	*3.963*	*4.127*	*0.099*
		Median	2.491	2.400	2.697	0.111	*4.060*	*4.231*	*0.101*
		Stdev	0.019	0.023	0.011	0.006	*0.337*	*0.364*	*0.008*
		Min	2.467	2.366	2.688	0.103	*3.294*	*3.406*	*0.082*
		Max	2.513	2.426	2.722	0.120	*4.267*	*4.457*	*0.106*
		n	7	7	7	7	7	7	7
Opalinus Clay	Clay-rich	Mean	2.475	2.368	2.713	0.127	*4.497*	*4.709*	*0.111*
		Median	2.475	2.368	2.713	0.127	*4.497*	*4.709*	*0.111*
		Stdev	0.018	0.021	0.007	0.005	*0.190*	*0.209*	*0.004*
		Min	2.463	2.354	2.708	0.123	*4.362*	*4.561*	*0.109*
		Max	2.488	2.383	2.718	0.131	*4.631*	*4.856*	*0.114*
		n	2	2	2	2	2	2	2
Staffelegg Fm.		Mean	2.463	2.385	2.665	0.105	*3.301*	*3.425*	*0.081*
		Median	2.466	2.389	2.711	0.108	*3.263*	*3.373*	*0.080*
		Stdev	0.093	0.098	0.116	0.025	*1.161*	*1.239*	*0.029*
		Min	2.313	2.243	2.462	0.071	*1.650*	*1.678*	*0.042*
		Max	2.563	2.519	2.739	0.132	*4.734*	*4.970*	*0.119*
		n	5	5	5	5	5	5	5
Klettgau Fm.		Mean	2.476	2.347	2.747	0.145	*5.425*	*5.749*	*0.134*
		Median	2.496	2.368	2.773	0.140	*4.951*	*5.209*	*0.125*
		Stdev	0.070	0.073	0.066	0.024	*1.125*	*1.272*	*0.028*
		Min	2.350	2.244	2.632	0.120	*4.315*	*4.510*	*0.107*
		Max	2.551	2.432	2.799	0.187	*7.432*	*8.028*	*0.182*
		n	6	6	6	6	6	6	6

4.3.1 Water content

Martin Mazurek & Lukas Aschwanden

As discussed in Section 3.4, water contents obtained by BRGM are mostly affected by partial evaporation of the samples in the dry atmosphere of the glovebox and so represent minimum values. In Tab. 4.3-3, the pertinent statistical data are therefore listed in italics. For samples with pycnometer porosity > 0.03, the degree of desaturation is moderate – on the average, water-loss porosity lies about 12%$_{rel}$ below pycnometer porosity. For samples with pycnometer porosity < 0.03, mostly representing clay-poor lithologies, desaturation is stronger and highly variable (Fig. 3.4-2). Water contents for these latter samples are screened out and not considered any further. Water contents for samples with pycnometer porosity > 0.03 are shown in graphics for comparison, bearing in mind that they represent minimum values.

The distribution of gravimetric water contents in the studied section Malm – Keuper is shown in Fig. 4.3-1. Water contents are relatively low in the «Felsenkalke» + «Massenkalk» and in the Schwarzbach Formation, and the lowest values are observed in the Villigen Formation. In the underlying Dogger, values increase abruptly, with typical values of 4 – 5 wt.-%. Values in the Triassic are heterogeneous, reflecting the lithological diversity in this section.

Water contents from gravimetry and from isotope diffusive exchange correlate well (Fig. 4.3-2), but the latter shows values that are consistently higher, about 13%$_{rel}$ on the average. 2 outliers in the Keuper can be identified:

- Klettgau Formation, 995.83 m: Heterogeneous dolomitic section in the vicinity of the Keuper aquifer, strongly affected by dissolution features. Bright, massive portions and dark, highly porous sections can be distinguished.
- Bänkerjoch Formation, 1'039.89 m: Heterogeneous sample with dolomite- and clay-rich beds.

The substantial heterogeneity in the 2 samples is illustrated in Fig. 4.3-3. To what degree this could explain the discrepancy between gravimetric water contents and those based of isotope diffusive exchange is unclear, given the fact that the gravimetric water contents shown in Fig. 4.3-2 have been obtained post mortem from the same material that was used for the isotope exchange experiments. Whether sample contamination (in case of sample 995.83 m) or the presence of some anhydrite (in case of sample 1'039.89 m) could contribute to the discrepancy is not clear.

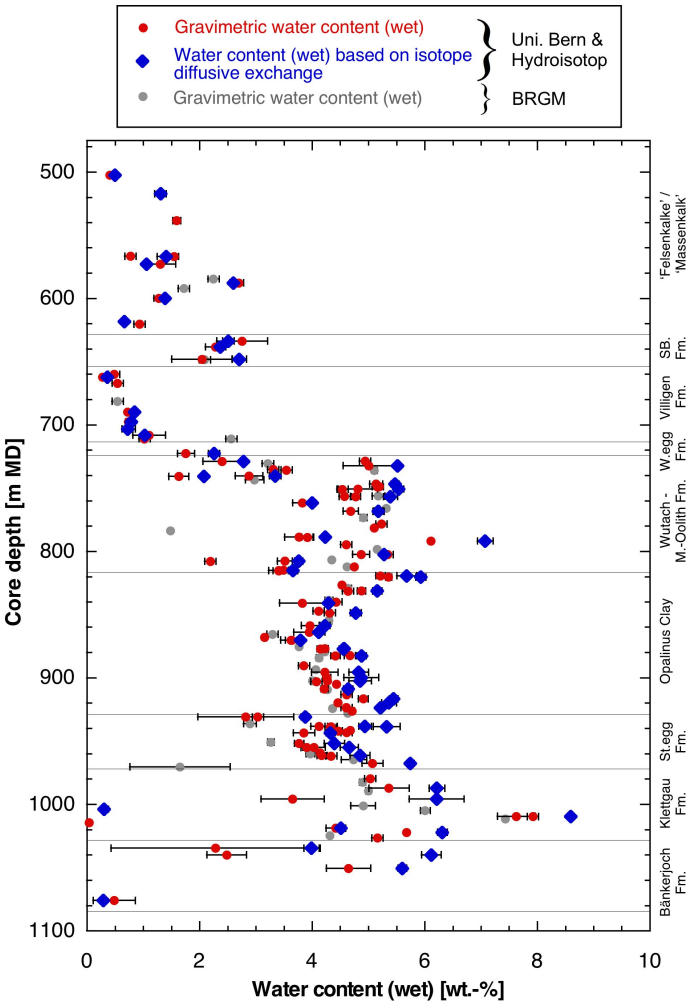

Fig. 4.3-1: Water content as a function of depth

Black bars for gravimetric water content indicate 1σ variability among 3 (University of Bern) or 2 (BRGM) aliquots of the same sample. Black bars for water content from isotope diffusive exchange represent the propagated analytical error. Data from BRGM are affected by partial desaturation and so represent minimum values.

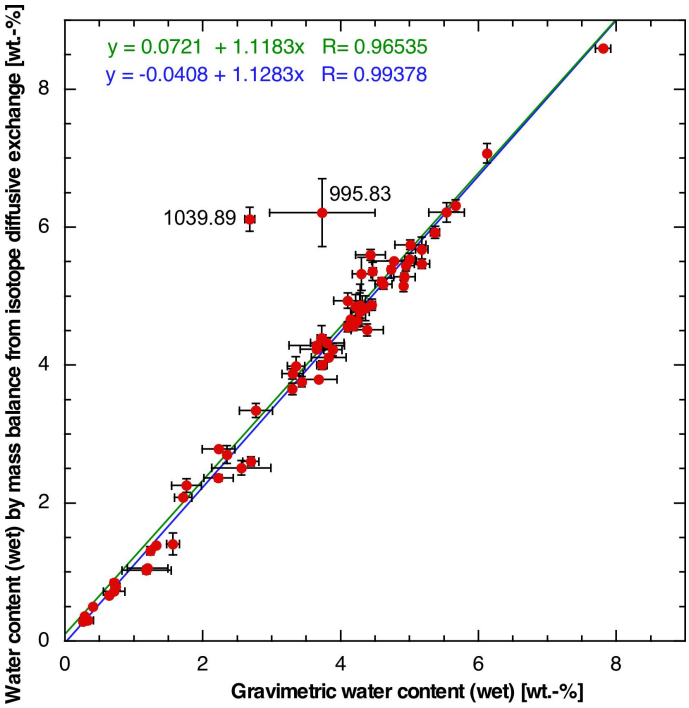

Fig. 4.3-2: Correlation of water contents based on gravimetry and on isotope diffusive exchange

All data originate from University of Bern / Hydroisotop GmbH. Black bars for gravimetric water content indicate 1σ variability among 2 aliquots of the same sample. Note that only the gravimetric water contents obtained from the aliquots used for the isotope diffusive exchange experiments are considered in this graph, so the correlation refers to identical sample materials. Black bars for water content from isotope diffusive exchange represent the propagated analytical error. Green regression line considers all samples, while the blue line excludes 2 outliers in the Triassic.

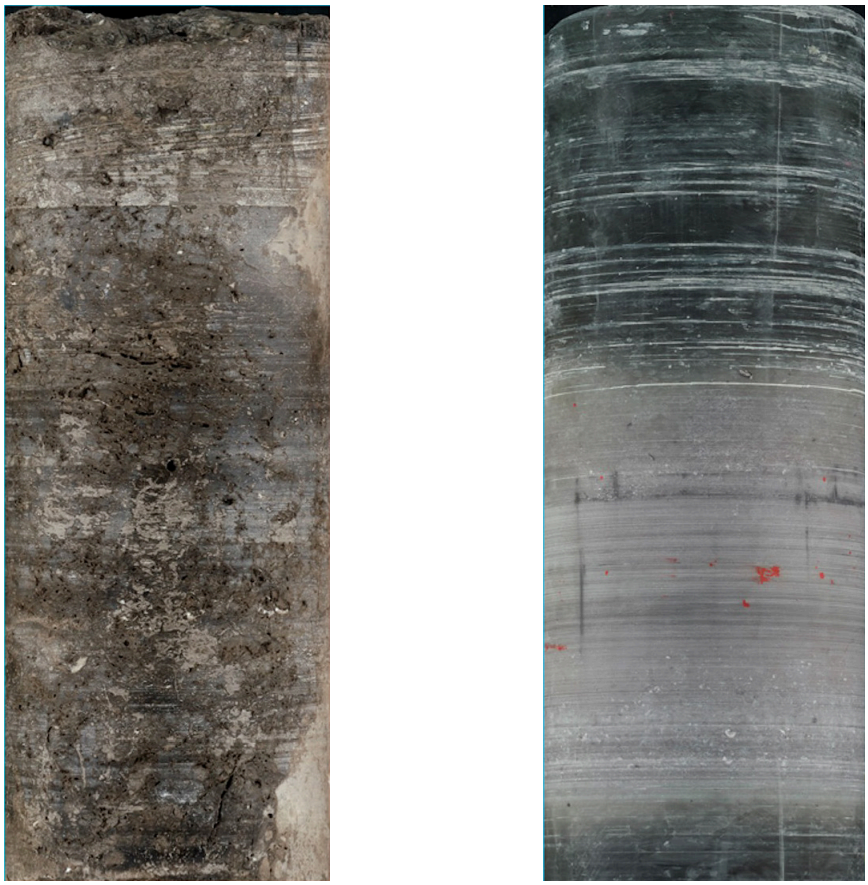

995.83 m 1039.89 m

Fig. 4.3-3: Core photographs of heterogeneous samples from the Keuper
Width of photographs is 10 cm.

A closer look at the clay-rich Lias – Dogger section

As shown in Fig. 4.3-4, water contents in the Staffelegg Formation and in the Opalinus Clay show systematic depth trends. These are similar for gravimetric water content and that obtained from isotope mass balance. Two distinct cycles of water contents decreasing upwards can be identified in the Staffelegg Formation. In the Opalinus Clay, the mixed clay-silt-carbonate sub-unit shows constant water contents except in the uppermost part where a decreasing trend is observed. This trend is broken in the overlying upper silty sub-unit and the sub-unit with silty calcareous beds, in which an upward trend of markedly increasing water contents can be identified. In the overlying «Brauner Dogger», no evident trends can be identified.

The observed trends of the water content correlate well with those identified for clay-mineral contents (Section 4.2.1, Fig. 4.2-3) and show a negative correlation with the ratio quartz/clay minerals. It is evident that a substantial part of the porewater is related to the presence of clay minerals.

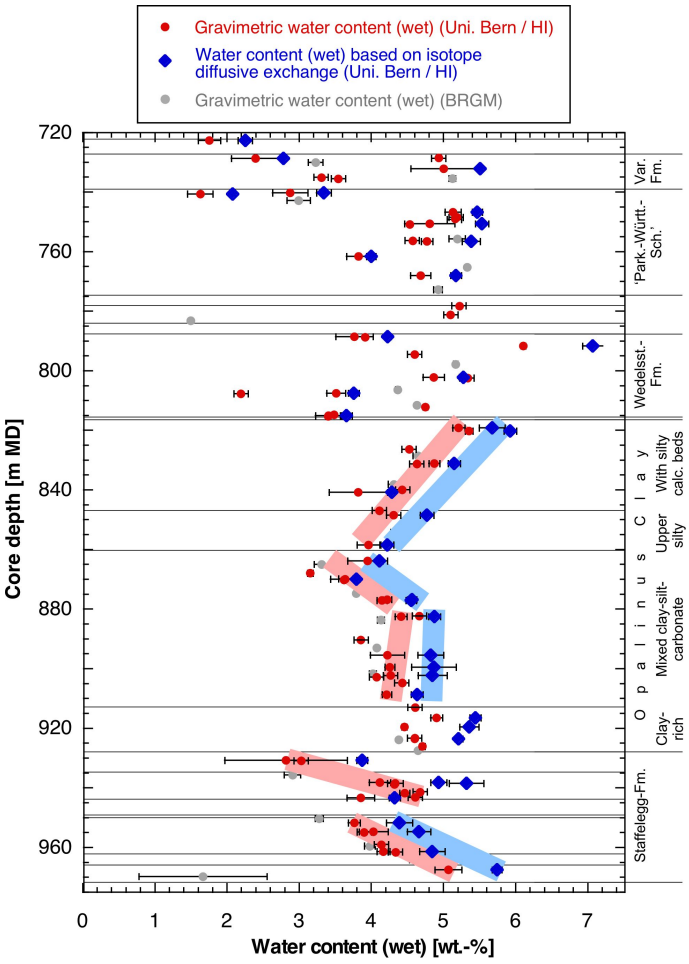

Fig. 4.3-4: Water content (wet) as a function of depth in the Lias-Dogger interval

Black bars for gravimetric water content indicate 1σ variability among 2 – 3 aliquots of the same sample. Black bars for water content from isotope diffusive exchange represent the propagated analytical error.

4.3.2 Grain density

Martin Mazurek & Lukas Aschwanden

The grain-density profile is shown in Fig. 4.3-5 (note that no data are available for samples analysed at Hydroisotop GmbH). Throughout the Malm, Dogger and Lias units, values are around 2.7 g/cm^3, with only limited scatter. The only conspicuous excursion is identified in the Rietheim Member of the Staffelegg Formation («Posidonienschiefer»), where high contents of organic matter (C_{org} = 3.1 – 7.8 wt.-%) lead to markedly lower grain-density values.

In the Keuper, values become larger, as does variability. This reflects the lithological heterogeneity, in particular the variable contents of dolomite and anhydrite with their high mineral densities. Fig. 4.3-6 shows the correlation between grain density and dolomite/ankerite contents. Grain density increases linearly with dolomite concentration (black line in Fig. 4.3-6), and outliers are due to the presence of anhydrite.

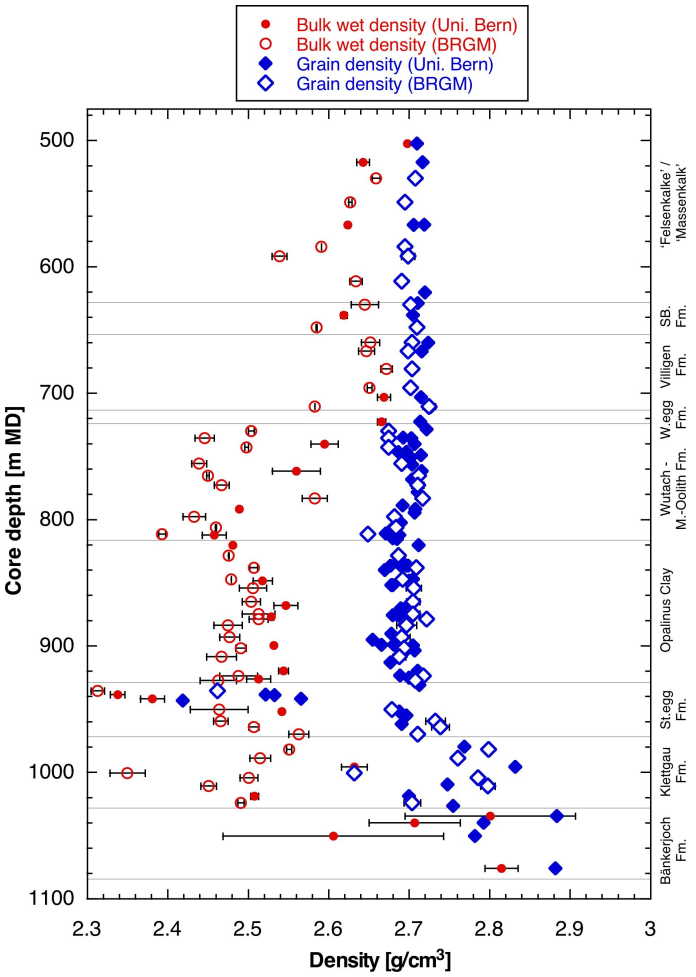

Fig. 4.3-5: Depth profile of bulk wet and grain densities

Black bars for bulk wet density indicate 1σ variability among several (2 – 3) pieces of the same sample. Analytical error bars for grain density are smaller than the symbol size.

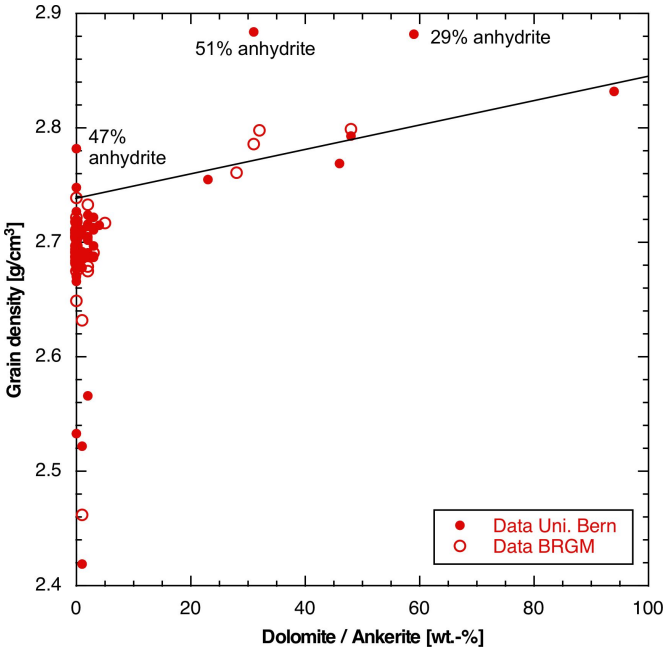

Fig. 4.3-6: Grain density as a function of the contents of dolomite/ankerite

All mineralogy data are from University of Bern, density data are from University of Bern and BRGM.

4.3.3 Bulk wet density

Martin Mazurek & Lukas Aschwanden

Data produced by University of Bern and BRGM are shown in Fig. 4.3-5 as a function of depth. Due to the partial desaturation of the samples studied by BRGM (particularly in the Malm), their bulk wet densities slightly underestimate the in situ values.

4.3.4 Porosity

Martin Mazurek & Lukas Aschwanden

Three different approaches were used to constrain rock porosity (for details see Waber ed. 2020):

- *Water-loss porosity:* calculation from the gravimetric water content using either bulk wet or grain density
- *Porosity from isotope diffusive exchange:* calculation from the water content obtained by mass balance using either bulk wet or grain density
- *Pycnometer porosity:* calculation from bulk dry and grain densities; bulk dry density is calculated from bulk wet density and water content.

Water-loss porosity and porosity from isotope diffusive exchange were calculated using bulk wet density by default. If the latter was not available, grain density was used, by which full water saturation of the pore space is assumed. The graphic in Fig. 4.3-7 shows that the two densities yield near-identical porosities, so the choice of the type of density for the calculation incurs no additional uncertainty.

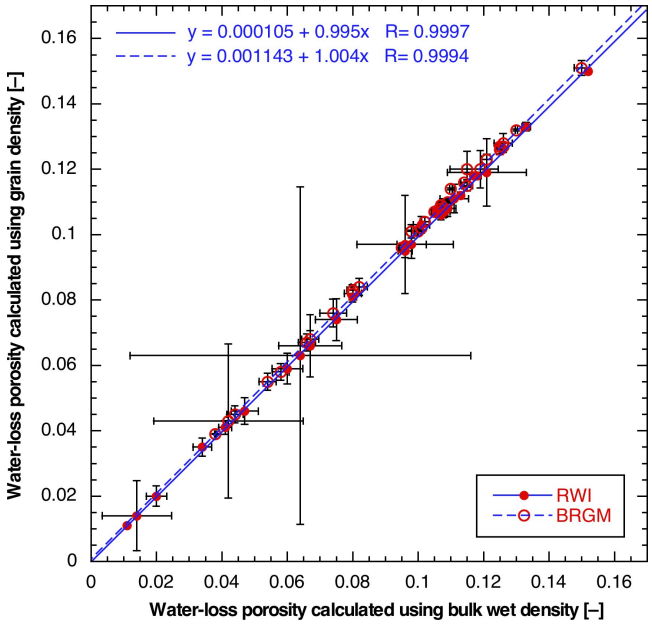

Fig. 4.3-7: Water-loss porosity calculated from gravimetric water content using either bulk wet or grain density

Bars indicate propagated errors. In case of the BRGM data, the fact that the samples are desaturated to some degree renders the calculation of water-loss porosity using grain density less accurate, even though this effect appears to be marginal.

Comparison of porosities obtained by different methods

- An excellent linear correlation is observed between water-loss porosity and porosity from isotope diffusive exchange (Fig. 4.3-8, based on data from University of Bern and Hydro-isotop GmbH). The latter yields about 11% higher values. Two outliers from the Triassic are likely due to sample heterogeneity (Fig. 4.3-3).
- A slightly less good linear correlation is found between pycnometer porosity and porosity from isotope diffusive exchange (Fig. 4.3-9, based on data from University of Bern). The latter yields about 22% higher values.
- The correlation between water-loss and pycnometer porosity is shown in Fig. 4.3-10. The slopes of the regression lines for the data sets of University of Bern and BRGM are slightly below 1. The partial desaturation of the BRGM samples results in a general shift of the data to the left, towards lower water-loss porosities.

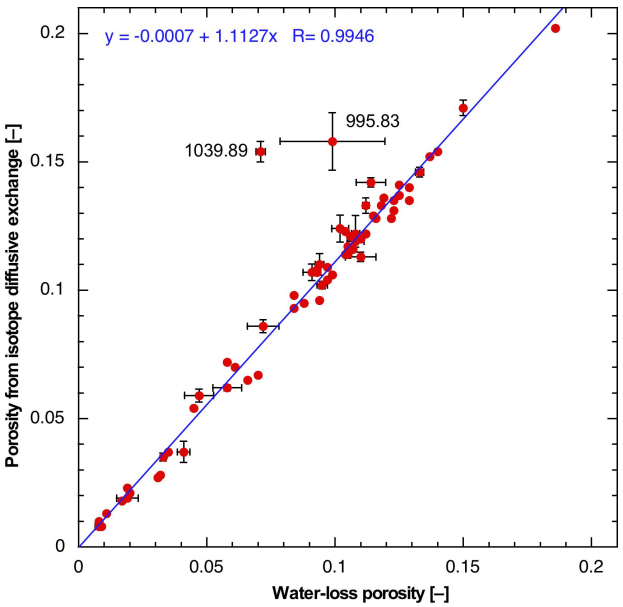

Fig. 4.3-8: Correlation of water-loss porosity and porosity from isotope diffusive exchange

All data from University of Bern and Hydroisotop GmbH. Bars indicate propagated errors for the University of Bern data. Note that only the gravimetric water contents obtained from the aliquots used for the isotope diffusive exchange experiments are considered for the x axis of this graph, so the correlation refers to identical sample materials. Heterogeneous outliers (illustrated in Fig. 4.3-3) were excluded for the regression line. In the absence of grain-density data for the Hydroisotop GmbH samples, a value of 2.7 g/cm^3 was used.

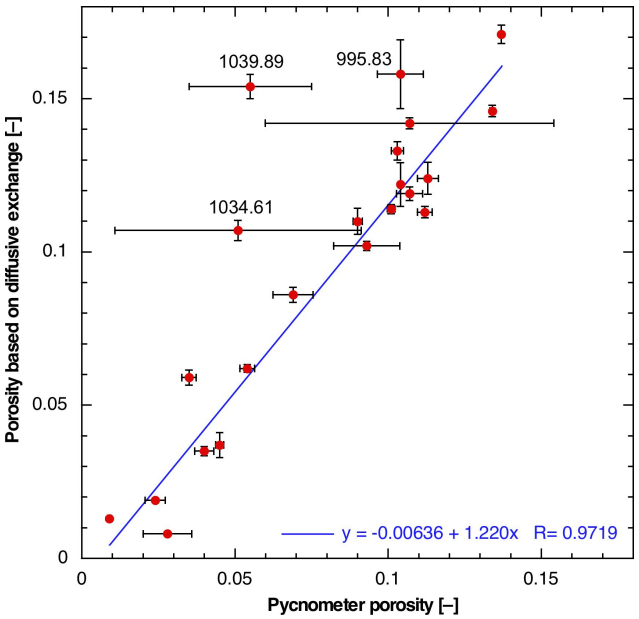

Fig. 4.3-9: Correlation of pycnometer porosity and porosity from isotope diffusive exchange

All data from University of Bern. Bars indicate propagated errors. Heterogeneous outliers were excluded for the regression line.

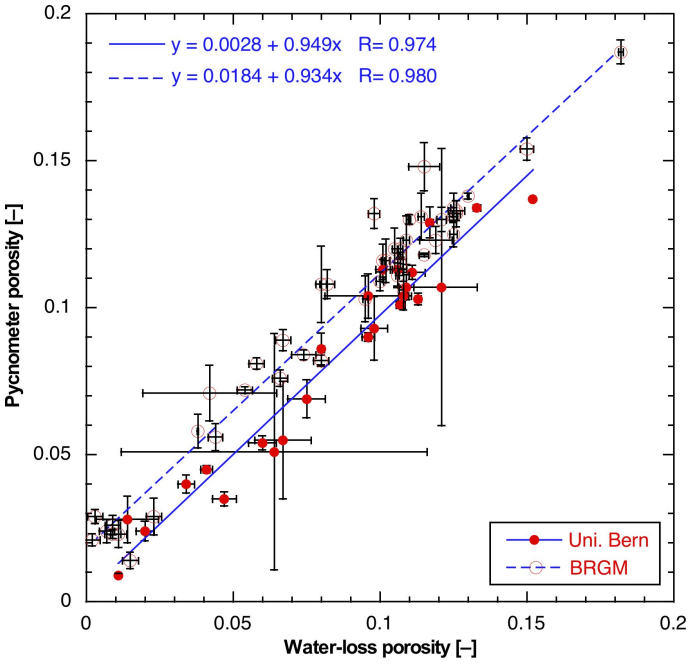

Fig. 4.3-10: Correlation of water-loss and pycnometer porosity

Bars indicate propagated errors. Due to partial desaturation of the BRGM samples, water-loss porosity is underestimated, leading to a shift of the data towards lower values.

Depth trends

In Fig. 4.3-11, porosity is shown as a function of depth. The shape of the profile is similar to that of water content (Fig. 4.3-1). Relatively low (but somewhat scattered) values in the «Felsenkalke» + «Massenkalk» contrast with very low porosities in the Villigen Formation. Porosity increases drastically in the underlying Dogger with typical values in the range of 0.10 – 0.13. Porosities in the Triassic units are highly heterogeneous, reflecting the lithological variability.

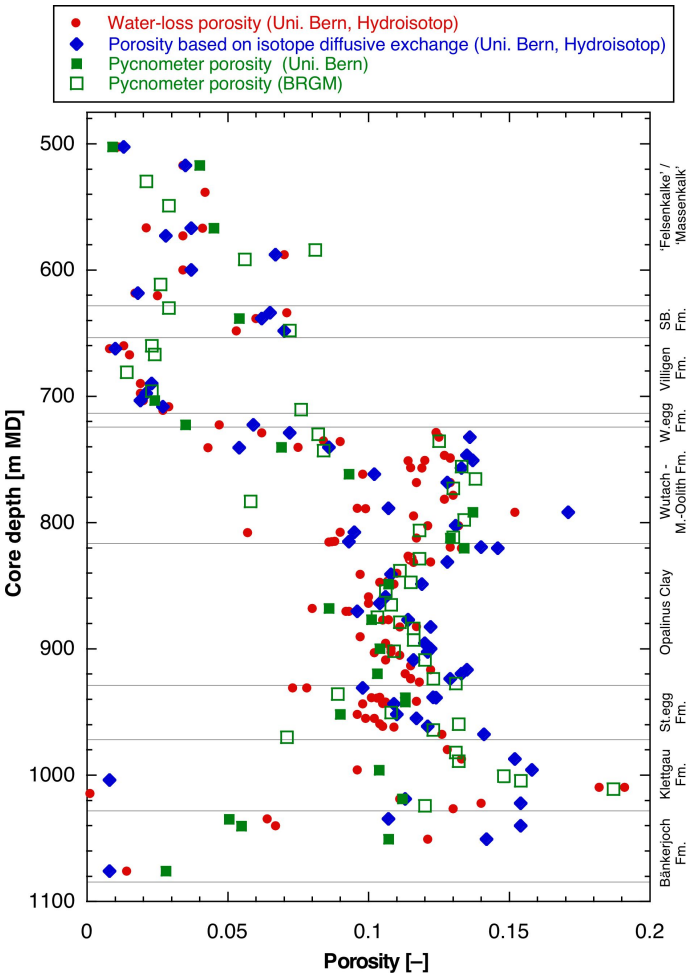

Fig. 4.3-11: Depth trends of porosities obtained by different methods and laboratories

Water-loss porosity based on BRGM data not shown due to the effects of partial desaturation.

Porosity as a function of mineralogical composition

The correlation of porosity with clay-mineral content is shown in Fig. 4.3-12. When considering all available data (Fig. 4.3-12a), a general positive correlation can be identified, but scatter is substantial. When samples containing > 20 wt.-% dolomite are excluded (Fig. 4.3-12b; all these samples originate from Triassic units), a better correlation is obtained. In particular, a number of highly porous samples with low clay-mineral contents are found in dolomite-rich lithologies. These were affected by diagenetic dissolution to some degree, either during the process of dolomitisation or at later stages. Thus, their porosity is not the result of compaction and cementation alone.

In Fig. 4.3-12b, the slope of the data is steeper for clay-mineral contents in the range of 0 – 30 wt.-% and becomes flatter at higher clay-mineral contents. Pycnometer porosities obtained by BRGM yield a higher scatter than the other data sets. Some outliers towards high porosity at low clay-mineral content can be correlated with silty samples (highlighted in Fig. 4.3-12b for quartz contents > 40 wt.-%).

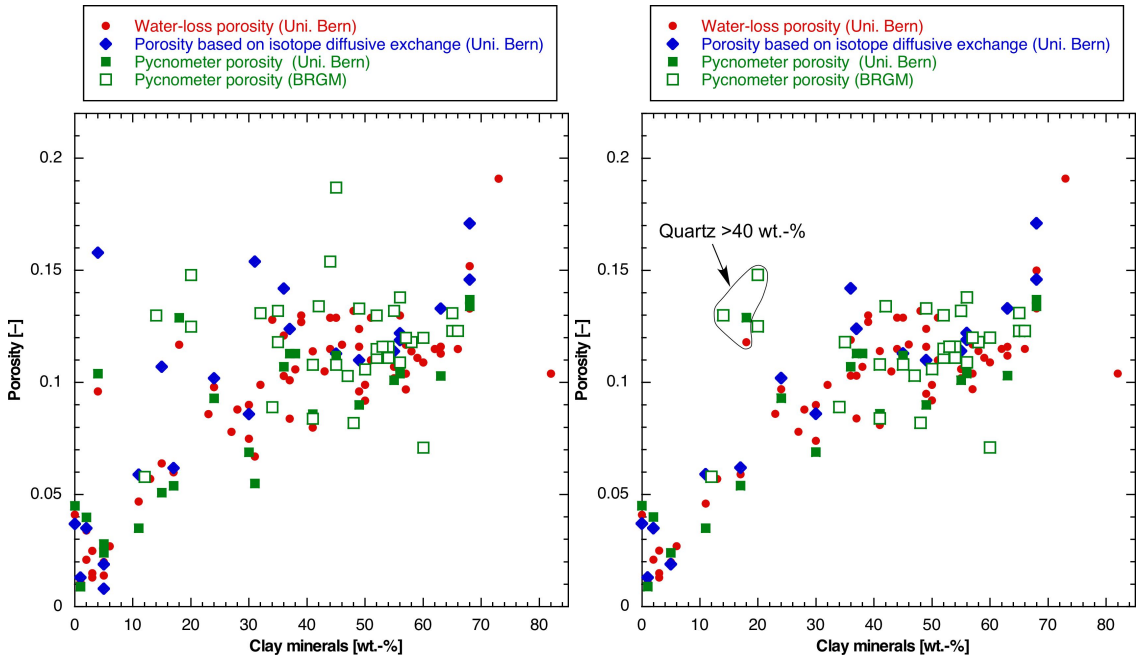

Fig. 4.3-12: Porosity as a function of clay-mineral content

a All data

b Data with dolomite contents >20 wt.-% excluded.

Water-loss porosity based on BRGM data not shown due to the effects of partial desaturation.

4.3.5 Specific surface area and pore size distributions from N_2 ad-/desorption

Thomas Gimmi

Depth trends

The specific surface area S_{BET} varies with the rock formation (Tab. 4.3-2 and Fig. 4.3-13). As N_2 cannot reach any interlayer pores of smectites, S_{BET} represents surfaces of external (non-interlayer) pores. Largest values in the range of about 25 to 35 m^2/g were generally found for clay-rich units, such as the Wutach – «Murchisonae-Oolith Formation», the Opalinus Clay and (partly) the Staffelegg Formation. The largest value of about 45 m^2/g is, however, located in the Klettgau Formation. Lowest values occur in predominantly calcareous lithologies, such as the Malm at the top of the sequence «Felsenkalke» + «Massenkalk», Villigen Formation). The large range of values found in the Staffelegg Formation points to a pronounced heterogeneity in this formation, as also evidenced by the clay-mineral contents (Fig. 4.2-3).

The variation of the specific surface area S_{BET} with depth is related to trends observed in other physical properties of samples from the Trüllikon-1-1 borehole, notably the bulk dry density, the gravimetric water content, the water-loss porosity or the clay-mineral content. Accordingly, clear correlations of specific surface area with these properties are found, as displayed in the following plots.

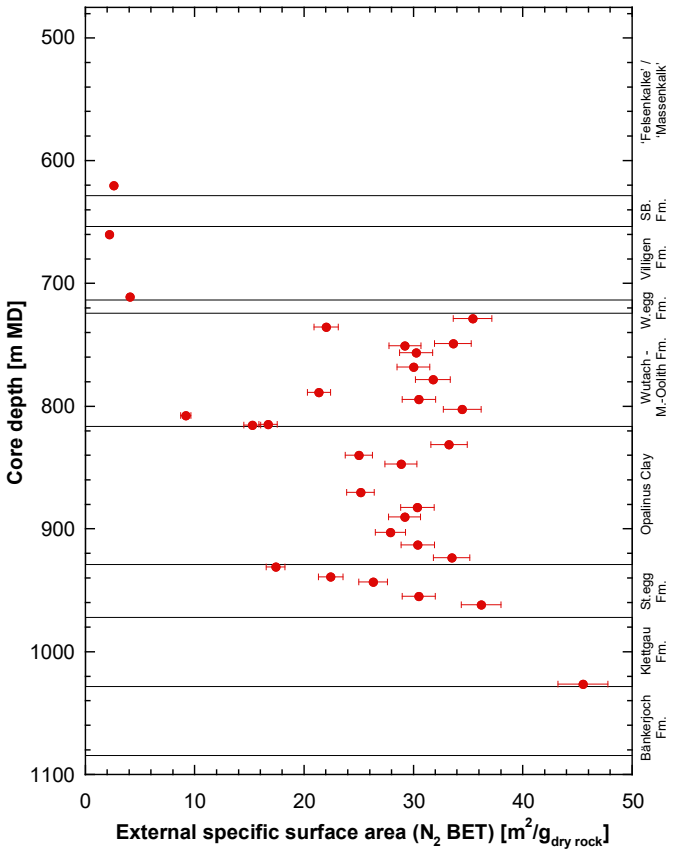

Fig. 4.3-13: Depth profile of specific surface area (S_{BET}) derived from N_2 adsorption

S_{BET} represents external surfaces only. The total specific surface area, including interlayer surfaces, would be larger depending on the smectite content of the sample. Errors resulting from sample preparation and handling are estimated to be ± 5% in general and ± 10% for $S_{BET} < 2$ m^2 g^{-1}, as given by the error bars.

Correlation of S_{BET} with other physical parameters

The relation between S_{BET} and the gravimetric water content relative to the dry sample mass follows an approximately linear trend (Fig. 4.3-14). We see that the largest S_{BET} values in the Dogger (Variansmergel Formation, «Parkinsoni-Württembergica-Schichten», «Humphriesioolith Formation», Wedelsandstein Formation, Opalinus Clay) are all related to comparably large water contents. The single data point from the Klettgau Formation plots above the linear regression, as it has a similar water content than the latter data but the largest S_{BET} value.

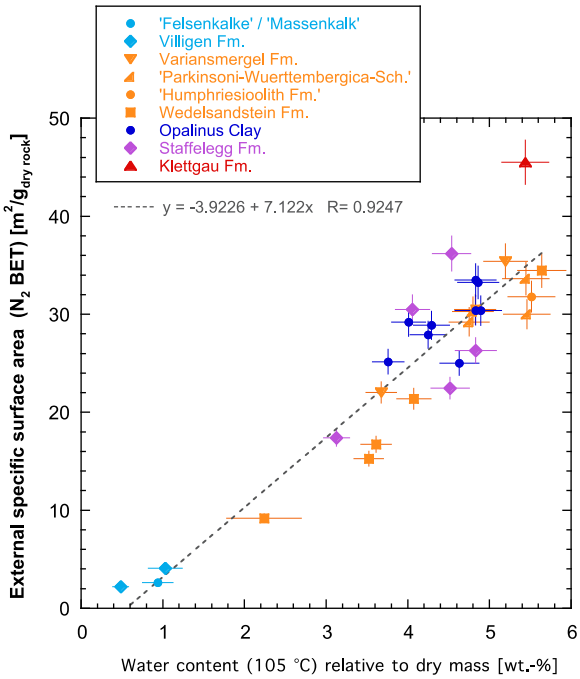

Fig. 4.3-14: Specific surface area (S_{BET}) derived from N_2 adsorption plotted against the gravimetric water content relative to the dry mass of the samples

Error bars show estimated errors for the water content (based on standard deviations of other samples) and estimated errors for S_{BET}.

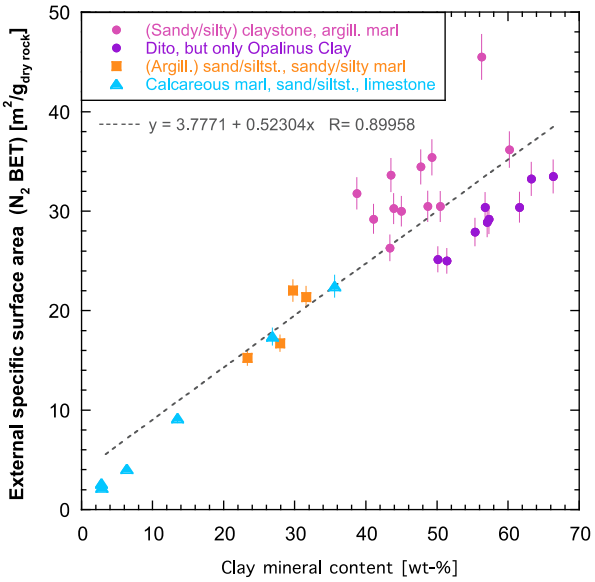

Fig. 4.3-15: Relation between external specific surface area (S_{BET}) derived from N_2 adsorption and content of clay minerals

The samples are assigned to three classes (Opalinus Clay, belonging to the first class, is additionally highlighted) according to their positions in the Füchtbauer diagram (i.e., according to lithological rock types). The linear regression is obtained for all samples.

The water content is related to the mineral composition of the samples, notably the clay-mineral content, as shown in previous subsections. Accordingly, the specific surface area S_{BET} is also positively correlated with the total content of clay minerals (Fig. 4.3-15). Three different lithological groups are distinguished in this figure, which differ in their ranges of clay-mineral contents. There is some scatter in the first group (claystones, argillaceous marls). The Opalinus Clay samples, being part of this group, have comparably large clay-mineral contents but comparably lower S_{BET} values. Thus, they plot somewhat below the other samples of this group.

A positive correlation of S_{BET} exists also with the contents of the illite end-member and weak correlations with those of the smectite and chlorite end-members (Fig. 4.3-16), whereas no clear correlation with the kaolinite end-member content is visible. The value of the Klettgau Formation fits approximately in the trend relation with the illite end-member content (or slightly below) but appears as an outlier in all other plots (above the general trends). Notably, its very low kaolinite content is against the trend of many other samples.

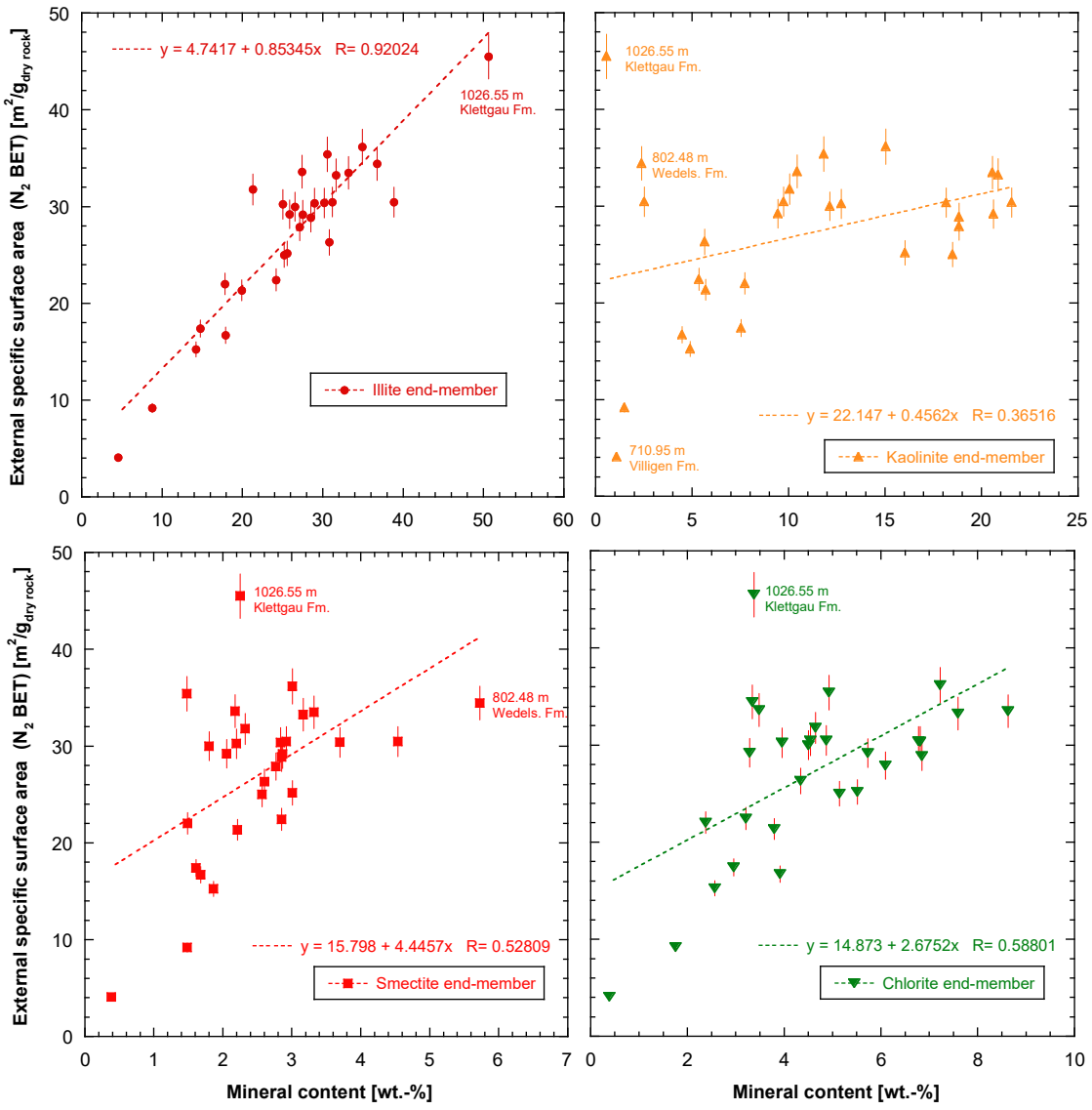

Fig. 4.3-16: Relation between external specific surface area (S_{BET}) derived from N_2 adsorption and contents of specific clay mineral end-members

Average sizes of external pores derived from S_{BET}

Average sizes of external pores were estimated from the specific surface area S_{BET} and the water content per dry mass WC_d as:

$$\overline{r_{ext}} = WC_d/(\rho_w S_{BET})$$

with ρ_w the water density taken to be 1 g/mL. This calculation assumes negligible pore volumes in interlayer pores, i.e. it attributes the measured water content to external pores only (which is not appropriate for samples with relevant smectite end-member contents).

From the inverse of the slope of the linear relation in Fig. 4.3-14 (the slope represents S_{BET}/WC_d), we obtain an overall average layer thickness (or radius) of external pores for all samples of 1.4 nm, which corresponds to about 5 to 6 water layers.

Instead of calculating an overall average from the linear regression, it is more interesting to derive an average layer thickness for each sample. Fig. 4.3-17 plots average external pore sizes (attributing all water to external surfaces) for each sample as a function of the gravimetric dry water content (a) and as a function of the total clay-mineral content (b). The derived values for the average external layer thickness (or pore radius) are rather small, below about 4 nm. There is a tendency of decreasing values with increasing clay-mineral contents, and thus also with increasing water contents. Values in the range of 2 – 4 nm were derived for the (few) Malm samples «Felsenkalke» + «Massenkalk», Villigen Formation) and one sample from the Wedelsandstein Formation, whereas values in the range of about 1 – 2 nm were calculated for the more clayey Dogger and Lias formations and the Keuper sample (Klettgau Formation).

One has to keep in mind that the samples with the largest clay-mineral fractions are very likely those with some interlayer water in smectites. Accordingly, these average external pore sizes may represent maximum values. A correction of average external pore sizes that accounts for the volume of interlayer water based on the smectite end-member content could be made assuming typical smectite particle geometries. However, in view of the involved uncertainties this is not done at present.

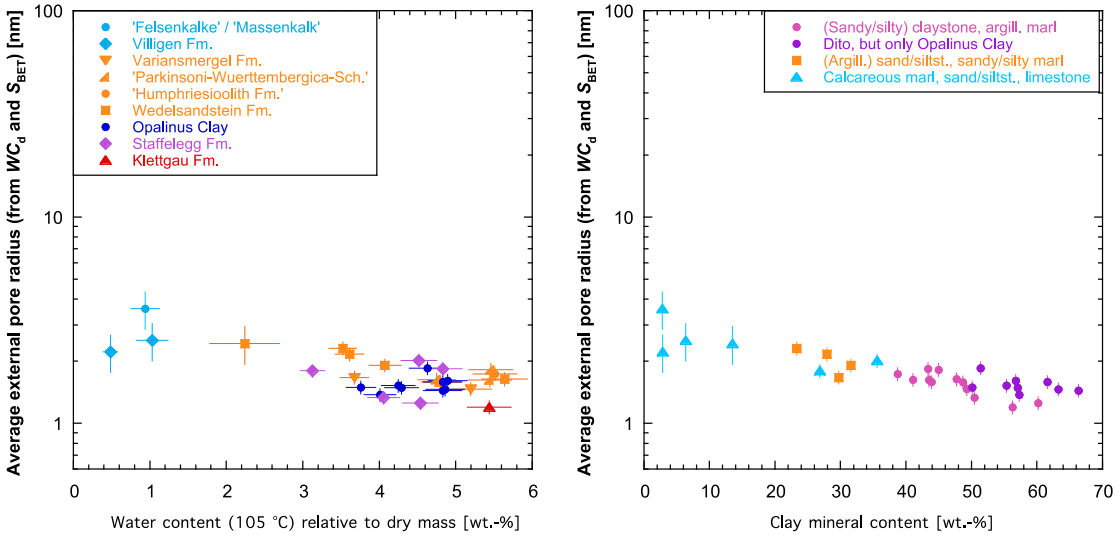

Fig. 4.3-17: Average external pore radius calculated from S_{BET} and the gravimetric water content (assuming insignificant interlayer pore volume) plotted against the gravimetric water content per dry mass of the samples (a) and against the total clay-mineral content (b)

Samples are grouped according to geological units (a) or according to rock lithology (b). Error bars show estimated errors for the water content (based on standard deviations of other samples) and propagated errors for the average external pore radius.

Distribution of external pore sizes derived from N_2 isotherms

Pore size distributions of external pores were derived by the standard BJH algorithm from N_2 ad- and desorption isotherms. The figures in the following present results from N_2 desorption for the samples of the different formations, grouped according to rock lithology. Most samples show more or less prominent peaks at a diameter of about 4 nm in the curves derived from desorption. These peaks are often related to the closure of the hysteresis of the isotherm and could thus be attributed to liquid instabilities rather than to a distinct pore volume in this size range. Such hysteresis is also related to a relatively complex pore architecture.

Pore size distributions of calcite-rich and clay-poor samples, classified as limestones, very calcareous sandstone/siltstone or calcareous marl according to the Füchtbauer nomenclature, are displayed in (Fig. 4.3-18a). The limestones from the Malm (TRU1-1 620.33, «Felsenkalke» + «Massenkalk»; TRU1-1 660.04 and 710.95, Villigen Formation) are characterised by small amounts of adsorbed N_2 volumes, consistent with their low porosities (Fig. 4.3-19), only a small peak at ~4 nm (i.e., little effect of hysteresis, pointing to comparably simple pore architecture), and a relevant peak at ~ 100 nm and (only TRU1-1 710.95) at ~ 10 nm. The very calcareous sandstone/siltstone (TRU1-1 807.74) from the Wedelsandstein Formation has a prominent peak at ~ 100 nm with an important shoulder at ~ 20 nm, whereas the two calcareous marl samples from the Staffelegg Formation (TRU1-1 930.99, Gross Wolf Member and 938.90, Rietheim Member) have a large peak at smaller sizes of ~ 6 – 8 nm, and a second important peak at ~ 100 nm and ~ 60 nm, respectively (besides the strong ~ 4 nm peaks pointing to hysteresis). The peaks of these two samples below 10 nm are likely related to their marly nature, but the high content of organic matter (C_{org} = 5 wt.-%) of the Rietheim Member sample could also play a role. In general, pore sizes (diameter) in the intermediate range of ~ 20 – 200 nm dominate in the limestone/calcareous

formations, except for the last two calcareous marl samples. The reliability of the results for these samples is corroborated by the fact that the maximum adsorbed amounts of N_2 at highest N_2 pressures, expressed as wt.-% H_2O, are very similar to the samples' water contents (Fig. 4.3-19). In other measurement campaigns, an increased risk of artefacts of too large maximum adsorbed amounts has been observed for low-porosity material. Here, such artefacts were not observed for the low-porosity samples.

Pore size distributions of samples classified as (argillaceous) sandstone/siltstone or sandy/silty marl according to the Füchtbauer nomenclature (Fig. 4.3-18b) all show a peak at ~ 4 nm related to the hysteresis closure. The pore size distribution of the sample from the Variansmergel Formation (TRU1-1 735.62) is skewed towards small diameters of 10 nm or below, with a small secondary shoulder at ~ 60 nm. The other three samples are from the Wedelsandstein Formation. Two of them have similar size distributions with equally important humps at ~ 100 nm and ~ 20 nm (TRU1-1 788.76) or a main peak at ~ 100 nm and a minor shoulder at ~ 20 nm (TRU1-1 815.28). The third one (TRU1-1 814.82) has a similar smaller peak at ~ 20 nm but then a large, broad peak at ~ 200 nm and above. The contrasting size distributions at diameters > 100 nm of the two Wedelsandstein samples located close to each other (TRU1-1 814.82 and 815.28) are not reflected in any clear differences of the physical or mineralogical data. However, the maximum adsorbed amount of N_2 of sample TRU1-1 814.82 is clearly larger than the corresponding water content determined on another aliquot (Fig. 4.3-19). This can be related to peculiarities of the sample used for the N_2 analysis due to small-scale heterogeneities, or to an artificially increased uptake of N_2 at high N_2 pressures.

Pore size distributions of samples classified as (sandy/silty) claystone or argillaceous marl are split into Fig. 4.3-18c and d, with d presenting all Opalinus Clay samples. All samples in the two subfigures show a very significant hysteresis peak at ~ 4 nm, indicating a complex pore architecture, as well as peaks at or below ~ 10 nm and at or below ~ 100 nm. The relative contributions of the latter two peaks to the pore size distribution vary to some degree but compared to the limestone samples and the (argillaceous) sandstone/siltstones or sandy/silty marls, the peaks at small pore sizes (at or below ~ 10 nm) are much more important. All Opalinus Clay samples have a dominating peak below 10 nm (TRU1-1 870.23 and 882.36: at ~ 10 nm) and a secondary, minor peak in the range of ~ 60 nm, ~ 60 – 100 nm, or ~ 100 nm. Similar pore size distributions (dominating peak at low pore diameters, minor peak at ~ 60 – 100 nm) were obtained for samples from the overlying Variansmergel Formation (TRU1-1 728.55), «Parkinsoni-Württembergica Schichten» (TRU1-1 748.98 to 768.29), «Humphriesioolith Formation» (TRU1-1 778.32), and a Wedelsandstein sample (TRU1-1 794.56) or for samples from the underlying Staffelegg Formation (TRU1-1 943.21, 955.02). The dominating peak tends to shift to lower pore diameters with increasing depth, reaching values of ~ 5 – 7 nm. The sample from the Klettgau Formation (TRU1-1 1'026.55) has a very strong peak towards ~ 5 nm (partly overlapping with the hysteresis peak) beside the minor peak at ~ 100 nm. As exceptions from the general trend, the peaks at ~ 100 nm were found to be equally important or even dominating over those at ~ 10 nm for a sample from the Wedelsandstein Formation (TRU1-1 802.84) and a sample from the Staffelegg Formation (TRU1-1 961.72). For the latter sample, the maximum adsorbed amount of N_2 exceeds the water content (Fig. 4.3-19), which may or may not mean that the fraction of large pores was overestimated in the N_2 measurements compared to the in situ situation (the same might apply to the Opalinus Clay sample TRU1-1 890.39).

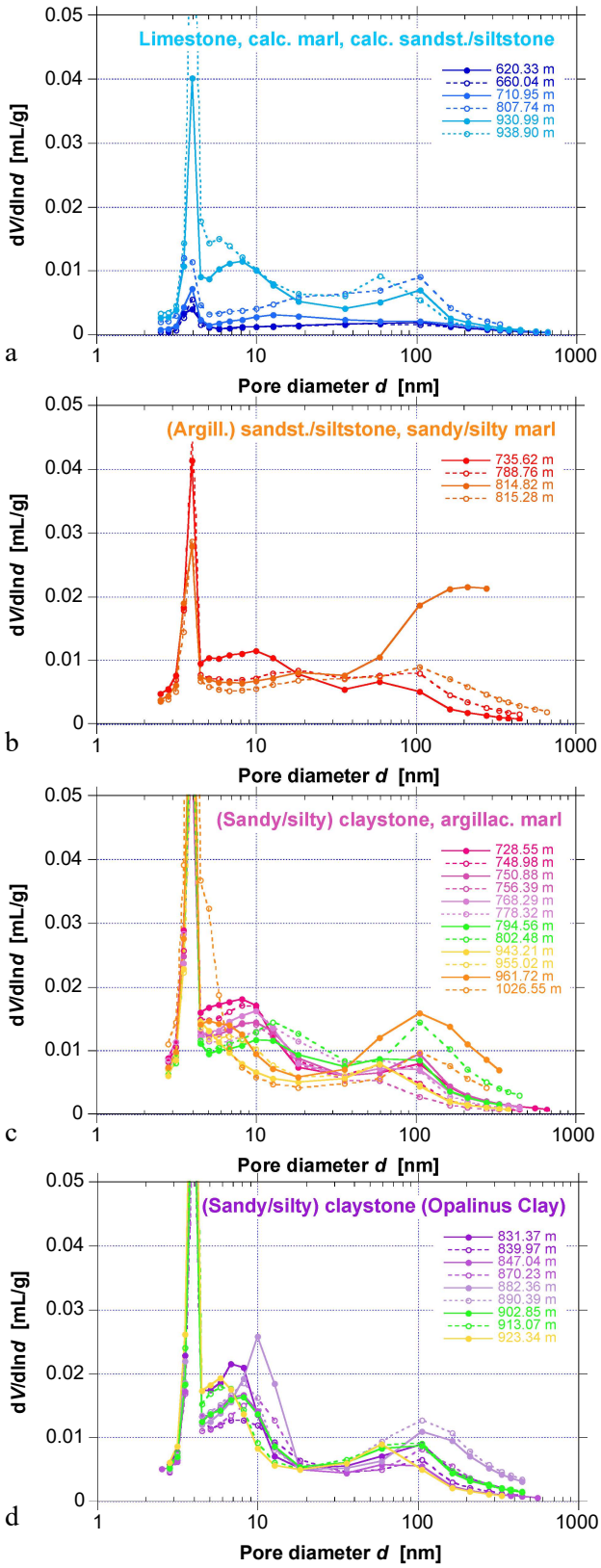

Fig. 4.3-18: Distribution of (external) pore sizes derived from N_2 desorption

(a) Limestone (620.33 m, 660.04 m, 710.95 m), very calcareous sandstone/siltstone (807.74 m) and calcareous marl samples (930.99 m, 938.90 m), (b) (argillaceous) sandstone/siltstone samples and a sandy/silty marl sample (735.62 m), and (c) and (d) (sandy/silty) claystone and argillaceous marl samples, with all Opalinus Clay samples shown in (d).

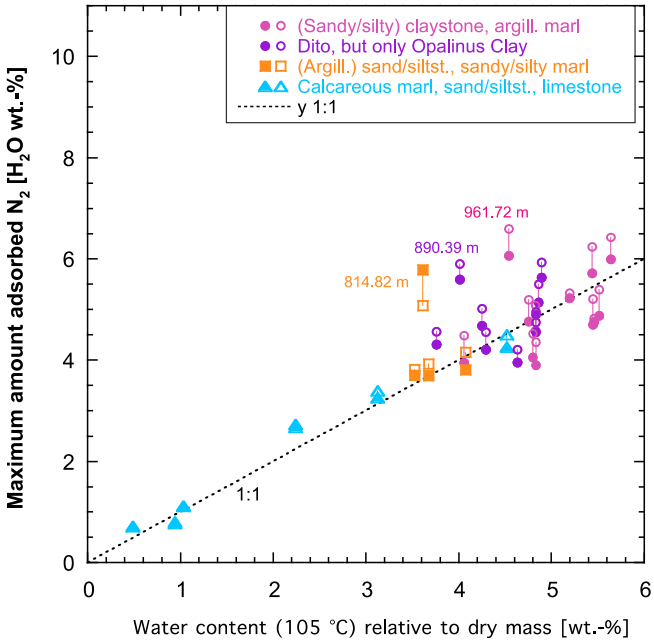

Fig. 4.3-19: Comparison of maximum amount of adsorbed N_2 (recalculated to H_2O wt.-%) with water content per dry sample mass

Open symbols: adsorption, closed symbols: desorption

Average sizes of external pores based on pore size distributions calculated from the N_2 isotherms

Average sizes of external pores cannot only be derived from S_{BET} and the water content as shown above but also directly from the pore size distribution derived from N_2 isotherms. In both cases, it is assumed that interlayer pore volumes (which are not probed by N_2 adsorption) are insignificant. Values directly derived by averaging the BJH pore size distributions (Fig. 4.3-20) are somewhat larger when compared with the average sizes determined from S_{BET} and the gravimetric water content (Fig. 4.3-17) but show the same tendencies: smaller values (around 3 – 4 nm here) for the claystones and argillaceous marls and somewhat larger values for the limestones (around 4 – 6 nm here). When comparing these numbers, one has to keep in mind that (a) any interlayer pores of smectites are not represented through N_2 adsorption, and (b) the maximum adsorbed N_2 volume partly deviates from the water content of the samples (Fig. 4.3-19), as discussed above. Here, for some of the clay-rich samples and one sandy sample the maximum adsorbed amount exceeds the water content. For these samples, the reported numbers thus tend to overestimate true average sizes.

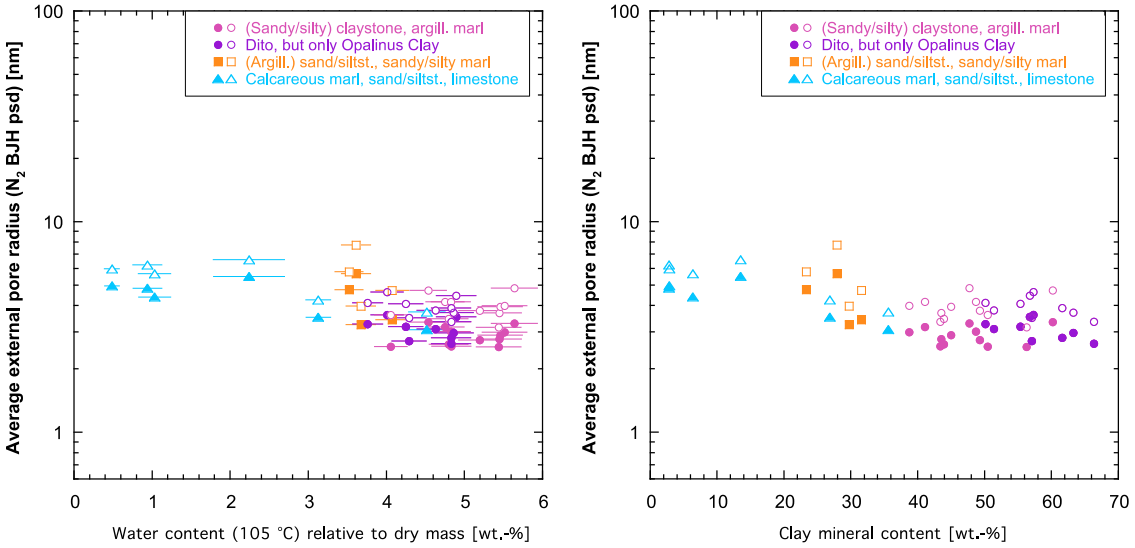

Fig. 4.3-20: Average external pore radius (assuming insignificant interlayer pore volume) based on the BJH pore size distribution from the N_2 isotherms (closed symbols: adsorption; open symbols: desorption) plotted against the gravimetric dry water content of the samples (a) and against the total clay-mineral content (b)

Samples are grouped according to rock lithology. Error bars show estimated errors for the water content per dry mass (based on standard deviations of other samples).

4.4 Data from aqueous extraction tests

Carmen Zwahlen

Aqueous extraction (AqEx) tests are a simple methodology to get insight into the porewater – rock system including the long-term evolutionary behaviour if conducted in regular intervals across a sequence of sedimentary rocks. This section provides the data from aqueous extraction tests conducted at a solid to liquid ratio (S/L) of 1 and, for two samples, at variable solid to liquid ratios. The full data set is provided in Appendix A and B. Integration of the data into context and – for chemically conservative compounds – conversion to porewater concentrations are given in Chapter 5. Details about the methodology are given in the method report by Waber (ed.) (2020).

4.4.1 Sample material and overview of analytical work

A total of 72 saturated drill core samples (PW, RP & AD samples) from different formations were subjected to aqueous extraction tests at a S*/L* ratio of approximately 1. Two of these samples were additionally extracted at variable S*/L* ratios of approximately 0.1, 0.25 and 0.5 using rock masses of about 3 g, 7.5 g and 15 g, respectively, while keeping the liquid mass constant at around 30 g. Tab. 4.4-1 lists all samples used for aqueous extraction tests and the analytical work performed on these samples. Note that the S*/L* refers to the ratio of the mass of wet rock to the mass of added water, i.e. to values measured at the onset of the experiment. In contrast, the S/L reflects the ratio of the mass of dry rock to the mass of added water and is calculated using the water content of the sample. In this Section we will only refer to the S/L.

Two thirds of the investigated samples were processed and analysed at BRGM in Orléans (France), the remaining samples at RWI, University of Bern. The two laboratories followed the method described in Waber (ed.) (2020). Nevertheless, there are some differences in the experimental protocols which are documented in Section 3.3. At BRGM the entire sample preparation is performed in a glove box with a nitrogen atmosphere. This leads to enhanced desiccation of the sample material (see Section 3.3). In contrast, sample preparation at RWI is carried out under atmospheric conditions, however, the exposure time of the samples is minimal (< 5 min; Waber ed. 2020). Thus, desiccation is in general negligible.

Additionally, the data of the extract solutions was used to model the mineral saturation states and the partial pressure of CO_2. These parameters were calculated with the PHREEQC Version 3 code (Parkhurst & Appelo 2013) and the PSI/Nagra thermodynamic data base (Thoenen et al. 2014) assuming a temperature of 25 °C.

Tab. 4.4-1: Summary of analytical work performed on samples for aqueous extraction tests

Sample type: PW/RP: porewater sample, AD: Advective displacement sample, AqEx: aqueous extraction tests.

Group	**Formation**	**Sample type**	**AqEx at S/L 1**	**AqEx at S/L 0.1, 0.25, 0.5**	**pH**	**Alkalinity**	**Anions**	**Cations**
RWI								
Malm	«Felsenkalke» + «Massenkalk»	PW, RP	3		3	3	3	3
Malm	Schwarzbach Fm.	PW	1		1	1	1	1
Malm	Villigen Fm.	PW	1		1	1	1	1
Malm	Wildegg Fm.	PW	1		1	1	1	1
Dogger	«Parkinsoni-Württembergica Sch.»	PW	2		2	2	2	2
Dogger	Wedelsandstein	PW, AD	2		2	2	2	2
Dogger	Opalinus Clay	PW, AD	7	1	10	10	10	10
Lias	Staffelegg Fm.	PW, AD	3	1	6	6	6	6
Keuper	Klettgau Fm.	PW	2		2	2	2	2
Keuper	Bänkerjoch Fm.	PW	4		4	4	4	4
BRGM								
Malm	«Felsenkalke» + «Massenkalk»	PW	5		5		5	
Malm	Schwarzbach Fm.	PW	2		2		2	
Malm	Villigen Fm.	PW	5		5		5	
Dogger	Variansmergel Fm.	PW	2		2		2	
Dogger	«Parkinsoni-Württembergica Sch.»	PW	4		4		4	
Dogger	«Humphriesioolith Fm.»	PW	1		1		1	
Dogger	Wedelsandstein	PW	3		3		3	
Dogger	Opalinus Clay	PW	13		13		13	
Lias	Staffelegg Fm.	PW	5		5		5	
Keuper	Klettgau Fm.	PW	6		6		6	
Total		PW,RP & AD	72	2	78	32	78	32

4.4.2 Aqueous extraction tests at different S/L ratios

Aqueous extraction tests at different S/L ratios are useful to discriminate non-conservative behaviour of ions, indicated by a nonlinear relationship between the ion concentration in the extract solution and the S/L ratio due to mineral dissolution or ion exchange reactions. In contrast, a linear relationship between the ion concentration in the extract solution and the S/L ratio is indicative for conservative behaviour. Such linearity is a necessary but not sufficient proof of conservative behaviour, as fast reaction kinetics (i.e. with respect to extraction time) or solute inventories significantly larger than the contribution from e.g. mineral reactions will also result in a linear behaviour (Waber & Rufer 2017).

There are two samples, one from 899.54 m depth from the Opalinus Clay and another from 951.78 m depth from the Staffelegg Formation, where aqueous extraction tests were conducted at S/L ratios of approximately 0.1, 0.25, 0.5 and 1. The two samples show a similar mineralogical composition and, based on the Füchtbauer nomenclature, they are described as very sandy/silty claystones.

4.4.2.1 Anions

Chloride concentrations exhibit a strong linear correlation with the S/L ratios, indicative for a conservative behaviour, as no Cl-bearing mineral phases are known to occur, and leakage of fluid inclusions was minimised by using crushed (and not milled) samples (Fig. 4.4-1). Bromide concentrations for these samples are below the detection limit but the same linear behaviour as for Cl was demonstrated in previous studies of the same stratigraphic formations in Northern Switzerland and at the Mont Terri Underground Rock Laboratory (Pearson et al. 2003, Wersin et al. 2013, Waber & Rufer 2017, Mazurek et al. 2021). Sulphate concentrations of the two samples are very similar and also show a linear relationship with the S/L ratio (Fig. 4.4-2). This observation, however, is not a sufficient argument to ascribe a conservative behaviour to SO_4 since the derived concentrations are significantly higher than those obtained from squeezing and advective displacement experiments (Section 5.3), suggesting possible contributions from mineral dissolution during leaching (Aschwanden & Wersin 2020, Mazurek et al. 2021). The sulphate data of aqueous extraction tests is further discussed in Section 5.3.

Both, F and alkalinity, show a nonlinear relationship with the S/L ratio with a relative decrease in concentration with increasing S/L ratio (not shown), which can be attributed to mineral reactions. Mineralogical analyses do not indicate the presence of a specific F mineral phase (Section 4.2) but fluorite (CaF_2) or another mineral, with F incorporated as solid solution, could be possible sources. Carbonate mineral dissolution is the likely reason for the observed alkalinity trend, supported by a positive correlation between the alkalinity and the Ca concentration.

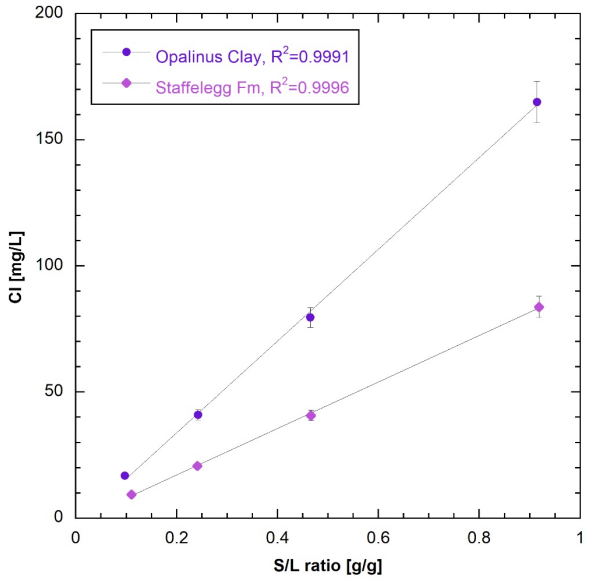

Fig. 4.4-1: Cl concentrations versus S/L ratios in aqueous extract solutions from the Opalinus Clay and the Staffelegg Formation

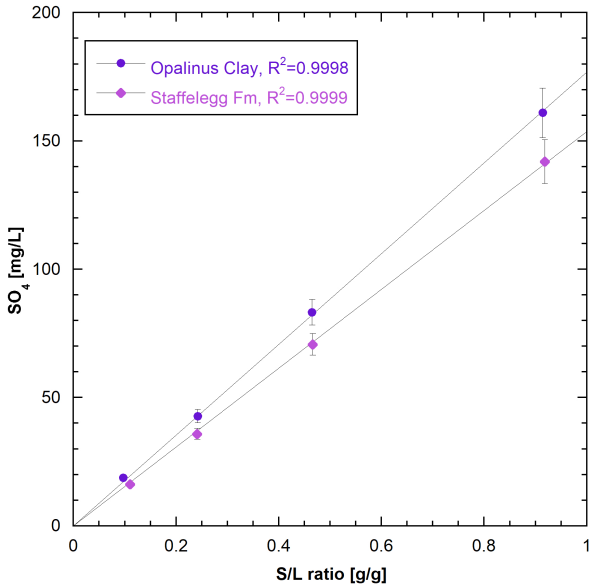

Fig. 4.4-2: SO_4 concentrations versus S/L ratios in aqueous extract solutions from the Opalinus Clay and the Staffelegg Formation

4.4.2.2 Cations

The Na concentrations in extract solutions present a linear trend (not shown) as a function of the S/L ratio, indicating that the porewater is a major source with an increasing contribution of cation exchange reactions as a function of decreasing S/L ratio. The remaining cations (K, Ca, Mg and Sr) show variable contributions from the porewater, mineral dissolution and cation-exchange reactions which are difficult to disentangle. The K concentration trend with the S/L ratio of the sample from the Staffelegg Formation is comparable to that of Na, however, the Opalinus Clay

sample presents no clear relationship between the K concentration and the S/L ratio. The Ca concentration in the extracts of the Opalinus Clay sample shows a linear trend with the S/L ratio, whereas the Ca concentration in the extracts of the Staffelegg Formation sample show a relative decrease with increasing S/L ratios. There is no clear relationship between the Mg concentration and S/L ratios. The Sr concentration increases nonlinearly with increasing S/L ratio. There is no clear trend between the Sr and Ca or SO_4 concentrations and hence the source of the Sr cannot clearly be deciphered.

4.4.2.3 Mineral saturation states, pH and partial pressure of CO_2

The pH shows a gradual decrease with increasing S/L ratios except for an outlier in the Opalinus Clay sample at a S/L ratio of 0.5 (Fig. 4.4-3). The log P_{CO2} is modelled using PHREEQC based on measured pH and alkalinity and is governed by the equilibrium with calcite. This log P_{CO2} correlates negatively with the pH and exhibits the same outlier in the Opalinus Clay sample at a S/L ratio of 0.5 (Fig. 4.4-3). The saturation index of calcite is close to equilibrium for both samples at all S/L with a slight oversaturation at higher S/L ratios decreasing to a slight undersaturation at lower S/L ratios. Gypsum, anhydrite, dolomite (disordered and ordered) and celestite are clearly undersaturated at all S/L ratios except for dolomite (ordered) which is in equilibrium at two S/L ratios (Tab. 4.4-2).

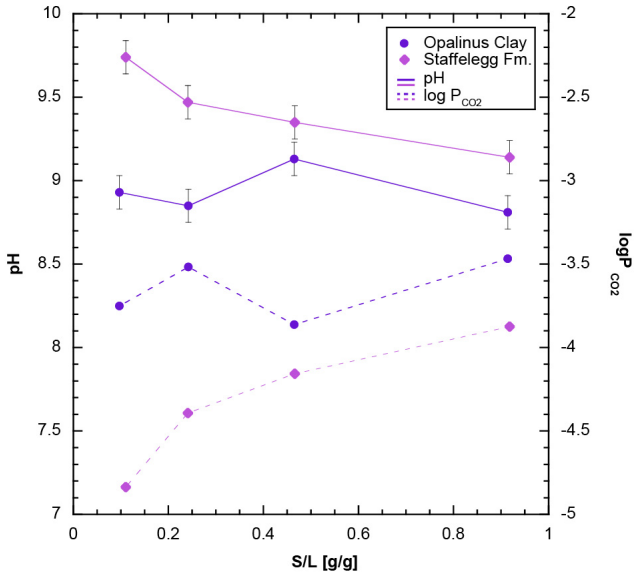

Fig. 4.4-3: pH and logP_{CO2} versus S/L ratio in aqueous extracts from the Opalinus Clay and the Staffelegg Formation

4.4.3 Aqueous extraction test at a S/L of 1

This Section presents the results of the aqueous extraction tests performed at a solid to liquid ratio of 1. In view of assessing the long-term porewater evolution across the Mesozoic sedimentary sequence, ion concentrations in aqueous extracts have a limited significance if they are not recalculated to porewater concentrations. For chemically conservative compounds this recalculation is established in Chapter 5. Thus, in this Section only ion ratios are presented as they are independent of the recalculation formalisms.

Two thirds of the aqueous extraction data set of the Trüllikon-1-1 borehole were produced at BRGM and do not include cation concentrations (see Tab. 4.4-1). The remaining third of the data set was produced at RWI and includes cation concentrations.

4.4.3.1 Drilling fluid contamination

During sample preparation approximately 1.5 cm of rim material is removed from the drill core samples to avoid contamination from the drilling fluid. However, in porous and permeable rocks such as e.g. dolostones or sandstones, the drilling fluid might reach the central parts of the drill core. This was observed in a few samples from the Bülach-1-1 borehole (Mazurek et al. 2021). The drilling fluid used in the Dogger section of the TRU1-1 borehole is potassium silicate mud particularly enriched in K, Si and organic carbon compared to the porewater. The criteria to discriminate contaminated samples include low Na/K ratios together with strongly elevated alkalinity and pH values compared to neighbouring samples (no data for Si is available for extracts of PW samples). There are 5 samples (1 PW and 4 AD) which fulfil these criteria and are therefore circled in red in all following figures. A porous (12 vol.-%) dolostone sample from the Klettgau Formation from 995.83 m depth exhibits a low Na/K ratio and high alkalinity and pH values (Figs. 4.4-5, 4.4-8) clearly indicating such contamination. This sample also yields an anomalous high Br/Cl ratio, which seems not reliable.

Aqueous extracts of all four AD samples from the Wedelsandstein Formation, Opalinus Clay and Staffelegg Formation show a distinctly lower Na/K ratio (i.e. owing to elevated K concentrations) compared to the neighbouring PW samples. Also, the Si concentrations appear to be elevated (Section 4.7.4). The AD samples are all clay-rich and exhibit a rather low permeability, which reduces the access of drilling mud to the central parts of the drill core samples. Alternatively, the contamination might have occurred during sample preparation (e.g. not enough rim material was disposed).

4.4.3.2 Anions

Br/Cl ratios in aqueous extract solutions from the Malm plot around and below the seawater ratio (Fig. 4.4-4). Samples from the underlying rock formations («Brauner Dogger», Staffelegg Formation, Opalinus Clay and Klettgau Formation) follow a linear trend diverging from the seawater line.

The depth profile of the Br/Cl ratios (Fig. 4.4-5) manifests a substantial variability in the Malm. The «Brauner Dogger», Opalinus Clay, Staffelegg Formation and Klettgau Formation exhibit nearly constant and remarkably uniform Br/Cl ratios significantly below the seawater value. There is one outlier in the Klettgau Formation (981.93 m), which shows a very low Br/Cl ratio. This extract was analysed by BRGM and thus, only limited chemical data is available (see Tab. 4.4-1), which does not allow an in-depth assessment of this data point. Thus, its significance is not clear.

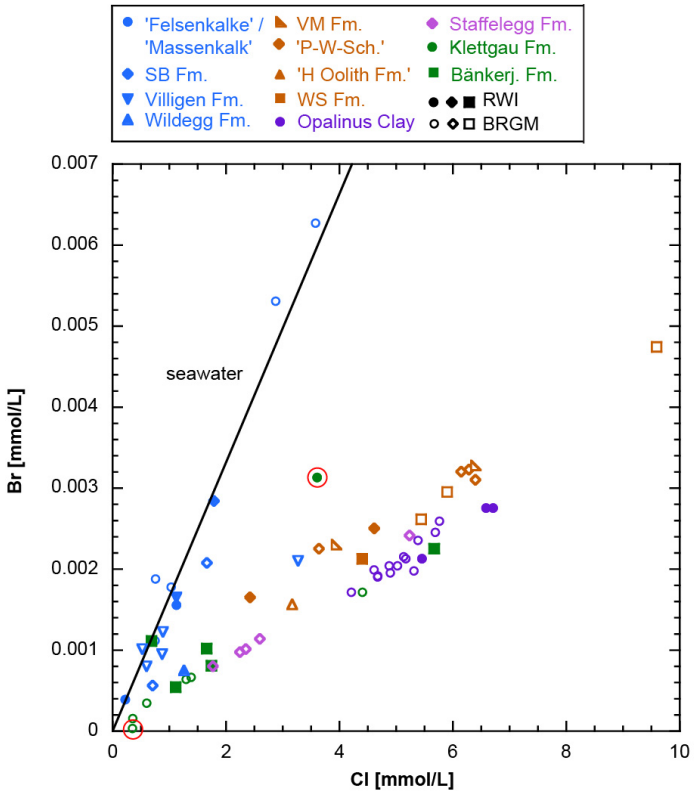

Fig. 4.4-4: Br versus Cl molar concentrations in aqueous extracts at a S/L ratio of 1

The analytical uncertanties for Cl and Br for RWI are 4% and 5%, respectively and 3% and 3%, respectively for BRGM. The samples with red circles appear to be contaminated by the drilling fluid. Note that two contaminated AD samples have a Br concentration below the detection limit.

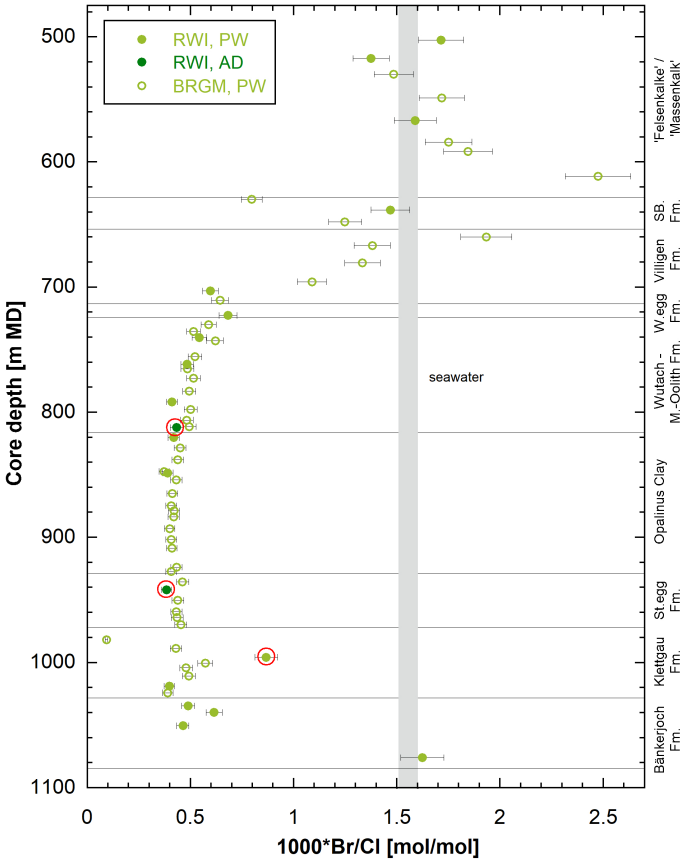

Fig. 4.4-5: Depth profile of the molar Br/Cl ratio in aqueous extracts at a S/L ratio of 1

Samples with red circles appear to be contaminated by the drilling fluid. Note that two contaminated AD samples have Br conentrations below the detection limit.

The depth profile of SO_4/Cl ratios in aqueous extract solutions (Fig. 4.4-6) shows a large scatter in the upper part of the Malm (i.e. in the «Felsenkalke» /«Massenkalk»), ranging from values below the seawater ratio up to high values of around 1 in the Schwarzbach Formation. The ratio decreases slightly throughout the Villigen Formation, the Wildegg Formation and the «Brauner Dogger». The samples of the «Brauner Dogger» analysed at RWI plot systematically below those analysed at BRGM, the latter showing a considerable scatter. A potential explanation for this difference could be oxidation during sample preparation at BRGM. However, this is rather unlikely, since BRGM prepares the samples exclusively under anaerobic conditions. At this stage the observed difference in SO_4/Cl ratios between the two laboratories remains unexplained.

Throughout the Opalinus Clay and the Staffelegg Formation, the SO_4/Cl ratios follow a smooth trend towards slightly higher values. This trend increases in the anhydrite-bearing Klettgau and Bänkerjoch Formations.

The F concentrations in aqueous extracts vary between 0.3 and 6.8 mg/L across the whole depth profile (not shown) with the highest values in the «Felsenkalke» + «Massenkalk», Schwarzbach and Staffelegg Formations. The alkalinity varies between 0.3 and 4.4 meq/L when excluding the contaminated samples with values of up to 26.7 meq/L (Tab. 4.4-2). The pH values are fairly constant between 8.6 and 9.3 but scatter in the Malm, Klettgau and Bänkerjoch Formations,

reaching values between 7.1 and 9.7 (Tab. 4.4-2). There is an outlier in the base of the Wutach Formation, and the contaminated sample in the Klettgau Formation has an exceptionally high value of 10.3.

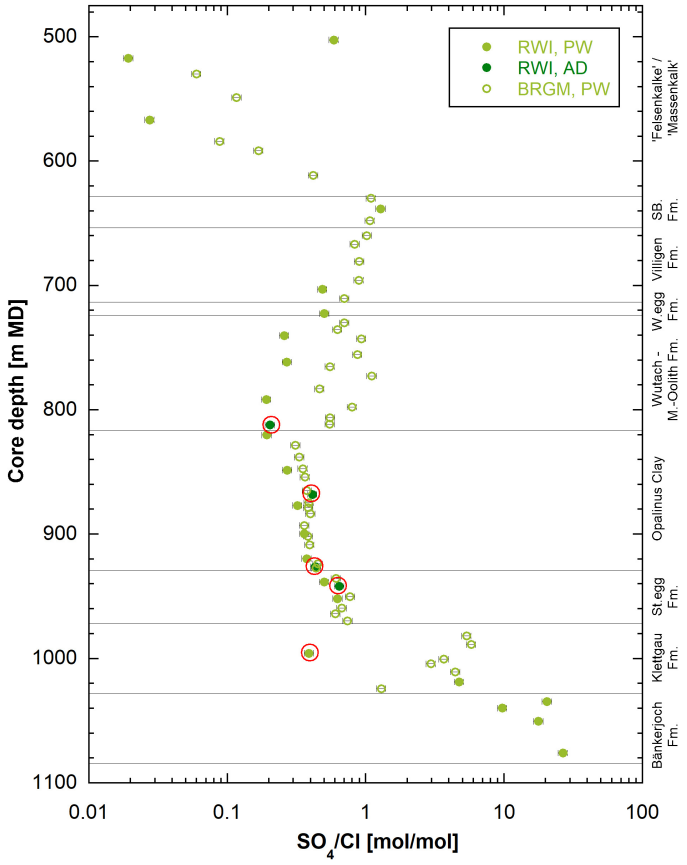

Fig. 4.4-6: Depth profile of SO_4/Cl molar concentration ratio in aqueous extracts at a S/L ratio of 1

Samples with red circles appear to be contaminated by drilling fluid.

4.4.3.3 Cations

The depth profile of Na/Cl ratios presents some scatter in the Malm section, a constant trend in the Dogger and a scatter in the Triassic (Fig. 4.4-7).

The depth profile of Na/K ratios shows rather constant values of around 40 in the Malm section (Fig. 4.4-8). The ratio then increases steadily throughout the «Brauner Dogger» to values of around 90, which remain constant throughout the Opalinus Clay (as outlined above, AD samples appear to be contaminated by the drilling fluid and thus, show distinctly lower values). In the Klettgau and Bänkerjoch Formation the Na/K ratios drop to values of around and below 20.

The Sr/Cl ratios (not shown) plot in a narrow range throughout the Malm – Lias section and then jump to distinctly higher values in the Keuper and Muschelkalk. This can be explained by the release of Sr from the dissolution of anhydrite during aqueous extraction. Moreover, some extracts of AD samples show higher Sr concentrations compared to extracts of adjacent PW samples. The reason for this is not known at this stage.

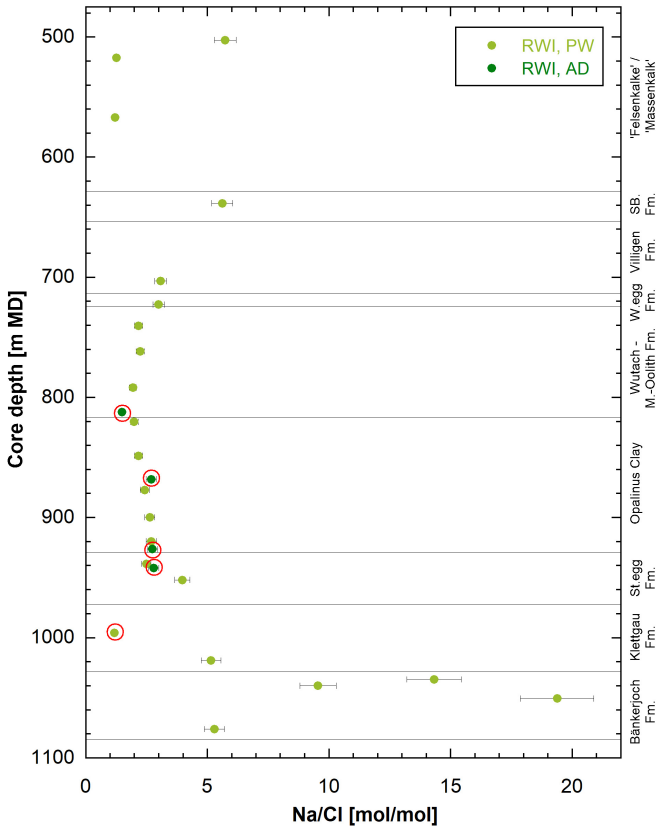

Fig. 4.4-7: Depth profile of the Na/Cl molar concentration ratio in aqueous extracts at a S/L ratio of 1

All data originate from the University of Bern. Samples with red circles appear to be contaminated with drilling fluid.

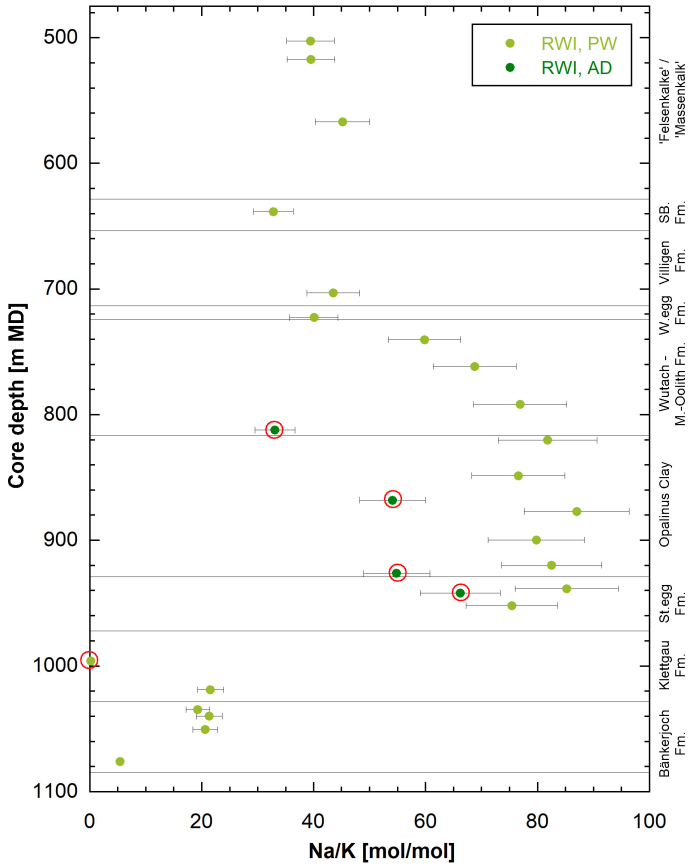

Fig. 4.4-8: Depth versus Na/K molar concentration ratio in aqueous extracts at a S/L ratio of 1

All data originate from Univ. Bern. Samples with red circles appear to be contaminated with drilling fluid.

4.4.3.4 Saturation indices

Most extracts of samples from the Malm, Dogger and Lias are close to saturation with respect to calcite but mostly undersaturated with respect to dolomite (disordered and ordered; Tab. 4.4-2). In the Klettgau and Bänkerjoch Formations the saturation indices for calcite and dolomite (disordered and ordered) vary strongly. The sample with drilling fluid contamination (995.83 m) shows a high oversaturation with respect to calcite and dolomite (disordered and ordered).

The sulphate minerals gypsum, anhydrite and celestite are undersaturated by 2 to 4 orders of magnitude in all extract solutions from the Malm to the Staffelegg Formation (Tab. 4.4-2). At the base of the Klettgau Formation, the extract solutions become generally saturated with respect to celestite and gypsum and are also close to saturation with respect to anhydrite. Exceptions form the extract solutions of a dolomitic marl sample in the Bänkerjoch Formation which are undersaturated with respect to gypsum and anhydrite and an anhydrite-bearing dolomite samples, which is undersaturated with respect to celestite but in equilibrium with gypsum. Re-examination of the XRD-patterns did not reveal quantifiable amounts of celestite in all these samples although trace amounts of < 1wt.-% cannot be completely excluded for samples 1'018.88, 1'034.61, 1'039.89 and 1'050.51. In turn, the calculated celestite saturation could be derived from anhydrite, calcite and dolomite dissolution, all of them known to have variable amounts of Sr incorporated as solid-solution.

Tab. 4.4-2: Saturation indices for calcite, dolomite (disordered and ordered), gypsum, anhydrite and celestite at variable S/L and S/L 1, pH and partial pressure of CO_2

Mineral saturation indices were calculated with the PHREEQC Version 3 code (Parkhurst & Appelo 2013) and the PSI/Nagra thermodynamic database (Thoenen et al. 2014) assuming a temperature of 25 °C. Note that a few samples lack a SI for dolomite due to Mg concentrations below the limit of detection.

Formation	**Depth** [m]	**S/L**	**SI Calcite**	**SI Dolomite (dis)**	**SI Dolomite (ord)**	**SI Gypsum**	**SI Anhydrite**	**SI Celestite**	**pH**	**pCO_2**
Variable S/L ratios										
Opalinuston	899.5	0.91	0.11	-0.79	-0.22	-2.75	-2.99	-2.44	8.81	-3.47
Opalinuston	899.5	0.47	0.20	-0.72	-0.15	-3.15	-3.39	-2.94	9.13	-3.86
Opalinuston	899.5	0.24	-0.08	-1.11	-0.54	-3.48	-3.72	-3.24	8.85	-3.52
Opalinuston	899.5	0.10	-0.17	-0.97	-0.40	-3.83	-4.07	-3.57	8.93	-3.75
Staffelegg Fm	951.8	0.92	0.08	-0.96	-0.39	-3.06	-3.30	-2.85	9.14	-3.87
Staffelegg Fm	951.8	0.47	0.16	-0.56	0.01	-3.38	-3.62	-3.35	9.35	-4.16
Staffelegg Fm	951.8	0.24	0.09	-0.54	0.03	-3.74	-3.98	-3.42	9.47	-4.39
Staffelegg Fm	951.8	0.11	-0.02	-1.07	-0.49	-4.25	-4.49	-3.91	9.74	-4.84
S/L ratio of 1										
Malm	502.5	0.98	0.06	-0.91	-0.34	-3.63	-3.87	-3.77	9.31	-4.61
Malm	517.1	0.96	-0.73	-2.78	-2.20	-4.01	-4.26	-4.52	8.19	-3.56
Malm	566.8	0.97	-0.29	-1.74	-1.17	-3.64	-3.88	-3.95	8.44	-3.67
Malm	638.2	0.94	0.05	-0.65	-0.08	-2.82	-3.06	-2.59	9.06	-3.97
Malm	703.1	0.97	0.04	-0.83	-0.26	-3.26	-3.50	-2.94	9.40	-4.55
Malm	722.7	0.94	0.25	-0.33	0.24	-2.76	-3.00	-2.46	9.09	-3.97
«Brauner Dogger»	740.3	0.95	0.03	-0.92	-0.35	-2.89	-3.13	-2.58	8.89	-3.69
«Brauner Dogger»	761.6	0.91	0.12	-0.68	-0.11	-2.96	-3.20	-2.61	9.06	-3.87
«Brauner Dogger»	791.7	0.88	-0.06	-1.06	-0.49	-2.84	-3.08	-2.51	8.65	-3.34
«Brauner Dogger»	812.2	0.89	0.05	-0.74	-0.17	-2.37	-2.61	-1.46	8.93	-4.10
Opalinus Clay	820.3	0.90	-0.04	-1.04	-0.47	-2.83	-3.07	-2.54	8.63	-3.30
Opalinus Clay	848.5	0.91	-0.03	-1.09	-0.51	-2.78	-3.02	-2.50	8.73	-3.46
Opalinus Clay	868.0	0.93	0.07			-2.79	-3.03	-2.41	8.89	-3.61
Opalinus Clay	876.8	0.91	0.10	-0.80	-0.23	-2.78	-3.02	-2.46	8.86	-3.56
Opalinus Clay	899.5	0.91	0.11	-0.79	-0.22	-2.75	-2.99	-2.44	8.81	-3.47
Opalinus Clay	919.7	0.90	0.07	-0.89	-0.32	-2.76	-3.00	-2.51	8.80	-3.47
Opalinus Clay	926.1	0.88	0.11			-2.70	-2.94	-2.42	8.84	-3.52
Staffelegg Fm.	938.5	0.90	-0.10	-1.20	-0.63	-2.47	-2.71	-2.01	8.71	-3.57
Staffelegg Fm.	941.8	0.90	-0.04	-0.97	-0.40	-2.26	-2.50	-1.72	8.62	-3.45
Staffelegg Fm.	951.8	0.92	0.08	-0.96	-0.39	-3.06	-3.30	-2.85	9.14	-3.87
Klettgau Fm.	995.8	0.91	0.76	1.29	1.86	-3.99	-4.23	-3.54	10.29	-4.74
Klettgau Fm.	1'018.9	0.90	-0.80	-3.11	-2.54	0.08	-0.15	0.12	7.12	-2.94
Bänkerjoch Fm.	1'034.6	0.95	0.51	-0.29	0.28	0.02	-0.22	0.00	8.22	-3.80
Bänkerjoch Fm.	1'039.9	0.93	0.52	0.08	0.65	-0.35	-0.59	0.15	8.37	-3.81
Bänkerjoch Fm.	1'050.5	0.92	0.10	-1.10	-0.53	0.14	-0.10	-0.03	7.79	-3.39
Bänkerjoch Fm.	1'076.0	0.99	0.10	-0.84	-0.27	-0.05	-0.29	-0.28	7.58	-2.95

4.4.4 Chloride and bromide concentrations in bulk porewater

The formalisms to recalculate Cl and Br concentrations in aqueous extracts to concentrations in bulk porewater are given in Waber (ed.) (2020). In clay-free rocks this recalculation is believed to directly deliver the in situ porewater concentrations of Cl and Br. In clay-bearing rocks this recalculation additionally has to account for anion-exclusion in order to obtain the porewater concentration. The derivation of the Cl and Br accessible porosity and calculation of porewater concentrations is further established in Chapter 5.

The recalculation of Cl and Br concentrations in aqueous extracts to concentrations in bulk porewater (Figs. 4.4-9, 4.4-10) requires the knowledge of the water content of the rocks. For aqueous extracts performed by RWI, the average of the three gravimetric water contents (PW subsample and the two subsamples used for diffusive-exchange experiments) was used. At BRGM the rock material suffered from desiccation during sample preparation. Thus, for the BRGM data the water content used for the recalculation was derived from the pycnometer porosity and the bulk dry density (see Section 3.4).

As presented in Section 4.3, the water content of various subsamples and methods shows some scatter. To illustrate the effect of this scatter, Fig. 4.4-11 includes the Cl concentrations in bulk porewater recalculated using three different water contents (i.e. gravimetrically derived, diffusive-exchange experiment derived and calculated from the pycnometer porosity and the bulk dry density). Overall, there is good agreement between the three methods.

The depth profiles of Cl concentrations in bulk porewater cover a range of 0.1 to 8 g/L and data of RWI and BRGM are broadly consistent (Fig. 4.4-9). At this stage, the observed trends should be treated with care because the recalculated Cl and Br concentrations still need to be corrected for anion accessibility, which, as mentioned above, is further established in Chapter 5.

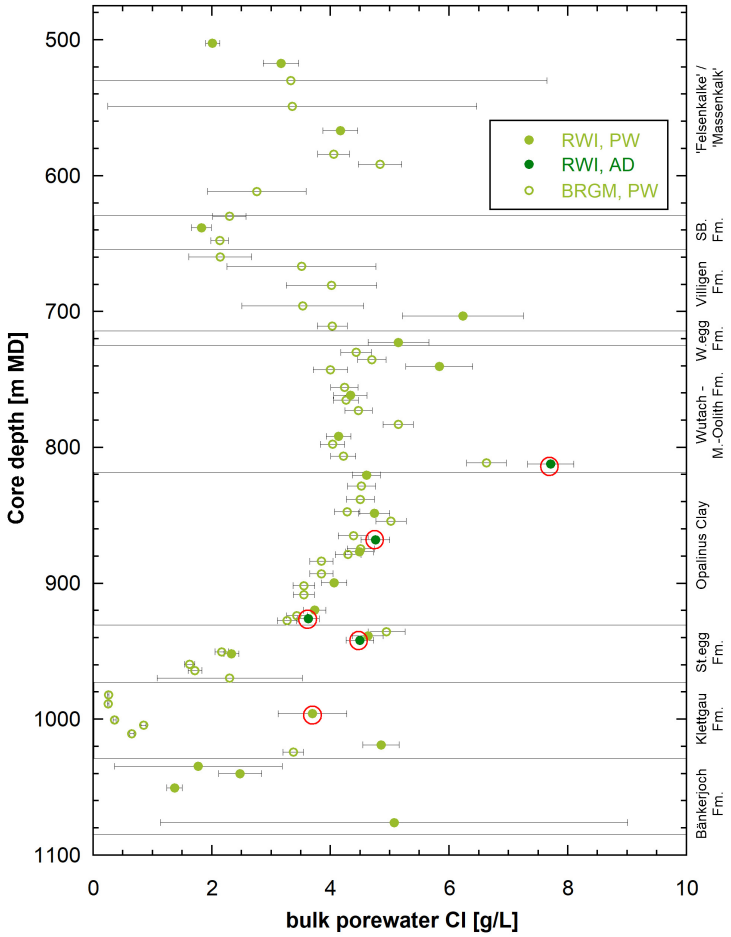

Fig. 4.4-9: Bulk porewater Cl concentrations versus depth from aqueous extracts

Samples with red circles appear to be contaminated by the drilling fluid. For RWI samples the average of the three gravimetric water contents was used for recalculation to the concentration in the bulk porewater. For the BRGM data the water content used for the recalculation to the concentration in bulk porewater was derived from the pycnometer porosity and the bulk dry density.

The depth profile of the Br concentration in bulk porewater shows a general decrease in concentrations from the Malm down to the Klettgau Formation (Fig. 4.4-10). There is little discrepancy between samples analysed by RWI and BRGM.

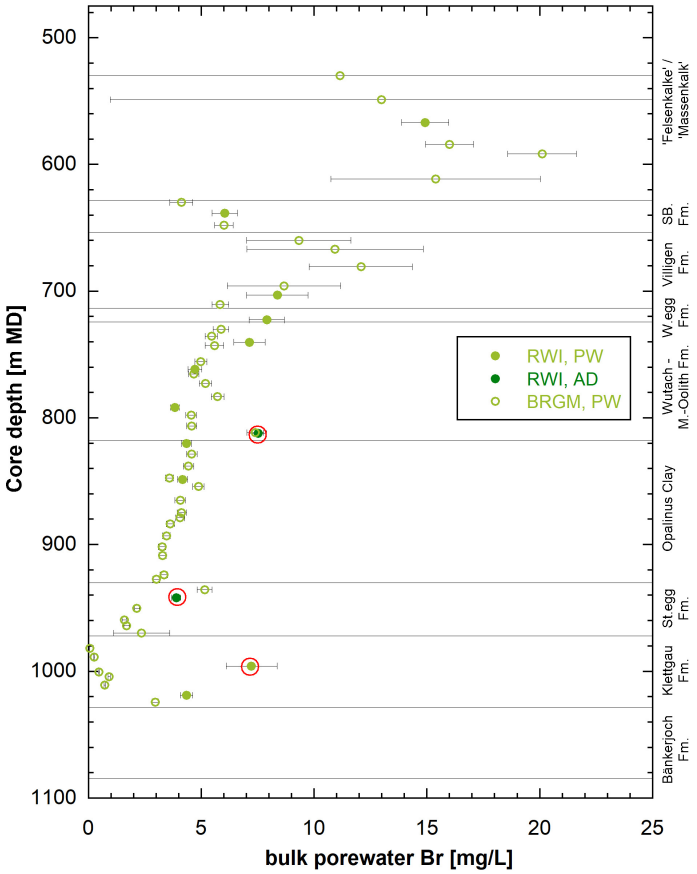

Fig. 4.4-10: Bulk porewater Br concentrations versus depth from aqueous extracts

Samples with red circles appear to be contaminated by the drilling fluid. For RWI samples the average of the three gravimetric water contents was used for the recalculation to the concentration in the bulk porewater. For the BRGM data the water content used for the recalculation to the concentration in bulk porewater was derived from the pycnometer porosity and the bulk dry density.

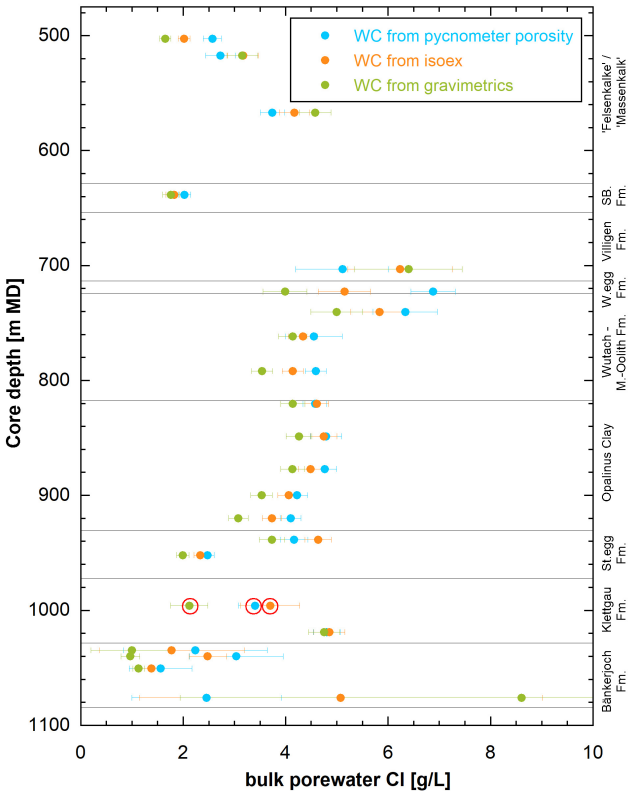

Fig. 4.4-11: Bulk porewater Cl of RWI data calculated with three different derived water contents: gravimetrically, from diffusive-exchange experiments and from pycnometer porosity

All data originate from University of Bern. Samples with red circles appear to be contaminated with drilling fluid.

4.5 Cation-exchange extraction data

Paul Wersin & Martin Mazurek

Four samples used for advective displacement experiments (AD samples) were analysed at the University of Bern with the nickel ethylenediamine (Ni-en) extraction method to determine the cation exchange capacity (CEC) and the composition of the clay exchanger (for methodology see Waber ed. 2020). For three samples, two subsamples on segments above and below the core used for AD experiments were analysed. For one sample (TRU1-1-926.14-AD) only one subsample representing a mixture of aliquots above and below the AD core was analysed.

Eleven samples were studied by the team at PSI using the $CsNO_3$ extraction method (Marques Fernandes & Baeyens *in prep.*). The objective of the Ni-en extraction study was (i) to help to evaluate the AD data (Section 4.7) and (ii) to compare and verify the PSI study with an alternative method. The data of PSI is presented and discussed in Section 5.7.2.

The CEC can be derived in two ways: (1) the consumption of the index cation (Ni in this case) during extraction and (2) the sum of extracted cations (ΣCAT). Note that the latter includes (i) the exchangeable cations, (ii) cations dissolved in the porewater and (iii) cations released from potentially dissolving minerals (e.g. carbonates, sulphates) during extraction. Thus, in principle, the CEC derived from the sum of cations requires correction from contributions of (ii) and (iii). Corrected CEC and exchangeable cation data are discussed in Section 5.7, where the data from the University of Bern is also compared with that of PSI.

Tab. 4.5-1 shows the Ni consumption and extracted cation data (Na, K, Ca, Mg, Sr, Ba, Fe) for solid/liquid ratios (S/L) around 1[6]. Anion data (Cl, Br, SO_4, NO_3) is depicted in Tab. 4.5-2. Note that Ni nitrate was added to the samples, which explains the high NO_3 contents. Note that these data represent averaged data of two subsamples for the samples at 812.24 m, 867.97 m and 941.80 m depth, whereas the sample at 926.14 m reflects one subsample. Data for individual subsamples can be found in the electronic Appendix.

Tab. 4.5-1: Cation data from Ni-en extracts at a S/L ratio around 1 (University of Bern data)

Type	Depth	Formation	S/L	Clay	Na	K	Ca	Mg	Sr	Ba	Fe	ΣCAT	Ni cons.
	[m]		[g/g]	[wt.-%]	[meq/$kg_{dry\ rock}$]								
AD	812.24	Wedelsandstein Fm.	0.866	18	26.2	3.8	20.3	8.5	1.2	0.03	< 0.002	60.0	51.3
AD	867.97	Opalinus Clay	0.904	41	34.2	4.6	28.7	10.7	0.7	0.02	< 0.002	78.9	84.0
AD	926.14	Opalinus Clay	0.849	65*	55.1	6.6	43.4	13.7	1.0	0.01	< 0.002	119.8	124.5
AD	941.80	Staffelegg Fm.	0.851	38	39.0	4.9	31.2	11.1	0.9	0.02	< 0.002	87.1	76.7

* Data from adjacent sample at 927.41 m.

[6] A water mass equal to the mass of the wet rock was added, leading to S/L (mass of dry rock/[mass of added water + porewater]) slightly below 1.

Tab. 4.5-2: Anion data from Ni-en extracts (University of Bern data)

Br contents are < 0.16 mg/L or < 0.002 meq/$kg_{dry\ rock}$ for all samples.

Type	**Depth**	**Formation**	**Cl**	**F**	**NO_3**[(a)]	**SO_4**
	[m]		[meq/$kg_{dry\ rock}$]			
AD	812.24	Wedelsandstein Fm.	10.6	0.03	363.1	3.5
AD	867.97	Opalinus Clay	4.1	0.03	349.2	2.3
AD	926.14	Opalinus Clay	5.1	0.06	238.0	3.1
AD	941.8	Staffelegg Fm.	6.1	0.04	375.1	5.0

[(a)] Nitrate is part of the added Ni-en stock solution.

The CEC derived from Ni consumption of the AD samples varies between about 50 and 125 meq/kg_{rock}, similar to the sum of cations. Note that the sum of cations needs to be corrected for porewater solutes and mineral dissolution as outlined in Section 5.7. The depth profiles of Ni consumption and ΣCAT data both show consistent trends (Fig. 4.5-1). The CEC data show a clear positive correlation with clay-mineral content ($R^2 = 0.991$ for Ni consumption data; Fig. 4.5-2).

Na and Ca are the main extracted cations, followed by Mg and K (Tab. 4.5-1). The Ca/Na ratio is constant for the four samples with a value of ~ 0.8. Mg correlates with Ca, thus the (Ca+Mg)/Na is also constant (~ 1.1). The K/Na and Sr/Na ratios exhibit a range of 0.12 – 0.15 (average: 0.13) and 0.02 – 0.05, respectively.

It should be noted that aqueous extraction data of the corresponding samples indicate contamination by the drilling fluid which is manifested by high K/Na ratios and elevated Si levels (Sections 4.4 & 4.7.4). This suggests that K data in the Ni-extracts are also potentially affected by drilling fluid. It is interesting to compare the TRU1-1 K/Na ratios in Ni-extracts with the ones obtained from the near-by Benken and Schlattingen-1 boreholes. For the Schlattingen-1 borehole, a range of 0.13 – 0.16 (average: 0.15) is obtained for samples from Opalinus Clay and confining units (Wersin et al. 2013). For the Benken borehole, a range of 0.09 – 0.23[7] (average: 0.15) for the same units was obtained (Mazurek 2017). From this comparison alone, it cannot be concluded that K levels obtained in the Ni-extracts for TRU-1-1 borehole were affected by drilling fluid contamination.

Speciation calculations on the Ni-en extracts for the individual subsamples were carried out with the PHREEQC Version 3 code (Parkhurst & Appelo 2013) and the PSI/Nagra thermodynamic database (Thoenen et al. 2014) assuming a temperature of 25 °C. The ethylene diamine complexes were taken from the MINTEC database (Allison et al. 1991) and included in the calculations. The concentration of ethylene diamine in the extracts, which was not analysed, was constrained by charge balance. The dissolved carbonate concentration (not measured) was constrained by assuming calcite equilibrium. The calculated partial pressures of CO_2 (pCO_2) and saturation indices for selected minerals are depicted in Tab. 4.5-3. The Ni-en extracts are clearly undersaturated with regard the carbonate minerals dolomite, and strontianite. They are also undersaturated with regard to the sulphate minerals gypsum and celestite but oversaturated with regard to barite.

[7] The very high value of 0.51 obtained in one sample (BEN 471.49) is considered as outlier and not considered here.

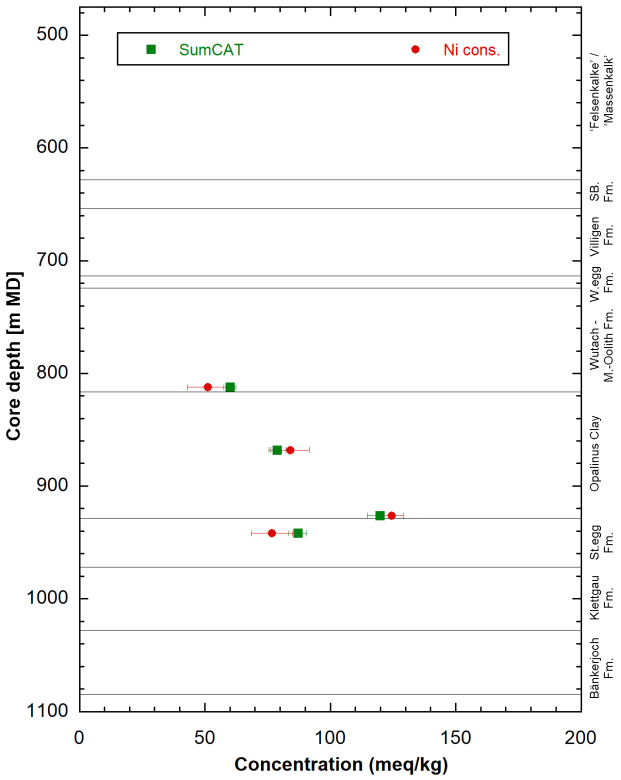

Fig. 4.5-1: Depth profile of Ni consumption and sum of cations (uncorrected)

Error bars reflect the range of the two individual subsamples except for the sample at 926.14 m depth where the analytical error is shown.

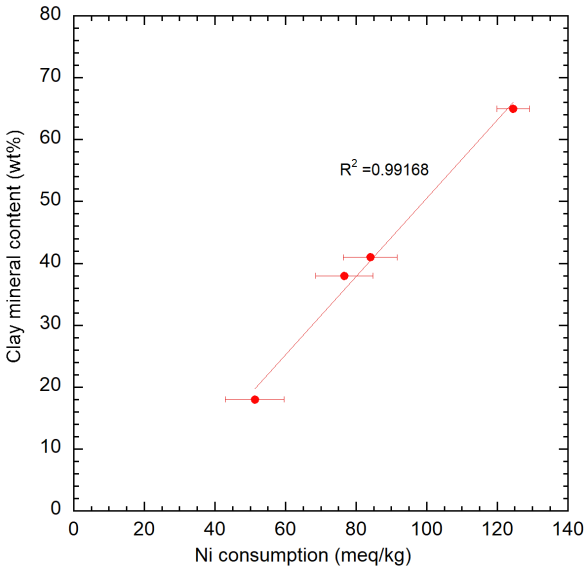

Fig. 4.5-2: Ni consumption vs. clay-mineral content

Error bars reflect the range of the two individual subsamples except for the sample at 926.14 m depth where the analytical error is shown. For the latter sample, the clay-mineral content was taken from an adjacent sample (PW 927.41).

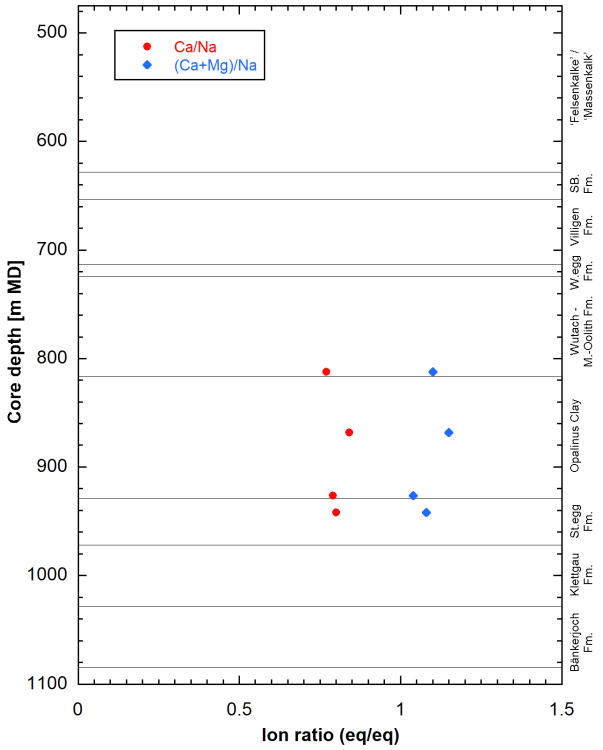

Fig. 4.5-3: Depth profiles of Ca/Na and (Ca+Mg)/Na ratios in Ni-en extracts

Tab. 4.5-3: Saturation indices of selected minerals and log(pCO_2) for Ni-en extract solutions (subsamples)

Calcite saturation was assumed in the calculations.

Sample ID	Depth	Formation	pH	logpCO_2 [log bar]	Gypsum	Celestite	Barite	Calcite	Dolomite (ord)	Dolomite (dis)	Strontianite
TRU1-1-AD	812.24	Wedelsandstein	8.38	-4.58	-1.48	-0.93	1.03	0.00	-0.28	-0.83	-0.71
TRU1-1-AD	812.24	Wedelsandstein	8.39	-4.41	-1.47	-0.41	1.08	0.00	-0.20	-0.75	-0.21
TRU1-2-AD	867.97	Opalinus Clay	8.28	-4.39	-1.58	-1.16	0.64	0.00	-0.30	-0.85	-0.85
TRU1-2-AD	867.97	Opalinus Clay	8.28	-4.54	-1.40	-0.92	0.82	0.00	-0.30	-0.85	-0.79
TRU1-4-AD	926.14	Opalinus Clay	8.35	-4.77	-1.27	-0.85	0.56	0.00	-0.37	-0.92	-0.85
TRU1-3-AD	941.80	Staffelegg Fm.	8.31	-4.48	-1.18	-0.67	1.03	0.00	-0.34	-0.89	-0.75
TRU1-3-AD	941.80	Staffelegg Fm.	8.31	-4.59	-1.17	-0.61	0.99	0.00	-0.31	-0.86	-0.71

4.6 Data from squeezing experiments

Martin Mazurek

A set of 6 samples from the interval «Brauner Dogger» – Staffelegg Formation were subjected to porewater squeezing. The mineralogical composition of the samples is listed in Tab. 4.6-1. All samples have clay-mineral contents > 40 wt.-%, except the one from the «Humphriesioolith Formation».

Tab. 4.6-1: Mineralogical composition of samples subjected to squeezing experiments

tr = trace, empty field = mineral not identified.

Depth [m]	**Formation**	**Member**	**S** [wt.-%]	**C(inorg)** [wt.-%]	**C(org)** [wt.-%]	**Quartz** [wt.-%]	**K-feldspar** [wt.-%]	**Plagioclase** [wt.-%]	**Calcite** [wt.-%]	**Dolomite / Ank.** [wt.-%]	**Siderite** [wt.-%]	**Pyrite** [wt.-%]	**Clay minerals** [wt.-%]
748.54	«Parkinsoni-Württembergica-Sch.»		1.15	2.92	0.68	19	3	2	24	tr		2.1	49
781.25	«Humphriesi-oolith Fm.»	«Blagdeni-Schichten»	0.56	3.25	0.58	28	3	2	26		1	1.0	38
826.39	Opalinus Clay	With silty calcareous beds	1.70	1.19	0.96	26	3	2	8		2	3.2	55
904.86	Opalinus Clay	Mixed clay-silt-carbonate	0.20	1.37	1.05	23	3	2	8	tr	4	0.4	59
941.54	Staffelegg Fm.	Rietheim Mb.	2.35	3.82	5.98	12	2	2	32	tr		4.4	42
959.22	Staffelegg Fm.	Frick Mb.	0.35	1.21	0.85	2	3	2	8	tr	2	0.7	81

4.6.1 Mass recovery

The water masses obtained by squeezing are listed in Tab. 4.6-2 and are shown graphically in Fig. 4.6-1 as a function of the squeezing pressure. The total mass recovery correlates with the initial water content of the sample (Fig. 4.6-2). The latter was measured at CRIEPI on the cut-off materials adjacent to the squeezed rock pieces. Samples from the «Brauner Dogger» and from the Opalinus Clay yielded first water aliquots at 200 MPa, while 300 MPa were needed for samples from the Staffelegg Formation. It is remarkable that sample 959.22 (Frick Member of the Staffelegg Formation) yielded limited amounts of water, in spite of the very high clay-mineral content. The total squeezed water mass corresponds to 11 – 17% of the total porewater in the sample.

Tab. 4.6-2: Water mass squeezed at different pressure steps

The initial water content was measured at CRIEPI on cut-off materials adjacent to the squeezed core, and this value was used here to calculate the initial mass of porewater in the sample. Squeezing was discontinued after 400 MPa for the two samples from the Opalinus Clay because sufficient water was obtained at lower pressures.

Depth [m]	**Formation**	**Initial sample mass (CRIEPI)** [g]	**Initial wet water content (CRIEPI)** [wt.-%]	**Mass of porewater prior to squeezing (CRIEPI)** [g]	**Mass squeezed at P =**						**Total mass squeezed** [g]	**Total mass squeezed** [% of total porewater]
					100 MPa [g]	**150 MPa** [g]	**200 MPa** [g]	**300 MPa** [g]	**400 MPa** [g]	**500 MPa** [g]		
748.54	«Parkinsoni-Württembergica-Sch.»	408.92	5.19	21.22			0.46	1.23	0.88	0.74	3.31	15.6
781.25	«Humphriesioolith Fm.»	420.54	5.10	21.45			0.16	1.19	1.09	1.26	3.70	17.2
826.39	Opalinus Clay	401.17	4.53	18.17			0.125	0.62	1.28		2.025	11.1
904.86	Opalinus Clay	407.60	4.43	18.06			0.199	0.97	0.96		2.129	11.8
941.54	Staffelegg Fm.	375.33	4.68	17.57				0.57	1.08	1.11	2.76	15.7
959.22	Staffelegg Fm.	365.16	4.14	15.12				0.21	0.75	0.97	1.93	12.8

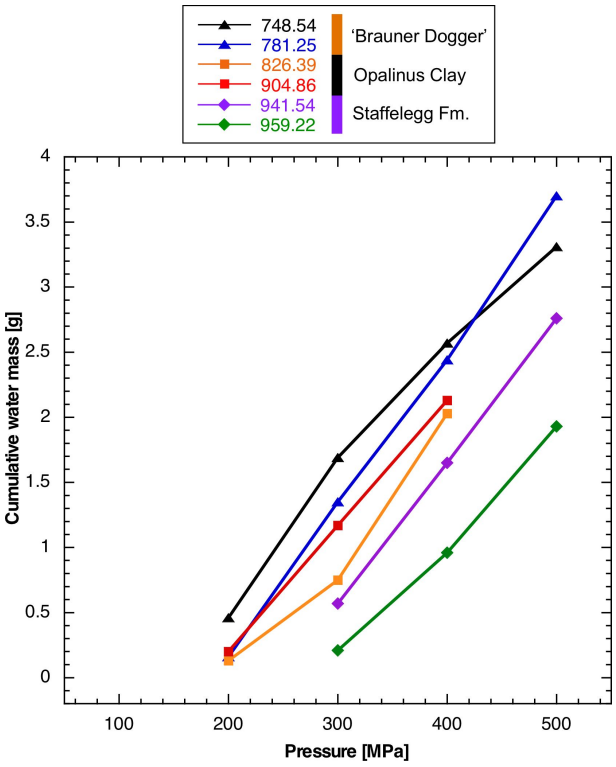

Fig. 4.6-1: Cumulative water mass obtained by squeezing as a function of the squeezing pressure

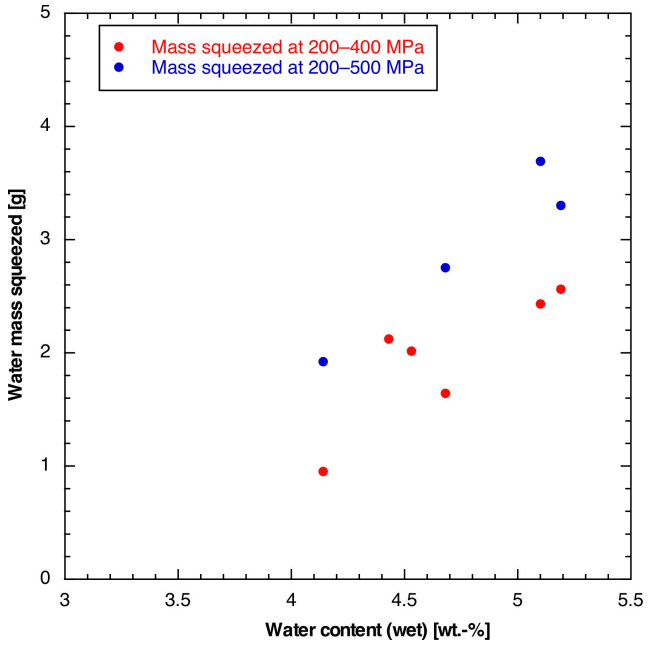

Fig. 4.6-2: Correlation of the original water content and total water mass obtained by squeeezing

4.6.2 Chemical composition of squeezed waters

Major-ion compositions of squeezed waters are listed in Tab. 4.6-3 and shown graphically as a function of squeezing pressure in Fig. 4.6-3. All waters are dominated by Na and Cl. The concentrations of monovalent ions (Na, K, Cl, Br, NO_3) generally decrease with squeezing pressure, likely due to ion-filtration effects that become important at higher pressures (Mazurek et al. 2015). Ca, Mg and Sr remain constant with pressure or increase slightly, which is considered to be due to the dissolution of carbonate minerals that becomes important at higher pressures. SO_4 concentrations increase slightly with pressure, even though mostly within analytical error. As discussed in Mazurek et al. (2015) and Rufer & Mazurek (2018), the composition of the first water aliquot recovered from a sample is considered to be closest to that of the porewater, and these analyses are highlighted by bold print in Tab. 4.6-3. F concentrations, in particular in the first squeezed aliquots, are contaminated by F leached from the fiberglass filters and so are not representative of the porewater. For clarity, the subset of the data that is considered to be useful for further interpretation is summarised in Tab. 4.6-4.

Tab. 4.6-3: Chemical composition of squeezed waters: full data set

Bold print indicates the selected ("best") aliquots. Italics refer to semi-quantitative analyses. F concentrations, in particular in the first squeezed aliquots, are contaminated by F leached from the fiberglass filters and so are not representative of the porewater. n.a. = no analysis. Aliquots squeezed at 500 MPa were not analysed because sufficient data were obtained for lower pressures.

Depth [m]	**Formation**	**Pressure** [MPa]	**Squeezing time** [d]	**Mass squeezed** [g]	**Na** [mg/L]	**K** [mg/L]	**Ca** [mg/L]	**Mg** [mg/L]	**Sr** [mg/L]	**F** [mg/L]	**Cl** [mg/L]	**Br** [mg/L]	**NO_3** [mg/L]	**SO_4** [mg/L]	**pH**	**TIC** [mg/L]	**TOC** [mg/L]	**TDS** [mg/L]	**Charge balance** [%]
748.54	«Parkinsoni-Württembergica-Sch.»	**200**	**2**	**0.46**	**4'573**	**71.5**	**750**	**204**	**34.7**	**10.8**	**7'627**	**8.1**	**14.18**	**1'060**	**n.a.**	**n.a.**	**n.a.**	**14'353**	**3.6**
		300	3	1.23	4'414	60.0	823	222	*36.1*	6.2	7'578	8.1	5.95	1'109	7.97	17.7	161.5	14'518	3.0
		400	2	0.88	3'578	36.9	824	232	*34.9*	3.7	6'485	7.1	2.43	1'093	8.23	< 50	148.7	12'450	2.7
781.25	«Humphriesioolith Fm.»	**200**	**2**	**0.16**	**5'495**	**94.6**	**932**	**250**	**36.6**	**8.6**	**9'200**	**9.4**	**12.07**	**1'241**	**n.a.**	**n.a.**	**n.a.**	**17'279**	**3.9**
		300	3	1.19	4'749	68.8	942	255	*35.6*	7.6	8'178	8.7	5.75	1'259	8.43	14.5	195.5	15'784	3.4
		400	2	1.09	4'457	56.8	916	244	*37.3*	4.1	7'818	8.0	3.29	1'287	8.50	15.2	147.6	15'061	2.5
826.39	Opalinus Clay	**200**	**3**	**0.13**	**4'798**	**81.5**	**809**	**223**	**33.3**	**14.7**	**7'997**	**7.6**	**13.24**	**1'063**	**n.a.**	**n.a.**	**n.a.**	**15'039**	**4.1**
		300[1]	2	0.62	4'443	58.7	935	245	36.9	9.9	7'655	7.3	8.20	1'165	n.a.	n.a.	n.a.	14'564	4.3
		400	2	1.28	4'188	43.4	892	236	*33.5*	4.5	7'245	6.9	5.72	1'211	8.29	*12.2*	163.4	14'095	3.5
904.86	Opalinus Clay	**200**	**3**	**0.20**	**4'566**	**74.8**	**823**	**207**	**26.1**	**12.4**	**7'456**	**6.4**	**9.29**	**1'269**	**n.a.**	**n.a.**	**n.a.**	**14'449**	**4.3**
		300[2]	2	0.97	4'540	54.1	974	212	*28.4*	7.9	7'564	6.7	5.13	1'530	7.20	< 25	253.8	15'181	3.9
		400	2	0.96	3'725	36.8	930	203	32.4	4.6	6'352	5.9	2.30	1'506	7.80	15.2	170.9	13'046	3.3
941.54	Staffelegg Fm.	**300**	**2**	**0.57**	**4'915**	**74.7**	**945**	**199**	**29.5**	**12.6**	**7'238**	**6.4**	**9.02**	**2'435**	**n.a.**	**n.a.**	**n.a.**	**15'865**	**4.5**
		400	2	1.08	4'536	54.2	990	223	*28.3*	5.5	6'814	6.2	5.23	2'529	8.40	*12.9*	233.7	15'496	4.0
959.22	Staffelegg Fm.	**300**	**2**	**0.21**	**3'360**	**46.4**	**333**	**69**	**< 10**	**17.2**	**4'163**	**3.8**	**8.43**	**1'737**	**n.a.**	**n.a.**	**n.a.**	**9'738**	**4.6**
		400	2	0.75	3'513	42.6	378	72	14.0	9.6	4'295	4.3	4.66	2'035	8.71	< 25	132.6	10'501	4.3

[1] Contains some white solid

[2] Contains some reddish solid

Tab. 4.6-4: Chemical composition of squeezed waters: summary of selected analyses to be used for interpretation

Due to the limited sample masses, no data are available for pH, TIC and TOC of the aliquots obtained at the lowest pressure. Data obtained from aliquots squeezed at higher pressures are listed in Tab. 4.6-3.

Depth [m]	**Formation**	**Pressure** [MPa]	**Squeezing time** [d]	**Na** [mg/L]	**K** [mg/L]	**Ca** [mg/L]	**Mg** [mg/L]	**Sr** [mg/L]	**Cl** [mg/L]	**Br** [mg/L]	**NO_3** [mg/L]	**SO_4** [mg/L]
748.54	«Parkinsoni-Württ.-Sch.»	200	2	4573	71.5	750	204	34.7	7'627	8.1	14.18	1'060
781.25	«Humphriesioolith Fm.»	200	2	5495	94.6	932	250	36.6	9'200	9.4	12.07	1'241
826.39	Opalinus Clay	200	3	4798	81.5	809	223	33.3	7'997	7.6	13.24	1'063
904.86	Opalinus Clay	200	3	4566	74.8	823	207	26.1	7'456	6.4	9.29	1'269
941.54	Staffelegg Fm.	300	2	4915	74.7	945	199	29.5	7'238	6.4	9.02	2'435
959.22	Staffelegg Fm.	300	2	3360	46.4	333	69	<10	4'163	3.8	8.43	1'737

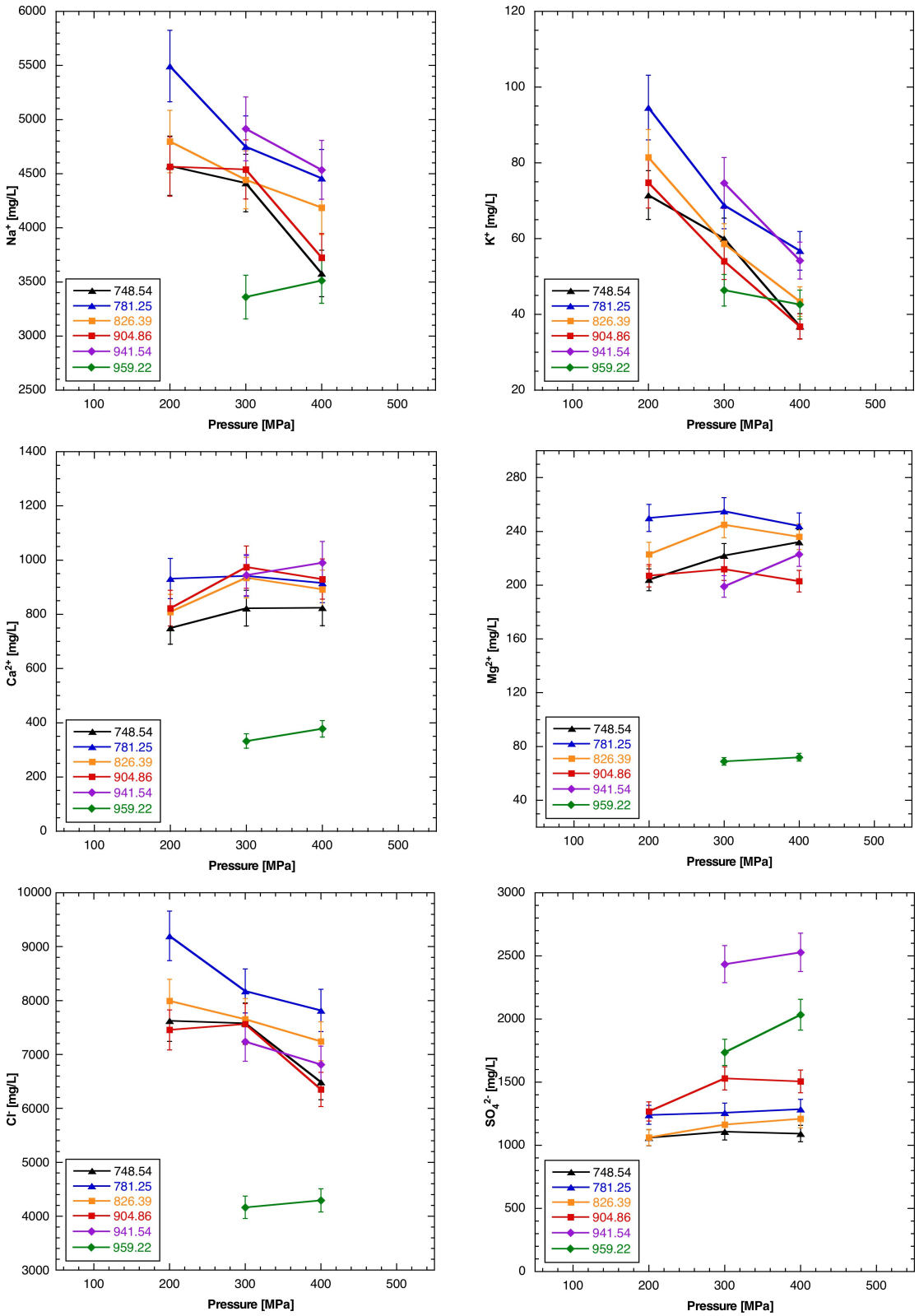

Fig. 4.6-3: Ion concentrations in squeezed waters as a function of squeezing pressure

Bars indicate analytical errors of ion-chromatography analysis.

4.6.3 Depth trends

Considering only the selected aliquots of each sample (Tab. 4.6-4), depth trends are illustrated in Fig. 4.6-4.

- Na, K, Mg, Sr, Cl and Br show their maximum concentrations in the «Brauner Dogger», with slightly decreasing values with depth. Substantially lower concentrations are observed in the lowermost sample at the base of the Staffelegg Formation.
- SO_4 concentrations are higher in the Staffelegg Formation in comparison with those in the overlying units.
- The molar ratio Br/Cl shows a decrease with depth, with a minimum at the base of the Opalinus Clay and a limited increase in the underlying Staffelegg Formation. All values are substantially below the modern seawater range of 1.52E-3 – 1.60E-3.
- The molar ratio SO_4/Cl lies around the value of modern seawater (about 0.0515) in the «Brauner Dogger» and the Opalinus Clay but then shows a substantial increase with depth in the Staffelegg Formation.

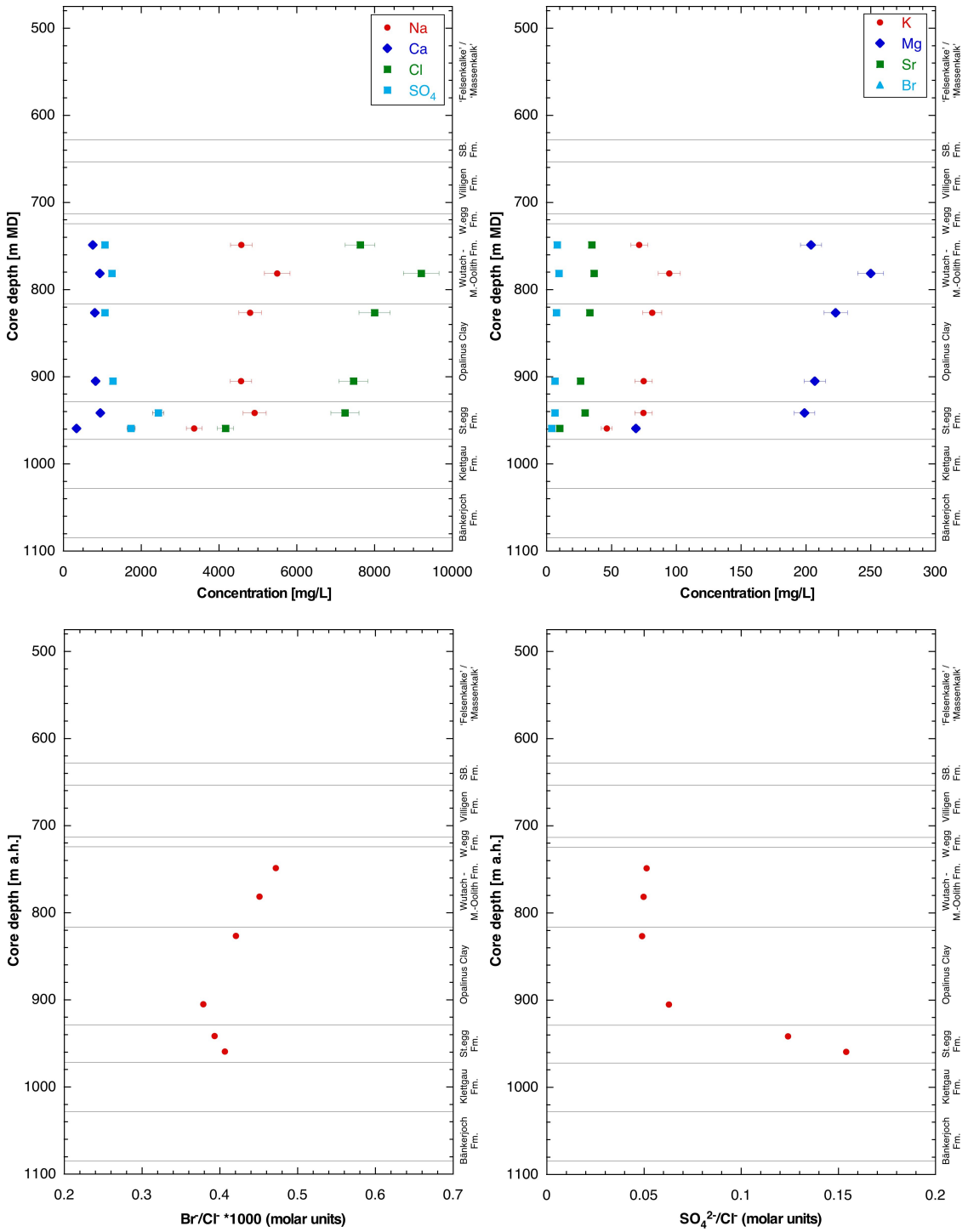

Fig. 4.6-4: Depth trends of ion concentrations and ion ratios in squeezed waters

Only the selected aliquots are shown for each sample. Bars indicate analytical errors of ion-chromatography analysis.

4.6.4 Geochemical modelling and mineral saturation states

Mineral saturation indices for squeezed waters were calculated using PHREEQC Version 3 and the PSI/Nagra thermodynamic data base (Thoenen et al. 2014) and are shown in Tab. 4.6-5.

- Squeezed waters are strongly oversaturated with respect to calcite and dolomite, a feature already known from previous studies (e.g. Mazurek et al. 2015). The oversaturation is possibly due to the fact that mineral solubility at high pressures during squeezing is higher than at atmospheric pressure. Further, outgassing of CO_2 during the squeezing process increases the pH and the saturation indices of calcite and dolomite (Tournassat et al. 2015). Further outgassing may take place into the headspace of the sample vials. The comparatively low calculated P_{CO2} suggest that some outgassing may have taken place, which also affects pH. However, this nevertheless does not markedly affect the obtained major-ion composition due to the large buffering capacity of the rock-water system in clay-rich lithologies. Last, lattice defects in carbonate minerals induced by deformation during squeezing might increase the solubility of these minerals. On the other hand, outgassing into the external atmosphere during sample storage in glass vessels is not considered to contribute to the low P_{CO2}. Such a process should also be seen by higher δ values of water isotopes, which is not the case (see Section 5.7).
- The waters are close to saturation with respect to strontianite for 3 out of 5 samples, and to celestite (except for the lowermost 2 samples).
- The waters are undersaturated with respect to gypsum, with the exception of sample 941.54 (Staffelegg Formation), which is close to saturation.
- Using the data from Tab. 4.6-3, squeezed waters are strongly oversaturated with respect to fluorite, which is a consequence of the contamination of F concentrations by the filter material. Therefore, no F data are listed in Tab. 4.6-4.

Tab. 4.6-5: Mineral saturation indices for squeezed waters

Depth [m]	**Formation**	**Pressure** [MPa]	**pH**	**TIC** [M]	**log(P_{CO2})**	**SI Calcite**	**SI Dolomite (ordered)**	**SI Dolomite (disordered)**	**SI Strontianite**	**SI Gypsum**	**SI Anhydrite**	**SI Celestite**	**SI Fluorite**
748.54	«Parkinsoni-Württem-bergica-Sch.»	200								-0.45	-0.67	-0.07	1.36
		300	7.97	1.50E-03	-3.20	0.81	1.38	0.83	-0.10	-0.40	-0.62	-0.04	0.91
		400	8.23							-0.39	-0.61	-0.05	0.46
781.25	«Humphriesi-oolith Fm.»	200								-0.34	-0.56	-0.03	1.21
		300	8.43	1.23E-03	-3.79	1.19	2.14	1.59	0.22	-0.32	-0.54	-0.02	1.11
		400	8.50	1.28E-03	-3.84	1.26	2.28	1.73	0.32	-0.31	-0.53	0.02	0.57
826.39	Opalinus Clay	200								-0.44	-0.65	-0.10	1.64
		300								-0.34	-0.56	-0.03	1.35
		400	8.29	1.03E-03	-3.70	0.98	1.71	1.16	0.00	-0.34	-0.55	-0.04	0.65
904.86	Opalinus Clay	200								-0.35	-0.56	-0.13	1.51
		300	7.20							-0.22	-0.43	-0.03	1.18
		400	7.80	1.28E-03	-3.09	0.62	0.91	0.36	-0.39	-0.22	-0.43	0.05	0.71
941.54	Staffelegg Fm.	300								-0.05	-0.27	0.16	1.55
		400	8.40	1.09E-03	-3.80	1.09	1.87	1.32	0.00	-0.02	-0.24	0.16	0.84
959.22	Staffelegg Fm.	300								-0.49	-0.71	-0.29	1.51
		400	8.71							-0.39	-0.61	-0.10	1.03

4.6.5 Water content and aqueous extraction of squeezed core material

After the squeezing experiment, each core was dried at 105 °C, from which the mass of water remaining in the sample was obtained. The dry core was then subjected to aqueous extraction, from which the mass of Cl remaining in the sample could be calculated. The results are summarised in Tab. 4.6-6. Given the fact that oven-drying was performed with air, some degree of rock oxidation occurred. Therefore, results are only given for the conservative constituents Cl and Br.

Tab. 4.6-6: Water contents and results of aqueous-extraction tests on previously squeezed samples

Depth [m]	**Formation**	**Water content (wet) of squeezed sample** [wt.-%]	**Mass of porewater in squeezed sample** [g]	**Aqueous extraction of squeezed sample**				
				Mass of dry rock [g]	**Mass of added water** [g]	**S/L** [g/g]	**Cl** [mg/$L_{extract\ solution}$]	**Br** [mg/$L_{extract\ solution}$]
748.54	«Parkinsoni-Württembergica-Sch.»	3.68	14.94	30.07	30.09	0.999	123	0.09
781.25	«Humphriesioolith Fm.»	3.88	16.16	30.04	30.09	0.998	151	0.12
826.39	Opalinus Clay	3.81	15.20	30.14	30.04	1.003	145	0.09
904.86	Opalinus Clay	3.94	15.98	30.18	30.11	1.003	122	0.08
941.54	Staffelegg Fm.	3.19	11.88	30.06	30.12	0.998	96	0.02
959.22	Staffelegg Fm.	3.59	13.04	30.19	30.05	1.004	59	0.05

4.6.6 Chloride-accessible porosity

Combining the data for squeezed waters (Tab. 4.6-3) and for the samples after squeezing (Tab. 4.6-6) permits the reconstruction of the total Cl and water inventories, therefore also the Cl concentrations in the bulk porewater. Assuming that the squeezed water represents the composition of the anion-accessible water, the Cl-accessible porosity fraction f_{Cl} can be calculated. The formalism is detailed in Mazurek et al. (2021).

The volume of the water remaining in the sample after squeezing is obtained from the water content of the squeezed core, assuming a porewater density of 1 g/cm^3. Note that the formalism also assumes that the dead volume of the squeezing system is negligible. While the dead volume is indeed likely small, a sensitivity calculation was performed on its impact. Assuming a dead volume of 1 mL results is an anion-accessible porosity fraction that is 0.01 – 0.04 higher than the value without consideration of a dead volume. The most strongly expressed shift is found in samples where only a small water volume was squeezed, while it becomes insignificant for samples with a good water yield.

The Cl-accessible porosity fraction is finally obtained from:

$$f_{Cl} = \frac{C_{Cl\ in\ bulk\ pore\ water}}{C_{Cl\ in\ squeezed\ water}}$$

The resulting Cl-accessible porosity fractions are listed in Tab. 4.6-7 and shown as a function of the clay-mineral content in Fig. 4.6-5. The mean value for f_{Cl} is 0.45, which is slightly lower than existing data from Mont Terri (Pearson et al. 2003) and Schlattingen-1 (Mazurek et al. 2015).

Tab. 4.6-7: Cl-accessible porosity fractions derived from squeezing and aqueous-extraction experiments

Depth [m]	**Formation**	**Cl-accessible porosity fraction f_{Cl}** [-]
748.54	«Parkinsoni-Württembergica-Schichten»	0.48
781.25	«Humphriesioolith Formation»	0.44
826.39	Opalinus Clay	0.51
904.86	Opalinus Clay	0.46
941.54	Staffelegg Formation	0.44
959.22	Staffelegg Formation	0.40

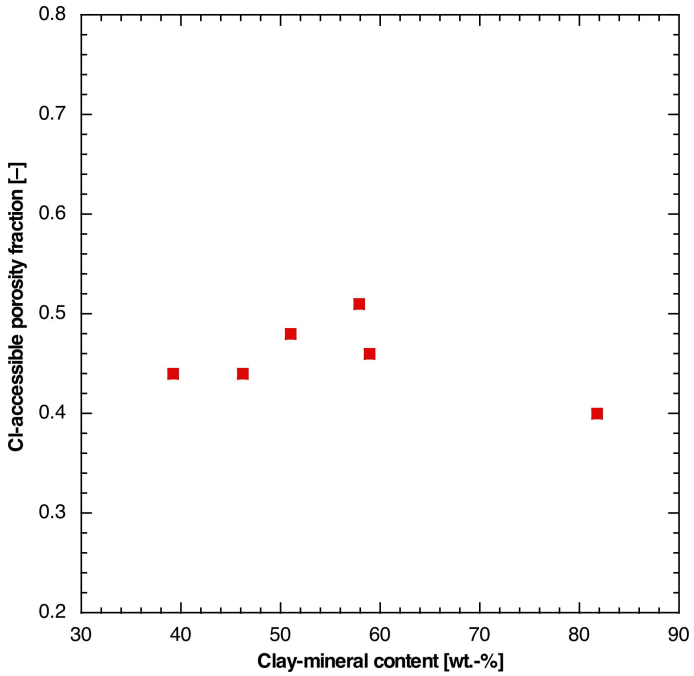

Fig. 4.6-5: Cl-accessible porosity fractions derived from squeezing experiments as a function of the clay-mineral content

4.6.7 Stable isotopic composition of squeezed water

Results of stable water-isotope analyses are listed in Tab. 4.6-8 and shown as a function of depth in Fig. 4.6-6. Note that due to the frequently limited masses of water aliquots obtained at the lowest pressure, data on water isotopes could sometimes only be produced for aliquots squeezed at higher pressures. In any case, data for the lowest available pressure were selected for further considerations (bold in Tab. 4.6-8). The following observations can be made:

- Within any sample, the variation of the δ values with squeezing pressure is small (typically within analytical error). In most cases, the δ values become marginally more negative with increasing pressure. This has already been observed in previous studies, and a discussion is provided in Mazurek et al. (2015).
- Both $\delta^{18}O$ and $\delta^{2}H$ decrease systematically with depth, with a gradient that becomes steeper with depth.
- In a plot $\delta^{18}O$ vs. $\delta^{2}H$ (Fig. 4.6-7), the shallower samples are located on the right side of the global ($\delta^{2}H = 8\ \delta^{18}O + 10$) and the local ($\delta^{2}H = 7.55\ \delta^{18}O + 4.8$) meteoric water lines. With increasing depth, the data come closer to the meteoric water lines, and the deepest sample from the base of the Staffelegg Formation is located on the left of the meteoric water lines.
- The same information can also be illustrated by the depth trend of deuterium excess ($\delta^{18}O - 8\ \delta^{2}H$), which increases systematically with depth (Fig. 4.6-8).

Tab. 4.6-8: Stable isotopic composition of squeezed waters

The aliquots selected for interpretation are shown in bold.

Depth [m]	**Formation**	**Pressure** [MPa]	**$\delta^{18}O$** [‰ VSMOW]	**$\delta^{2}H$** [‰ VSMOW]	**D excess** [‰]
748.54	«Parkinsoni-Württembergica-Sch.»	**200** 300 400	**-4.58** -4.46 -4.71	**-42.4** -41.9 -42.9	**-5.8** -6.2 -5.2
781.25	«Humphriesioolith Fm.»	**300** 400	**-4.66** -4.80	**-41.9** -42.5	**-4.6** -4.2
826.39	Opalinus Clay	**400**	**-5.24**	**-43.0**	**-1.0**
904.86	Opalinus Clay	**300** 400	**-6.40** -6.50	**-45.8** -46.3	**5.4** 5.7
941.54	Staffelegg Fm.	**300** 400	**-7.39** -7.42	**-50.1** -50.6	**9.0** 8.8
959.22	Staffelegg Fm.	**400**	**-8.50**	**-55.2**	**12.8**

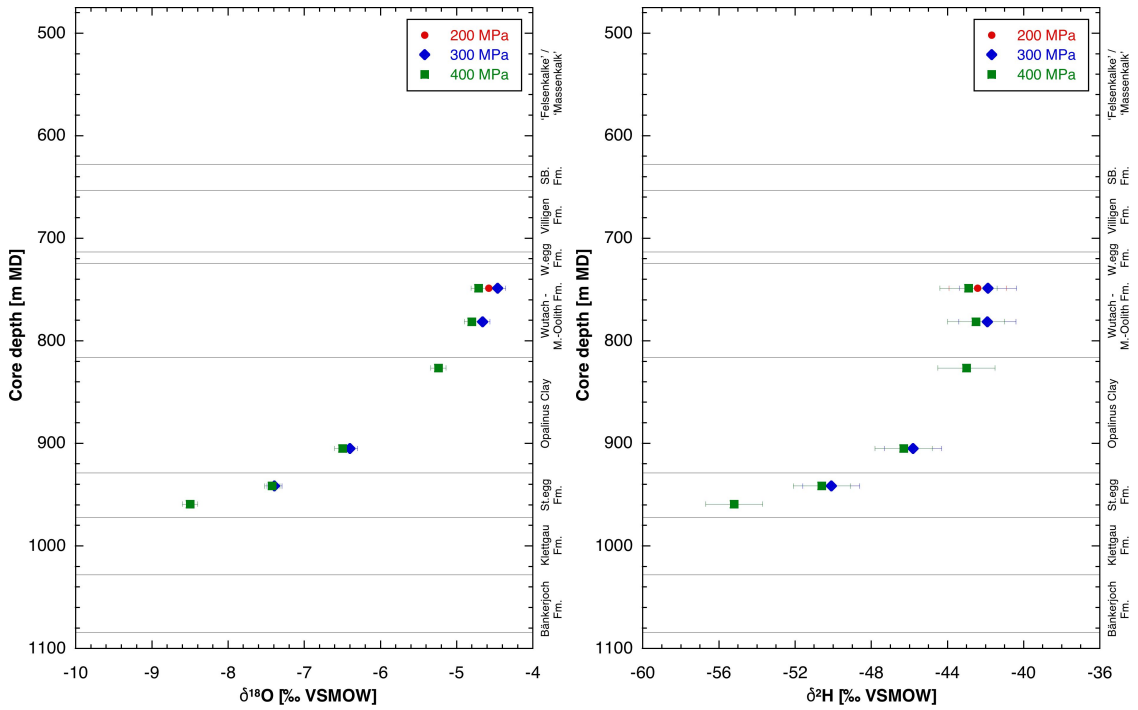

Fig. 4.6-6: Depth trends of $\delta^{18}O$ and $\delta^{2}H$ in squeezed waters

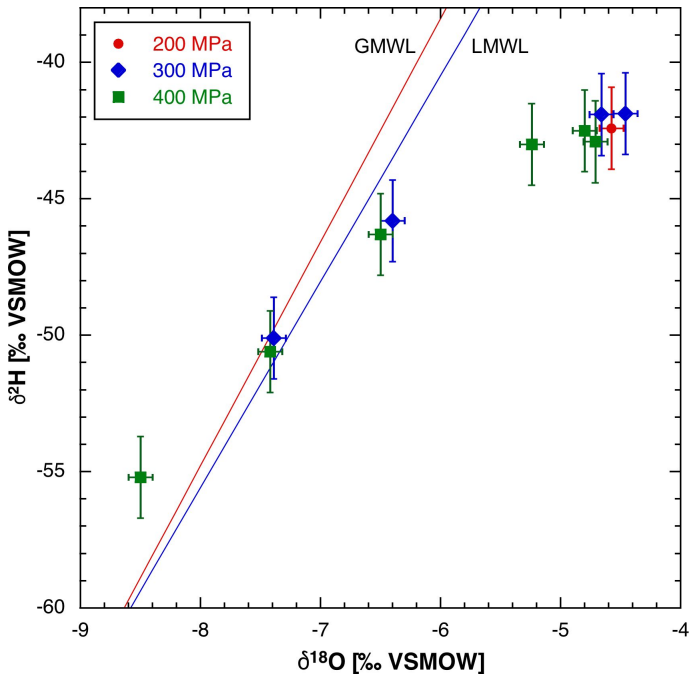

Fig. 4.6-7: Plot of $\delta^{18}O$ vs. $\delta^{2}H$ for squeezed waters

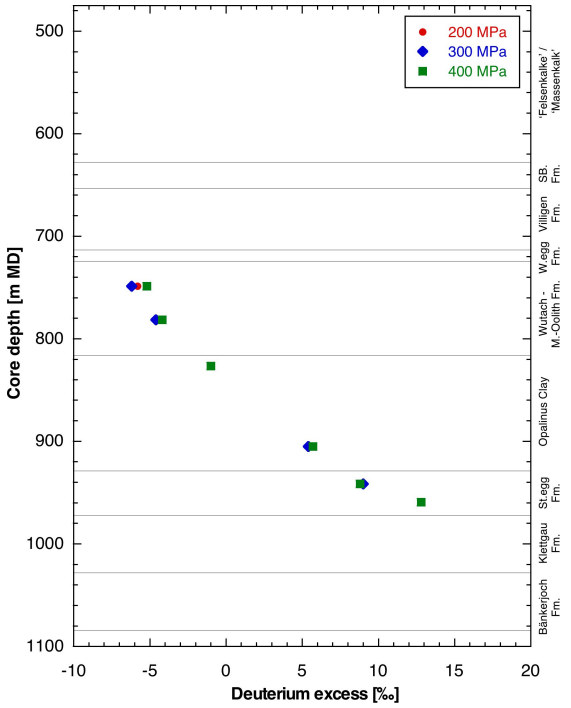

Fig. 4.6-8: Depth trend of deuterium excess

4.7 Data from advective displacement experiments

Mirjam Kiczka, Andreas Jenni, Urs Mäder & H.-Niklaus Waber

Advective displacement (AD) experiments are a methodology for a comprehensive physico-chemical characterisation, including porewater chemistry and certain transport properties (details in method report, Waber ed. 2020). This section presents summary data, and details where important, with short comments. The full data sets are provided in Appendix D. Integration of the data into context and depth profiles is included in Chapter 5.

Four samples from the clay-rich Dogger units were processed. One experiment failed (distinct leak of confining fluid into the core assembly and out of the outflow capillary) and yielded only data from pre-characterisation. The other three experiments were successful and were subjected to a similar analytical programme, with differences mainly related to the duration of an experiment (number of sampled fluid aliquots) and to the extent of post-mortem characterisation. The programme fulfilled the planned work, but only one experiment (Wedelsandstein Formation) was monitored long enough to achieve a full breakthrough of anions. The duration of the percolation period was 20 – 90 days, transporting 0.2 – 2.8 pore volumes of fluid. The analytical programme for post-mortem analysis was reduced compared to the one for Bülach-1-1, i.e. comprising only water-content measurements but no aqueous extracts and no CEC/cation-selectivity measurements were performed.

4.7.1 Sample material and overview of analytical work

The sample cores of the three successful experiments (Fig. 4.7-1) are all from the Dogger, covering the interval at 812 – 926 m depth. One core is from the Wedelsandstein Formation («Brauner Dogger») and two cores are from the Opalinus Clay. The experiment in the Staffelegg Formation (942 m) was not successful but yielded data from pre-characterisation.

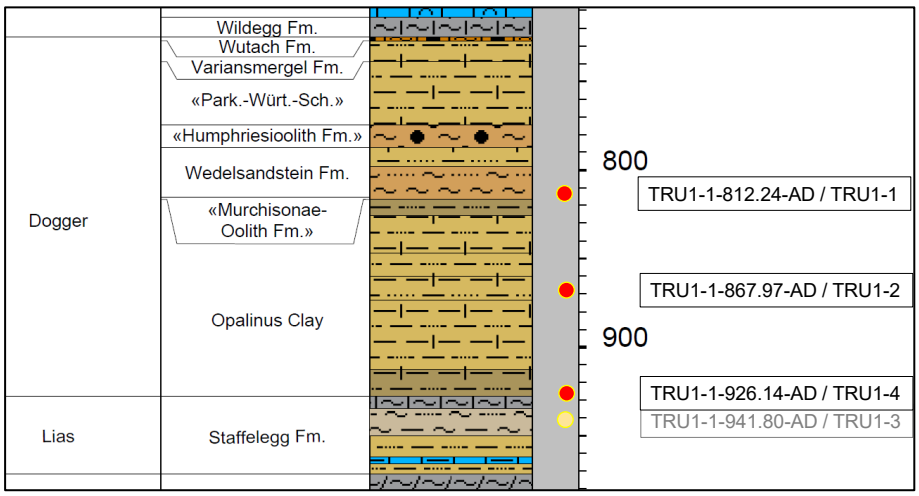

Fig. 4.7-1: Location of samples used for advective displacement experiments (red dots)

Short labels are consecutively numbered laboratory abbreviations. Sample TRU1-1941.80-AD (yellow dot) was not successful and was aborted.

X-ray computed tomography (CT) was performed on a medical scanner (Waber ed. 2020) for sample selection (Fig. 4.7-2), detection of disturbing features (fractures, pyrite concretions, macro-fossils etc.). Dry cutting was used for obtaining a central core segment for AD experiments, and adjacent 1 or 2 discs for accompanying characterisation (green in Fig. 4.7-2). The central core segment (yellow in Fig. 4.7-2) was turned on a lathe to 80 mm diameter.

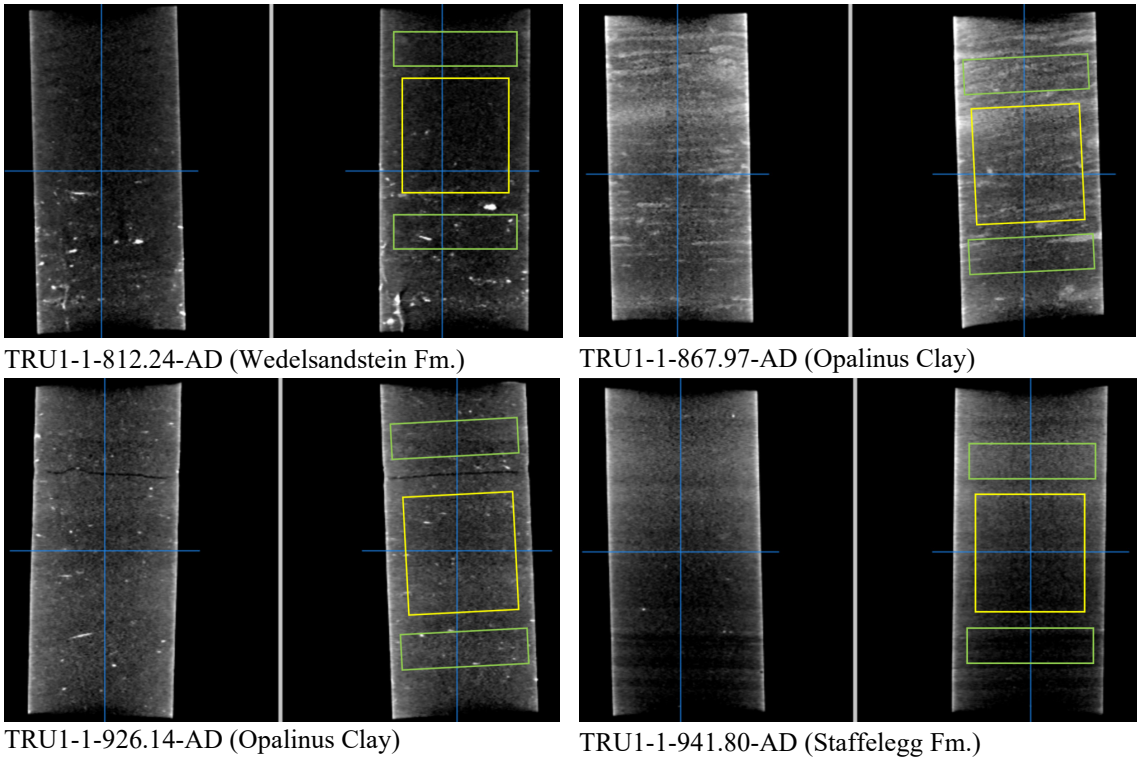

Fig. 4.7-2: X-ray CT images of AD samples

Central sections parallel to core axis at right angle. Grey scale range setting is 1'700 – 2'500 HU. Yellow segments are used for advective displacement, green segments for pre-characterisation. Darker grey (low X-ray absorbance) represents clay/quartz-rich sections, slightly lighter grey indicates carbonate-richer parts, siderite is brighter, and pyrite is white (strongest absorbance). Black lines/gaps represent fractures.

Tab. 4.7-1 lists all analytical work performed on the four samples. Samples taken during abrasion of outermost 7.5 mm on a lathe during trimming of cores for the AD experiments are related to an upcoming study of drilling fluid contamination.

Tab. 4.7-1: Summary of analytical work perfomed on samples for advective displacement experiments

Parameter	**TRU1-1**	**TRU1-2**	**TRU1-4**	**TRU1-3**
Sample ID RWI	TRU1-1-812.24-AD	TRU1-1-867.97-AD	TRU1-1-926.14-AD	TRU1-1-941.80-AD
Lab sample ID	TRU1-1xx-AD	TRU1-2xx-AD	TRU1-4xx-AD	TRU1-3xx-AD
Depth [m]	812.24	867.97	926.14	941.80
Geol. unit	Wedelsandstein Fm.	Opalinus Clay	Opalinus Clay	Staffelegg Fm.
AD_exp	y	y	y	n
Pre_WC	2+2	2+2	1+1	2+2
Pre_M	y	y	y	y
Pre_V,A,L	y	y	y	y
Pre_Min	1+1	2+2	n	1+1
Pre_Clay	1+1	2+2	n	1+1
Pre_AqEx	2+2	2+2	1+1	2+2
Pre_Ni-en	1+1	1+1	ave	1+1
Post_WC	5	5	5	na
Post_M	y	y	y	na
Post_V,A,L	y	y	y	na
Post_AqEx	n	n	n	na
Post_Ni-en	n	n	n	na
Abras_Drilling_Fl	5	5	n	5

y = yes = done; n = no = not done; integer numbers refer to the number of samples processed; +: samples from above (left number) and below (right number) a core were processed; 2: duplicate samples; Pre: sample pre-characterisation; Post: post-mortem characterisation; WC: water content; M: mass; V,A,L: core volume, sectional area and length; Min: mineralogy; Clay: clay mineralogy; AqEx: aqueous extracts; Ni-en: cation selectivity with Ni-en method; Post_WC: post-mortem water content determined along a profile with 5 segments; AD_exp: complete analysis of fluid sample aliquots collected during advective displacement; Abras_Drilling_Fl: samples taken during abrasion of outermost 7.5 mm on a lathe during trimming of cores.

4.7.2 Conditions of advective displacement experiments

Sample preparation was performed according to Waber (ed.) (2020). The overview table (Tab. 4.7-2) presents some experiment specific parameters such as sample processing dates, storage time and other characteristic times like arrival of first fluid drop and its electric conductivity. A single layer of PEEK fabric filter was used below and above the core, as detailed in Waber (ed.) (2020). Numbers of samples taken and analysed are listed as well as average pressures for confining and injection. The number of pore volumes percolated are based on the water content determined from pre-characterisation. Confining pressure was set to 58 to 60 bar, pressurised by Ar on water. Average pressure for the infiltration of the artificial porewater (APW) was set by He to ~ 48 bar for TRU1-4 and initially also for the TRU1-1 experiment. Due to the high hydraulic conductivity of the TRU1-1 core, the infiltration pressure was reduced after one day to ~ 29 bar for this experiment and the TRU1-2 experiment that infiltrated from the same APW tank. The hydraulic gradients are large with around 350 m_{H2O}/m in TRU1-1 and TRU1-2 experiments and almost 6'000 m_{H2O}/m for the TRU1-4 experiment (sample dimensions are in

Tab. 4.7-4). Experiments 1 and 2 started within a week after sample delivery, while the core for experiment TRU1-4, which replaced the failed TRU1-3 experiment, was stored for 73 days at University of Bern in cold storage prior to preparation. The time until arrival of a first fluid drop at the electric conductivity cell (outflow, before sampling syringe) ranged from less than 1 day (Wedelsandstein Formation) to 17 days (Opalinus Clay, 867.97 m) after start of infiltration.

Tab. 4.7-2: Conditions of advective displacement experiments

Parameter	**TRU1-1**	**TRU1-2**	**TRU1-4**	**TRU1-3**
Depth [m]	812.24	867.97	926.14	941.80
Geol. unit	Wedelsandstein Fm.	Opalinus Clay	Opalinus Clay	Staffelegg Fm.
Drilled	24.11.2019	11.12.2019	15.12.2019	15.12.2019
Delivered	02.12.2019	16.12.2019	23.12.2019	23.12.2019
Prep_AD	05.12.2019	19.12.2019	05.03.2020	07.01.2020
Injection	07.12.2019	20.12.2019	06.03.2020	AD experiment failed
First drop	08.12.2019 00:38	07.01.2020 01:46	09.03.2020 20:00	na
Days to first drop	0.6	17.4	3.2	na
Initial gas [mL]	0.0	0.9	0.0	na
End_AD	05.03.2020 08:40	19.03.2020 08:35	26.03.2020 07:45	na
Duration [d]	88.9	89.7	19.7	failed
Pore-volumes	2.8	0.2	0.2	na
EC_initial (25 °C) (max. in 1st 24 h) [mS/cm]	31.6	23.5	26.7	na
Filter	PEEK	PEEK	PEEK	PEEK
AD-samples	17	5	6	0
AD-samp_chem	15	4	5	0
AD-samp_isotopes	15	4	5	0
in-line pH	4	3	3	0
P_Conf [bar]	60	58	60	na
P_Inf [bar]	30	29	48	na
Gradient [m_{H2O}/m]	3584	3486	5863	na

4.7.3 Mineralogy and petrophysical properties

Mineralogy was determined on subsamples cut adjacent to the core segment used for the AD experiments (Tab. 4.7-1). Averaged values for subsamples (Tab. 4.7-3) are plotted in Section 4.2 and cover a range of clay contents from 18 – 41 wt.-%, calcite contents of 12 – 34 wt.-%, and quartz contents of 12 – 53 wt.-%. All samples contain pyrite, between 0.8 – 3.3 wt.-%. The dominant clay minerals are illite (30 – 33 wt.-% of clay fraction), illite/smectite mixed layers (26 – 50 wt.-% of clay fraction), and kaolinite (9 – 32 wt.-% of clay fraction). The ratio of (illite/smectite+smectite)/(total_clay) spans a range from 0.27 to 0.5.

Included are also carbon, nitrogen and sulphur analysis. Pyrite contents are moderately low because pyrite-rich lithologies were avoided based on X-ray CT characterisation (Fig. 4.7-2). More details, including end-member clays, are included in Appendix D.

Tab. 4.7-3: Mineralogy of advective displacement samples, including C, N and S analyses

Average values of subsamples (see text); b.d.: below detection limit.

Parameter	**Unit**	**TRU1-1**	**TRU1-2**	**TRU1-3**
Depth	[m]	812.24	867.97	941.80
Geological unit		Wedelsandstein Fm.	Opalinus Clay	Staffelegg Fm.
S	[wt.-%]	0.4	0.4	1.8
C(inorg)	[wt.-%]	1.8	2.8	4.4
C(org)	[wt.-%]	0.5	0.9	5.0
N	[wt.-%]	b.d.	0.1	0.1
Quartz	[wt.-%]	53	27	12
K-feldspar	[wt.-%]	8	5	3
Plagioclase	[wt.-%]	5	3	2
Calcite	[wt.-%]	12	22	34
Dolomite / Ankerite	[wt.-%]	3	1	4
Siderite	[wt.-%]	b.d.	2	b.d.
Anhydrite	[wt.-%]	b.d.	b.d.	b.d.
Celestite	[wt.-%]	b.d.	b.d.	b.d.
Pyrite	[wt.-%]	1	1	3
Clay minerals	[wt.-%]	18	41	38
Illite	[wt.-%]	6	13	13
Illite/smectite ML (85-90)	[wt.-%]	2	6	15
Illite/smectite ML (75-80)	[wt.-%]	6	3	1
Illite/smectite ML (50-70)	[wt.-%]	1	2	1
Illite/smectite ML (20-40)	[wt.-%]	b.d.	b.d.	0.7
Smectite	[wt.-%]	b.d.	b.d.	0.4
Kaolinite	[wt.-%]	1.6	13.0	4.0
Chlorite	[wt.-%]	1.0	0.9	1.3
Chl/Sm ML (85-95)	[wt.-%]	1.0	0.9	1.3
Total illite/smectite	[wt.-%]	8	11	19
(tot_ill/sm+sm)/(total_clay)		0.45	0.27	0.50
(tot_ill+ill/sm+sm)/(total_clay)		0.79	0.58	0.83

A plethora of petrophysical parameters may be derived from sample dimensions, mass, water content, and changes in these parameters determined before and after an AD experiment (Tab. 4.7-4). Derived quantities include porosity, bulk density, grain density, water uptake during the experiments, or unsaturated porosity (saturation ratio). The relationships are given in Waber

(ed.) (2020). Note that the water content determined for pre-characterisation is based on 2 – 4 subsamples adjacent to the AD core segment, but it is determined for post-mortem characterisation along a 5-sample profile of the entire AD core segment itself. Accounting for the usually observed slight core volume expansion during an AD experiment, one can derive a net water uptake (initially gas-filled porosity fraction) and a corrected initial water content.

Core volume is seen to increase by 1.1% for sample TRU1-4, whereas it remains constant for the others (the small negative volume changes of TRU1-1 and TRU1-2 are within measurement uncertainty; Tab. 4.7-4). Absolute water uptake of the cores ranges from 1.25 to 5.2 g. The net water uptake after accounting for any volume expansion reflects an initially small volume of unsaturated porosity, ranging from 0.5 to 3.7 mL, or a saturation ratio in the range 0.97 – 0.99 for TRU1-1 and TRU1-4 and 0.90 for TRU1-2. Thus, for the TRU1-1 and TRU1-4 experiments, the initial state can be considered saturated in agreement with negligible amounts of gas expelled at the beginning of the experiments, whereas a slightly undersaturated state for the TRU1-2 experiment agrees with notable higher initial gas release (i.e. 0.9 ml; Tab. 4.7-2).

Tab. 4.7-4: Core dimensions and derived petrophysical parameter

n.m.: not measured.

Parameter	**Unit**	**TRU1-1**	**TRU1-2**	**TRU1-4**	**TRU1-3**
Depth	[m]	812.24	867.97	926.14	941.80
Geol. unit		Wedelsandstein Fm.	Opalinus Clay	Opalinus Clay	Staffelegg Fm.
Pre_Core_M	[g]	**1'017.14**	**1'034.91**	**1'038.30**	**961.17**
Pre_Core_DM	[cm]	8.02	8.02	8.02	8.01
Pre_Core_L	[cm]	8.19	8.04	8.19	8.01
Pre_Core_A	[cm^2]	50.52	50.52	50.45	50.39
Pre_Core_V	[cm^3]	413.86	406.28	413.09	403.63
Post_Core_M	[g]	**1'018.39**	**1'037.72**	**1'043.48**	**n.m.**
Post_Core_DM	[cm]	8.02	8.01	8.02	n.m.
Post_Core_L	[cm]	8.19	8.04	8.27	n.m.
Post_Core_A	[cm^2]	50.47	50.44	50.50	
Post_Core_V	[cm^3]	413.41	405.36	417.79	
Delta_M	[g]	**1.25**	**2.82**	**5.18**	
Delta_Core_DM	[cm]	-0.004	-0.006	0.004	
Delta_Core_L	[cm]	-0.001	-0.006	0.085	
Delta_Core_A	[cm^2]	-0.047	-0.079	0.050	
Delta_Core_V	[cm^3]	**-0.450**	**-0.923**	**4.693**	
Delta_Core_V-%	[%]	-0.109	-0.227	1.136	
Pre_Bulk_WD	[g/cm^3]	**2.458**	**2.547**	**2.513**	**2.381**
Post_Bulk_WD	[g/cm^3]	**2.463**	**2.560**	**2.498**	
Delta_Bulk_WD	[g/cm^3]	0.006	0.013	-0.016	
Delta_Bulk_WD-%	[%]	0.232	0.501	-0.630	

Tab. 4.7-4: continued

Parameter	**Unit**	**TRU1-1**	**TRU1-2**	**TRU1-4**	**TRU1-3**
Pre_GD measured	[g/cm^3]	**2.688**	**2.699**		**2.566**
Pre_GD calulated	[g/cm^3]	2.650	2.682	**2.717**	2.546
Post_GD	[g/cm^3]	**2.664**	**2.711**	**2.712**	
Delta_GD*	[g/cm^3]	0.014	0.028	-0.005	
Corr_Pre_GD	[g/cm^3]	**2.652**	**2.684**	**2.708**	
Pre_WCw		**0.0475**	**0.0315**	**0.0471**	**0.0447**
Post_WCw		**0.0489**	**0.0344**	**0.0502**	
Delta_WCw		0.0014	0.0029	0.0030	
Corr_Pre_WCw		**0.0478**	**0.0318**	**0.0454**	
Pre_H2O_Core	[g]	**48.32**	**32.63**	**48.95**	**42.93**
Post_H2O_Core	[g]	**49.83**	**35.71**	**52.33**	
Delta_H2O_Core	[g]	1.52	3.08	3.39	
Corr_Pre_H2O_Core	[g]	**48.58**	**32.89**	**47.15**	
Unsat_Vol	[mL]	1.70	3.74	0.49	
Pore_Vol_tot	[mL]	50.28	36.64	47.64	
Sat_ratio		**0.97**	**0.90**	**0.99**	
Pre_Poro_WL		**0.1167**	**0.0803**	**0.1185**	**0.1064**
Post_Poro_WL		**0.1205**	**0.0881**	**0.1253**	
Delta_Poro_WL		0.0038	0.0078	0.0068	
Delta_Poro_WL-%	[%]	3.2553	9.6937	5.7212	
Corr_Pre_Poro_WL		**0.1174**	**0.0810**	**0.1141**	
Corr_Pre_Poro_tot		**0.1215**	**0.0902**	**0.1153**	

L = length; _A = area; _V = volume; _M = mass; WD = wet density; GD = grain density; WCw = water content rel. to wet mass; _WL = water loss; Delta_GD* calculated with measured data if available, Pre: sample pre-characterisation; Post: post-mortem characterisation; Delta: difference between Pre and Post values; Corr: corrected

There are significant differences in water content measured in adjacent samples (pre-characterisation) and in the core itself (post-mortem) of 3 – 10%, even when accounting for core expansion (Fig. 4.7-3). This leads to different values of bulk wet density, water-loss porosity and grain density (assuming saturated conditions) derived from pre-characterisation and post-mortem data. This spread is significantly larger than measurement uncertainties and illustrates that the largest contribution to uncertainty is sample heterogeneity for parameters that depend on water content. In contrast, measurements on replicate samples agree well within measurement uncertainty. Differences in water content commonly correlate with differences in clay content, such that this heterogeneity is mainly an issue of lamination in fine-grained sediments.

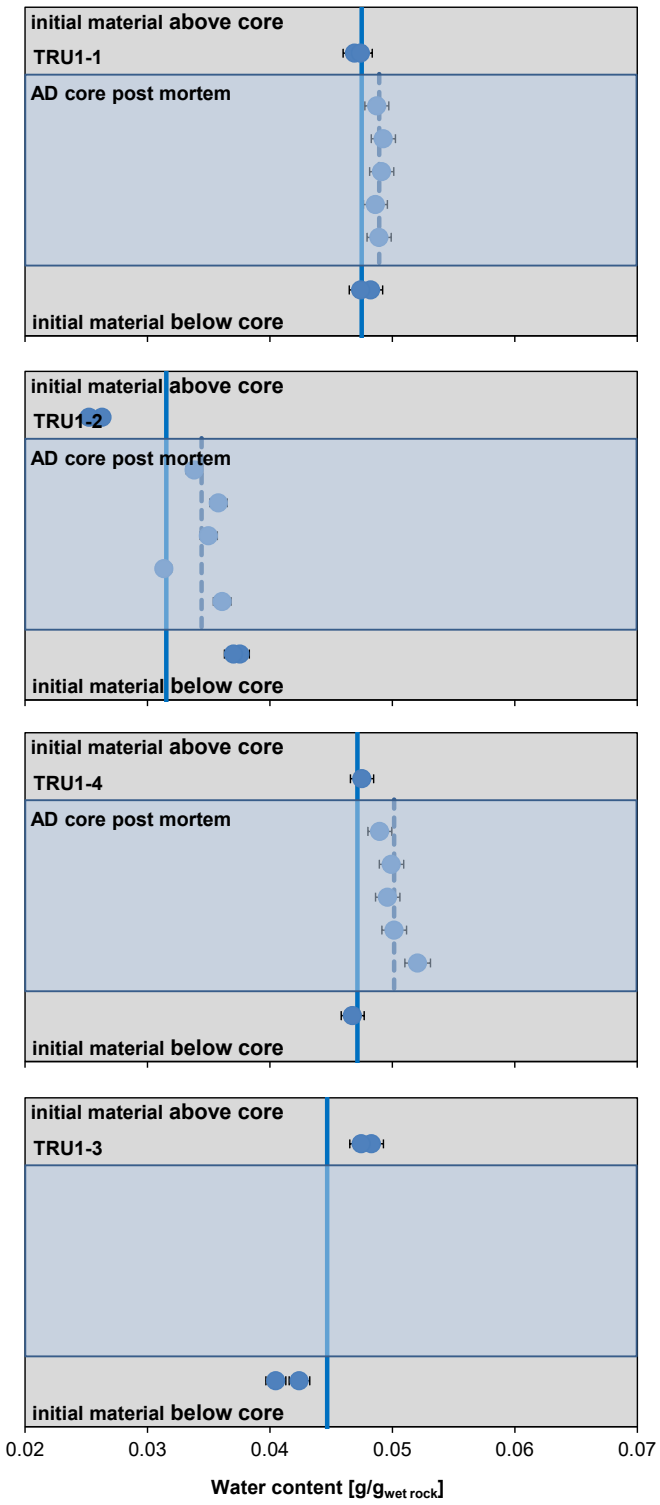

Fig. 4.7-3: Details of water content measurements before and after AD experiments

TRU1-1 = 812.24 m (Wedelsandstein Fm.); TRU1-2 = 867.97 m (Opalinus Clay); TRU1-4 = 926.14 m (Opalinus Clay); TRU1-3 = 941.80 m (Staffelegg Fm.); Average values are indicated for pre-characterisation (solid line) and post-mortem characterisation (dashed line). Error bars refer to measurement uncertainty of 2%.

4.7.4 Aqueous extracts, CEC and cation selectivity of AD samples

Aqueous extracts, CEC and cation selectivity determinations were carried out on all AD samples during pre-characterisation. No post-mortem analyses were performed. Detailed analyses are provided in Appendix D. Methods are the same as used for other core samples (Waber ed. 2020), with the exception of sample masses that may have been smaller than used for regular core sample analysis. Averaged data – also used for integrative data plots – are presented in this section. Averaging refers to duplicates (except for TRU1-4) and to measurements performed on pieces above and below the segment used for the AD experiments (indicated in Fig. 4.7-2 and Tab. 4.7-5).

Tab. 4.7-5: Average composition of aqueous extract solutions from pre-characterisation

The full data set is provided in Appendix D.

Parameter	**Unit**	**TRU1-1**	**TRU1-2**	**TRU1-4**	**TRU1-3**
Depth	[m]	812.24	867.97	926.14	941.80
Geol. unit		Wedelsandstein Fm.	Opalinus Clay	Opalinus Clay	Staffelegg Fm.
averaging		top+base (2+2)	top+base (2+2)	top+base (1+1)	top+base (2+2)
$1/WC_w \cdot L/S_w$		22.42	34.18	22.88	23.84
Rock wet	[g]	29.88	30.14	29.60	29.88
Water	[g]	30.40	30.46	30.52	30.36
WC_w	[g/g_{wet}]	0.048	0.032	0.047	0.045
S/L (S_d/(L+PW))		0.895	0.929	0.884	0.901
pH at Titration		8.928	8.890	8.840	8.623
Na	[mg/L]	334	255	285	347
NH4	[mg/L]	2.6	1.6	1.4	1.7
K	[mg/L]	17.1	8.0	8.8	8.9
Ca	[mg/L]	7.8	3.3	3.7	6.4
Mg	[mg/L]	2.1	< 1	< 1	1.6
Sr (OES)	[mg/L]	1.2	0.1	0.1	0.4
Ba (OES)	[mg/L]	0.12	< 0.01	< 0.025	< 0.01
Si (OES)	[mg/L]	1.90	2.01		3.63
F	[mg/L]	1.4	2.0	4.0	3.3
Cl	[mg/L]	344	144	159	189
Br	[mg/L]	0.34	< 0.16	< 0.16	0.16
NO3	[mg/L]	0.77	0.60	0.47	0.45
SO4	[mg/L]	190	161	186	331
I	[mg/L]	< 0.08	n.a.	n.a.	n.a.
Alk (tit)	[meq/L]	1.47	3.83	4.23	2.96
Alk as HCO3	[mg/L]	89.7	233.8	257.8	180.6
TOC	[mg/L]	7.71	9.54	11.15	14.74

Tab. 4.7-5: continued

Parameter	Unit	TRU1-1	TRU1-2	TRU1-4	TRU1-3
TIC	[mg/L]	14.9	42.6	41.9	30.7
lactate	[mg/L]	< 2	< 2	< 2	< 2
acetate	[mg/L]	7.94	< 2	8.46	2.98
propionate	[mg/L]	< 2	< 2	< 2	2.285
formate	[mg/L]	< 2	< 2	< 2	< 2

WC_w: Water content wet; L: Liquid added; S_w: solid wet; S_d: solid dry; PW: porewater

All averaged aqueous extract solutions (Tab. 4.7-5) processed at S/L ≈ 1 contain low concentrations of NH_4 (1.4 – 2.6 mg/L) and NO_3 (0.45 – 0.77 mg/L). Magnesium and bromide concentrations are below the detection limit in aqueous extract solution of Opalinus Clay samples but detected in small amounts in the extract solutions of samples from the Wedelsandstein and Staffelegg Formation. Iodide was measured only in one sample but below detection limit. The factor ($1/WC_w*L/S_w$) given in Tab. 4.7-5 refers to the scaling factor required to scale the extract concentrations of conservative components to concentrations in the bulk porewater (i.e. at water loss porosity).

Molar Ca/Mg and Br/Cl ratios in the aqueous extract solutions of the samples from the Wedelsandstein and Staffelegg Formations are similar, while they could not be defined for the Opalinus Clay samples as Mg and Br concentrations are below the detection limit. The SO_4/Cl ratio systematically increases with depth. TIC and the titratable acetate concentrations account for most of the titrated alkalinity. TOC concentrations indicate a slight increase with depth but remain below 15 mg/L. A maximum of 42% of the TOC occurs as low-molecular weight organic acids (mainly acetate).

As shown in Section 4.4 (Fig. 4.4-8), the Na/K ratios in these aqueous extracts are smaller than the trend defined by other samples across the clay-rich section. This is tentatively attributed to contamination of K by the potassium-silicate drilling fluid. Only a minute amount of this highly concentrated fluid would be required to induce a notable perturbation. In an upcoming study of contamination by drilling fluid with samples including these advective displacement core samples, a significant penetration depth was demonstrated for K across the examined radial thickness of 7.5 mm. Also, the Si concentrations appear to be elevated (Tab. 4.7-5) and would lead to a gross quartz supersaturation when upscaled to water content. This is also taken as an indication that a K-silicate component might have affected these aqueous extraction tests. The apparent absence of such a contamination in the PW samples may be due to a much larger sample size that was processed in the conventional PW samples, permitting a more generous discarding of material from the core margin. The contamination does not affect anion concentrations and the overall chemistry of the extracts and does allow its use to establish chloride or bromide-accessible porosities as done further below.

Tab. 4.7-6: Ion ratios and details of carbon system in aqueous extract solutions from pre-characterisation

Parameter	**Unit**	**TRU1-1**	**TRU1-2**	**TRU1-4**	**TRU1-3**
Depth	[m]	812.24	867.97	926.14	941.80
Geol. unit		Wedelsandstein Fm.	Opalinus Clay	Opalinus Clay	Staffelegg Fm.
Br/Cl*1000	[mol/mol]	0.43	Br <0.16	Br <0.16	0.38
SO_4/Cl	[mol/mol]	0.20	0.41	0.43	0.64
Ca/Mg	[mol/mol]	2.23	Mg <1	Mg <1	2.41
Ca/Sr	[mol/mol]	14	49	62	33
(Ca+Mg)/(Na+K)	[eq/eq]	0.026	0.014	0.015	0.021
Alk (tit)	[meq/L]	1.47	3.83	4.23	2.96
TIC	[meq/L]	1.24	3.54	3.48	2.55
acetate	[meq/L]	0.13	<0.03	0.14	0.05
TOC	[mg/L]	7.7	9.5	11.2	14.7
Acetate (as C)	[mg/L]	3.23	<0.814	3.44	1.21

Calculation of speciation and saturation indices (Tab. 4.7-7) of the aqueous extract solutions from Tab. 4.7-5 reveal a systematic surplus cationic charge as positive imbalance that is largely explained by acetate that was not included in the speciation calculations (included in the table as equivalent for illustration). Solutions are at or very close to calcite saturation (on average slightly > 1.00), and not far from dolomite saturation (no SI for Opalinus Clay due to Mg concentrations below detection). Extracts are distinctly undersaturated with respect to sulphates. TIC was used as input for the carbon system because the titrated alkalinity would also include acetate.

Tab. 4.7-7: Saturation indices calculated for averaged aqueous extract solutions from Tab. 4.7-5 from pre-characterisation

The full data set is provided in Appendix D.

Parameter	**Unit**	**TRU1-1**	**TRU1-2**	**TRU1-4**	**TRU1-3**
Depth	[m]	811.12	863.66	877.03	924.18
Geol. unit		Wedelsandstein Fm.	Opalinus Clay	Opalinus Clay	Staffelegg Fm.
Charge	[eq/kgw]	5.7E-04	2.5E-04	6.3E-04	8.2E-04
Charge %-error	[%]	1.88	1.11	2.52	2.70
Acetate	[eq/kgw]	1.3E-04	< 3.0E-05	1.4E-04	5.0E-05
Ionic strength	[mol/kgw]	0.017	0.013	0.014	0.019
tot_alk	[eq/kg]	1.38E-03	3.78E-03	3.69E-03	2.66E-03
pH		8.93	8.89	8.84	8.62
Log P_{CO2}	[bar]	-4.11	-3.60	-3.55	-3.47
SI(calcite)		0.082	0.125	0.114	-0.026
SI(dolomite)		-0.05	-	-	-0.31
SI(gypsum)		-2.37	-2.80	-2.70	-2.26
SI(celestite)		-1.46	-2.41	-2.42	-1.72
SI(strontianite)		-0.26	-0.75	-0.87	-0.74
SI(anhydrite)		-2.59	-3.02	-2.92	-2.48

WATEQ4F thermodynamic data base and ordered dolomite; kgw=kg water; charge=Σ(cation charge) - ׀Σ(anion charge)׀ ; Charge %-error=100 charge/ (Σ(cation charge) + ׀Σ(anion charge)׀).

Cation exchange capacities and cation selectivities determined by the Ni-en method (Waber ed. 2020) were performed on the same subset of sample material as used for aqueous extracts (see also Section 5.6). Averaged values (Tab. 4.7-8) indicate uncorrected (for porewater contribution and mineral dissolution/precipitation) capacities of 60 – 120 meq/kg (dry rock) with errors of up to ~ ±5%. For the Opalinus Clay samples, Ni consumptions is ~ 5% higher than the sum of cations, whereas for the samples from the Wedelsandstein and Staffelegg Formation Ni consumption was 14% and 12%, respectively lower. Ni consumptions of individual samples from top and bottom of the processed core sample (data in Appendix D) differ by 37% (Opalinus Clay) to 60% (Staffelegg Formation), largely explained by different clay-mineral content of the samples (see Section 4.5 for a more detailed discussion). Ammonium was not measured but is expected to be present on the exchanger judged by the presence of 1.4 to 2.6 mg/L of NH_4 in the aqueous extracts performed at the same S/L ratio (Tab. 4.7-5).

Br concentrations are below the detection limit of 0.16 mg/l for all samples, which is in agreement with the low to non-detectable Br concentrations in aqueous extracts. Interestingly, the SO_4/Cl ratios are significantly and systematically lower in the Ni-en solutions compared to the aqueous extracts, suggesting that there is either a sulphate source in the aqueous extracts or a sink in the Ni-en solutions. Seemingly, K levels obtained in the Ni-extracts are not affected by contamination with the drilling fluid (see Section 4.5) as is the case for the aqueous extracts.

The cation occupancies (selectivities) derived from Ni-en extracts and applying a correction for the porewater contribution are presented in Section 4.5.

Tab. 4.7-8: Composition of average Ni-en extract solutions and related parameters from pre-characterisation

The entire data set with the results of individual samples is provided in Appendix D.

Parameter	**Unit**	**TRU1-1**	**TRU1-2**	**TRU1-4**	**TRU1-3**
Depth	[m]	812.24	867.97	926.14	941.80
Geol. unit		Wedelsandstein Fm.	Opalinus Clay	Opalinus Clay	Staffelegg Fm.
averaging		top+base (ave 1+1)	top+base (ave 1+1)	top+base (ave 1+1)	top+base (ave 1+1)
$1/WC_w \cdot L/S_w$		23.16	35.22	23.80	25.23
Rock wet	[g]	30.62	29.48	29.93	29.38
Solution	[g]	32.23	30.64	32.17	31.66
WC_w	$[g/g_{wet}]$	0.05	0.03	0.05	0.04
S/L (S_d/(L+PW))		0.87	0.90	0.85	0.85
pH (initial)		8.28	8.27	8.37	8.27
Ni (initial)	[mg/L]	8'407	8'425	5'566	8'367
pH (final)		8.39	8.28	8.35	8.31
Na	[mg/L]	520	712	1'076	764
K	[mg/L]	128	162	220	164
Mg	[mg/L]	89.5	118	142	114
Ca	[mg/L]	350	520	738	534
Sr	[mg/L]	44.9	28.4	36.8	35.3
Ba	[mg/L]	1.65	1.20	0.70	1.15
Fe	[mg/L]	< 0.05	< 0.05	< 0.05	< 0.05
Ni	[mg/L]	6'744	5'944	2'229	6'109
F	[mg/L]	0.51	0.48	0.92	0.69
Cl	[mg/L]	325	133	153	185
Br	[mg/L]	< 0.16	< 0.16	< 0.16	< 0.16
NO_3	[mg/L]	19'498	19'584	12'534	19'798
SO_4	[mg/L]	146.5	101.4	128.0	204.5
TDS	[mg/L]	27'848	27'304	17'258	27'911
Na	[meq/kgd]	26.2	34.2	55.1	39.0
K	[meq/kgd]	3.8	4.6	6.6	4.9
Mg	[meq/kgd]	8.5	10.7	13.7	11.1
Ca	[meq/kgd]	20.3	28.7	43.4	31.2
Sr	[meq/kgd]	1.18	0.72	0.99	0.95
Ba	[meq/kgd]	0.03	0.02	0.01	0.02
Fe	[meq/kgd]	< 0.002	< 0.002	< 0.002	< 0.002
SumCat	[meq/kgd]	60.0	78.9	119.8	87.1
SumCat_err	[meq/kgd]	2.45	3.28	5.07	3.64

Tab. 4.7-8: continued

Parameter	Unit	TRU1-1	TRU1-2	TRU1-4	TRU1-3
Ni_cons	[meq/kgd]	51.3	84.0	124.5	76.7
Ni_cons_err	[meq/kgd]	8.30	7.65	4.60	8.10
Br/Cl	[mol/mol*1000]	-	-	-	-
SO_4/Cl	[mol/mol]	0.17	0.28	0.31	0.41

kgd = kg dry rock; WC_w: Water content wet; L: Liquid added; S_w: solid wet; S_d: solid dry; PW: porewater

4.7.5 Chemical and isotopic evolution of displaced porewater aliquots

An artificial porewater (APW) composition was injected to force advective displacement. The outflow of each experiment was continuously sampled in small syringes (Waber ed. 2020). These syringe aliquots were analysed for chemical and water isotopic composition. Hydraulic conductivity was evaluated for each sampled aliquot (Darcy's law), and any expelled gas was also recorded, although gas-tightness is commonly good but cannot be ensured for a syringe sampling system. Most data for each experiment are included in tables and graphs in this section, and more details are provided in Appendix D.

According to the method of advective displacement (Mäder 2018), it is expected that the first few sampled aliquots are of similar composition and represent the displaced porewater from the sample core. After this, a gradual breakthrough of the injected APW should be observed, until full breakthrough of conservative components (e.g. Cl, Br), given enough time.

4.7.5.1 Artificial porewater used for advective displacement

In the absence of constraining data, an artificial porewater composition (Tab. 4.7-9) was chosen that was based on work performed for the deep geothermal well in Schlattingen-1 (advective displacement experiments detailed in Mäder & Waber 2017). The composition was calculated with PHREEQC for 25 °C, to be saturated with respect to calcite and dolomite, and a partial pressure of CO_2 of $10^{-2.2}$ bar. This partial pressure was imposed by bubbling with an Ar/CO_2 gas mixture during mixing and again when the fluid reservoir was filled before experiments. A recipe with the appropriate amounts of PA-grade chemicals is given in Tab. 4.7-10.

Deuterium was added as a water tracer for advective-diffusive transport, aiming for a δ^2H of approximately +100 ‰ (VSMOW). There is no Br contained in the APW and therefore bromide-breakout can be used as an anionic tracer in the case of significant Br concentrations in the porewater. If the Cl concentration in the APW is significantly different from the displaced early aliquots, Cl breakthrough forms an additional anionic tracer for transport.

Two different batches of APW were used for the three successful experiments (Tab. 4.7-9). Both batches were prepared according to the same recipe and concentrations of major ions are equal within analytical uncertainty. A larger difference of 20% is present for δ^2H. The APW was injected from PFA-coated fluid tanks containing the APW and a pressurised headspace filled with He after bubbling with the Ar/CO_2 gas mixture mentioned above.

Tab. 4.7-9: Composition and recipe for the artificial porewaters

Parameter	**Unit**	**Recipe**	**APW TRU1-1, TRU1-2**		**APW TRU1-4**		**Compounds**
			Calculated*	**Measured**	**Calculated***	**Measured**	
pH		7.19		7.48		7.38	
Na	[mg/L]	3'989	3'988	4'029	3'988	4059	NaCl; $NaHCO_3$; Na_2SO_4
NH_4	[mg/L]			< 10		< 10	
K	[mg/L]	79.4	79.5	75.0	79.3	78.7	KCl
Ca	[mg/L]	503	503	501	504	506	$CaCl_2 \cdot 2H_2O$
Mg	[mg/L]	226	226	223	226	208	$MgCl_2 \cdot 6H2O$
Sr	[mg/L]			3.95		< 0.25	
Ba	[mg/L]			0.08		< 0.25	
Si	[mg/L]			< 0.5		< 2.5	
Al	[mg/L]			< 2.5		0.279	
F	[mg/L]			< 1.6		< 1.6	
Cl	[mg/L]	5'992	5'984	5'918	5'986	5'826	$CaCl_2 \cdot 2H_2O$; KCl; $MgCl_2 \cdot 6H_2O$
Br	[mg/L]			< 1.6		< 1.6	
NO_3	[mg/L]			6.8		5.25	
SO_4	[mg/L]	2'305	2'305	2'175	2'303	2'132	Na_2SO_4
I	[mg/L]			n.m		n.m	
TOC	[mg/L]			7.22		7.4	
TIC	[mg/L]	29.3	29.3	31.5	29.32	28.0	$NaHCO_3$
lactate	[mg/L]			< 20		< 20	
acetate	[mg/L]			< 20		< 20	
propionate	[mg/L]			< 20		< 20	
formate	[mg/L]			< 20		< 20	
$\delta^{18}O$	[‰ VSMOW]		-11.43	-11.53	-11.43	-11.52	
$\delta^{2}H$	[‰ VSMOW]	100	106.8	107.9	91.9	90.8	D_2O

* Calculated from the weighed-in chemical compounds; CO_2-Ar bubbling not taken into account.

Tab. 4.7-10: Recipe and preparation for the artificial porewater for a 2-litre batch

Chemical	**Manufacturer**	**Grade**	**Recipe**		**APW for TRU1-1, TRU1-2**	**APW for TRU1-4**
			[g/kgw]	[g/2kgw]	Weighted in [g/2L]	Weighted in [g/2L]
$NaHCO_3$	Merck	p.a.	0.2051	0.4101	0.4102	0.4102
$CaCl_2 \cdot 2H_2O$	Merck	p.a.	1.8465	3.6930	3.6923	3.6944
KCl	Merck	p.a.	0.1514	0.3029	0.3031	0.3026
$MgCl_2 \cdot 6H_2O$	Merck	p.a.	1.8907	3.7814	3.7824	3.7827
NaCl	Merck	p.a.	7.1916	14.3831	14.3800	14.3838
Na_2SO4	AnalaR NORMA-PUR	Ph.Eur.	3.4089	6.8177	6.8171	6.8114
D_2O (100%)	Roth	> 99.8%D	0.0318	0.0635	0.0659	0.0607

4.7.5.2 Physical conditions, hydraulic conductivity, sampling, and pore volume equivalents

All core samples were subjected to 58 – 60 bar hydraulic confining pressure. The TRU1-1 experiment was started with an initial infiltration pressure set by a He headspace of 47 bar. There was a He leak initially at the top of the injection tank (a small fissure in the stainless-steel top annulus) that could not be fixed from the outside. The pressure was put to zero after 8 hours and the crack was fixed from the inside, and injection resumed at 40 bar pressure 3 hours later. The pressure was reduced to 30 bar after two days to counteract a rather large flux observed for this experiment. The infiltration pressure was slowly and gradually decreasing with time (displaced APW, and any small He leak), and was replenished 2 times during the course of experiment TRU1-1. Experiment TRU1-2 was fed from the same infiltration tank but started 3 weeks after TRU1-1 and thus was subjected to the same infiltration pressure, which covered a range of 26.5 to 30 bar over the experimental runtime. The TRU1-4 experiment was initiated at 47.5 bar and pressure varied between 47.3 to 48.4 bar.

Temperature conditions were stable without diurnal fluctuations, ranging seasonally from 21.4 to 22.3 °C. Critical temperature-sensitive measurements, such as electric conductivity, pH and hydraulic conductivity, were temperature-compensated, either intrinsically or explicitly (details in Waber ed. 2020).

Hydraulic conductivity referenced to 25 °C was evaluated for all sampled aliquots based on sample mass and Darcy's law (detailed data in Appendix D, method in Waber (ed.) 2020). Earliest aliquots commonly show lower apparent hydraulic conductivities due to the expulsion of gas from the dead volume in the outflow, and saturation of any small initially unsaturated volume in the sample core itself. TRU1-1 and TRU1-2 cores (Fig. 4.7-4) show an initial maximum hydraulic conductivity that is gradually decreasing with time, and in the case of the long-lasting TRU1-1 core (Wedelsandstein Formation) it is approaching a steady-state value. No decrease in hydraulic conductivity is seen for the TRU1-4 core, which might be due to the short runtime. The values for the early conductivity and that measured towards the end of the experiments (Tab. 4.7-11) span a relatively narrow range for each core and are approximately one order of magnitude higher for the core from the Wedelsandstein Formation ($0.9 – 1.1 \times 10^{-12}$ m/s) than for the samples from the Opalinus Clay ($0.6 – 2.4 \times 10^{-13}$ m/s). This conductivity refers to a direction perpendicular to

bedding and a sample length of 8 – 9 cm, measured at very large hydraulic gradients (Tab. 4.7-2). A gradual but rather minor decrease after an early maximum value may be due to slow sample consolidation, which was also observed in earlier work (Mäder 2018). These latter values are most representative for in situ conditions, although the confining stress of 60 bar (6 MPa) in the experiments is still considerably less than those at 800 – 1'000 m depth.

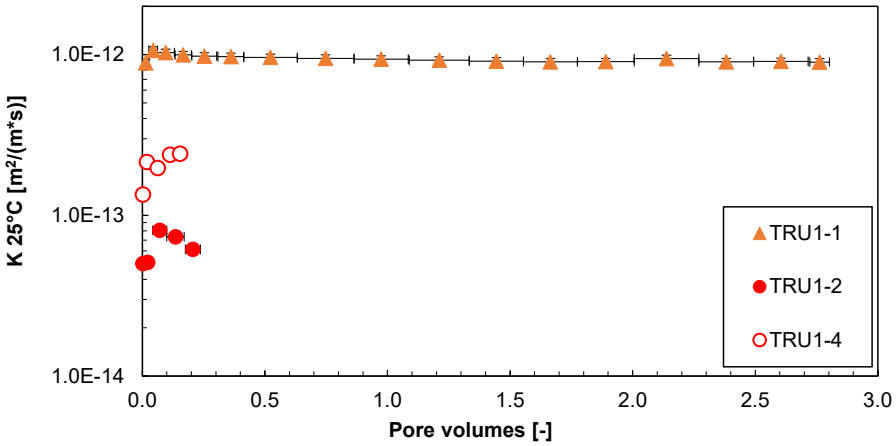

Fig. 4.7-4: Evolution of hydraulic conductivity during advective displacement experiments

TRU1-1 = 812.24 m (Wedelsandstein Fm.); TRU1-2 = 867.97 m (Opalinus Clay); TRU1-4 = 926.14 m (Opalinus Clay); Pore volume fractions relate to transport time based on water content. Experiment duration is 20 – 90 days. Horizontal length of symbol bar covers the sampling interval, vertical bars are within symbol size and are an estimate of combined uncertainties.

Tab. 4.7-11: Hydraulic conductivity of AD samples

Parameter	**Unit**	**TRU1-1**	**TRU1-2**	**TRU1-4**
Depth	[m]	812.24	867.97	926.14
Geol. unit		Wedelsandstein Fm.	Opalinus Clay	Opalinus Clay
Early_max. K (25 °C)	[m/s]	1.06E-12	8.07E-14	2.42E-13
Late_K (25 °C)	[m/s]	8.99E-13	6.14E-14	2.42E-13

The time axis for all data representations of sequential fluid aliquots is converted to pore volume fractions by dividing the cumulative sample mass (volume) by the water content of the core. In this way, experiments with very different hydraulic conductivities or different water contents can be represented in a meaningful way for transport. There may be some minor ambiguities in case where water contents from pre-characterisation deviate from the true water content of a sample core, or if a significant initial unsaturated porosity fraction would be present. The chosen approximation is sufficient for a visual presentation of data.

Sampled aliquots (mass) plotted versus pore volume fraction (time) provide an overview of all syringe samples taken for the three successful AD experiments (Fig. 4.7-5). For the two experiments of the Opalinus Clay focus was on the first porewater aliquots (5 – 6 samples collected), whereas for the experiment of the Wedelsandstein Formation 17 samples could be collected in a reasonable experimental duration.

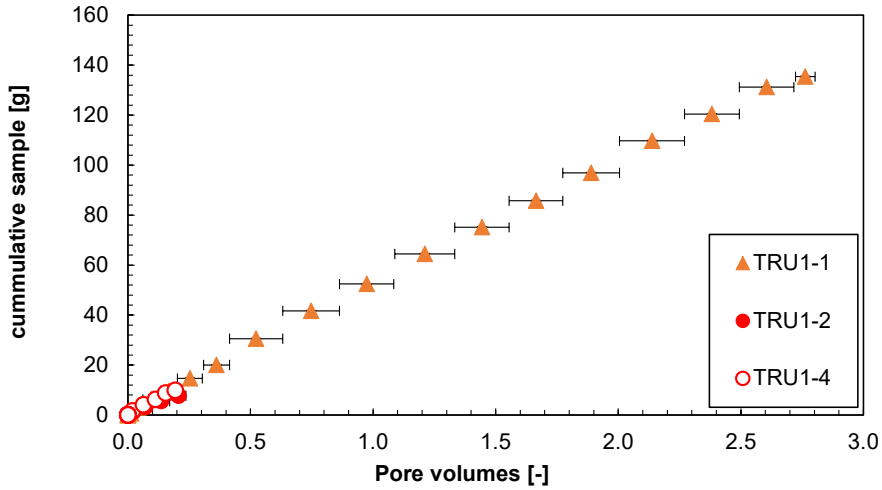

Fig. 4.7-5: Sampling schedule and sample volumes taken

TRU1-1 = 812.24 m (Wedelsandstein Fm.); TRU1-2 = 867.97 m (Opalinus Clay); TRU1-4 = 926.14 m (Opalinus Clay); Each data point represents a syringe aliquot taken, with the horizontal bar indicating the duration for sampling, here converted to pore volume fraction percolated. The slopes reflect volumetric flow rates scaled by porosity.

4.7.5.3 Inline measurement of electric conductivity and pH

Electric conductivity (EC) was continuously monitored in all experiments (Fig. 4.7-6, Waber ed. 2020, for method). Conductivity cells were initially calibrated but may show a drift to a varying extent over time due to electrode corrosion, commonly resulting in low apparent readings. Therefore, electric conductivity values are only meant to provide an indication of salinity but are not used quantitatively.

The electric conductivities generally show a maximum in the early percolated porevolumes ranging from 20 to 28.5 mS/cm (22 °C laboratory reference). The injected artificial porewater has a lower (experiments TRU1-1 and TRU1-4) to similar (experiment TRU1-2) conductivity compared to the displaced porewater. The value of the APW is gradually approached with progress of advective displacement. In the long-lasting experiment of the Wedelsandstein Formation, however, the electric conductivity drops 3 mS/cm below the APW value, where it remains rather constant after 1.5 PV percolated. This offset presumably is due to corrosion effects of the electrode as mentioned above. Post-experiment calibration of the conductivity cell used for TRU1-2 did indeed show a significant decrease of EC readings by approximately 3 mS/cm, but the cell for TRU1-1 was not recalibrated. Corrosion may not only affect the inner surface of the flow-through electrodes but may also lead to diffusion-dominated short-circuits between the two electrodes. Similar calibration offsets were already established between pre-and post-experiment calibrations performed in earlier experiments (Mazurek et al. 2021). Alternatively, the data may indicate that a full breakthrough of the APW is not achieved, and some ionic strength is precipitated in the samples (e.g. sulphates). Nevertheless, in the present case this is considered less likely, given the well-matched concentrations on major ions in late syringe samples and the APW (Section 4.7.5.4).

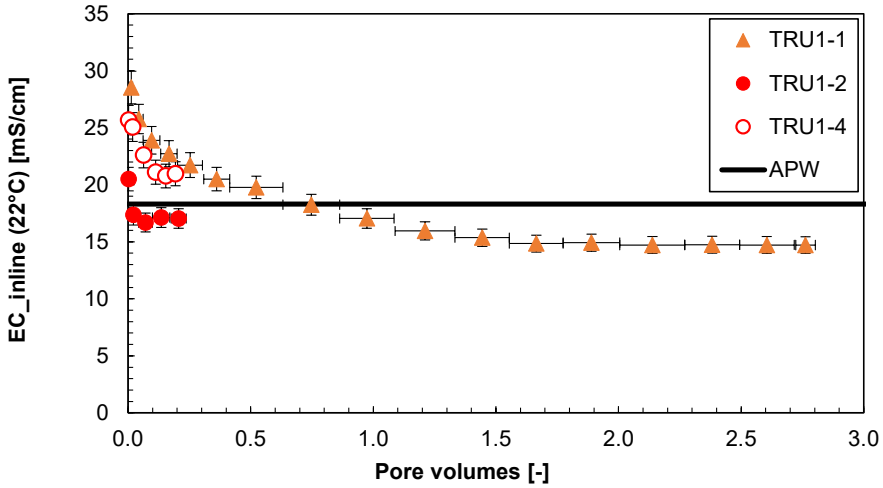

Fig. 4.7-6: Evolution of electric conductivity (22 °C) during advective displacement experiments

TRU1-1 = 812.24 m (Wedelsandstein Fm.); TRU1-2 = 867.97 m (Opalinus Clay); TRU1-4 = 926.14 m (Opalinus Clay); Pore volume fractions relate to transport time based on water content. Experiment duration is 20 – 90 days. Horizontal length of symbol bar covers the sampling interval, vertical bars are an estimate of combined uncertainties.

The aim was to measure pH inline three times before/after sampling of the first four aliquots, and less frequently at later times (method in Waber ed. 2020). Due to the fast arrival of first sample aliquots in the TRU1-1 experiment (Wedelsandstein Formation) and problems with the in-line pH measurement unit, first in-line pH measurement was recorded during syringe 4 only. Measurements took ~ 3 hrs and 12 – 24 hrs for TRU1-1 and TRU1-4, respectively, to ensure that the dead volume of the very small flow-through pH cell was sufficiently flushed given the very slow flow rates of the experiments. The micro-electrode was left installed in the flow-through cell and was checked before and after each pH measurement period with a standard solution. The initial calibration was made at pH 7 and 9, and simple drift checks and corrections were made with a standard solution at pH 7. In most cases, drift corrections over 12 – 24 hrs were ≤ 0.1 pH units. The overall uncertainty is difficult to assess because these small electrodes may respond to manipulations at the flow-through cell (response to small strains) and also small gas bubbles may temporarily affect readings. It is estimated that an error of ± 0.2 pH units is appropriate for most measurements. pH values of early aliquots are also tabulated below.

These in-line pH measurements (Fig. 4.7-7) are rather tricky and require careful handling of equipment. Criteria to accept a value include a small drift of the two pH standards measured before and after the sample measurement and a reasonably well-defined pH-plateau. It cannot be excluded that for long measurement durations some effect from outgassing or in-gassing may influence the readings. The measurements for each experiment span a range of less than 0.5 pH units and point to a systematic trend over the experimental duration of each experiment, thus indicating that random errors or disturbed signals are not a dominant feature. More details are discussed further below.

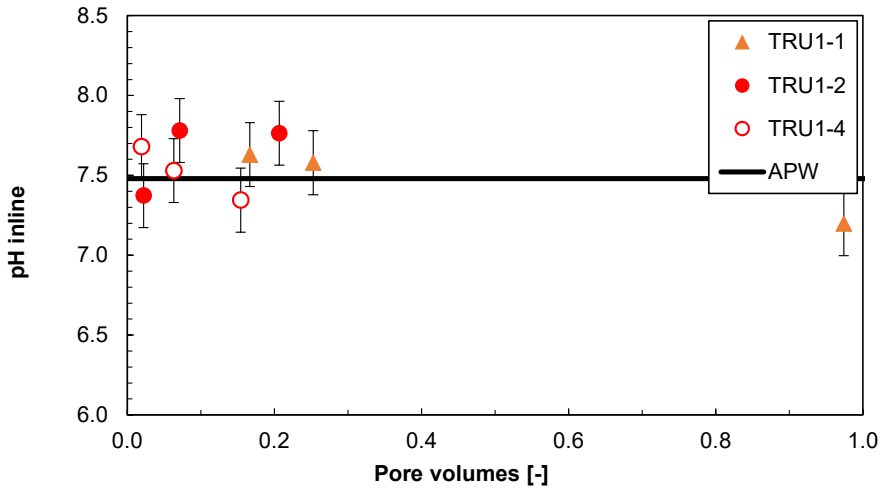

Fig. 4.7-7: Evolution of inline pH during advective displacement experiments

TRU1-1 = 812.24 m (Wedelsandstein Fm.); TRU1-2 = 867.97 m (Opalinus Clay); TRU1-4 = 926.14 m (Opalinus Clay); Pore volume fractions relate to transport time based on water content. Amount sampled per in-line pH measurement is small and would correspond to less than symbol width. Experiment duration is 20 – 90 days. X-axis is truncated at 1 PV, omitting an additional pH measurement of TRU1-1 at 2.6 PV of pH 7.22. Vertical bars are an estimate of combined uncertainties.

4.7.5.4 Evolution of major and minor components

Evolution of concentrations with progress of percolation are shown in Figs. 4.7-8 to 4.7-13. Selected analytical data for the first two aliquots sampled are summarised in Tab. 4.7-12 further below, with full details in Appendix D. The composition of the earliest aliquots displaced from the core samples are the most representative for the pore fluid extracted, and this is highlighted and interpreted in a separate Section 4.7.5.5.

Major components (Cl, SO_4, Na, Ca, Mg) displaced initially are all more concentrated than in the APW (Fig. 4.7-8) except for sulphate that elutes initially at concentrations below the APW (Wedelsandstein Formation, upper Opalinus Clay sample) or only slightly above (deeper Opalinus Clay sample). In the Wedelsandstein Formation experiment (TRU1-1) a convergence of anions and cations to the APW concentration can be observed, and APW concentrations are well matched by displaced porewater concentrations after approximately 1.5 percolated pore volumes. The comparable convergence behaviour of Na and Ca with Cl, for example, indicate that the major cation ratios in the APW are compatible (although different in ionic strength) with the ion-exchanger population in situ. An exception is Mg that tends to decrease with time (pore volume) to concentrations below the APW, indicating that the ion-exchange equilibrium with the APW is not yet reached across the entire sample core and would require several more pore volumes of percolation. Sr concentrations are shown further below at an expanded scale. In the Opalinus Clay experiments, experimental duration was too short for an evaluation of the convergence phase.

The same information as depicted in Fig. 4.7-8 is summarised for select components for all three experiments (Fig. 4.7-9), this visualises some differences in the evolution of the early porewater aliquots. In AD experiments, several components show a relatively small change with time over the first 2 – 3 aliquots, which is interpreted to represent the porewater composition displaced from the core sample at the imposed physical conditions. For the Wedelsandstein Formation, a clear plateau in most major components can be observed, which spans the percolation period required for 0.4 pore volume fractions. Note, that the elevated concentrations in the first syringe of this

experiment are interpreted to be due to evaporation i) from the core surface during cutting and preparation (likely a minor affect) and ii) during fluid sampling because the syringe piston was expelled, and the open and overflowing syringe left overnight, and thus this datum was not used for interpretation. In the Opalinus Clay experiments, the plateau is less pronounced than in the Wedelsandstein experiment, and a steepening of the gradient can already be detected after approximately 0.1 percolated pore volume fractions. A choice was made to use average compositions of the first two analysed aliquots to represent the porewater composition. In the experiment from the Wedelsandstein Formation, the second and third sample were used instead, because of the inferred evaporation artefact mentioned above. The resulting porefluid compositions are summarised in Tab. 4.7-12 (Section 4.7.5.5) and are also used in the integrative plots in Chapter 5.

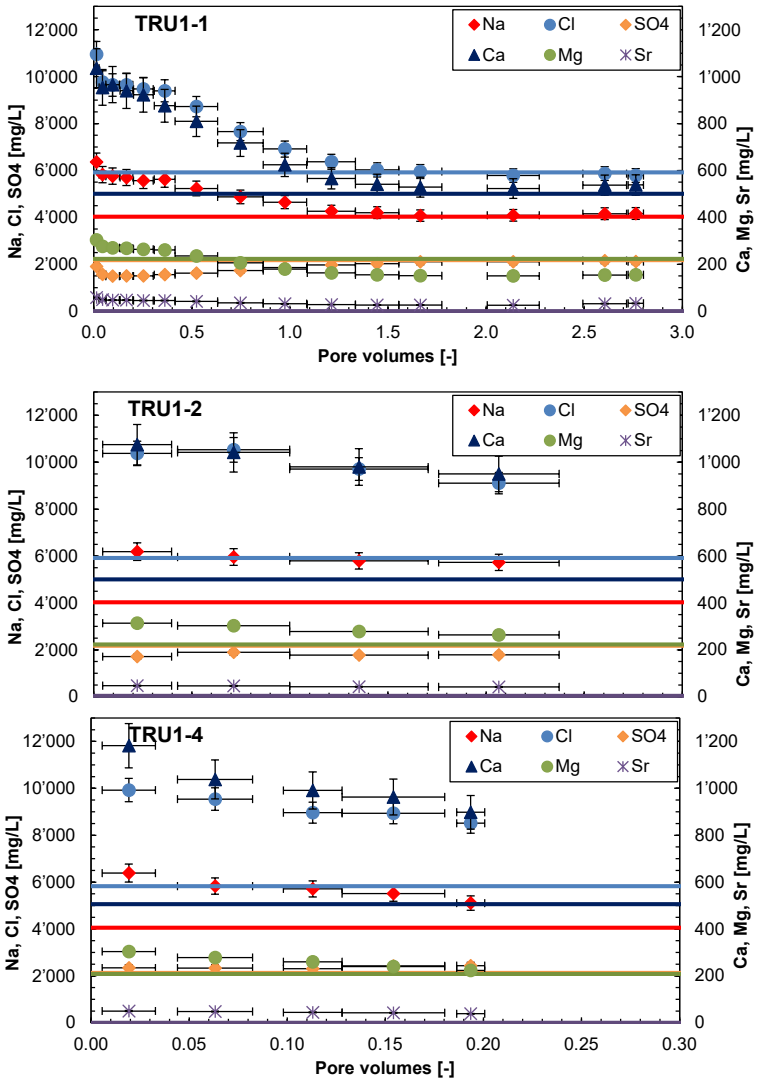

Fig. 4.7-8: Evolution of major components during advective displacement experiments

TRU1-1 = 812.24 m (Wedelsandstein Fm.); TRU1-2 = 867.97 m (Opalinus Clay); TRU1-4 = 926.14 m (Opalinus Clay); Pore volume fractions relate to transport time based on water content. Experiment duration 20 to 90 days. Horizontal length of symbol bar covers the sampling interval, vertical bars are an estimate of combined uncertainties. Horizontal lines represent the composition of the injected APW, differences between the two batches are within line thickness. Note the different X-axis scale for long-running TRU1-1 and the short TRU1-2/TRU1-4 experiments.

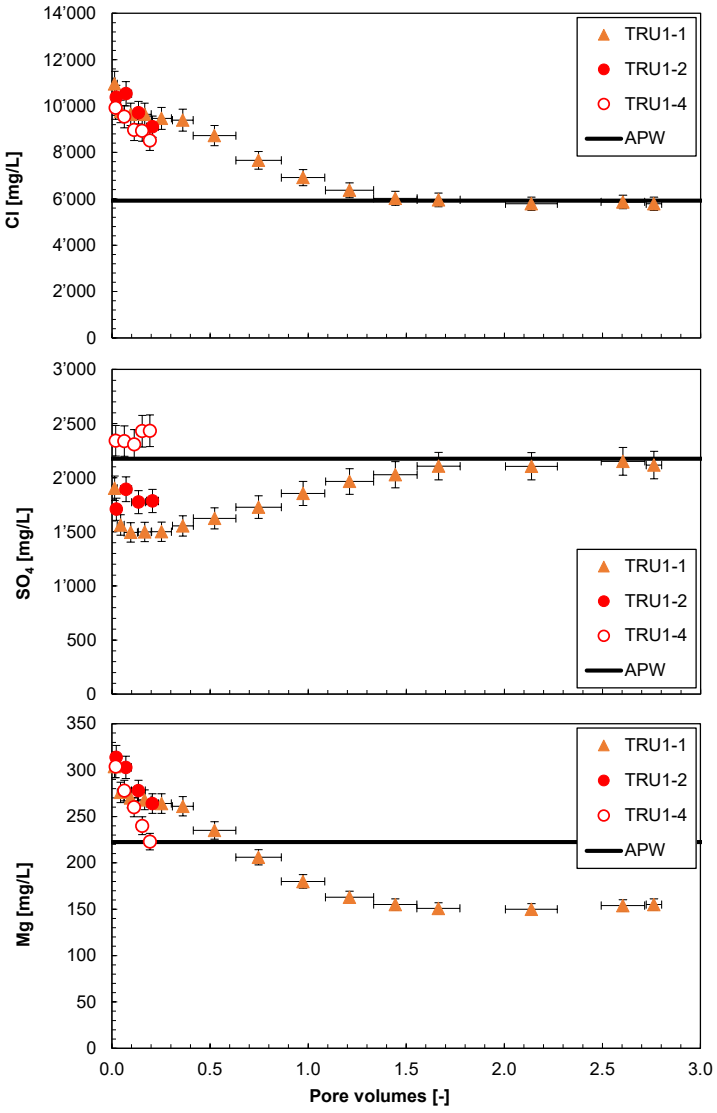

Fig. 4.7-9: Evolution of selected major components during advective displacement experiments

TRU1-1 = 812.24 m (Wedelsandstein Fm.); TRU1-2 = 867.97 m (Opalinus Clay); TRU1-4 = 926.14 m (Opalinus Clay); Pore volume fractions relate to transport time based on water content. Experiment duration 20 to 90 days. Horizontal length of symbol bar covers the sampling interval, vertical bars are an estimate of combined uncertainties. Horizontal lines represent the composition of the injected APW, differences between the two batches are within line thickness.

Of the **minor components (Br, NO_3, K, Sr, Si)**, only potassium is present in the injected APW. Its evolution is decreasing from concentrations near and above the APW to lower values, until in the long-lasting Wedelsandstein Formation experiment it again approaches the APW concentration after more than two percolated pore volumes, thus indicating some transient effects of ion-exchange (Fig. 4.7-10). An exception is the first aliquot from the lower Opalinus Clay sample (TRU1-4), which exhibits a strongly elevated K concentration. A crack in the original core just above the AD core segment (Fig. 4.7-2) may have caused a drilling fluid contamination (by K-silicate) in the upper-most part of the core sample.

Strontium concentrations are gradually decreasing from 50 to 40 mg/L in the first 0.2 pore volume aliquots sampled in the Opalinus Clay experiments and down to 25 mg/L at 2 pore volumes percolated in the Wedelsandstein Formation experiment. Latest aliquots in the latter experiment show again increasing Sr concentrations (details in Fig. 4.7-11). This is likely a coupling to the also increasing sulphate concentrations (Fig. 4.7-9; and the observed celestite saturation, discussed below). Bromide elutes from initial values representative of the pore fluid (7 – 10 mg/L) to below detection limit after ~ 1.2 pore volumes, just by being flushed out (details in Fig. 4.7-11). In the Wedelsandstein Formation experiment, this can be used as a reversed breakthrough of an anionic tracer (see below). Dissolved silica elutes at rather constant concentrations in the range of 3.7 to 5 mg/L.

Nitrate concentrations gradually decrease from 24 and 43 mg/L in in the early sample aliquots of the Opalinus Clay experiments (TRU1-2 and TRU1-4), to 10 and 20 mg/L, respectively. In contrast, in the sample from the Wedelsandstein Formation, the evolution of NO_3 shows an initial increase to concentrations of not more than 15 mg/L at 0.1 pore volume percolated, subsequently decreasing to below or close to detection limit after 0.5 pore volumes. Ammonium (NH_4) was only determined for two samples, where it is below the detection limit of 10 mg/L.

Iodide was only analysed in the early aliquots from the Wedelsandstein Formation experiment (TRU1-1) and the first Opalinus Clay experiment (TRU1-2), and concentrations are around 4 mg/L and 2 – 2.6 mg/L, respectively.

Ba and Al were measured by ICP-OES but always below the detection limits. The detection limits depend on dilution factors and were 0.25 – 0.5 mg/L for Ba, and 2.5 – 10 mg/L for Al.

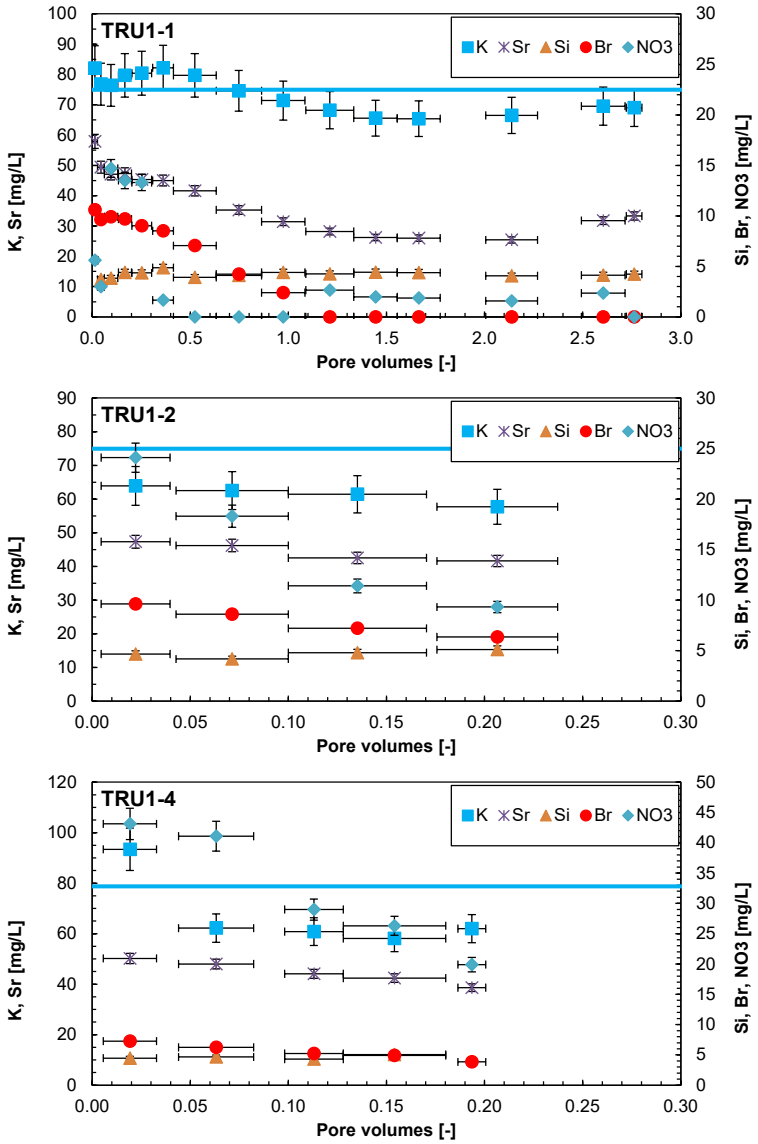

Fig. 4.7-10: Evolution of minor components during advective displacement experiments

TRU1-1 = 812.24 m (Wedelsandstein Fm.); TRU1-2 = 867.97 m (Opalinus Clay); TRU1-4 = 926.14 m (Opalinus Clay); Pore volume fractions relate to transport time based on water content. Experiment duration 20 to 90 days. Horizontal length of symbol bar covers the sampling interval, vertical bars are an estimate of combined uncertainties. Horizontal line represent the composition of the injected APW for K (0 for others). Note the different X-axis scale for long-running TRU1-1 and the short TRU1-2/TRU1-4 experiments.

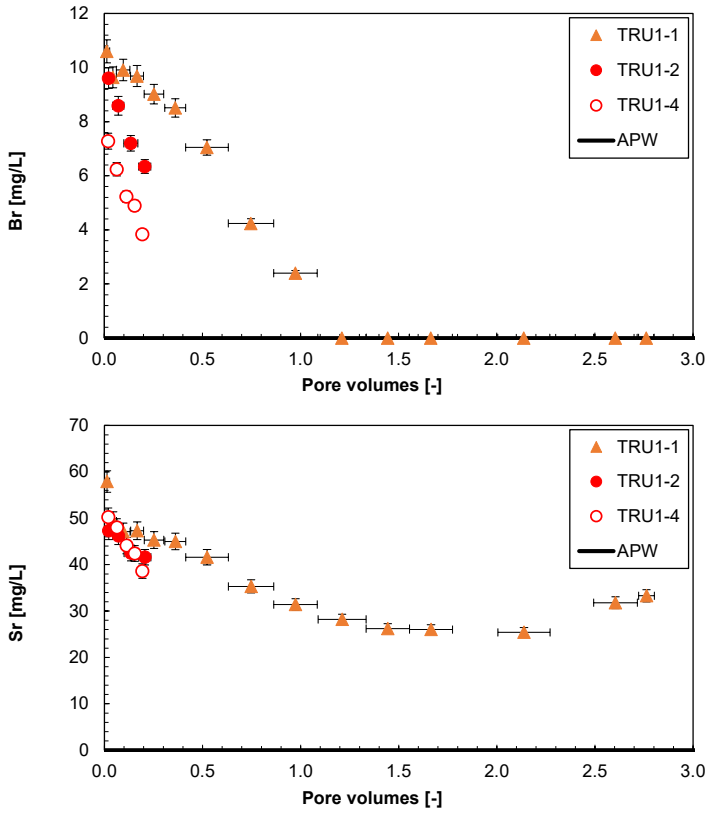

Fig. 4.7-11: Evolution of selected minor components during advective displacement experiments

TRU1-1 = 812.24 m (Wedelsandstein Fm.); TRU1-2 = 867.97 m (Opalinus Clay); TRU1-4 = 926.14 m (Opalinus Clay); Pore volume fractions relate to transport time based on water content. Experiment duration 20 to 90 days. Horizontal length of symbol bar covers the sampling interval, vertical bars are an estimate of combined uncertainties. Br and Sr in the APW are 0 mg/L. Br concentrations below detection are plotted at 0.

The **carbon system (TIC, TOC, TC, LMWOA)** shares a common feature, namely that relatively large TOC concentrations are eluted initially (280 – 500 mg/L) and gradually decrease to 20 – 100 mg/L with progressive percolation (Fig. 4.7-12, Tab. 4.7-12 shows averages of first 2 aliquots). TOC clearly dominates the total dissolved carbon inventory (TC) at early times. In most samples between 15 – 35% of TOC is explained by acetate, the only low-molecular-weight organic acid (LMWOA) found above a detection limit of 20 mg/L (other analysed LMWOA included formate, propionate, and lactate). Aqueous extracts (Tab. 4.7-6) show TOC values around 150 – 300 mg/L when scaled to porewater content, thus in agreement with the values observed in early aliquots of the advective displacement experiments (Tab. 4.7-12).

TIC elutes initially at much lower concentrations than TOC, with concentrations in the range of 20 – 40 mg/L (Figs. 4.7-12, 4.7-13). There are two unusually large TIC values of 115 mg/L obtained for the 2nd and 3rd analysed syringes of TRU1-2 (Opalinus Clay), which is accompanied by a drop in TOC and acetate concentrations in those samples. Thus, it can be speculated that this anomaly is due to microbial activity either in the syringe itself (i.e. during sampling/storage) or at the surface of the core sample, whereby a part of organic carbon is oxidised to inorganic carbon, e.g. coupled with sulphate reduction. This phenomenon was observed in some tests from the Marthalen MAR1-1 borehole, where syringes were stored for several weeks, and analysed before and after storage.

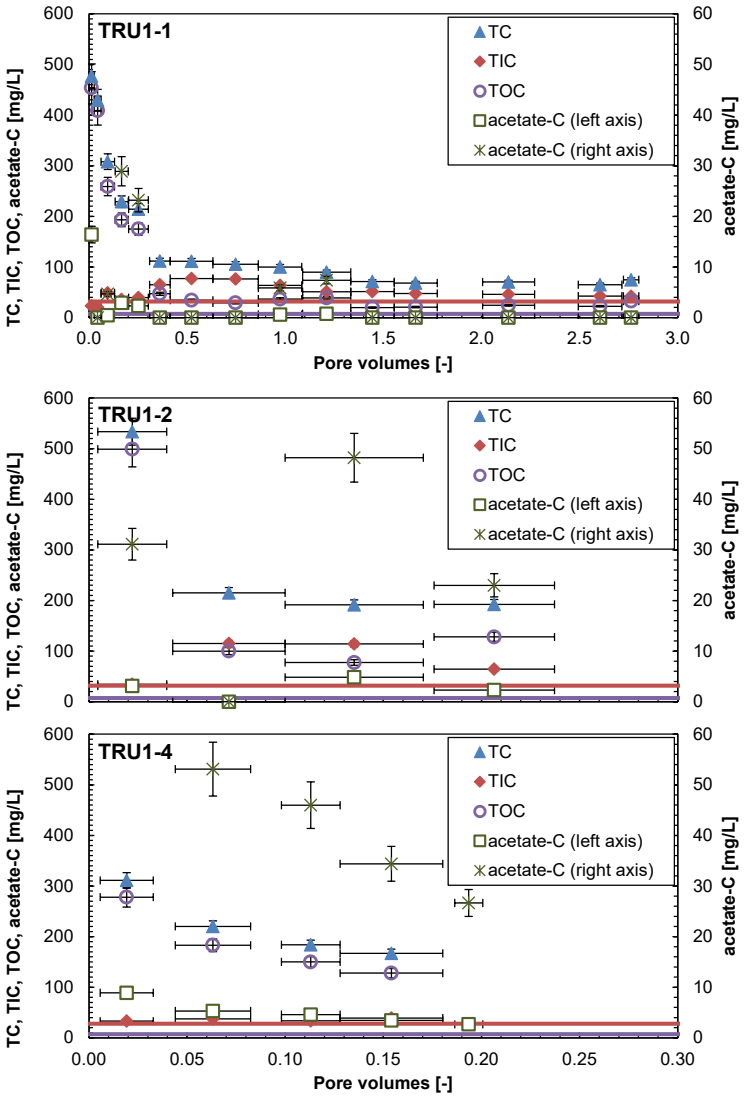

Fig. 4.7-12: Evolution of carbon system during advective displacement experiments

TRU1-1 = 812.24 m (Wedelsandstein Fm.); TRU1-2 = 867.97 m (Opalinus Clay); TRU1-4 = 926.14 m (Opalinus Clay); Pore volume fractions relate to transport time based on water content. Experiment duration 20 to 90 days. Horizontal length of symbol bar covers the sampling interval, vertical bars are an estimate of combined uncertainties. Horizontal line represent the composition of the injected APW. Note the different X-axis scale for long-running TRU1-1 and the short TRU1-2/TRU1-4 experiments.

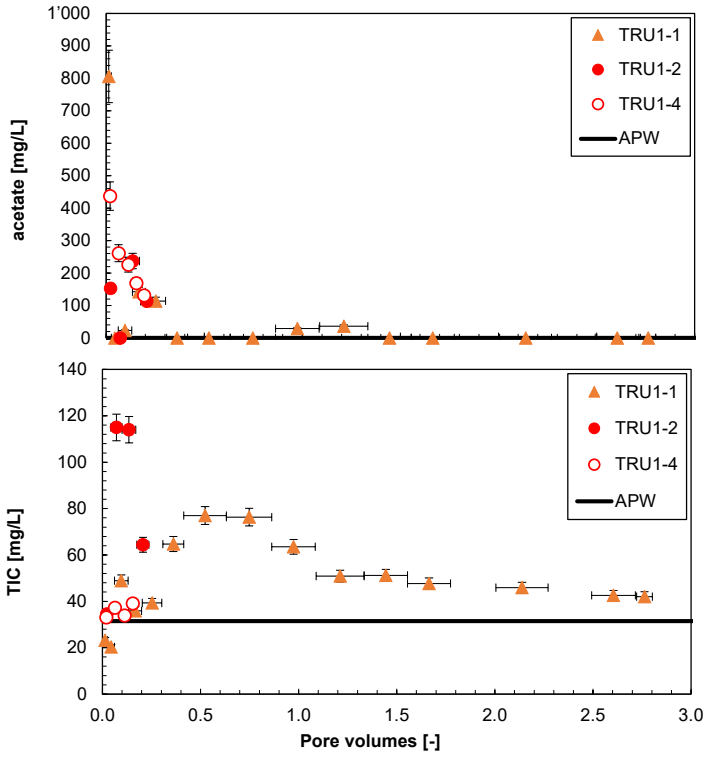

Fig. 4.7-13: Evolution of selected carbon components during advective displacement experiments

TRU1-1 = 812.24 m (Wedelsandstein Fm.); TRU1-2 = 867.97 m (Opalinus Clay); TRU1-4 = 926.14 m (Opalinus Clay); Pore volume fractions relate to transport time based on water content. Experiment duration 20 to 90 days. Horizontal length of symbol bar covers the sampling interval, vertical bars are an estimate of combined uncertainties. Horizontal lines represent the composition of the injected APW. Concentrations below detection (acetate) are plotted at 0.

The **measurement of pH** was performed in-line between some of the sampling intervals (set-up in Waber ed. 2020) and in the laboratory when syringe aliquots were prepared/preserved for analysis. The latter was done in most cases very shortly after sampling (one to a few hours), or after a few days of storage at room temperature. The total range covered for all samples, in-line and laboratory, is 7.0 – 7.9 (Fig. 4.7-14), with laboratory values showing more spread than the in-line measurements.

All experiments show an early decreasing trend for pH measured in the laboratory, but this is less clearly seen in the early in-line values. The in-line pH series define relatively smooth trends with percolation progress but not a very systematic behaviour. The spread is relatively small, ranging from 0.3 – 0.4 pH units. Some of the low apparent pH values measured in syringe samples (e.g. two early samples from the TRU1-1, Wedelsandstein Formation experiment) may relate to sample storage issues, including microbial activity, as already discussed in the previous section for the 2nd and 3rd syringes in the TRU1-2 Opalinus Clay experiment. The partial pressure of CO_2 is larger than atmospheric in the aliquots, and this bears the potential for outgassing and resultant supersaturation with respect to calcite, and possibly some loss of Ca and TIC by precipitation.

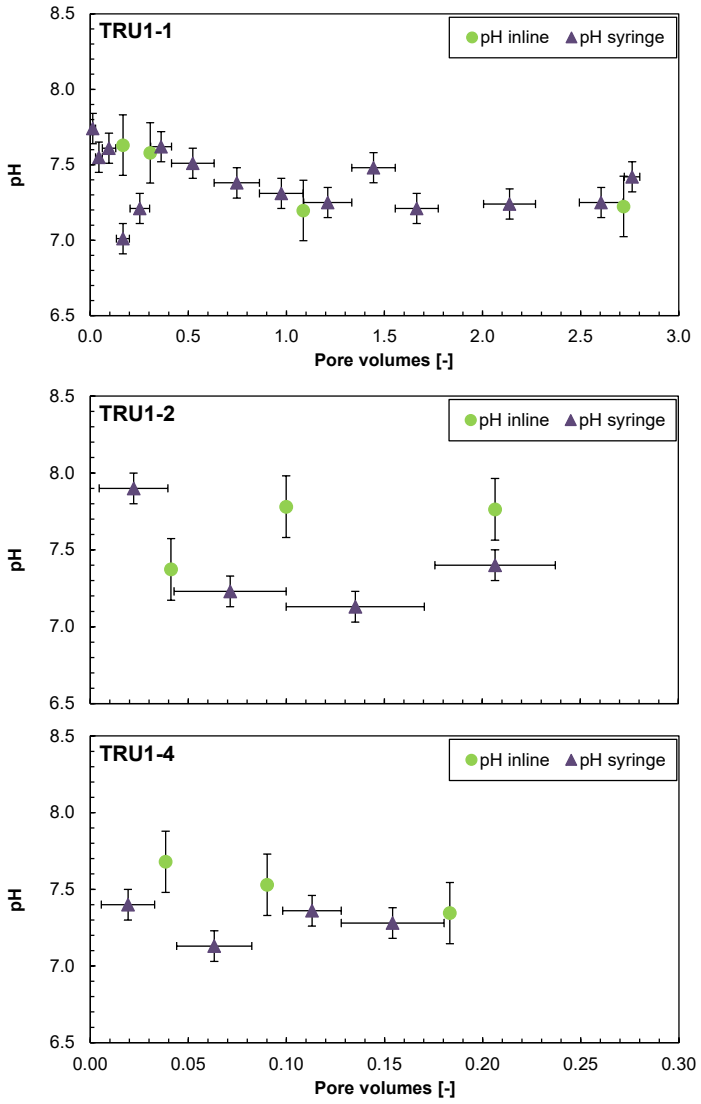

Fig. 4.7-14: Evolution of pH during advective displacement experiments

TRU1-1 = 812.24 m (Wedelsandstein Fm.); TRU1-2 = 867.97 m (Opalinus Clay); TRU1-4 = 926.14 m (Opalinus Clay); Pore volume fractions relate to transport time based on water content. Experiment duration 20 to 90 days. Horizontal length of symbol bar covers the sampling interval of the sample syringe (in-line pH measurements cover a pore volume smaller than symbol width), vertical bars are an estimate of combined uncertainties.

4.7.5.5 Early displaced aliquots representing the porewater composition

Early displaced aliquots were generally obtained by averaging the first two measured samples (Tab. 4.7-12). For the experiment of the Wedelsandstein Formation (TRU1-1) the first measured sample was neglected, as the syringe piston popped out from the syringe during sampling due to fast initial flow, thus exposing the sample to atmosphere that potentially introduced some artefacts, e.g. evaporation and outgassing.

Interpretation of these early displaced aliquots as being representative of the in situ porewater contained in the core at the time of the experiment requires integration and interpretation of the entire data set supported with geochemical calculations. Only speciation calculations are included in this data report for the early compositions. Speciation calculations for all individual syringes are provided in Appendix D. The laboratory pH values were used for the speciation calculations. TIC was used as constraint for inorganic carbon.

Tab. 4.7-12: Average composition of earliest aliquots from advective displacement experiments

Parameter	**Unit**	**TRU1-1**	**TRU1-2**	**TRU1-4**
Depth	[m]	812.24	867.97	926.14
Sample ID RWI		TRU1-1-812.24-AD	TRU1-1-867.97-AD	TRU1-1-926.14-AD
Geol. unit		Wedelsandstein Fm.	Opalinus Clay	Opalinus Clay
pH inline	[-]	7.63	7.58	7.60
pH lab	[-]	7.58	7.57	7.27
Na	[mg/L]	5'791	6'075	6'108
NH4	[mg/L]	n.d.	n.d.	n.d.
K	[mg/L]	76.6	63.2	77.8*
Ca	[mg/L]	960	1'059	1110
Mg	[mg/L]	273	309	291
Sr	[mg/L]	48.3	46.8	49.1
Ba	[mg/L]	< 0.5	< 0.5	< 0.25
Si	[mg/L]	3.8	4.4	4.6
Al	[mg/L]	< 10	< 10	< 2.5
F	[mg/L]	< 1.6	< 1.6	< 1.6
Cl	[mg/L]	9'706	10'455	9'734
Br	[mg/L]	9.8	9.1	6.8
NO3	[mg/L]	8.84	21.2	42.1
SO4	[mg/L]	1'529	1'801	2'340
I	[mg/L]	4.26	2.45	n.d.
TOC	[mg/L]	334	300	231
TIC	[mg/L]	34.6	74.8	35.1
lactate	[mg/L]	< 20	< 20	< 20
acetate	[mg/L]	23	153	349
propionate	[mg/L]	< 20	< 20	< 20
formate	[mg/L]	< 20	< 20	< 20
$\delta^{18}O$	[‰VSMOW]	-4.53	-4.92	-6.41
$\delta^{2}H$	[‰VSMOW]	-41.6	-45.1	-46.9

* Large difference between first and second aliquot, presumably drilling fluid contamination in the first aliquot (93.4 mg/L).

The speciation calculations (Tab. 4.7-13) reveal a cation charge surplus (positive 'Charge') that is 1 – 3.3% (6 – 22 meq/L) and partially explained by significant acetate concentrations that were not included in the speciation but listed in the table. The aliquots are all significantly oversaturated with respect to calcite and also dolomite. Such oversaturation may result from shifts in pH linked to potential in-gassing or outgassing of CO_2 during sampling and storage. Alternatively, the large TOC (and TC) contents pose analytical difficulties to obtain TIC and associated errors may be larger than commonly assigned to TIC measurements. There is also evidence that TIC may be produced during sampling and storage from the oxidation of organic carbon (see Section 4.7.5.4).

Saturation is also slightly exceeded for celestite but not for gypsum. The implication is that the ion-activity product ($[Sr]\cdot[SO_4]$) is a controlling factor, but this does not necessarily mean that celestite is also present in the core before the experiments. The sulphate concentration in the injected APW is similar to the concentrations in the early extracts of the Opalinus Clay samples but distinctly higher than in the early aliquots obtained from the Wedelsandstein (Fig. 4.7-8). Ca and Sr are eluted initially at much higher concentrations compared to the APW and are decreasing quite rapidly. To maintain above mentioned ion-activity product at the value of the equilibrium constant, the decreasing cation concentrations are compensated by increasing activity coefficients as a function of decreasing ionic strength. These cation trends are therefore coupled to the relatively rapid breakthrough of the anions that dictate the evolution of the ionic strength. A more in-depth analysis and interpretation will have to be carried out, including reconstructions by geochemical modelling.

Tab. 4.7-13: Saturation state of earliest aliquots from advective displacement experiments

Parameter	**Unit**	**TRU1-1**	**TRU1-2**	**TRU1-4**
Depth	[m]	812.24	867.97	926.14
Geol. unit		Wedelsandstein Fm.	Opalinus Clay	Opalinus Clay
Charge	[eq/kg]	1.7E-02	6.6E-03	2.2E-02
Carge %-error		2.71	0.98	3.32
Acetate	[eq/kg]	3.9E-04	2.6E-03	5.9E-03
Ionic strength	[mol/kgw]	0.35	0.38	0.38
tot_alk	[eq/kg]	0.00	0.01	0.00
pH (Lab)		7.58	7.23	7.27
Log P_{CO2}		-2.53	-1.86	-2.23
SI(calcite)		0.74	0.73	0.46
SI(dolomite-o)		1.30	1.31	0.71
SI(dolomite-d)		0.75	0.76	0.16
SI(gypsum)		-0.30	-0.22	-0.09
SI(celestite)		0.12	0.15	0.27
SI(strontianite)		-0.11	-0.17	-0.45
SI(anhydrite)		-0.51	-0.43	-0.30

WATEQ4F thermodynamic data base; 25 °C; dolomite-o: ordered dolomite; dolomite-d: disordered dolomite.
Charge = Σ(cation charge) - ׀Σ(anion charge)׀ ; Charge %-error = 100 charge/(Σ(cation charge) + ׀Σ(anion charge)׀).

4.7.5.6 Initial values and evolution of stable water isotope composition

$\delta^{18}O$ values in the TRU1-1 experiment (Wedelsandstein Formation) evolve from a scattered plateau comprising samples from the first 0.4 percolated pore volumes towards the APW value, which is finally reached after approximately 2 percolated pore volumes (Fig. 4.7-15). In contrast, $\delta^{18}O$ values in the experiments from the Opalinus Clay immediately decrease. A final convergence with the APW, however, could not be evaluated due to short experimental duration. The last two samples in experiment TRU1-4 show higher $\delta^{18}O$ values than the previous samples. This presumably relates to issues of sampling, storage and sample preparation, because very small sample volumes had to be processed in some cases and these are prone to evaporation effects.

For the TRU1-1 and TRU1-2 experiment, the evolution of $\delta^{2}H$ is characterised by an initial slight decrease in the first 0.1 percolated pore volumes followed by a short plateau. For the long-running TRU1-1 experiment, after around 0.3 percolated pore volumes, $\delta^{2}H$ values start to increase and converge towards the heavy $\delta^{2}H$ value of the APW. The extent of breakthrough is much less compared to $\delta^{18}O$ for reasons that are not intuitively obvious.

One hypothesis is that there is an effect from dry cutting the core surfaces during sample preparation. This may induce evaporation of small amounts of porewater in the close vicinity of the cut surfaces, thus, enriching the residual porewater in heavy isotopes. Percolation would then first yield isotopically heavy signatures, which are then gradually mixed with the in situ signature, and increasingly also affected by the breakthrough of the traced APW (ca. +100 ‰ VSMOW for $\delta^{2}H$ and -11.5 ‰ VSMOW for $\delta^{18}O$). This would explain the observed trends for $\delta^{2}H$ in the TRU1-1 experiment. Note, that the experiments TRU1-2 and TRU1-4 were terminated prior to the onset of the tracer breakthrough. In case of the oxygen isotopes the APW is significantly lighter than the in situ porewater and accordingly, the trend of $\delta^{18}O$ will always decrease as a function of replaced pore volumes (i.e. first by mixing with the non-evaporated porewater and later with the APW). This could explain the apparently immediate breakthrough behaviour in experiment TRU1-2. The suspected evaporation effect on $\delta^{18}O$ would be less compared to $\delta^{2}H$ due to the prevalence of kinetic isotope fractionation during evaporation. In laboratory experiments a slope of $a = 4.34$ was observed for the relation $\delta^{2}H = a\ \delta^{18}O\text{-}c$ (Cappa et al. 2003). In the $\delta^{2}H$ vs. $\delta^{18}O$ plot (Fig. 4.7-16) the early samples of the experiment, prior to the start of APW breakthrough follow a trend with a similar slope. A more in-depth analysis is attempting to quantify this process. In past studies, wet cutting was used rather than dry cutting, and this led to a small component of contamination by tap water for the early extracted water isotopes (Mäder & Waber 2019). The high concentrations of DOC may also influence the water isotopic system, or any microbial activity, as well as any precipitation of hydrous minerals that may be induced by advective displacement.

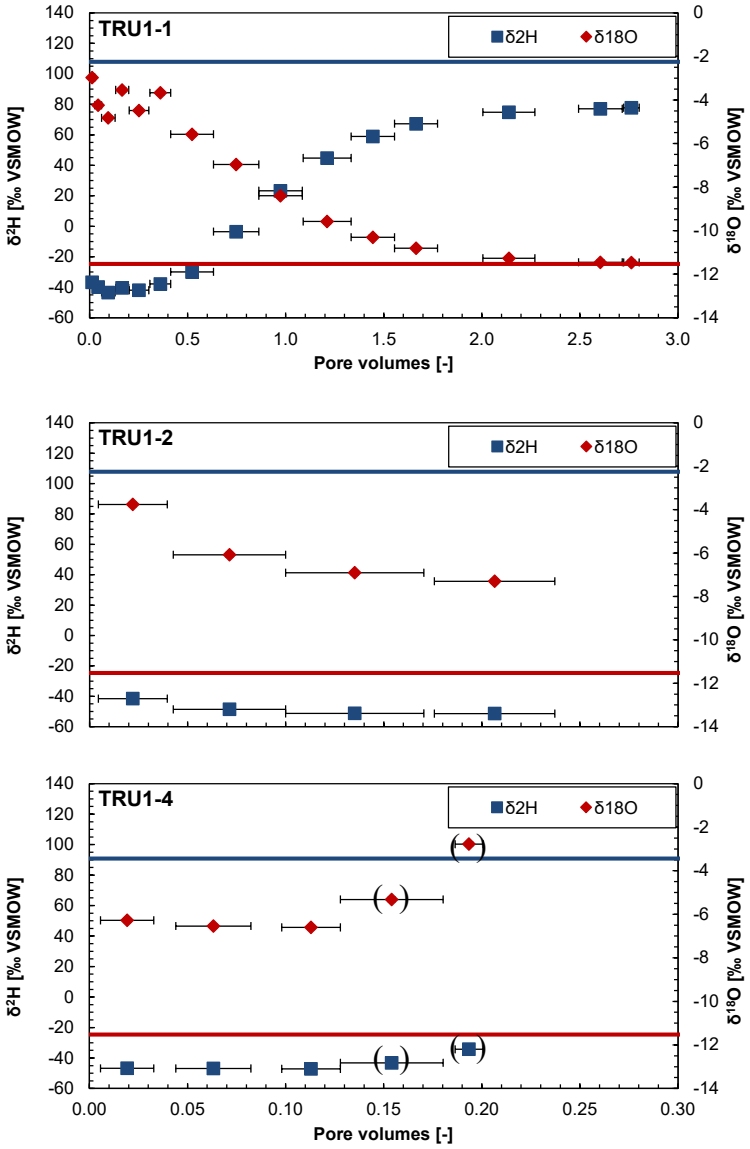

Fig. 4.7-15: Evolution of δ^2H and $\delta^{18}O$ during advective displacement experiments

TRU1-1 = 812.24 m (Wedelsandstein Fm.); TRU1-2 = 867.97 m (Opalinus Clay); TRU1-4 = 926.14 m (Opalinus Clay); Pore volume fractions relate to transport time based on water content. Experiment duration 20 to 90 days. Horizontal length of symbol bar covers the sampling interval. Measurement errors are 1.5 ‰ for δ^2H and 0.1 ‰ for $\delta^{18}O$. Symbols in brackets indicate less reliable datapoints.

The observed differences between $\delta^{18}O$ and δ^2H concerning the extents of breakthrough are discussed below.

The stable isotope compositions in $\delta^{18}O$ vs δ^2H coordinates (Fig. 4.7-16) for the experiment from the Wedelsandstein Formation display a slightly curved data array extending from the earliest and isotopically lightest (δ^2H) / heaviest ($\delta^{18}O$) extracts towards the APW isotopic composition. For the short-running Opalinus Clay experiments, no indication of a breakthrough of the isotopically

heavy (δ^2H) APW was observed. Earliest aliquots of each experiment (on right side of arrays) define a trend distinctly below the global meteoric water line, and also slightly inclined towards the GMWL with increasing sample depth. This is compared to other data sources in more detail in Chapter 5.

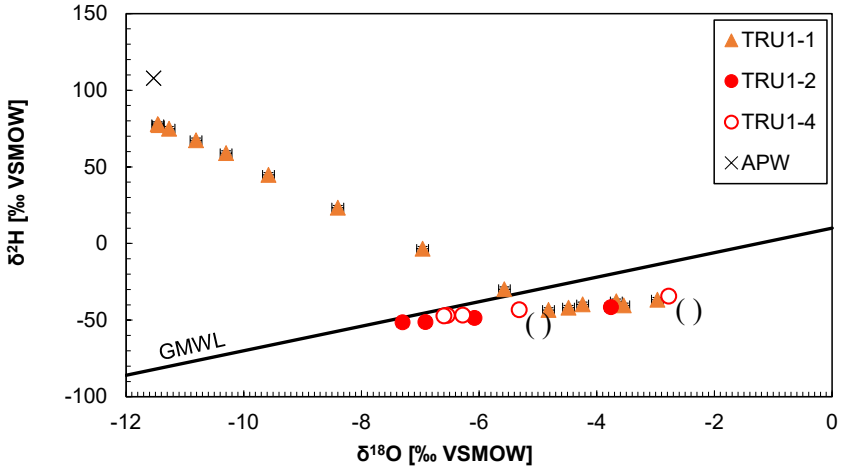

Fig. 4.7-16: Stable isotope composition of aliquots from advective displacement experiments

TRU1-1 = 812.24 m (Wedelsandstein Formation); TRU1-2 = 867.97 m (Opalinus Clay); TRU1-4 = 926.14 m (Opalinus Clay); Measurement errors are 1.5 ‰ for δ^2H and 0.1 ‰ for $\delta^{18}O$. GMWL is the global meteoric water line. 1st aliquots are located the furthest to the right, and evolve towards the left. Symbols in () are considered non-reliable.

4.7.6 Derivation of anion-accessible porosity

There are several ways by which chloride and bromide accessible porosity fractions may be obtained. The principle is the same: namely the ratio between the anion concentration obtained from aqueous extracts up-scaled to porewater content divided by that obtained from earliest extracts from the percolation experiments (discussion in Waber ed. 2020 and Mäder 2018). There are some variants depending on how water contents were measured and averaged, or how inferred water losses may be corrected. In the case where a full breakthrough is captured for chloride, such a ratio may also be obtained by post-mortem aqueous extracts and the latest aliquots sampled before the end of the experiments (for the outlet / top), or the injected APW (for the inlet / base). However, for borehole Trüllikon-1-1, no post-mortem aqueous extracts were performed. Data for bromide is limited to the Wedelsandstein Formation sample due to too low Br concentrations for the Opalinus Clay samples.

The top two data lines (Tab. 4.7-14) list the average concentrations (Cl, Br) for the first two aliquots as shown in Tab. 4.7-12. The subsequent six lines list the up-scaled concentrations to water content, in three different ways for both chloride and bromide. The following three lines list different Cl concentrations up-scaled to water content: for the sample from above the AD core (_upscaled_top), for the sample from below (_upscaled_base) and a corrected and averaged value (top and base). The correction compensates for a small amount of water loss (unsaturated volume) commonly observed and evaluated from a measured net water uptake. The net water uptake is the measured water uptake (mass gain of the core during the experiment) corrected for a commonly measured volume increase during the experiment (Section 4.7.3 and Tab. 4.7-3). The correction hinges on the assumption that sample treatment for the AD core and the off-cuts share the same

history (core handling, storage, sample preparation) and therefore also potentially underwent similar water losses. These corrections are rather small for TRU1-1 and TRU1-4, with small net water uptakes, whereas for TRU1-2 desaturation was larger and resulted in a correction of 8% (relative) for chloride. The following three lines contain the same data for Br. The range in up-scaled Cl and Br concentrations of top and bottom samples is an indication of heterogeneity, mainly in clay content. A homogeneous sample with respect to the degree of anion-exclusion should yield the same up-scaled Cl and Br concentrations, despite differences in water content. A consistent proportion of anion-accessible porosity would then be evaluated regardless of choosing a sample from the top or from the base as a reference for the early displaced aliquots.

The final data block (Tab. 4.7-14) lists the accessible porosity fraction obtained by various combinations and averaging. The first four lines list values that would be derived without knowledge from post-mortem analysis (water content from pre-characterisation), with the most meaningful combinations shaded in grey. Shaded in blue are the "best" values after applying a correction for water contents as mentioned above.

There is in general excellent agreement and consistency among the different ways of evaluation and pre-characterisation and post-mortem water content measurements. This renders this data set quite robust. Sample 812.24 m (Wedelsandstein Formation) shows some modest discrepancy between top and average evaluations, due to a 10% difference between aqueous extract solutions upscaled to porewater concentrations derived from top and bottom samples. For these samples, clay-mineral content differed significantly with 22% and 14% in top and bottom sample, respectively. There is also very good agreement between the accessible porosity fraction derived for chloride and bromide for sample 812.24 m (Wedelsandstein Formation), attesting among other factors to the excellent analytical work for bromide analysis at low concentrations in the aqueous extracts.

The two experiments from the Opalinus Clay span a range of accessible porosity fraction for chloride from 0.37 to 0.47. This is consistent with earlier work from Opalinus Clay and clay-rich «Brauner Dogger». In contrast, chloride and bromide accessible porosity fractions calculated for the Wedelsandstein Formation are significantly higher, ranging from 0.73 to 0.79, which is in agreement with the low average clay-mineral content of only 18 wt.-% (Tab. 4.7-3). The accuracy is limited by the basic assumptions underlying the approach and by sample heterogeneity to some degree, mainly in water content. The combined measurement uncertainties are dominated by the analytical error associated with Cl and Br concentrations and are probably not more than ±10%.

Tab. 4.7-14: Chloride and bromide-accessible porosity fractions

Preferred values are shaded in blue.

Parameter	**Unit**	**TRU1-1**	**TRU1-2**	**TRU1-4**
Depth	[m]	812.24	867.97	926.14
Geol. unit		Wedelsandstein Fm.	Opalinus Clay	Opalinus Clay
Cl-AD_ave (1-2)	[mg/L]	9'706	10'455	9'734
Br-AD_ave (1-2)	[mg/L]	9.78	9.10	6.76
Cl-AqEx-upscaled_top	[mg/L]	7'358	4'920	3'641
Cl-AqEx-upscaled_base	[mg/L]	8'060	4'654	3'611
Cl-AqEx-upscaled_ave_corr	[mg/L]	**7'450**	**4'419**	**3'589**
Br-AqEx-upscaled_top	[mg/L]	7.10	bd	bd
Br-AqEx-upscaled_base	[mg/L]	7.92	bd	bd
Br-AqEx-upscaled_ave_corr	[mg/L]	7.25	bd	bd
Cl-AqEx_top / Cl-AD_ave		0.76	0.47	0.37
Br-AqEx_top / Br-AD_ave		0.73	bd	bd
Cl-AqEx_ave / Cl-AD_ave		0.79	0.46	0.37
Br-AqEx_ave / Br-AD_ave		0.77	bd	bd
Cl-AqEx_ave_corr / Cl-AD_ave		0.77	0.42	0.37
Br-AqEx_ave_corr / Br-AD_ave		0.74	bd	bd

4.7.7 Transport properties marked by breakthrough of δ^2H, $\delta^{18}O$, Cl and Br

There are four components that can be used to elucidate on transport properties by their breakthrough behaviour, namely Cl, Br, and the water isotopes δ^2H and $\delta^{18}O$. Chloride is a good tracer in these experiments because the APW is distinctly less saline than the in situ porewater (negative breakthrough). The resolution towards a full breakthrough is diminished because small differences between large concentrations can no longer be resolved. Bromide is a break-out tracer that is gradually flushed out of the core (no Br in the APW). Again, as a full break-out is approached, bromide concentrations tend to fall below the detection limit. Water tracers also feature a contrast between the in situ porewater (Tab. 4.7-12) and the APW. Particularly δ^2H was traced to ca. +100‰ VSMOW in the APW, but also $\delta^{18}O$ has a contrast of nearly 8 ‰ VSMOW. Given the short duration of the two experiments from the Opalinus Clay, breakthrough curves are only calculated for the experiment of the Wedelsandstein Formation.

For comparison (Fig. 4.7-17) all breakthrough data are normalised to 1 and the breakout of chloride and bromide is inverted to mimic a breakthrough behaviour. The normalised breakthrough of chloride, for example, is given by $1-(Cl-Cl_{APW})/(Cl_{PW}-Cl_{APW})$, where Cl_{PW} refers to the value of the first aliquot of the plateau that most closely represents the in situ porewater composition. Chloride and bromide breakthrough are identical. This same behaviour was illustrated in earlier work by Mäder (2018), where a very slightly faster breakthrough for Br was observed. Cl and Br achieve a full breakthrough after around 1.6 percolated pore volumes. Bromide breakthrough cannot be tracked beyond the percolation progress where it drops below detection (seemingly missing points in Fig. 4.7-17). There is some ambiguity in dealing with data scatter

that may be present in the first few syringe compositions (e.g. Br, Cl), and the choice made to define the initial value that is used for normalisation of breakthrough curves. Different choices may shift curves somewhat, but this is a minor effect for these relatively smooth data trends.

$\delta^{18}O$ breaks through more slowly compared to the anions Br and Cl and reaches a full breakthrough just after more than 2 percolated pore volumes. $\delta^{2}H$ displays an anomalous behaviour during the early breakthrough, possibly for reasons discussed in Section 4.7.5. Deuterium lags considerably behind oxygen suggesting some sort of retardation mechanism that is presently not well understood. The two water tracers may interact differently with the accessible porewater volumes and mineral surfaces. This behaviour was also observed with samples from the Schlattingen-1 geothermal well (Mäder & Waber 2017) and also for samples from the Bülach-1-1 borehole (Mazurek et al. 2021).

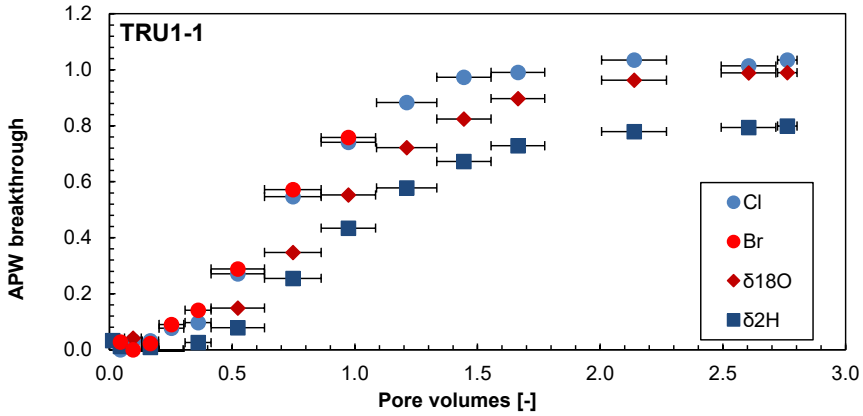

Fig. 4.7-17: Breakthrough of Cl, Br, $\delta^{2}H$ and $\delta^{18}O$ during advective displacement experiments

TRU1-1 = 812.24 m (Wedelsandstein Fm.). Pore volume fractions relate to transport time based on water content. Experiment duration is 89 days. Horizontal length of symbol bar covers the sampling interval.

4.7.8 Concluding remarks and open issues

Three successful advective displacement experiments were conducted on samples from the clay-rich Dogger units, especially focussing on the derivation of a representative porewater composition and with less emphasis on transport properties. Thus, the number of samples, extent of characterisation and experimental duration was less than for Bülach-1-1 (Mazurek et al. 2021). Nevertheless, a systematic and consistent data set on petrophysical and geochemical properties was obtained, not only of value for the specific site characterisation but also for interpretation of porewater chemistry and chloride / bromide accessible porosity fractions across all TBO drilling sites.

Advective displacement experiments on samples from the clay-rich Dogger units supplied a large amount of systematic, consistent and plausible data on petrophysical and geochemical properties of high quality. Samples covered a clay-mineral content of 18 (Wedelsandstein Formation) to 41 wt.-% (Opalinus Clay). This rather large range in clay-mineral content is reflected in derived anion-accessible porosity fractions ranging from 0.76 – 0.83 (Wedelsandstein Formation) to around 0.44 (Opalinus Clay) and hydraulic conductivities for the two formations differ by one order of magnitude.

Earliest displaced aliquots are most representative of the porewater contained in the sample cores, possibly subject to some artefacts, but these aliquots are not equally representative for the in situ porewater due to issues of drilling, unloading, temperature change, handling and storage. While derived Cl and Br concentrations are robust with respect to such artefacts, the sulphate system in all aliquots appears to be controlled by celestite equilibrium. This either implies that such a control is imposed by this mineral being initially present, or that a disturbance causes to reach such a solubility-product control. In the latter case, the reconstruction of the porewater sulphate concentration is more challenging and may also influence the carbonate system and clay-exchanger complex by ways of interdependent thermodynamic mass-action equilibria.

Like in all earlier work, there are unusually high concentrations of DOC mobilised in the earliest aliquots, decreasing gradually to values more in line with aqueous extracts but still at significant concentrations. Remarkably, earliest aliquots show moderate nitrate concentrations (9 – 43 mg/L) that gradually decrease to 2 – 4 mg/L at later sampling times, a feature not observed in samples from Bülach-1-1. Corresponding aqueous extracts also show values of 0.5 – 1 mg/L nitrate that would up-scale to 12 – 24 mg/L at the measured water content. The origin of this nitrate is likely the kerogenous solid organic matter, but there is relatively little data and experience to compare such findings.

An interesting feature – not yet well understood – is the observed delayed breakthrough of deuterium (δ^2H traced in the APW) compared to $\delta^{18}O$ that elutes more regularly as expected for a water tracer. However, compared to observations from more clay-rich units in the Bülach-1-1 borehole (Mazurek et al. 2021), the delay in deuterium breakthrough determined here for the Wedelsandstein Formation is clearly less pronounced, thus indicating some different interaction of the water tracers with clay surfaces or accessible porosity fractions.

An initial decreasing trend of deuterium isotopic signatures in early displaced aliquots is suspected to be the result of evaporation from the surface during dry cutting of the core. Evaporation would also affect the concentration of ions in the earliest displaced aliquots. Calculations based on the deuterium isotopic signatures would indicate an evaporation of 1 – 8% of the porewater obtained in the earliest aliquots.

It appears that there was a small component of contamination of potassium (and silica) from the potassium-silicate drilling fluid, as observed in the aqueous extracts and in one of the first sampling syringes from an Opalinus Clay experiment. However, this disturbance does not affect the critical data required for our key-observations.

There are no fundamental adaptations needed to the methods prompted by this study. The mechanical, hydraulic and electronic or sensor aspects of the experimental set-up reliably performed for the duration of the experiments and even longer as shown in previous experiments. Likewise, the analytical procedures were already optimised and adequate, naturally limited by very small sample volumes for some cases.

4.8 Water-isotope data from diffusive-exchange experiments

H. Niklaus Waber

The porewater isotope composition ($\delta^{18}O$, $\delta^{2}H$) was derived by isotope diffusive-exchange experiments conducted on core material of 68 samples collected over a depth interval between 502.5 and 1'076.0 m borehole length. The obtained highly resolved profiles for $\delta^{18}O$ and $\delta^{2}H$ cover the lithologies from the «Felsenkalke» + «Massenkalk» to the Bänkerjoch Formation.

Isotope diffusive-exchange experiments were conducted in two different laboratories for reasons of quality assurance and optimisation of data production time. Hydroisotop GmbH conducted experiments and analyses on 46 samples between 538.4 and 1'022.2 m of depth at high sampling frequency. Larger sampling intervals were covered by the 22 samples investigated at RWI, University of Bern, between 502.5 and 1'076.0 m.

The data set of Hydroisotop GmbH is given in their data report in Appendix E. The calculated porewater data produced at RWI, University of Bern, are summarised in Appendix A. The complete experimental data underlying the final calculations of the porewater isotope compositions and water contents including their mathematical evaluation are deposited in the TRU1-FileMaker™ database at RWI, University of Bern.

4.8.1 Data evaluation

4.8.1.1 Experimental and analytical data

Both laboratories followed the experimental protocol given in Waber (ed.) (2020). The analytical protocols of the two laboratories are described in Waber (ed.) (2020; for RWI) and Appendix E (for Hydroisotop GmbH).

The conduction of isotope diffusive-exchange experiments by different laboratories asked for a standardised evaluation of the experimental data underlying the derivation of the water stable isotope composition of the in situ porewater. Hydroisotop GmbH provided in addition to their data report (Appendix E) the complete experimental data, which were then re-processed applying the same criteria as used by RWI, University of Bern.

The success or failure of isotope diffusive-exchange experiments depends on several factors with some of them being unknown at the time of sample preparation. Thus, the set-up of the initial experiment conditions strongly relies on experience. Whereas large experience exists with clay-rich rocks with water contents of about 3 – 10 wt.-% and highly mineralised to saline porewater compositions, experience with lithologies of extreme water content (very low/high), extreme porewater mineralisation (highly saline to brine) and special mineralogical compositions (e.g. anhydrite- and/or salt-bearing lithologies) is still limited but growing.

In order to qualify an isotope diffusive-exchange experiment as successful, the following criteria had to be met (within the propagated analytical uncertainties) by the two experiments (so-called LAB and NGW or ICE experiments) conducted for one core sample:

- Equal mass of experiment container including rock and testwater before and after experiment (no severe leakage).
- Equal mass of rock + testwater before and after the experiment. Small differences in this mass might not be detectable outside the analytical error in the total mass of the set-up but might indicate minor evaporation of the porewater – testwater mixture.

  Evaporation of < 10% of the porewater – testwater mixture by leakage can reasonably be corrected by applying Rayleigh-distillation calculations to the measured isotope value before calculating the porewater isotope ratio.
- Reasonable ratio of testwater to porewater yielding a change in the isotope signal of the test-water after equilibration (i.e. outside the propagated analytical uncertainty).
- Limited transfer of testwater to rock or vice versa due to too large salinity difference between testwater and porewater.
- Limited transfer of testwater to rock because of hydrating mineral phases (e.g. anhydrite, halite).
- Stable isotope analyses of testwater solutions within the required accuracy.

Of the 68 investigated samples (or 136 experiments, respectively) only 3 experiment couples did not pass these criteria. The reasons were a too large transfer of porewater to testwater during the experiment (sample 538.43, «Felsenkalke» + «Massenkalk»), a too low mass of porewater in an anhydrite-rich sample of the Klettgau Formation (sample 1'014.37, no mineralogy data available) at Hydroisotop GmbH and a leaking vial and induced strong evaporation during isotope analyses (sample 566.84, «Felsenkalke» + «Massenkalk») at RWI, University of Bern. In addition, core sample 995.83, a dolostone from the Seebi Member of the Klettgau Formation, had a very wet surface at its arrival in the laboratory. This sample was collected within the water-conducting zone in the Klettgau Formation. According to the aqueous extraction data, the sample suffered from contamination by a mixture of drilling fluid and groundwater (*cf.* Chapter 4.4).

An artefact not related to the experimental or analytical procedure was observed for the third preparation campaign performed during December 2019. The experiments of these samples (TRU1-1-722.66-PW, TRU1-1-740.28-PW, TRU1-1-761.64-PW, TRU1-1-791.71-PW, TRU1-1-820.28-PW) fulfil all above criteria. However, it was recognised that the calculated $\delta^{18}O$- and $\delta^{2}H$-values were significantly more negative compared to neighbouring samples investigated at Hydroisotop GmbH. The testwater solutions used for these experiments (LAB-21 and NGW-21) revealed aberrant isotope compositions enriched in ^{18}O and ^{2}H compared to the testwater stock solution. This enrichment was confirmed by re-analyses of these solutions during June/July 2021. It appears that the aliquots of testwater solutions (LAB-21 and NGW-21) used for this sample batch suffered from evaporation during their storage after preparation until they were analysed in May 2020. A reason for this misbehaviour can well be associated with the challenging work conditions in the lab during the COVID lockdown in early 2020. The porewater isotope composition of samples TRU1-1-722.66-PW, TRU1-1-740.28-PW, TRU1-1-761.64-PW, TRU1-1-791.71-PW, TRU1-1-820.28-PW was, therefore, calculated using the average of LAB and NGW testwater samples of the two preceding and the two following preparations campaigns. This results in good agreement of the porewater isotope composition with neighbouring samples although the uncertainty is somewhat larger.

4.8.1.2 Calculation of porewater composition

Hydroisotop GmbH initially calculated the porewater isotope composition from the analysed testwater $\delta^{18}O$- and $\delta^{2}H$-values and the mass of rock used in the experiments (Equation 72 in Appendix A in Waber (ed.) 2020). This approach bases on the assumption that the water content is identical in the two experiments (LAB and NGW or ICE, respectively). Whereas this is generally the case for argillaceous rocks with elevated water content (ca. > 3 wt.-%), larger differences may occur in lithological heterogeneous rocks of lower water content. For such rocks the recalculation of the analysed testwater $\delta^{18}O$- and $\delta^{2}H$-values preferably occurs based on the individual water contents of the rock samples used in the experiment, which may differ (Equation 76 in Appendix A in Waber ed. 2020). The data by Hydroisotop GmbH were thus reprocessed using the same mass balance formulation as used by RWI, University of Bern (i.e. using Equation 76 in Appendix A in Waber (ed.) 2020).

The difference in the resulting porewater $\delta^{18}O$- and $\delta^{2}H$-values when using the mass balance equation assuming equal water contents of the two subsamples, or when using the mass balance equation with the individual measured water contents, respectively, is shown in Fig. 4.8-1. For samples with water contents above about 3 wt.-% the difference in the porewater composition calculated by the two equations is negligible. These findings are important as they allow an adequate comparison of porewater isotope data produced for the argillaceous low-permeability rocks (e.g. Opalinus Clay, Staffelegg Formation) from the present boreholes with those of older boreholes (e.g. Benken, Schlattingen-1?) where the necessary basic experimental information is no longer accessible.

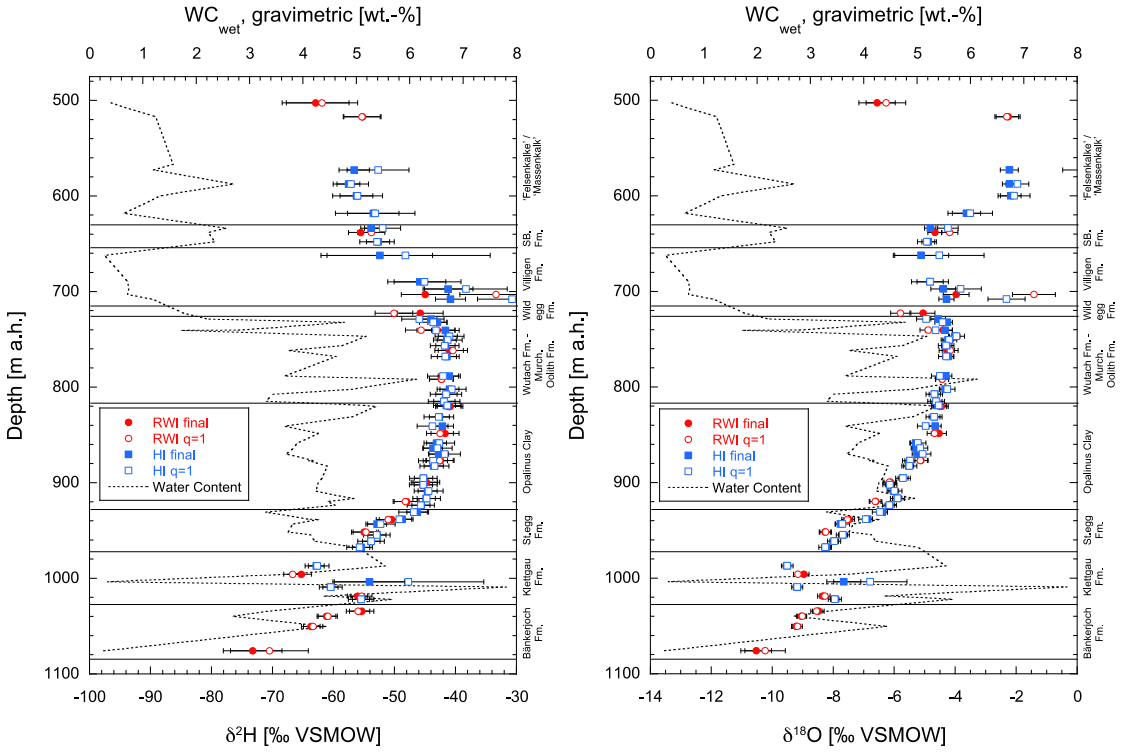

Fig. 4.8-1: Comparison of all porewater $\delta^{18}O$- and $\delta^{2}H$-values derived by isotope-diffusive exchange experiments and calculated by isotope mass balance based on the individual water contents (closed symbols, final) and based on assuming equal water contents (open symbols, q = 1) for the rock in both experiments

Laboratories: RWI = RWI, University of Bern, HI = Hydrosisotop GmbH.

Somewhat larger differences are obtained for limestone, dolostone and anhydrite-bearing rock samples with water contents of about < 3 wt.-%. In these samples of the «Felsenkalke» + «Massenkalk» to Villigen Formation and the Klettgau and Bänkerjoch Formations lithological differences and associated differences in water content occur on the cm-scale what makes it difficult to have equal water contents in the two experiments. As a consequence, the propagated uncertainty of such samples may strongly increase and render the obtained porewater $\delta^{18}O$- and $\delta^{2}H$-values less reliable. For most samples, however, the difference of the porewater $\delta^{18}O$- and $\delta^{2}H$-values calculated by the two approaches is still within this larger propagated uncertainty (Fig. 4.8-1).

The only exceptions in the TRU1-1 borehole are 2 limestone samples from the Hornbuck Member at the base of the Villigen Formation (samples 703.13 and 707.99). The $\delta^{18}O$- and $\delta^{2}H$-values calculated for these samples by assuming identical water contents of the two experiments suggest an excursion towards less negative values. In turn, this excursion disappears when the calculation is performed using the measured ratio q of the water contents (or the mass of porewater, respectively) of the rock masses used in the two experiments (Fig. 4.8-1).

The robustness of the calculated porewater $\delta^{18}O$- and $\delta^{2}H$-values with respect to in situ conditions is further tested according to the following criteria:

1. A relative difference of less than 20% between the average water contents reckoned back from $\delta^{18}O$ and $\delta^{2}H$ data derived from the experiment with testwater depleted in ^{18}O and ^{2}H (NGW/ICE subsamples) divided by the water content based on $\delta^{2}H$.
2. A relative difference of less than 20% between the average water content calculated by isotope mass balance from $\delta^{18}O$ and $\delta^{2}H$ data and the average of the gravimetric water content of the two subsamples used in the experiments.

If the relative difference in the various water contents is larger than 20% the calculated porewater $\delta^{18}O$- and $\delta^{2}H$-values become unreliable. Some of such data nevertheless may be used for further interpretation by accepting the larger propagated uncertainty if the reason for the deviation is clearly known (e.g. contamination with drilling fluid).

All the 65 samples that passed the experimental quality criteria (*cf.* Section 4.8.1.1) also pass criterion 1 above (Fig. 4.8-2), which gives good confidence in the derived porewater isotope compositions. Criterion 2 is met by 63 samples (Fig. 4.8-3). The 2 samples that do not meet the criterion are sample 995.83 from the Seebi Member of the Klettgau Formation and sample 1'039.80 from the Bänkerjoch Formation.

Sample 995.83 has an elevated relative difference of 17% in criteria 1 (Fig. 4.8-2) and a relative difference of 40% in criterion 2 (Fig. 4.8-3). As mentioned above, this dolostone displays clear indication of contamination by a mixture of drilling fluid and groundwater by its appearance upon arrival in the lab and by the aqueous extraction data (*cf.* Chapter 4.4). Therefore, the porewater isotope composition derived for this sample has to be treated with care.

Sample 1'039.80 has a relative difference of only 6% in criterion 1 (Fig. 4.8-2) and a high relative difference of 56% in criterion 2 (Fig. 4.8-3). Aqueous extraction data of this sample do not indicate obvious contamination with drilling fluid (*cf.* Chapter 4.4). However, the aqueous extract solution displays an elevated SO_4 concentration (ca. 1.5 g/L) suggesting the presence of anhydrite. Although anhydrite was not detected in the mineralogical analyses (*cf.* Chapter 4.2), the rocks in the Bänkerjoch Formation frequently contain heterogeneously distributed anhydrite nodules and/or layers. The effect of potential anhydrite hydration on the isotope diffusive-exchange

experiments is unknown so far. Based on that, the porewater isotope composition of sample 1'039.80 should be treated with care.

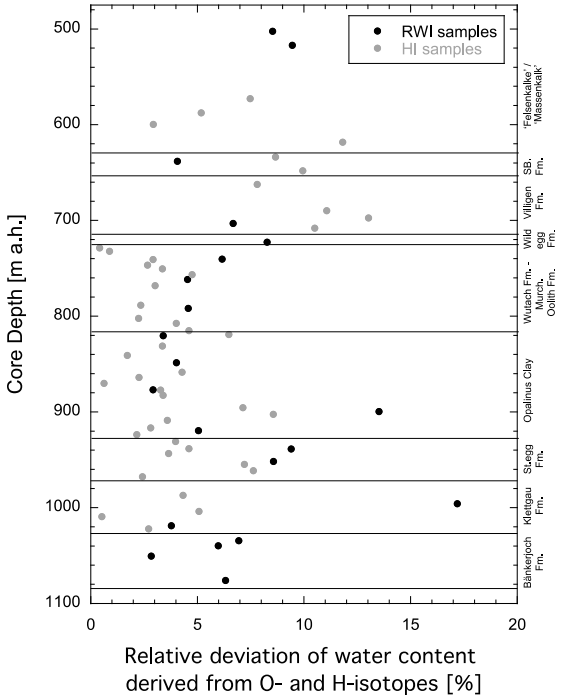

Fig. 4.8-2: Relative deviation of water contents obtained from $\delta^{18}O$ and $\delta^{2}H$ mass balance

The relative deviation is defined as the difference between the water contents obtained from $\delta^{18}O$ and $\delta^{2}H$ data from the experiments with testwater depleted in ^{18}O and ^{2}H (NGW or ICE, respectively) divided by the water content based on $\delta^{2}H$.

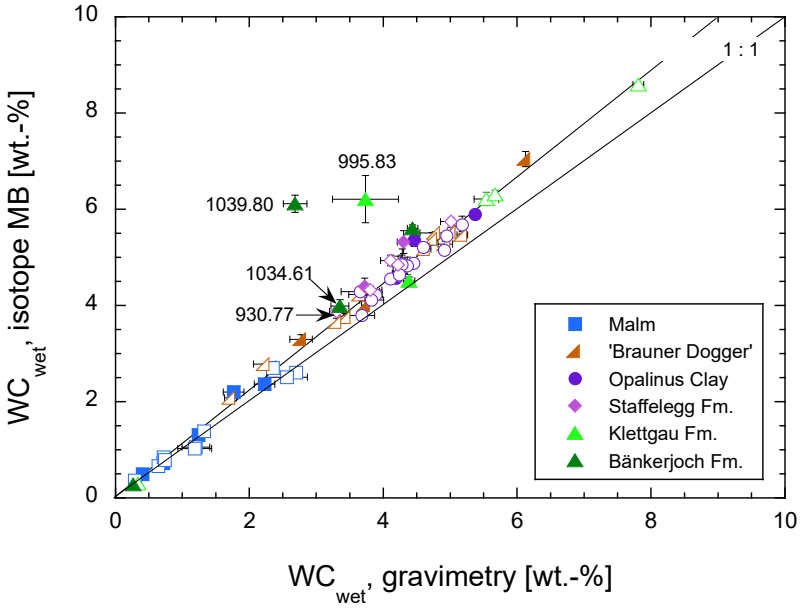

Fig. 4.8-3: Average water content obtained by water-loss at 105 °C (WC_{wet} gravimetry) of the subsamples LAB and NGW/ICE used in isotope diffusive-exchange experiments vs. the average water content calculated from $\delta^{18}O$ and $\delta^{2}H$ mass balance from the NGW/ICE samples (WC_{wet} isotope MB)

Closed symbols: samples investigated at RWI, University of Bern; open symbols: samples investigated at Hydroisotop GmbH.

An interesting case is indicated for samples 1'034.61 (RWI) and 930.77 (HI). The first sample consists of marl with anhydrite layers of the Bänkerjoch Formation and the second sample consists of interlayered calcareous marl of the Gross Wolf Member in the Staffelegg Formation. The water content derived by isotope mass balance differs by 43% and 27%, respectively, when compared to the average gravimetric water content of all three subsamples. However, the difference reduces to 16% and 15%, respectively, when the water content derived by isotope mass balance is compared to only the gravimetric water content of the two subsamples used in the isotope diffusive-exchange experiments (Fig. 4.8-3). The reason for this is the lithological heterogeneity within the drillcore samples. Sample preparation for isotope diffusive-exchange experiments focuses on rock material with high water content, i.e. clay-rich layers. In contrast the material of the PW subsample was collected to be representative for the entire 25 cm long drill core sample (covering its heterogeneity). Therefore, in heterogeneous samples the two different sets of subsamples may differ lithologically and also in their petrophysical properties. Thus, especially in heterogeneous rocks, the water content derived from isotope diffusive-exchange experiments should only be compared to the water content of the two subsamples used in the experiments.

For all remaining 63 samples, the relative difference between the average water content derived from isotope mass balance and the average gravimetric water content of the subsamples used for the experiments is < 20%, thus passing all the experimental quality criteria. All these samples display the consistent, well-known relation between the average water content derived by isotope mass balance and the average of the gravimetric water content of the subsamples used in the experiment in that the difference between these water contents is around 10% and increases with increasing absolute water content (Fig. 4.8-3). As the increase in water content is generally well correlated with the clay content of the rocks (*cf.* Chapter 4.3), it was postulated that this difference might be associated to minor exchange with water of different isotope composition adsorbed on clay minerals (e.g. Pearson et al. 2003).

4.8.2 $\delta^{18}O$- and $\delta^{2}H$-values of porewater

4.8.2.1 Data comparison RWI – Hydroisotop GmbH

All the porewater isotope data that pass the various quality criteria are illustrated in Fig. 4.8-4 as a function of depth. Porewater $\delta^{18}O$- and $\delta^{2}H$-values produced at Hydroisotop GmbH and RWI, University of Bern, generally agree well within the propagated uncertainty across the entire profile and especially across the clay-rich lithologies of the Opalinus Clay and Staffelegg Formation (Fig. 4.8-4).

4.8.2.2 Depth profiles of porewater isotope composition

Similar as in previous studies, the concentration profile developed by the $\delta^{2}H$-value as a function of depth displays less scatter (compared to the propagated uncertainties) than that of the $\delta^{18}O$-values.

In the Malm units from the «Felsenkalke» + «Massenkalk» to the base of the Villigen Formation porewater $\delta^{2}H$-values show a rather smooth trend towards less negative values with depth (Fig. 4.8-4). In contrast, the $\delta^{18}O$-values display a more curved profile with porewater isotope compositions most enriched in ^{18}O in the limestones of the «Felsenkalke» + «Massenkalk». Across the units of the «Brauner Dogger» the porewater isotope composition remains rather constant with $\delta^{18}O$-values around –4.5 ‰ VSMOW and $\delta^{2}H$-values around –42 ‰ VSMOW. These values further extend down to about 850 m of depth into the Opalinus Clay before the porewater isotope composition becomes gradually more negative towards $\delta^{18}O$- and $\delta^{2}H$-values of about –9.1 ‰ VSMOW and –67 ‰ VSMOW, respectively, at around 995 m depth in the water-conducting zone of the Seebi Member in the Klettgau Formation (Fig. 4.8-4). The gradient towards more negative isotope compositions is still weak between about 850 and 920 m depth, whereas it becomes more accentuated in lithologies of the Staffelegg Formation and Klettgau Formation between 920 and 970 m of depth.

From the Seebi Member in the Klettgau Formation porewater $\delta^{18}O$- and $\delta^{2}H$-values appear to describe a second curved profile down to the base of the Bänkerjoch Formation and with the most enriched isotope composition occurring at the interface of the Klettgau Formation to the Bänkerjoch Formation (Fig. 4.8-4). However, owing to the comparatively larger sample spacing and the heterogeneity of the Triassic lithologies, this profile is less well defined.

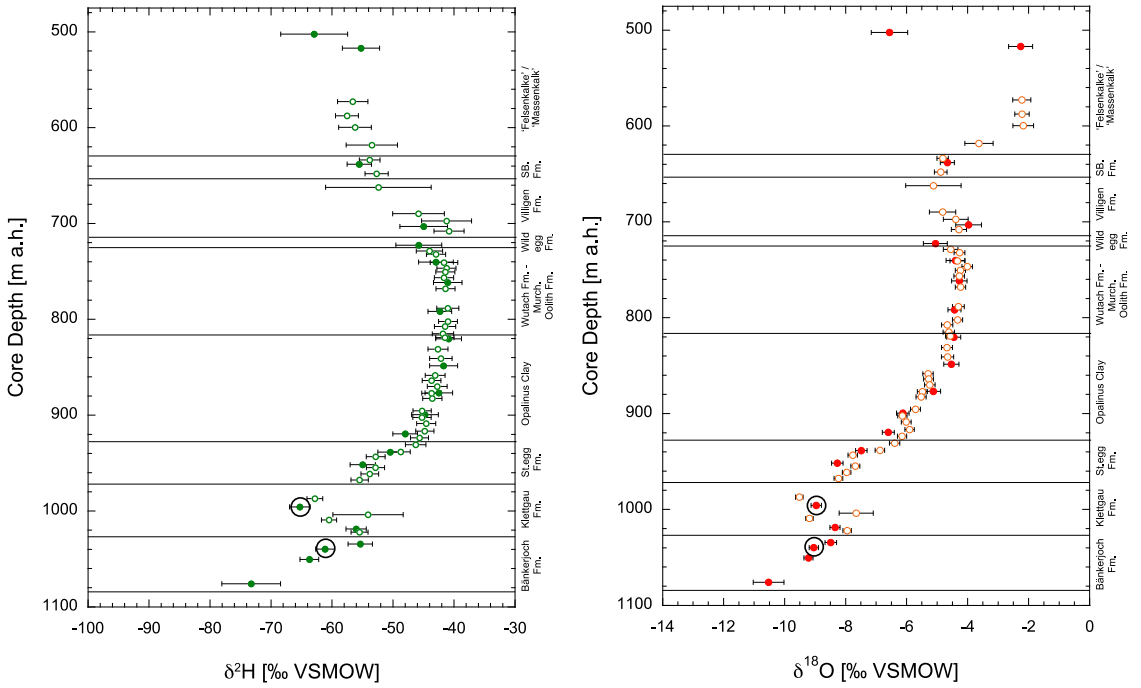

Fig. 4.8-4: Depth distribution of approved porewater $\delta^{18}O$- and $\delta^{2}H$-values obtained from isotope diffusive-exchange experiments

Closed symbols: samples investigated at RWI, University of Bern; open symbols: samples investigated at Hydrosisotop GmbH; samples with black circles are less reliable, see text.

In the $\delta^{18}O$ – $\delta^{2}H$-diagram the isotope composition of porewater in the lithologies encountered by the TRU1-1 borehole display a remarkable constant trend, except for the samples of the «Felsenkalke» + «Massenkalk» units (Fig. 4.8-5). From the Villigen Formation across the «Brauner Dogger» units, Opalinus Clay to the Staffelegg Formation the porewater isotope composition evolves from $\delta^{18}O$- and $\delta^{2}H$-values that fall to the right of the Global Meteoric Water Line (GMWL) towards values that plot on the GMWL indicating a strong meteoric component in the porewater of the lower Staffelegg Formation. Similarly, the isotope composition of porewater in lithologies of the Klettgau Formation and Bänkerjoch Formation has a meteoric signature and evolves towards most negative values in the water-conducting zone of the Seebi Member of the Klettgau Formation (Fig. 4.8-4; see Chapter 5.7 for further discussion).

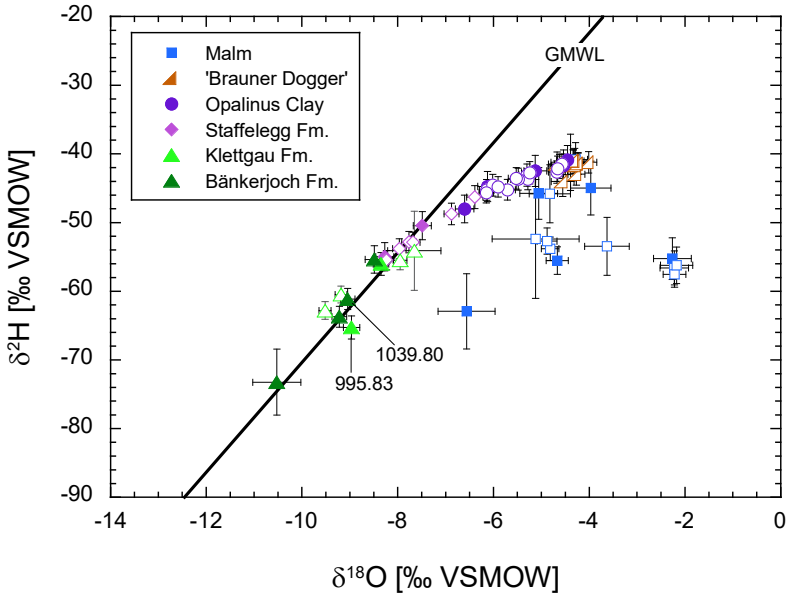

Fig. 4.8-5: $\delta^{18}O$ vs. $\delta^{2}H$-values of porewater obtained from isotope diffusive-exchange experiments

Closed symbols: samples investigated at RWI, University of Bern; open symbols: samples investigated at Hydrosisotop GmbH; samples 995.83 and 1'039.80 are less reliable, see text; GMWL = Global Meteoric Water Line ($\delta^{2}H = 8 \times \delta^{18}O + 10$ ‰ SMOW).

5 Discussion of porewater data

5.1 Chloride data and estimation of Cl^- and Br^--accessible porosity

Paul Wersin & Martin Mazurek

Chloride, a major compound in the porewater, has been determined by squeezing (Section 4.6), advective displacement (Section 4.7) and aqueous extraction (Section 4.4). This anion is considered to behave as a conservative species with no or very limited interaction with the minerals. The same can be said for bromide, which occurs at much lower concentrations in the porewater. In argillaceous rocks, anions are repelled from the negative structural charge of the clay-mineral surfaces and are thus affected by ion exclusion. In other words, they only "see" part of the total water-filled porosity, the fraction of which is often termed anion-accessible porosity (Pearson et al. 2003).

Knowing the concentration of Cl and/or Br in a sample from aqueous extraction ($C_{Cl\ in\ bulk\ porewater}$), the anion accessible porosity fraction f can be estimated from Cl and/or Br measurements in squeezing ($C_{Cl\ in\ squeezed\ water}$) or advective displacement ($C_{Cl\ in\ adv.\ displaced\ water}$) experiments:

$$f_{Cl} = \frac{n_{anion-accessible}}{n_{total}} = \frac{C_{Cl\ in\ bulk\ pore\ water}}{C_{Cl\ in\ squeezed\ or\ adv.displaced\ water}}$$

$C_{Cl\ in\ bulk\ porewater}$ is calculated from:

$$C_{Cl\ in\ bulk\ pore\ water} = \frac{C_{Cl\ in\ aq.extract}}{WC_{dry}\ {}^{S}/_{L}}$$

with C = concentration [mg/L], n = porosity [–], WC_{dry} = water content relative to dry rock mass [g/g], S/L = solid/liquid ratio of aqueous extraction experiment [g/g]. The Br-accessible porosities are derived in an analogous fashion.

The anion-accessible porosities have been derived according to the above equation for squeezed and advectively displaced porewaters (Tabs. 4.6-7 and 4.7-14). In the case of the squeezed waters, it is assumed that the waters squeezed at the lowest pressure reflect the in situ porewater (Mazurek et al. 2015, Wersin et al. 2016). For the advectively displaced waters, the first two aliquots are assumed to be the most representative of the in situ porewater (Section 4.7).

A further possibility to estimate anion-accessible porosities in argillaceous rocks is via through-diffusion tests with anionic tracers (Cl) in combination with a water tracer (e.g. HTO). Such a data set was acquired for 30 samples from the TRU1-1 borehole by Van Loon & Glaus (*in prep.*). The samples span across a 400 m thick rock sequence (from «Felsenkalke» + «Massenkalk» to Klettgau Formation) and include a wide range of clay-mineral contents. From the initial transient phase of the through-diffusion tests, the diffusion-accessible porosity of HTO and Cl was calculated (approach described in Van Loon 2014).[8]

The derived values of the Cl-accessible porosity fraction (f_{Cl}) for the three data sets are shown as a function of the clay-mineral content in Fig. 5.1-1. Consistent porosity fractions are obtained from the three different methods, thus varying around a value of ~ 0.45 at higher clay-mineral

[8] It should be noted that two of the diffusion samples failed to yield reliable data (Van Loon & Glaus *in prep.*) and are not reported here.

contents and suggesting an increasing trend towards lower clay-mineral contents. The onset of this increasing trend is not obvious in view of the scatter of the data and their uncertainties. Moreover, almost all data at lower clay-mineral contents stem from the through-diffusion data set. For clay-poor lithologies, i.e. clay-mineral contents < 20 wt.-%, only a limited number of data with large uncertainties are available, thus not enabling to define a proper range of f_{Cl}. The mean f_{Cl} value at clay-mineral contents of > 20 wt.-% and > 40 wt.-% is 0.470 ± 0.074 (1σ) and 0.449 ± 0.051, respectively. These values are somewhat lower than the corresponding mean f_{Cl} values that were derived for the Schlattingen-1 borehole (0.52 ± 0.05) (Wersin et al. 2016) or the Bülach-1-1 borehole (0.52 ± 0.06) (Mazurek et al. 2021). Increasing f_{Cl} values towards lower clay-mineral contents were also derived for the latter borehole but only for clay-poor samples with clay-mineral contents < 20 wt.-%. At higher clay-mineral contents, f_{Cl} values were rather constant with no obvious trend. These slight differences of the relationship between clay-mineral content and f_{Cl} at BUL1-1 and TRU1-1 should not be over-emphasised at this stage, given the fact that the number of data points is limited, in particular on the clay-poor side. It should be noted that the scatter of f_{Cl} data is considerably even for clay-mineral contents > 40 wt.-%, showing a range of 0.37 – 0.54 for most data points from all three methods. Considering the mean value of 0.45, this reflects an uncertainty of about 20%. Overall, the uncertainty band of 0.45 ± 20% well represents these data.

Within the interval between the Malm and Keuper aquifers, the lithologies in the TRU-1 profile vary substantially. In order to derive a porewater profile for Cl, anion accessibility in these lithologies must be known or assumed. On the basis of the f_{Cl} -clay-mineral content relationship, a f_{Cl} value of 0.45 is used for clay-mineral contents ≥40 wt.-%. For the range from 40 to 0 wt.-% clay-mineral content, a linear increase towards 1 is assumed. An uncertainty range of ± 20% is considered for f_{Cl}, which is probably sufficient for clay-rich lithologies but may still be an underestimation for clay-poor rocks. This uncertainty propagates into the calculated Cl concentrations per anion-accessible porewater, i.e. an error of ± 20% must be considered in addition to the propagated analytical error. The fact that f_{Cl} shows such a wide range when plotted against the clay-mineral content suggests that the latter is not the only parameter that determines anion accessibility. Correlations with individual clay minerals (e.g. illite or smectite end-members) are not better than those with the total clay-mineral content. Mean grain size, grain-size distribution, fabric and other phases are expected to affect anion accessibility as well. Furthermore, according to theory, anion accessibility also varies with the salinity and composition of the porewater, i.e. is not just a material property. All these partly interdependent effects cannot be properly quantified at this stage, which severely limits the application of theoretical models.

For Br, only advective displacement data from a clay-poor sample (clay-mineral content of 18 wt.-%) from the Wedelsandstein Formation are available (not shown). The derived f_{Br} value is 0.77 which is close to the corresponding f_{Cl} value (0.79). In view of the limited data for Br, the same anion-accessible porosity fractions as for Cl are used for Br.

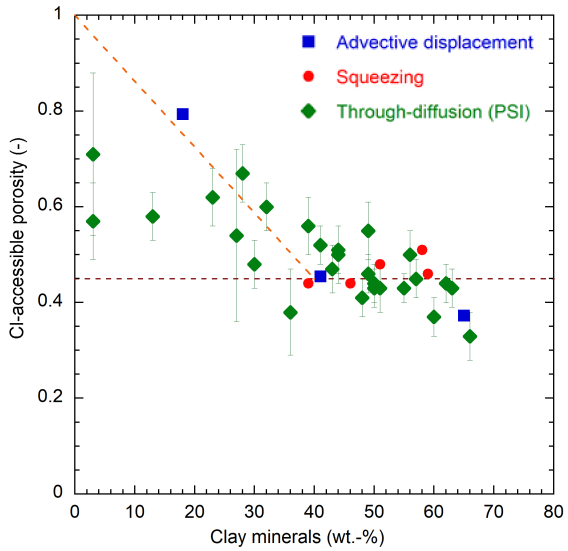

Fig. 5.1-1: Cl-accessible porosity fraction as a function of the clay-mineral content

Errors bars on diffusion data indicate propagated anayltical errors. Error bars on squeezing and advective displacment data are indicated as 20% which represents a rough estimate based on previous studies. Brown dashed line: average f_{Cl} value for clay-mineral contents > 40 wt.-%. Orange dashed line: Linear extrapolation from clay-mineral content 40 to 0 wt.-% (see text).

Fig. 5.1-2 illustrates the Cl-accessible porosity fraction as a function of depth. The upper confining unit, the «Brauner Dogger», exhibits large variations in f_{Cl} values, which is likely mainly due to the large mineralogical and textural heterogeneity within this unit. The f_{Cl} values for the Opalinus Clay show constant values at ~ 0.45 with no clear depth trend, except for the lowermost data points where f_{Cl} is < 0.4. In the underlying Staffelegg Formation the f_{Cl} data suggest a jump in the uppermost sample, followed by a sharply decreasing trend with depth, remarkably similar to what was observed for BUL1-1. In parallel, the clay-mineral content of the samples from this formation shows a tendency to increase with depth in this formation. This may suggest the influence of the clay mineral charge on the anion-accessible porosity. On the other hand, the porewater chloride concentrations and salinity (see next section) also show a strong decrease with depth in the Staffelegg Formation, which may affect the anion-accessible porosity as well as indicated from through-diffusion experiments (Wigger & Van Loon 2017). The results showed that the Cl-accessible porosity fraction increased from 0.35 to 0.61 when increasing the ionic strength from 0.1 to 1.0.

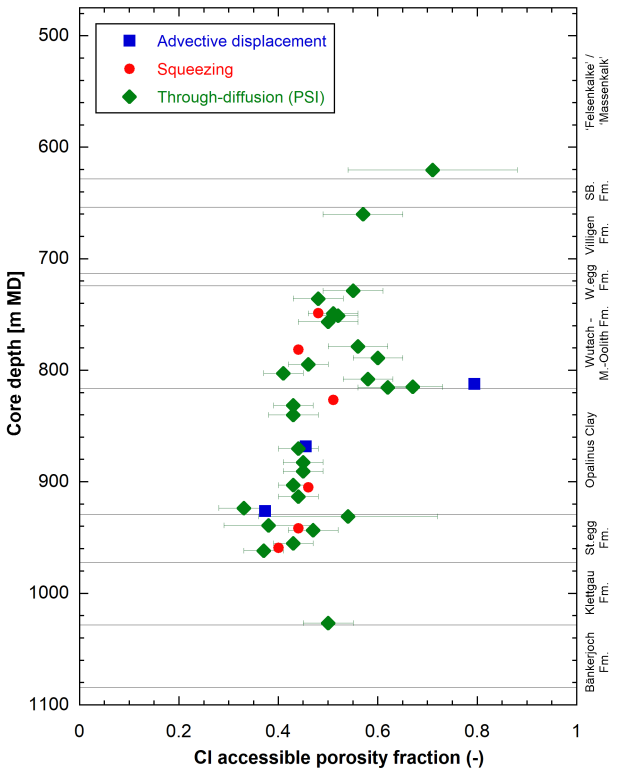

Fig. 5.1-2: Cl-accessible porosity fraction (f_{Cl}) as a function of depth

5.2 Chloride, bromide and Br/Cl profiles

Paul Wersin & Martin Mazurek

In order to calculate the Cl concentration in bulk porewater on the basis of aqueous-extraction data, the water content of the sample must be known (see equation in Section 5.1). For samples studied at Uni Bern, the measured water contents were used for the recalculation. In case of the BRGM samples, measured water contents are more or less strongly affected by evaporation during sample preparation (Section 3.4). Therefore, water content (WC_{dry}) obtained from pycnometer porosity (Φ_{pyc}) was used instead:

$$WC_{dry} = \frac{\phi_{pyc}\,\rho_{pw}}{\rho_{bd}}$$

with ρ_{bd} = bulk dry density, ρ_{pw} = porewater density.

The chloride profile depicted in Fig. 5.2-1 includes aqueous extraction data recalculated to in situ conditions assuming the relationship between clay-mineral content and f_{Cl} as discussed in Section 5.1. The Cl data based on squeezing and advective displacement, as well as those for the groundwaters in the Malm and in the Keuper, are also shown. The error bars include the propagated analytical uncertainty and an additional 20% that reflect the uncertainty related to f_{Cl} (see Section 5.1, Fig. 5.1-1).

Data from all three methods are consistent within the extended error bars. The data from advective displacement tend to be slightly higher than those obtained from squeezing. Note that contamination by drilling fluid was identified in one sample from the Klettgau Formation used for aqueous extraction (Section 4.4). This sample is not included in Fig. 5.2-1 and the following graphics.

The Cl profile between the Malm und the Keuper aquifers indicates a bell-shaped curve, with the highest Cl concentrations in the Opalinus Clay and the «Brauner Dogger» of ~ 10 g/L, decreasing towards the upper and lower aquifer, respectively. A similar Cl profile was derived for the Benken borehole (Gimmi & Waber 2004) from the same siting area and for the nearby Schlattingen-1 borehole (Wersin et al. 2013), even though the upward decrease of the Cl concentration towards the Malm aquifer is more strongly expressed in the TRU1-1 borehole. The Cl concentrations were generally somewhat lower in those boreholes, with maximum concentrations of ~ 7 g/L. The Cl profiles in these boreholes could be explained by diffusive exchange between the low permeability sequence of the Staffelegg Formation – Opalinus Clay – «Brauner Dogger» and bounding aquifers having occurred during the last 0.5 – 1 My (Gimmi & Waber 2004, Wersin et al. 2021).

A closer look at the profile shows a general steady upward increase starting at the level of the Keuper aquifer (~ 1'000 m depth) where a good match between the porewater and groundwater data is manifested. Thus, Cl concentrations increase from ~ 1 near the Keuper aquifer to ~ 10 g/L in the central part of the Opalinus Clay (~ 860 m depth), above which concentrations remain constant up to the top of the formation (826 m depth). The Cl profile in the heterogeneous «Brauner Dogger» displays a significant scatter, owing to the uncertainty related to the water content and, more importantly, to the uncertainty related to the anion-accessible porosity. In the overlying Malm units, a limited scatter is seen, but a decreasing trend towards the aquifer in the «Felsenkalke» + «Massenkalk» can be discerned. The porewater data show good agreement with the groundwater sample in that zone. The profile, however, suggests a local minimum (~ 2'400 mg/L) at around 640 – 660 m depth, located in the Schwarzbach Formation and the top of the Villigen Formation, about 20 – 40 m below the groundwater sample, whose concentration is higher (~ 4'200 mg/L). A similar excursion in the interval at 620 – 660 m depth is observed in the Br profile (see below), as well as in the $\delta^{18}O$ profile (but not in the $\delta^{2}H$ profile) in the depth interval of 660 – 680 m (Section 5.7). Based on the information from core and mud logging, two alternative hypotheses can be invoked to explain these profiles (Section 5.8).

In summary, a consistent Cl profile between the Malm and Keuper aquifers is obtained from squeezing, advective displacement and aqueous extraction data. The profile shape is similar to those derived for the Benken and Schlattingen-1 boreholes. A well-defined profile is identified in the Opalinus Clay, but some more scatter is seen in the confining units (Staffelegg Formation and «Brauner Dogger») and in the Malm units. This scatter is related predominantly to the uncertainty in anion accessible porosity and to a lesser extent to the uncertainty in the water content. In this analysis, a simple relationship of anion-accessible porosity with clay-mineral content (as proxy of surface charge) based on through-diffusion, squeezing and advective displacement data was used. It is worth noting that other relationships with the clay-mineral content (e.g. linear extrapolation from clay-mineral content < 20 wt.-%, < 30 wt.-% or < 50 wt.-%) resulted in a slightly larger scatter in the data. Also, considering relationships between f_{Cl} and smectite or illite content did not result in less data scatter.

The Cl profile below the Keuper aquifer (located in the Seebi Member of the Klettgau Formation) exhibits an increasing trend with depth until the deepest sample at 1'076 m in the Bänkerjoch Formation. Two rather clay-rich samples located in the Ergolz Member, fall off this trend and show much higher Cl concentrations. The reason for this is not clear; it might be related to drilling fluid contamination in this generally sandy lithology, although no indication thereof could be seen from the composition of the aqueous extracts (Section 4.4). Another possibility is that the anion-

accessible porosity fraction (assumed to be related to the clay-mineral content) is overestimated for these clay-rich samples. These two samples do not contain any carbonate minerals, which is exceptional, even though it is unclear if and how this could affect the derived Cl concentrations in the porewater (distinct fabric properties?).

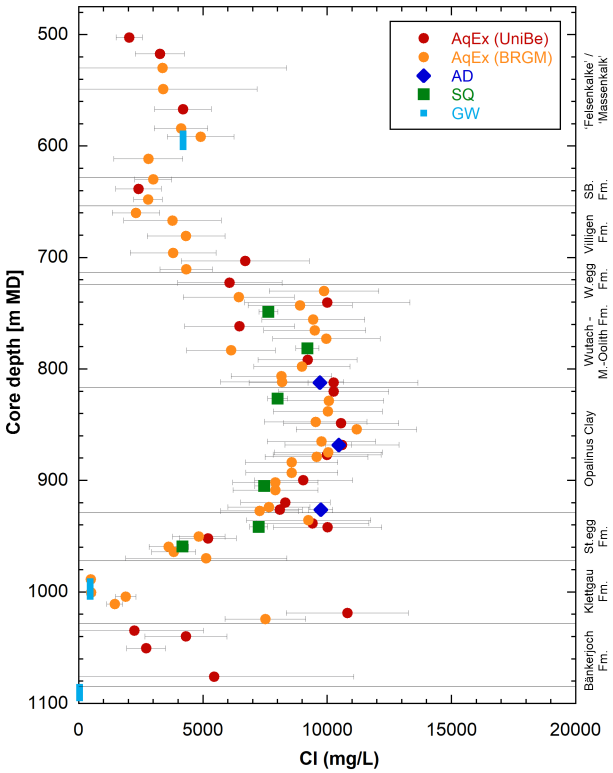

Fig. 5.2-1: Cl profile with data from squeezing, advective displacement, aqueous extraction, and groundwater samples

Aqueous extraction data recalculated to Cl-accessible porosity assuming the relationship between accessibility and clay-mineral content as discussed in Section 5.1. Error bars on the data from aqueous extraction include propagated analytical uncertainty plus another 20% that reflect the uncertainty related to f_{Cl}.

The Br profile shows an increasing trend from the Keuper aquifer up to the top of the Opalinus Clay (Fig. 5.2-2). Above, the increasing trend continues up to the Malm aquifer, but the profile is less defined and displays a considerable scatter. The Br profile is thus similar as the Cl profile in the lower units but diverges from the latter in the upper ones. This can also be illustrated in the Br/Cl ratios which are approximately constant in the lower part of the rock sequence but increase towards the upper part. The Br/Cl profile reveals a remarkable consistency between the three data sets with very little variability except for the Malm units where some scatter is noted. The much smaller scatter is because rock heterogeneity and uncertainty related to anion-accessibility do not affect the Br/Cl ratio contrary to the individual concentrations.

The (1'000*Br/Cl) (molar units) ratio in the Klettgau Formation up to the top of the Dogger is 0.4 – 0.6. This is much lower than that of modern seawater (~ 1.55). In the Opalinus Clay, the mean ratio is 0.41 ± 0.03, thus depicting a narrow range. The Br/Cl ratio in the Keuper groundwater is somewhat higher (0.86) than those of the corresponding porewaters (0.4 – 0.6). The reason for this difference is not clear. Potential effects may be due to contamination of the ground-

water samples by drilling fluid or the fact that different laboratories analysed the pore- and groundwaters. In the Malm aquifer and in the corresponding porewaters, the Br/Cl scatters around that of seawater, although, as mentioned above, there is considerable variability in the porewater values.

Br aqueous extraction data of samples from the Bänkerjoch Formation were below detection limit (< 0.16 mg/L in extract).

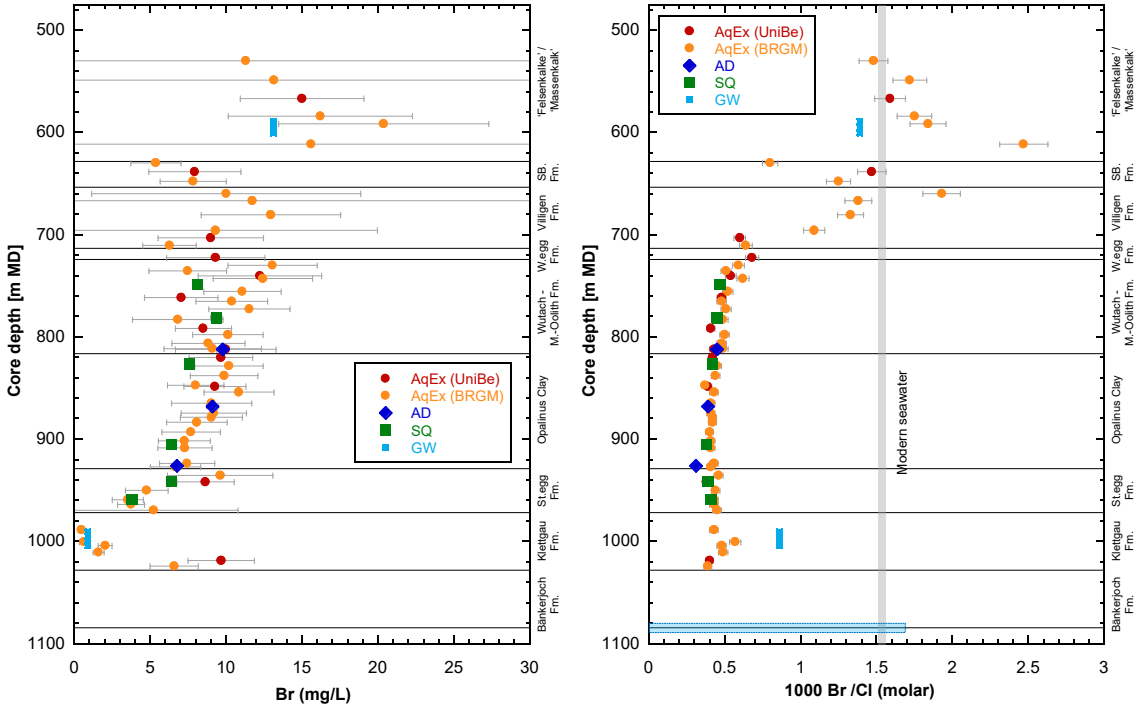

Fig. 5.2-2: Br and Br/Cl profiles with data from squeezing, advective displacement, aqueous extraction and groundwater samples

Aqueous extraction data in the Br profile recalculated to Br-accessible porosity assuming the relationship between accessibility and clay-mineral content as discussed in Section 5.1. In the Br graphic (left), error bars on the data from aqueous extraction include propagated analytical uncertainty plus another 20% that reflect the uncertainty related to f_{Br}. Error bars for Br/Cl (right graphic) represent propagated analytical uncertainties, given the fact that anion accessibility is not needed to calculate the ion ratio. Samples affected by drilling-fluid contamination (Section 4.4) are omitted. Note that the Br concentration in the Muschelkalk groundwater is below detection limit (0.1 mg/L) and the molar 1'000 Br/Cl ratio below 1.66 (shown as light blue bar in right figure).

5.3 Sulphate and SO_4/Cl profiles

Paul Wersin & Martin Mazurek

Sulphate data from squeezing, advective displacement, aqueous extraction and groundwaters are illustrated in logarithmic and linear scales in Fig. 5.3-1. Note that the groundwater sample from the Malm aquifer was affected by microbial disturbance caused by the drilling fluid which led to sulphate reduction and to erroneously low sulphate levels which are thus not presented in Fig. 5.3-1. Data from aqueous extraction were recalculated to concentrations in bulk porewater assuming conservative behaviour of sulphate. This assumption is not true at least in anhydrite-bearing lithologies in the Bänkerjoch Formation where mineral dissolution contributed to SO_4 concentrations in the extracts. Anion exclusion has not been considered at this stage. Data from the University of Bern were recalculated using the measured water content, while water content obtained from pycnometer porosity was used for the BRGM data (see Section 5.2 for justification). Note that the groundwater concentrations of sulphate are not corrected for drilling fluid contamination, which, however, is considered to be minor regarding the conservative constituents for the sampled Keuper and Muschelkalk groundwaters (Lorenz 2020).

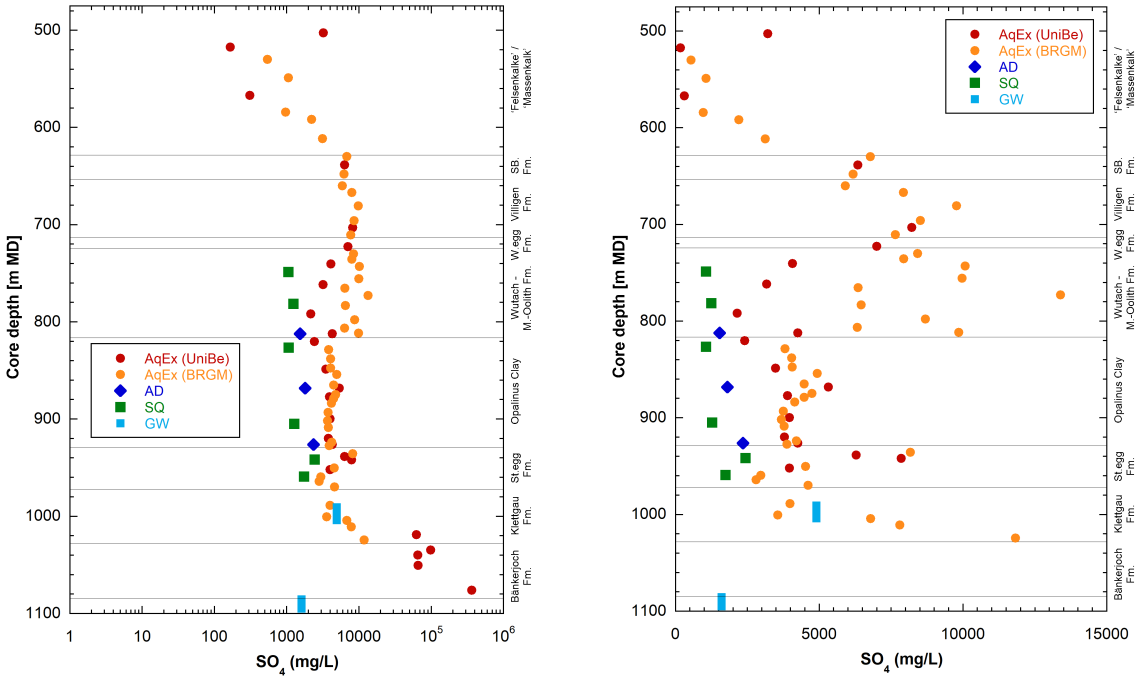

Fig. 5.3-1: SO_4 profile with data from squeezing, advective displacement, aqueous extraction, and groundwater samples

Left: entire data (logarithmic scale); right: data with SO_4 concentrations < 15 g/L (linear scale).

Aqueous extraction data recalculated to contents in bulk porewater using water content. Samples affected by drilling-fluid contamination (Section 4.4) are omitted.

From a qualitative perspective, the highest sulphate levels based on aqueous extraction are observed in the Bänkerjoch Formation, whereas lower but scattered levels are displayed from the Staffelegg Formation to the Schwarzbach Formation. Starting in the Villigen Formation, a well-defined decreasing trend towards the sampled Malm aquifer is noted.

The very high SO_4 concentrations obtained for the recalculated aqueous extracts in the Bänkerjoch Formation and the lowermost one in Klettgau Formation are not meaningful because of anhydrite dissolution during extraction. The corresponding porewaters are likely controlled by anhydrite or gypsum equilibrium, which is also manifested in most of these S/L ≈ 1 extracts (Section 4.4). In this context, it should be noted that the Keuper groundwater (although slightly contaminated by the drilling fluid) is undersaturated with respect to gypsum as suggested from speciation calculations with PHREEQC (Parkhurst & Appelo 2013).

SO_4 concentrations based on squeezing and advective displacement yield distinctly lower and less scattered values in comparison to the recalculated data from aqueous extraction. A closer look at the Opalinus Clay and the under- and overlying confining units (Staffelegg Formation and «Brauner Dogger») reveals consistent concentrations between squeezing and advective displacement data and a slightly increasing trend with depth, from about 1 to 2 g/L (Fig. 5.3-1, right). Conversely, the recalculated aqueous extraction data exhibit systematically higher and more variable concentrations. The scatter of aqueous extraction data produced by BRGM and their mismatch relative to aqueous extraction data of University of Bern are larger in the Staffelegg Formation and «Brauner Dogger» than in the Opalinus Clay. A part of these BRGM data appear to be affected by sulphide oxidation during extraction, as indicated from the SO_4/Cl ratio (see below and Section 4.4); this is a priori not expected given the fact that sample preparation and extraction were performed in an anaerobic glovebox (Section 3.4).

The discrepancy between aqueous extraction and squeezing/advective displacement data becomes even larger when anion exclusion is considered, e.g. by assuming the same relationship between anion-accessible porosity and clay-mineral content as that applied for Cl (Fig. 5.3-2). However, it should be noted that the anion exclusion effect of SO_4 in the considered rocks is not well known. From double layer theory, the exclusion of SO_4 in clayrocks is predicted to be higher because of its higher charge (Gimmi & Alt-Epping 2018). On the other hand, SO_4 has a larger tendency to form weak complexes, such as with alkaline earths, thus partly compensating the charge effect.

A similar discrepancy between squeezing/advective displacement data on the one hand and aqueous extraction data on the other has been observed for other boreholes, such as Schlattingen-1 (Wersin et al. 2013) and Bülach-1-1 (Mazurek et al. 2021), as well as in in the Mont Terri rock laboratory (Wersin et al. 2021). In the latter case, waters sampled from packed-off boreholes exhibit similar sulphate concentrations and SO_4/Cl ratios as waters squeezed from near-by drillcores. All porewaters from squeezed and advectively displaced samples are close to equilibrium with regard to celestite (except for one squeezed sample in the Staffelegg Formation at 959.22 m depth which is undersaturated). Celestite could be identified in the matrix of the Opalinus Clay and «Brauner Dogger» samples at Mont Terri and Schlattingen-1 by a combined SEM/microprobe study (Jenni et al. 2019). In the case of Bülach-1-1, where in view of the higher sulphate levels, higher amounts of sulphate phases such as anhydrite and celestite could be expected, no such phase (with grain sizes of > 3 μm) could be identified by SEM analysis so far. Samples from advective displacement and squeezing are generally undersaturated with regard to gypsum except for two samples (at 926.14 and 951.54 m) which are close to saturation with regard to this phase.

The reason for the higher sulphate levels derived from aqueous extraction compared to squeezing / advective displacement data is not understood at this stage, in spite of a recent systematic aqueous extraction study on Opalinus Clay including Mont Terri and BUL1-1 samples (Debure & Gailhanou 2019, Aschwanden & Wersin 2020). Interestingly, the SO_4 concentrations obtained from recalculated Ni-en extracts used for obtaining cation exchange parameters are systematically lower than those obtained from aqueous extraction but still higher than those displayed by squeezing/advective displacement data (Fig. 5.3-2). The reason for this difference is not known at this point.

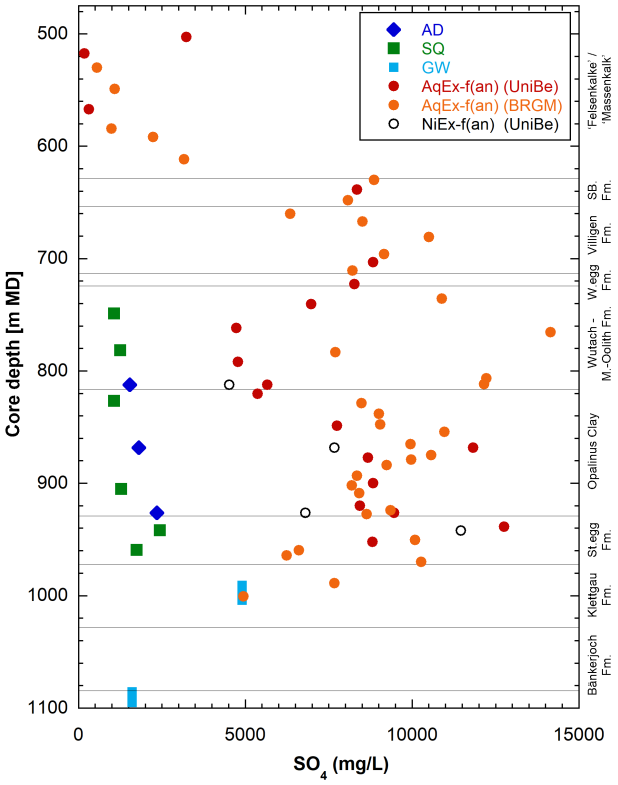

Fig. 5.3-2: SO_4 profile with data from aqueous and Ni-en extraction, compared with squeezing, advective displacement and groundwater data

Aqueous and Ni-en extraction data recalculated to SO_4-accessible porosity assuming the same relationship between accessibility and clay-mineral content as applied above for Cl. Samples affected by drilling-fluid contamination (Section 4.4) are omitted.

The depth profile of SO_4/Cl ratios (Fig. 5.3-3) shows similar trends as the SO_4 profile. The high molar SO_4/Cl ratios up to more than 10 in aqueous extracts in the lower sequence of the profile point to the dissolution of sulphate-bearing mineral phases during extraction. In the central part, SO_4/Cl ratios remain below 1, whereby the values obtained from squeezing and advective displacement are clearly lower. The ratios in the aqueous extracts increase strongly upwards in the interval «Brauner Dogger» to Schwarzbach Formation, from where they decrease again, reaching low values in the «Felsenkalke» + «Massenkalk».

The Keuper groundwater sample displays a ratio of 3.95, clearly above that of modern seawater (0.052). The ratio increases up to ~ 22 in the Muschelkalk groundwater sample. The ratios of squeezing/advective displacement samples show a slight downward increase in the Staffelegg Formation, above they remain constant at levels close to that of seawater.

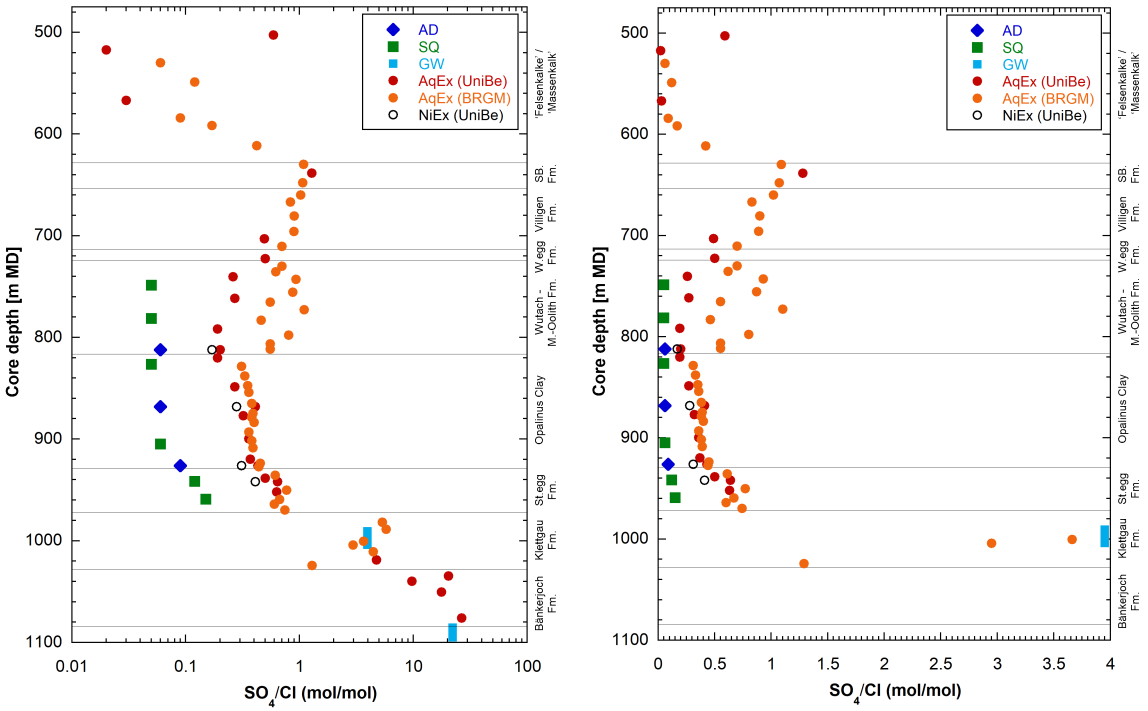

Fig. 5.3-3: Profiles showing molar SO_4/Cl ratios obtained from different methods in logarithmic and linear scales

Data from aqueous extracts not shown for the Bänkerjoch Formation in the right graphic (most points would fall out of the plotted range). Samples affected by drilling-fluid contamination (Section 4.4) are omitted.

5.4 Cation concentrations in porewaters

Urs Mäder

5.4.1 General considerations

Deriving cation concentrations in porewaters involves a discussion about controlling processes and disturbing effects (mineral dissolution/precipitation, cation exchange, oxidation, others) that operate invariably when handling drill core samples, in our case for performing aqueous extractions, Ni-en extractions, porewater squeezing and advective displacement experiments.

The seemingly least-affected cation is Na (no mineral source except for halite if present), not because it does not interact, but because it is in most units the major positive charge-carrying cation and thus is not sensitive to small relative changes, and a priori correlates well with chloride concentrations where chloride is the major anion charge-carrier. With increasing sulphate concentrations (and ionic strength), however, charge compensation may increasingly also relate to Ca concentrations, and Na forms an important ligand for sulphate complexation ($NaSO_4^-$) and is no longer a quasi-conservative component. In some porewater models, Na is used to top up cation charge to balance the sum of anionic charge, with other major cation concentrations constrained by mineral equilibria and measured exchanger composition.

All cations interact to variable degrees with the clay exchanger, an inventory that far exceeds the dissolved load (except in very clay-poor limestones), and disturbances are thus interlinked. Some cations are directly involved in mineral saturation equilibria (calcite, dolomite, sulphates where present), and all are directly or indirectly linked to the carbonate system (detailed in Section 5.5).

Some data were obtained for minor or trace cations such as Ba and Fe. These are not drivers for interactions but may be controlled by mineral saturation equilibria. A minor cation of some significance is ammonium (NH_4) that is known to be present in porewater and on the clay exchanger, but relatively few data exist. The Fe-system is analytically not well-constrained for the solutes and exchanger concentrations due to the inherent sensitivity of Fe to redox processes: it is normally constrained by modelling and linked to the more reactive Fe-bearing minerals pyrite and Fe-carbonates. Fe was measured in 22 aqueous extract samples but was below a detection limit of 0.025 mg/L in these samples. Little comprehensive data exists on trace cations (e.g. transition metals) and none were measured in this study.

5.4.2 Constraints from aqueous extract data

A somewhat leaner data set is available for TRU1-1 compared to BUL1-1: only aqueous extracts performed at the University of Bern (22 PW samples, 4 AD samples) were analysed for anions and cations. The PW samples processed by BRGM (46 samples) were only analysed for selected anions.

Aqueous extracts are affected by mineral dissolution of calcite to saturation, by dolomite to a variable degree and by anhydrite where present (Bänkerjoch Formation), as detailed in Section 4.4.3.3. This adds Ca and some Mg to the extract solutions, charge-compensated by alkalinity and sulphate in case of anhydrite. Ionic strength is low in extracts compared to porewater, and this is causing a much stronger preference for the divalent cations relative to Na and K to populate the clay exchanger. This combined disturbance renders all cation concentrations to be non-conservative and therefore they cannot be scaled to porewater concentrations (by water content). This is occasionally done for Na, but as discussed above, it is an approximation, and likely fails for porewaters that are not of Na-Cl type.

It may be possible to perform modelling calculations to back-track mineral dissolution contributions during aqueous extraction and the dilution induced by the added water, and so arrive at a model porewater composition. This has not yet been rigorously attempted and it remains to be demonstrated that it is possible to constrain a unique reaction pathway for back-calculation.

5.4.3 Constraints from porewater squeezing and advective displacement data

The two so-called direct sampling methods, porewater squeezing (6 SQ samples) and advective displacement (3 AD samples), aim at obtaining sample aliquots that are porewater like. Both approaches mobilise porewater and it is thought that this mobile part is more kin to the free porewater (not affected by electrostatic effects / charged clay surfaces and interlayers). Past experience and comparison to through-diffusion experiments attest some degree of consistency to this end. One method implies high-pressure deformation and destruction of the rock fabric to squeeze porewater, the other applies large hydraulic gradients and an artificial porewater to displace the in situ porewater. The two methods are therefore quite contrasting regarding the mechanism of extraction, and some method-specific artefacts may be expected. Both methods are also expected to show agreement in a subset of characteristic porewater parameters. Also important are additional constraints for certain parameters by independent methods to identify any systemic shortcomings.

Most significant for porewater composition are the squeezed aliquots at lowest pressures (Tabs. 4.6-3, 4.6-4) and the first 1 – 3 small sample aliquots from advective displacement (Tab. 4.7-12, average of first 2 aliquots; Appendix D for all data). The small sample volumes available typically allow not for analysing all parameters, and it may lead to high detection limits for some parameters due to required dilution, and analytical uncertainties may be larger than commonly adopted for standard analytical procedures. The aliquots squeezed at lowest pressures all lack pH measurements and information on TIC/TOC and are thus of limited value in constraining porewater composition (further addressed in Section 5.5).

The measured concentrations of major and some minor cations in squeezing aliquots from lowest pressure and the average concentration from the first two aliquots from advective displacement (Figs. 5.4-1, 5.4-2) are discussed below. Data interpretation is on-going, and data below thus represent squeezed or displaced aliquot concentrations, potentially subject to experimental artefacts as indicated below.

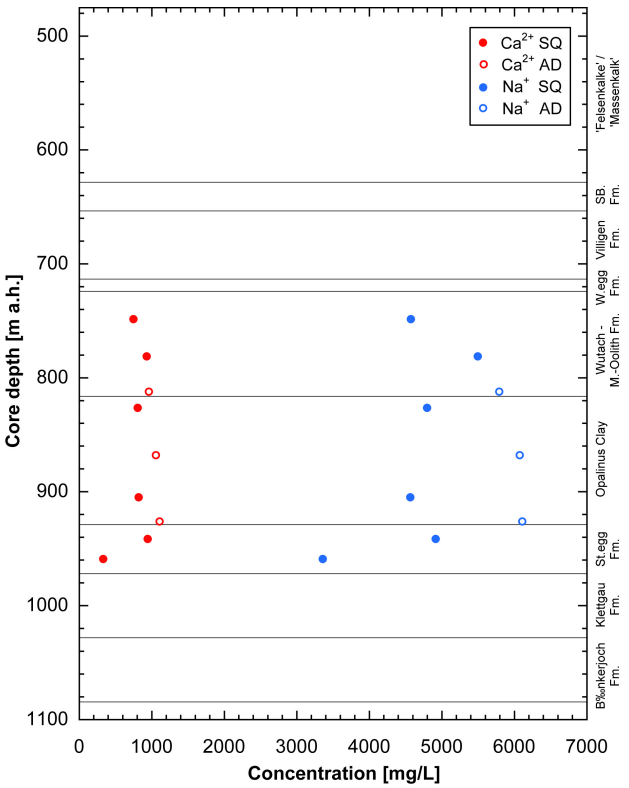

Fig. 5.4-1: Concentrations of Na and Ca in aliquots from squeezing experiments and advective displacement experiments

Only aliquots squeezed at lowest pressures are shown, and average values for the first two aliquots obtained from advective displacement.

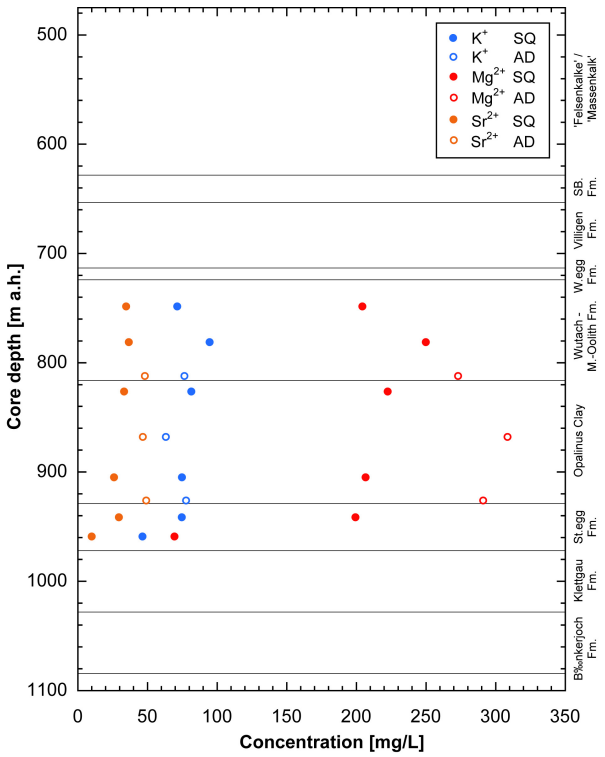

Fig. 5.4-2: Concentrations of K, Mg and Sr in aliquots from squeezing experiments and advective displacement experiments

Only aliquots squeezed at lowest pressures are shown, and average values for the first two aliquots obtained from advective displacement.

5.4.3.1 Differences and commonalities between porewaters obtained from squeezing and advective displacement

On close inspection of squeezing (SQ) data (Section 4.6) and advective displacement (AD) data (Section 4.7), the following differences are obvious or may be derived:

- Chloride concentrations from AD samples do not suggest significant gradients with depth: 9'700 mg/L (812 m, Wedelsandstein Formation), 10'450 mg/L (868 m, Opalinus Clay) and 9'730 mg/L (926 m, base of Opalinus Clay). Chloride concentrations in squeezing aliquots from clay-rich samples from the same depth range (3 samples) yield 8'000, 7'450 and 7'240 mg/L and are thus significantly less saline by ~ 20% (Fig. 5.2-1). This is the same situation as observed for BUL1-1 samples (Mazurek et al. 2021). Further below, Cl decreases towards the Keuper aquifer (captured in SQ samples, no AD samples).
- Sulphate concentrations from the same clay-rich section as for chloride, increase in AD samples from 1'500 to 2'300 mg/L but are only 1'000 to 1'300 mg/L in squeezing samples from Opalinus Clay and show a high value of 2'400 mg/L in one of the samples from the Staffelegg Formation. Both data sets show trends towards increasing SO_4 with depth.
- Because the sum of anion charge in SQ samples is ca. 20% smaller than that in AD samples, also the sum of cations is 20% smaller. A comparison value-by-value is therefore not meaningful, and approximately all cation concentrations in SQ samples are smaller than those

in AD samples (except for K, Fig. 5.4-2). Ca concentrations are similar, and so Ca is enriched in SQ samples relative to Cl and compared to AD samples. This is reflected in generally higher degrees of calcite supersaturation in SQ samples vs. AD samples.

- The carbonate system (details in Sections 4.6, 4.7 and 5.5) in SQ samples squeezed at higher pressures is characterised by pH values of 7.2 – 8.7 (but none are measured at lowest squeezing pressures), strong supersaturation with respect to calcite (SI 0.6 – 1.3 at higher squeezing pressures) and a low calculated partial pressure of CO_2 (-3.1 to -3.8 in log-bar units, at higher squeezing pressures). pH values from first AD aliquots cluster at 7.6, SI values of calcite are 0.5 – 0.7 and log-P_{CO2} (bar) ranges from -1.9 to -2.5. An assessment of the carbonate system for the most relevant aliquots from lowest squeezing pressures cannot be made due to the lack of a measured pH (and TIC/alkalinity).
- Dissolved organic carbon contents were not measured in SQ samples from lowest pressures and range from 130 – 250 mg/L in aliquots squeezed at higher pressures. TOC measured in AD samples range from 230 – 330 mg/L, and this is distinctly lower compared to findings from the BUL1-1 borehole where much higher initial concentrations were measured (details in Section 5.5).
- Saturation indices for celestite are at or slightly above saturation, and those for gypsum are below saturation in both data sets, except for aliquots squeezed from a sample of the Staffelegg Formation that are at gypsum saturation.
- Calculated chloride-accessible porosity fractions obtained from AD samples are 0.41 and 0.47 for Opalinus Clay, and 0.8 for a sample from the Wedelsandstein Formation (only 18% clay content, 53% quartz). Cl-accessible porosity fractions of 0.51 and 0.46 were obtained from squeezing data for Opalinus Clay, and the entire data set ranges from 0.40 to 0.51 (clay contents 40 – 80 wt.-%). Data from through-diffusion experiments cover a range from 0.33 – 0.71 (Fig. 5.1-2) with clay contents of 3 – 66%. The three data sets therefore overlap largely (detailed discussion in Section 5.1). It is interesting to note that the difference of 20% in thebchloride concentration of the aliquots (AD vs. SQ, see first bullet point above) does not lead to different Cl-accessible porosity fractions, despite that both methods relate the extracted aliquots to the same basis, namely the initial bulk porewater concentration. The SQ samples therefore also contain systematically less Cl in aqueous extract samples normalised to water content compared to the AD samples.

5.4.3.2 Significance of porewater aliquots from advective displacement

The aqueous extract data for chloride concentrations and for Br/Cl ratios are rather smooth across the Opalinus Clay and define a plateau or slightly curved maximum concentrations (Sections 4.4, 5.2, Fig. 5.2-1) that coincide with the closely spaced aqueous extract samples up-scaled with a Cl-accessible porosity fraction of 0.45 (Fig. 5.2-1). There is some divergence in the data towards the transition to the Staffelegg Formation where Cl concentrations start to drop steeply towards the Keuper aquifer. The squeezing data yield samples that are less saline (by ca. 20% in Opalinus Clay), and the lack of measured pH and TIC in the aliquots squeezed at lowest pressures render the SQ data set not appropriate for constraining the porewater composition. This is not to say that advective displacement is not associated with some artefacts.

5.4.3.3 The sulphate issue and its link to porewater cation concentrations

Substantial efforts over the past few years in form of dedicated laboratory studies and some modelling work had been directed to better constrain the sulphate concentration in porewaters (e.g. Aschwanden & Wersin 2020, Wersin et al. 2021). While a detailed analysis is not within the scope of this data report, some points that are directly evident from measurements and speciation calculations presented in this report are briefly addressed.

The sulphate issue relates to the observation that sulphate concentrations in aqueous extracts for the marine strata appear to be largely derived from porewater without an obvious or significant contribution from mineral dissolution (details in Section 4.4 and also 5.3). Such concentrations up-scaled to porewater content – even without considering an anion-exclusion effect – are larger than those observed in advective displacement aliquots or squeezing aliquots. SQ and AD data tend to agree rather well on sulphate concentrations, and the disagreement with aqueous extract data has been observed in the BUL1-1 borehole as well as in previous boreholes (Schlattingen-1, Mont Terri), and at Mont Terri long-term sampling of seepage waters also tends to agree with sulphate concentrations from squeezing.

The issue is enigmatic in the sense that the smooth SO_4/Cl profiles and other evidence (Debure & Gailhanou 2019, Aschwanden & Wersin 2020) indicate that neither celestite nor pyrite are obvious sources for SO_4 during aqueous extraction, but also a potential precipitation of celestite during SQ or AD experiments is limited by the rather low Sr inventory available from the clay exchanger (ca. 1% of the CEC).

Cation concentrations are directly linked to the sulphate concentration (by charge balance) and any correction of either aqueous extracts or the SQ/AD aliquots relates corrected sulphate concentrations to some specific cations, with significant effects on the cation ratios in the porewater.

5.4.4 Implications for defining formation and location-specific porewaters

The corollary of the sulphate issue is that at present the sulphate concentration in the porewater of the drill core samples cannot be deduced reliably but may be gauged by two end-members: one with concentrations from advective displacement and squeezing samples and one from restoration of sulphate from aqueous extract data. The latter requires modelling to speciate and re-distribute sulphate and sulphate complexes across the two porosity domains. A higher-sulphate variant will accordingly contain a larger cation inventory, and this will also require a modelling interpretation based on possible processes that are supported by our data.

Based on the good consistency of advective displacement and squeezing experiments, as well as seepage waters at Mont Terri (see Section 5.4.3.3), the sulphate concentrations obtained by these methods appear to represent conditions in the free porewater reasonably well. Thus, for a low-sulphate end-member, values may be derived from advective displacement data (Tab. 4.7-12) by restoring calcite – dolomite equilibrium, and observing that the model porewater does not become supersaturated with respect to gypsum and celestite. Such a preliminary composition had been defined in 2020 for the purpose of laboratory experiments (through-diffusion tests performed at PSI, among others).

5.5 Dissolved carbon species (inorganic, organic), alkalinity, pH and P_{CO2}

Urs Mäder

5.5.1 General considerations

The carbonate system (dissolved inorganic species / alkalinity, carbonate minerals, P_{CO2}) plays a pivotal role for porewater composition as it links measurable parameters like pH, alkalinity/TIC (total inorganic carbon) to difficult-to-measure quantities like partial pressure of CO_2. Inorganic carbon species in combination with the solid carbonate system (calcite, dolomite etc.) intimately link dissolved Ca and Mg to the exchange complex that contains an inventory of cations that far exceeds the dissolved load (except for pure limestones). Via this link to the exchanger, also Sr, K and – to a lesser extent – Na are interlinked. Due to potentially solubility-limiting sulphates (anhydrite, gypsum, celestite), there is also a link to the sulphate system. With other words: the controlling carbonate equilibria, or any disturbing effects to the carbonate system, affect the entire porewater composition. By the same token, the exchanger capacity has a buffering effect on external disturbances.

Constraining the in situ porewater composition – or even that of the porewater chemical state of a sample core after drilling – involves different levels of data interpretation based on geochemical equilibrium models (like PHREEQC) and cannot be simply derived from aqueous extracts by scaling (like for conservative anions) or from a one-to-one adoption of concentrations in advective-displacement or squeezing aliquots. This data report does not include such modelling interpretation and therefore can only elucidate on some aspects of porewater composition.

The dissolved organic carbon species pose analytical challenges, cannot be characterised to any degree of completeness, and the measured TOC (total dissolved organic carbon) contents seem to be dependent on sample handling and sampling techniques. There is evidence that some TOC components may readily get involved in microbial processes. The link of TOC to the solid organic matter is not well understood.

We use solely TOC in referring to dissolved organic carbon, and not TOC and DOC, with the latter being designated to filtrated solutions. In most cases, our TOC concentrations represent DOC values. Filtration was commonly applied to aqueous extract samples (0.2 µm) but not to small aliquots from squeezing or advective displacement experiments, except for few cases where suspended particles were visible after dilution. In-line filtration was involved in IC analysis for low-molecular-weight organic acids.

5.5.2 Organic carbon

Available data includes (LMWOA: low-molecular-weight organic acids):

1. TOC in aqueous extracts associated with AD experiments (4 samples, clayey sequence)
2. TOC in aliquots from AD (3) and SQ (6) experiments (clayey sequence)
3. Organic C in rock samples (PW samples, AD, SQ, DI, GM)
4. LMWOA only in 4 AD aqueous extract samples
5. LMWOA in direct samples of 4 AD experiments
6. TIC and TOC concentrations are available for the Malm, Keuper and Muschelkalk aquifer waters, but LMWOA were only measured in the Keuper groundwaters and were below a detection limit of 10 mg/L.

Organic C in rock samples (Fig. 5.5-1) shows consistent and typical values near 1 wt.-% organic carbon for Opalinus Clay (average of 1.02 wt.-%, range of 0.76 – 1.39, Tab. 4.2-1), and lower values on average, but more variable, in the «Brauner Dogger» and Staffelegg and Klettgau Formations. Highest values of 3 – 6 wt.-% are associated with the Rietheim Member («Posidonienschiefer») in the Staffelegg Formation. There were no specific analyses performed for further characterisation of the solid organic matter.

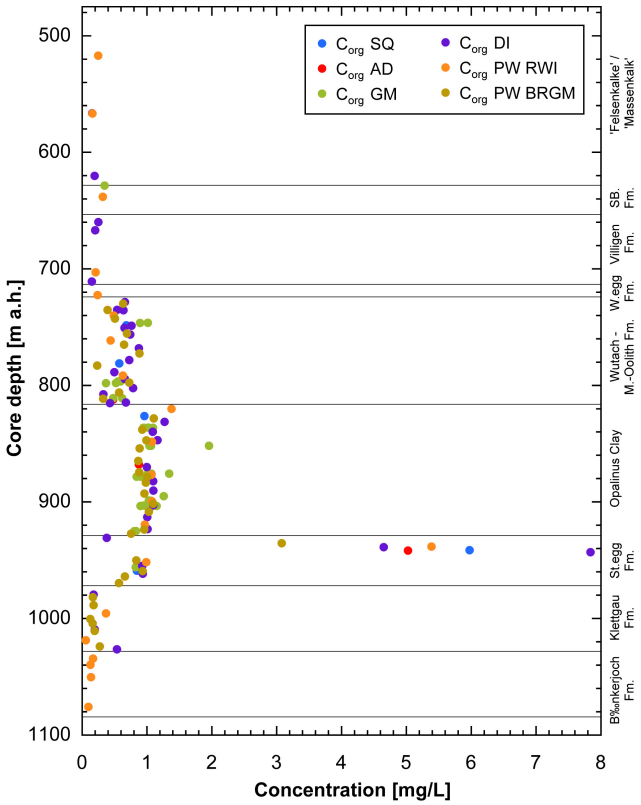

Fig. 5.5-1: Organic carbon in rock samples

Colour coding is according to sample type.

Organic carbon in liquid samples (TOC) is either determined by direct measurement (NPOC, non-purgeable organic carbon) or by difference (total carbon – TIC). Almost all TOC determinations for this study were performed by difference.

TOC (DOC) measurements for earliest sample aliquots from advective displacement (AD) contain elevated TOC of 230 – 330 mg/L for the clayey sequence (Fig. 5.5-2). No data are available for aliquots squeezed at lowest pressures, but those at more elevated pressures range from 130 to 250 mg/L. TOC values from aqueous extracts from AD samples (pre-characterisation, 7.7 – 14.7 mg/L) are in a similar range as the AD aliquots, when up-scaled to porewater content. Such an upscaling may be subject to debate, because the nature of the organic species is mostly not known, except that a portion is present as acetate (see below). Acetate is expected to show some kind of anion-exclusion effect, resulting in higher calculated concentrations in the anion-accessible part of the porewater. Also shown is a value of 17 mg/L for TOC measured in groundwater samples from the Keuper aquifer. This value is likely affected by contamination from organic additives of the drilling fluid.

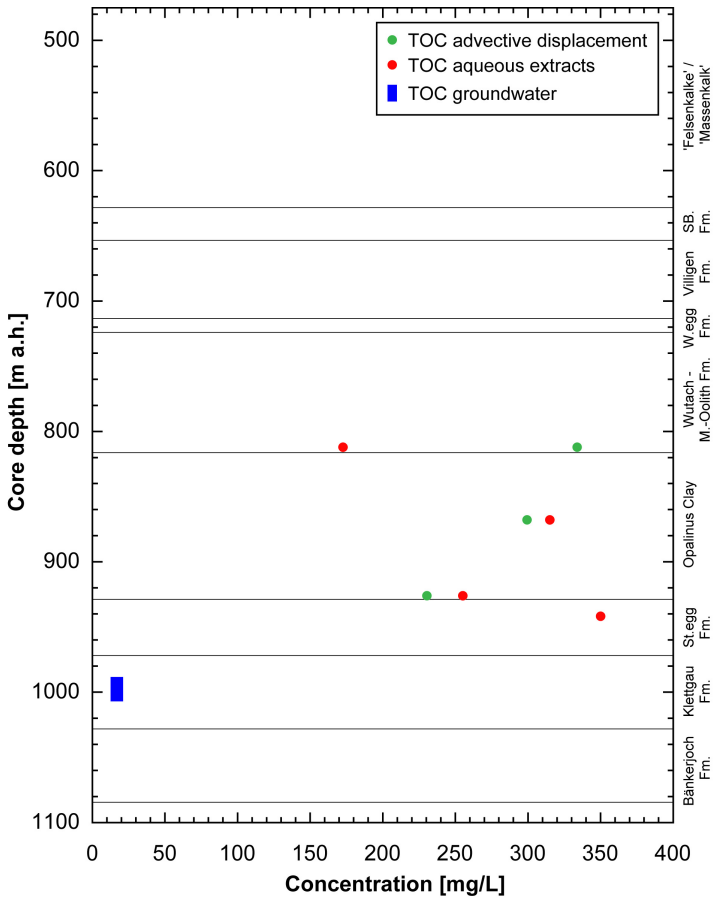

Fig. 5.5-2: TOC in aliquots from AD, upscaled from aqueous extracts, and the Keuper aquifer

Aqueous extract samples from AD samples are scaled to water content (TOC_WC). The value of the Keuper aquifer is likely affected by contamination from organic additives of the drilling fluid.

Low-molecular-weight organic acids (LMWOA) that are detectable by our IC separation column include acetate, formate, lactate and propionate. These acids were only analysed in aqueous extracts from four AD samples, in aliquots from three AD experiments and in groundwater samples from the Keuper aquifer (but not detected, with a limit of 10 mg/L). Of these acids, acetate was present in aqueous extracts above a detection limit of 2 mg/L in 3 out of 4 samples (3 – 8 mg/L), and propionate was only detected in one sample at 2.3 mg/L (Rietheim Member, «Posidonienschiefer»). Early aliquots from AD experiments contain 20 – 350 mg/L acetate and other acids below a detection limit of 20 mg/L. A highest value of 800 mg/L acetate was measured in the first aliquot from sample 812.24 m (Wedelsandstein Formation), but this seems to be somewhat aberrant in view of later samples. Organic acids were not evaluated in aqueous extracts from PW samples.

Note that an upscaling of concentrations in aqueous extracts to the chloride-accessible porosity proportion is not necessarily correct, because these organic acids are not only subject to purely electrostatic effects but also to interactions specific to functional groups or surfaces. It should be viewed as an illustration.

Acetate concentrations recalculated to water content (aqueous extracts of AD samples, Tab. 4.7-5) range from 71 to 194 mg/L (and < 70 mg/L in one sample of Opalinus Clay) and may be significant in the clayey sequence («Brauner Dogger» – Opalinus Clay – Staffelegg Formation). These up-scaled concentrations (to water content) overlap with the concentrations seen in earliest AD aliquots, ranging from 20 to 350 mg/L.

It is not straightforward to interpret or transfer this data directly to in situ porewater conditions. The process of aqueous extraction, porewater squeezing (limited data in this study) and advective displacement seems to mobilise TOC and LMWOA above values that have been determined from long-term in situ sampling (e.g. at Mont Terri Rock Laboratory). Furthermore, TOC concentrations strongly decrease with progress of advective displacement (Section 4.7), and the advection process seems to wash out this labile initial TOC pool. Likewise, TOC concentrations also decrease with increasing squeezing pressure (Section 4.6, but no data for lowest-pressure aliquots) and seem to be preferentially mobilised during early squeezing stages (observed for BUL1-1 samples and earlier work). It seems certain, however, that TOC and LMWOA are part of the porewater system, presumably in some kind of long-term disequilibrium situation with the solid organic matter (some kind of sorbed form?) and the inorganic carbon system. Apparently, any disturbance (drilling, sampling, EDZ, experiments etc.) is able to mobilise TOC significantly.

5.5.3 Dissolved inorganic carbon, alkalinity

Inorganic carbon species are either analysed directly as TIC or titrated as alkalinity. The latter is a summation parameter for all acids that can be protonated to a pH of ~ 4.3, such that it would also include acetate, for example.

The inorganic carbon system in aqueous extracts is affected by calcite/dolomite dissolution induced by dilution and does not reflect porewater composition. Alkalinity in these samples largely reflects the carbonate alkalinity. Because calcite/dolomite dissolution evolves in a closed and initially CO_2-free system during extraction, the pH rises strongly (pH 8 – 10 for Malm to Staffelegg Formation, for example) and bears no similarity to porewater pH.

The sample aliquots from advective displacement and porewater squeezing potentially may yield information on porewater TIC. TIC analyses were conducted within hours after sample collection for AD-sample aliquots and after some weeks including an air-freight transport for the SQ aliquots. Alkalinity titration is not advisable for early aliquots because it may be dominated by organic acids (acetate) and thus overestimates carbonate alkalinity, and alkalinity titration also requires more sample volume than is commonly available. TIC concentration in earliest AD aliquots ranges from 35 to 75 mg/L for the clayey sequence (Tab. 4.7-12). Straight speciation of these AD aliquots results in significant supersaturation with respect to calcite with SI values of 0.45 to 0.75, such that a geochemical modelling interpretation to restore calcite saturation may adjust some of these TIC values. No TIC measurements were possible for samples squeezed at lowest pressures, and thus no evaluation of saturation states is possible except for sulphates.

In summary, a tentative range of 3 – 6 mmol/L of inorganic carbon is covered by AD sample aliquots, but this somewhat large range may also be due to method-specific artefacts, and this will have to be further constrained by geochemical modelling analysis.

5.5.4 pH and partial pressure of CO_2

Like for carbonate alkalinity, it is not possible to adopt pH and calculated partial pressures of CO_2 from aqueous extract solution for reasons explained above.

pH measurements were done for advective displacement experiments, both in-line during sampling and shortly after sampling (one to few hours) on aliquots collected in closed syringes. Earliest in-line measurements cluster at pH 7.6 (Fig. 4.7-14, Tab. 4.7-12) and laboratory measurements range from pH 7.3 – 7.6 (Fig. 4.7-14, Tab. 4.7-12), covering the clayey units («Brauner Dogger» – Opalinus Clay). No pH measurements were possible for aliquots squeezed at lowest pressures.

Partial pressures of CO_2 in log-bar units from first AD aliquots range from -1.9 to -2.5 based on straight speciation calculations, without restoration of calcite equilibrium at this stage. Depending on how calcite saturation is restored (CO_2 in/outgassing or adjustments to carbonate alkalinity), this will somewhat adjust both pH and P_{CO2} values.

The ranges for pH and calculated P_{CO2} observed in this study are quite comparable to those obtained from the BUL1-1 borehole and other sites (Mont Terri Rock Laboratory, Schlattingen-1 geothermal well), although only a more limited data set was available for the latter. The large acetate concentrations have not yet been rigorously addressed in the modelling interpretations but may have some impact on the carbonate system and pH control (buffering processes). The exact process of liberation of acetate is at present poorly constrained, and so are potential interactions. Apart from effects discussed above, there are also potentially disturbing processes involved that are common to all methods, namely related to drilling, unloading, sample handling and cooling from in situ temperature. Also, these processes will have to be included in restoring in situ porewater compositions.

5.6 Cation exchange capacity and exchangeable cation population

Paul Wersin & Martin Mazurek

5.6.1 Corrected exchangeable cation data

As mentioned in Section 4.5, in order to obtain the exchangeable cation concentrations, the extracted cation data need to be corrected for cations dissolved in the porewater and the cations released from (potential) mineral dissolution. As shown from previous work (e.g. Hadi et al. 2019), carbonate mineral dissolution can be largely suppressed with the appropriate S/L ratio, extraction time and pH conditions. Such conditions were applied for the University of Bern data set.

Two correction methods were applied based on the concentrations of the main anions chloride and sulphate (Bradbury & Baeyens 1998, Hadi et al. 2019). The first correction method ($NaCl/Na_2SO_4$) attributes dissolved Cl and SO_4 from the Ni-extracts to Na and leaves the other cations unchanged. The second method ($NaCl/CaSO_4$) attributes Cl to Na and SO_4 to Ca, leaving the other cations unchanged. In both methods, the CEC is calculated from the sum of cations (ΣCAT) minus the concentrations (normalised to $meq/kg_{dry\ rock}$) of Cl and SO_4. The corresponding data is shown in Tab. 5.6-1. The data correspond to the average of two subsamples collected at the top and the base of the AD core, respectively, except for the sample at 926.14 m depth, where only one subsample was collected.

The relative difference between the uncorrected and corrected sums of extracted cations (ΣCAT) is within 7 – 24%. The largest difference is noted for a clay-poor sample at 812.24 m depth from the Wedelsandstein Formation.

The correlation between Ni consumption and ΣCAT is illustrated in Fig. 5.6-1. The slope is below 1 (0.878 and 0.801 for the uncorrected and corrected data, respectively), indicating the generally slightly larger CEC values derived from Ni consumption. Further, Fig. 5.6-2 indicates good correlation between clay-mineral content and CEC parameters.

The exchangeable cations are expressed as cation occupancies (in equivalent fractions) in Tab. 5.6-1. Na and Ca are the main exchangeable cations, followed by Mg and K. The Sr occupancies are considerably lower (below 3%).

Tab. 5.6-1: Sum of cations and cation occupancies obtained from Ni-en extraction after correction (University of Bern data)

First line for each sample indicates cation occupancies obtained by the $NaCl/Na_2SO_4$ correction method, the second line those obtained by the $NaCl/CaSO_4$ method. n.m. = not measured.

Type	**Depth** [m]	**Formation**	**Clay-mineral content** [wt.-%]	**ΣCAT raw** [meq/kg$_{rock}$]	**ΣCAT corr.** [meq/kg$_{rock}$]	**Na**	**K**	**Ca**	**Mg**	**Sr**
						Fractional occupancy (equivalent units)				
AD	812.24	Wedelsandstein Fm.	18	60.0	45.84	0.26	0.08	0.44	0.19	0.026
						0.34		0.36		
AD	867.97	Opalinus Clay	41	78.9	72.37	0.38	0.06	0.40	0.15	0.010
						0.42		0.36		
AD	926.14	Opalinus Clay	n.m.	119.8	111.58	0.42	0.06	0.39	0.12	0.009
						0.45		0.36		
AD	941.80	Staffelegg Fm.	38	87.1	75.92	0.37	0.06	0.41	0.15	0.012
						0.00		0.35		

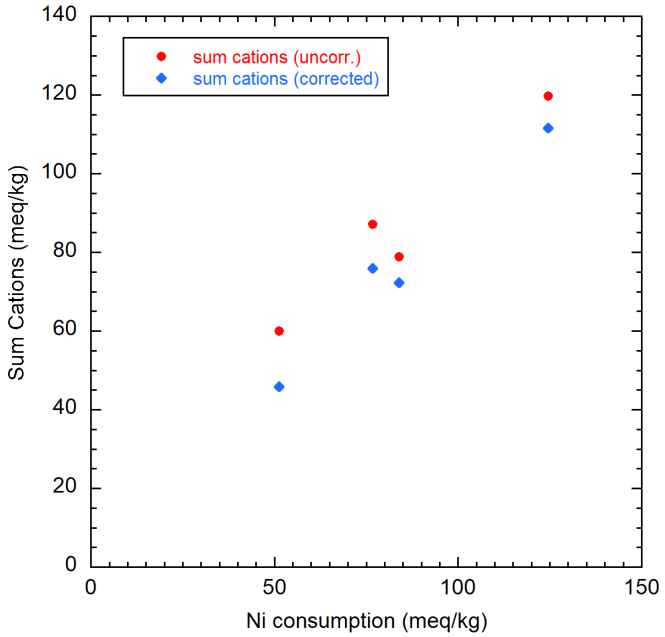

Fig. 5.6-1: Ni consumption vs. sum of cations (data of University of Bern)

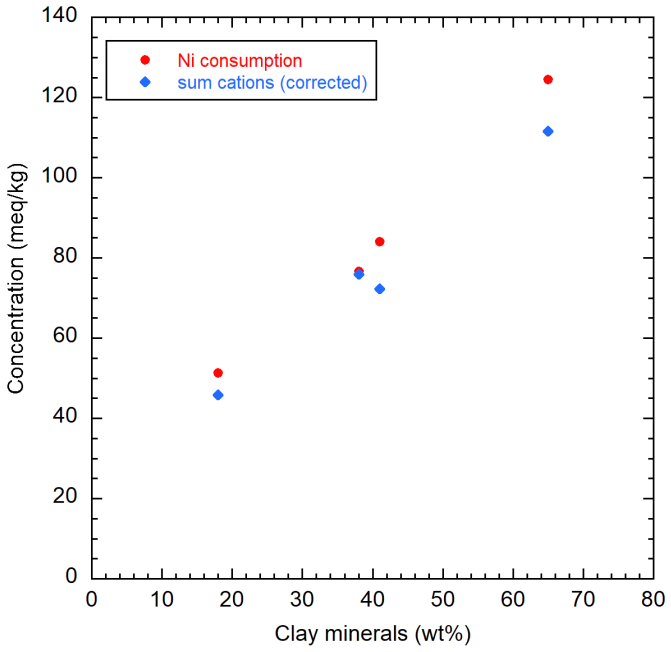

Fig. 5.6-2: CEC parameters as a function of clay-mineral content (data of University of Bern)

5.6.2 Comparison with data from PSI

A data set including eleven samples from the TRU1-1 borehole was elaborated by PSI (Marques Fernandes & Baeyens *in prep*). Besides samples from the Opalinus Clay and confining units («Brauner Dogger» and Staffelegg Formation), one sample from the Wildegg Formation was investigated.

In a first step, the CEC at PSI was determined for all samples from Ni consumption with the Ni-en extraction method. Subsequently, the main data set was generated via $CsNO_3$ extraction, from which the CEC and the exchanger population were obtained. The CEC was derived by subtracting the anions (Cl, SO_4, HCO_3/CO_3) from the cations (Na, Ca, Mg, K, Sr). The exchanger population was derived by two correction methods: (1) attributing Cl and SO_4 to Na and TIC to Ca, and (2) attributing Cl to Na and SO_4 and TIC to Ca. Note that these two methods are analogous to the ones used for the University of Bern samples presented above, except for the additional consideration of TIC.

The conditions applied in the different extraction methods of PSI and University of Bern are compared in Tab. 5.6-2. Important differences of the PSI methods relative to that of the University of Bern are (i) the lower and more variable solid/liquid ratios and (ii) the smaller amount of solid mass.

Tab. 5.6-2: Extraction conditions applied by the University of Bern and PSI

	University of Bern	**PSI**	**PSI**
Extraction method	Ni-ethylenediamine	Ni-ethylenediamine	$CsNO_3$
Extract solution concentration	91 – 139 mmol/L *	2.5 mmol/L	34 – 39 mmol/L
Solid/Liquid ratio	~ 0.9 kg/L	~ 0.028 kg/L	0.04 – 0.23 kg/L
Amount of solid used	~ 30 g	~ 1 g	~ 1.5 – 8 g a)
Extraction time	24 h	24 h	24 h
Final pH	8.3 – 8.4	8.1 – 8.3	8.4 – 8.8
Sample disaggregation	Disintegration by hand to a few mm^3 pieces	Milled and passed through 1 mm sieve	Milled and passed through 1 mm sieve
Sample storage time prior to preparation	1 – 14 days	Several months	Several months
Extraction in glovebox	Yes	No	Yes

* Adjusted to obtain the expected index cation consumption-to-CEC ratio.

Cation exchange capacity and corrected sum of extracted cations

The Ni-en consumption and the corrected ΣCAT data (the latter from Ni-en extraction in the case of University of Bern and $CsNO_3$ in the case of PSI) are shown in Fig. 5.6-3. From the comparison of these two data sets, the following findings can be derived (see also Fig. 5.6-4):

- The CEC values obtained from Ni consumption exhibit similar values for both data sets. In this context it should be noted that the two data sets were not performed on the same samples, thus CEC variations at similar depths due to mineralogical variation are expected. This becomes explicit for the samples close to the Opalinus Clay / «Brauner Dogger» boundary, where the clay-rich sample in the Opalinus Clay measured by PSI displays a higher CEC than the carbonate-rich sample in the Wedelsandstein Formation measured by Uni Bern.
- In general, the good correlation of Ni consumption data with clay-mineral content (Fig. 5.6-5a) supports the consistency of CEC values of University of Bern and PSI based on Ni-en extraction.
- The PSI data set indicates broad linear correlation between Ni consumption and corrected ΣCAT data, the latter, however, being systematically higher (difference 1 – 50%). Conversely, the University of Bern data set shows closer agreement between Ni consumption and corrected ΣCAT data (1 – 14%), but the latter values tend to be slightly lower (although within the analytical uncertainty).
- The corrected ΣCAT data of University of Bern shows a very good correlation with the clay-mineral content ($R^2 = 0.985$), whereas that of PSI indicates more scatter ($R^2 = 0.802$) which, however, also contains a larger data set. It should be noted, however, that the latter data set shows a better correlation with the sum of smectite end-member and illite end-member, because some PSI samples display rather large fractions of kaolinite and chlorite which contribute much less to the CEC (Marques Fernandes & Baeyens *in prep.*).

These findings are interpreted as follows:

- The Ni-consumption data from both laboratories and corrected ΣCAT data from University of Bern are considered to be the most representative measures of the CEC.

- The corrected ΣCAT of PSI is probably somewhat too high with regard to CEC determined via Ni-en because of selective leaching of K (see discussion below) and likely because of some other unknown side-reactions.

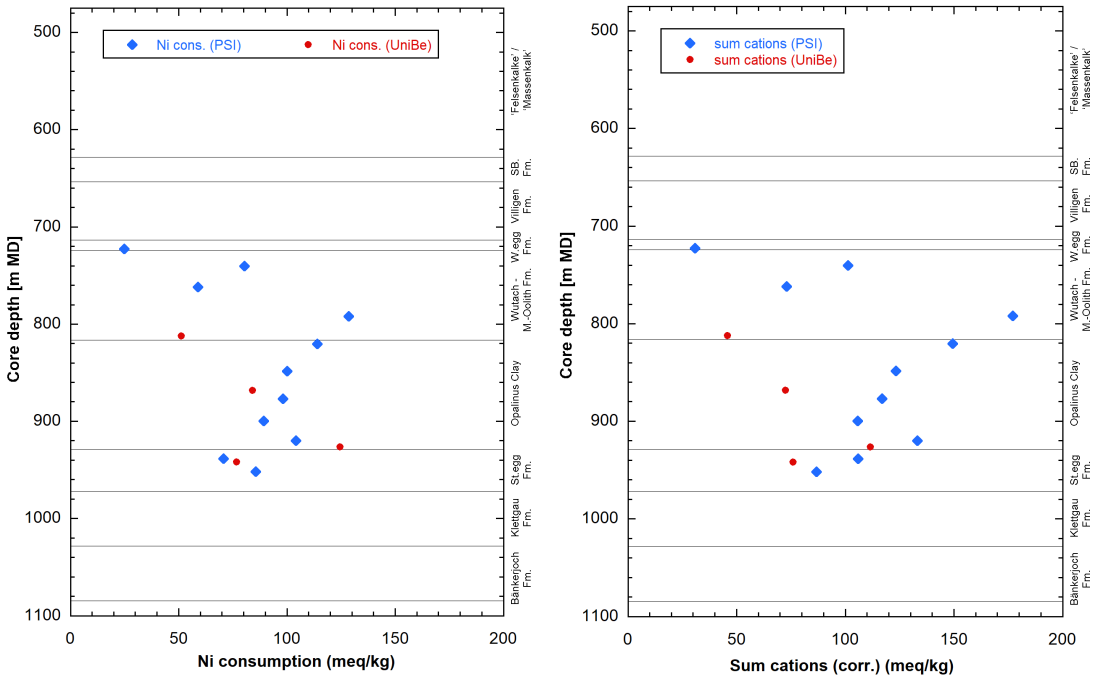

Fig. 5.6-3: Comparison of CEC data from University of Bern and from PSI

Left: Ni consumption data

Right: Corrected sum of cations

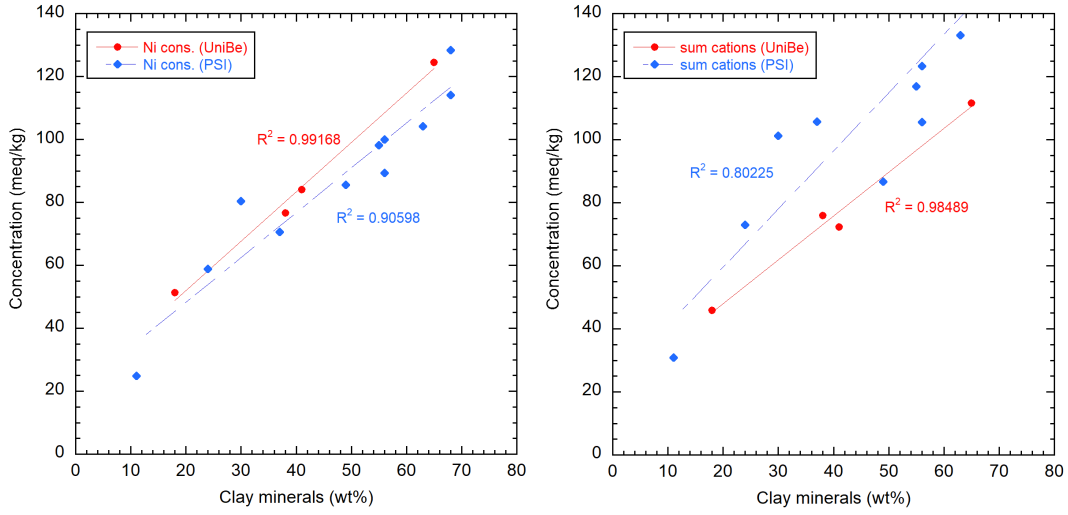

Fig. 5.6-4: CEC data as function of the clay-mineral content

Left: Ni consumption data

Right: Corrected sum of cations

Exchangeable cation occupancies

The advantage of comparing fractional cation occupancies rather than the extracted cation concentrations is that they are normalised to the sum of cations (as proxy for the CEC) and do not directly depend on the clay-mineral content of the sample.

Fig. 5.6-5 shows the Na and Ca occupancies derived from the two correction methods. Note that in method 1 Cl and SO_4 are attributed to Na, whereas in method 2, SO_4 and, in the case of PSI data, also TIC is attributed to Ca. Thus, the Na fraction is minimised in method 1 and maximised in method 2, while the opposite is true for Ca.

Comparison of University of Bern and PSI data illustrates consistent data for all measured exchangeable cations (Na, Ca, Mg, K, Sr) as illustrated in Figs. 5.6-5 to 5.6-8. However, there is one sample from the Wedelsandstein Formation (812.24-AD) that somewhat falls off the general trend exhibiting higher amounts of extracted divalent cations (Ca, Mg, Sr) and lower ones of Na, as well as higher amounts of extracted Cl. Disregarding this sample, the two data sets reveal similar fractional occupancies for all measured cations except for K (see below). For Ca, data from the University of Bern derived with correction method 1 ($NaCl/Na_2SO_4$) show slightly higher values compared to the remaining data sets, which might result from an overcorrection of Na by this method.

The occupancies for the main cations Na and Ca. and consequently also the Ca/Na ratio, are rather constant across the Opalinus Clay and «Brauner Dogger» units. In the Staffelegg Formation, no clear trends can be discerned.

Regarding K, the data set from PSI systematically shows higher fractional occupancies (by a factor of about two) than those obtained from University of Bern samples. The same feature was observed for the Bülach-1-1 borehole (Mazurek et al. 2021). While both data sets show a strong correlation between illite content and the concentration of extracted K, the dependence is much stronger for the PSI data (Fig. 5.6-8). This suggests that an additional pool of K present in illite (possibly from the interlayer) is mobilised by Cs in the case of PSI, which is less the case for the Ni method used by University of Bern. As shown in Sections 4.4 and 4.7, aqueous extraction data from AD samples suggest that K data are affected by drilling-fluid contamination. For the Ni extracts, however, this is difficult to confirm or disconfirm. At any rate, even if this artefact has led to increased K, this effect would be much smaller than the preferential mobilisation of K caused by the Cs-extraction method applied by PSI.

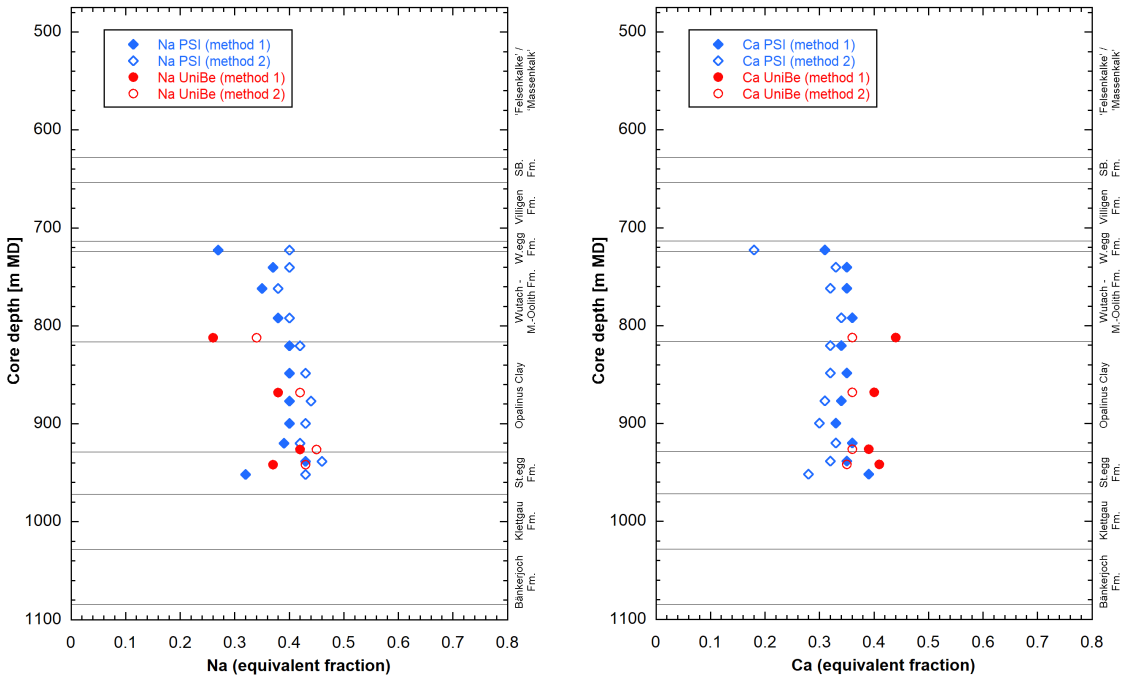

Fig. 5.6-5: Na (left) and Ca (right) fractional occupancies according to University of Bern and PSI data

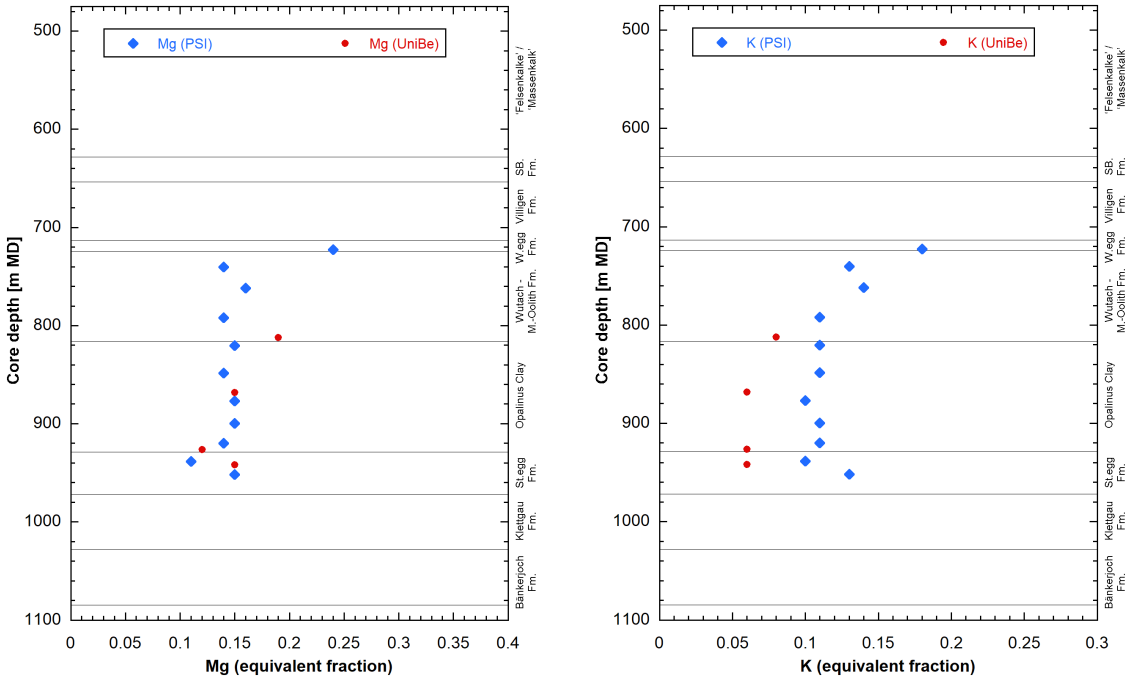

Fig. 5.6-6: Mg (left) and K (right) fractional occupancies according to University of Bern and PSI data

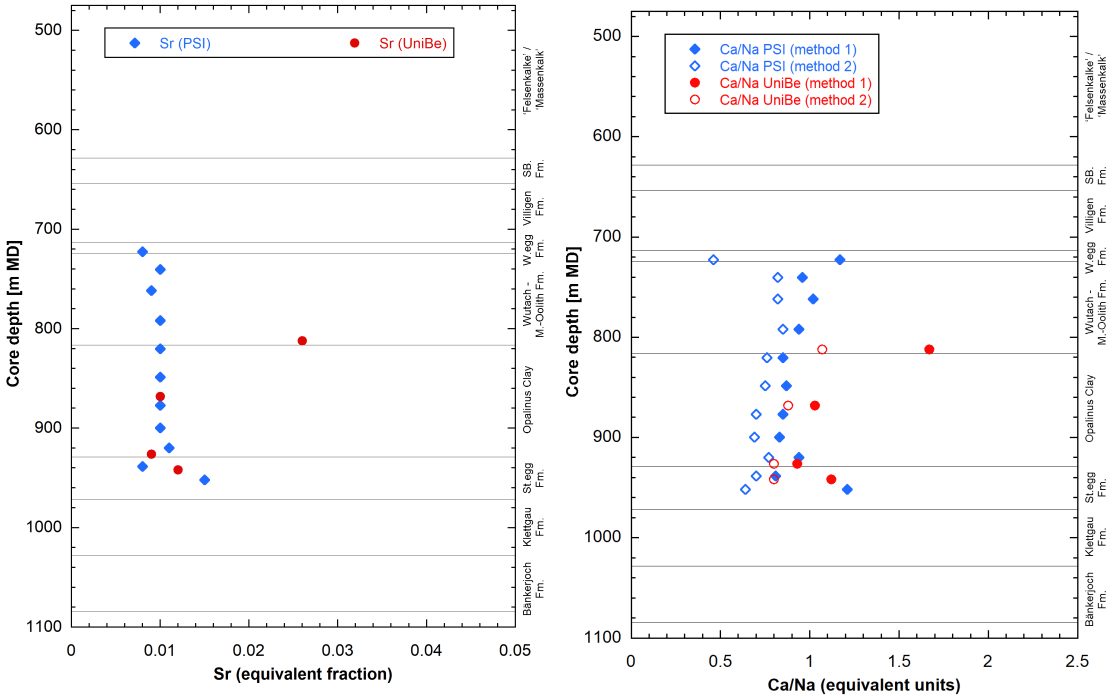

Fig. 5.6-7: Sr fractional occupancies (left) and Ca/Na ratios (right) according to University of Bern and PSI data

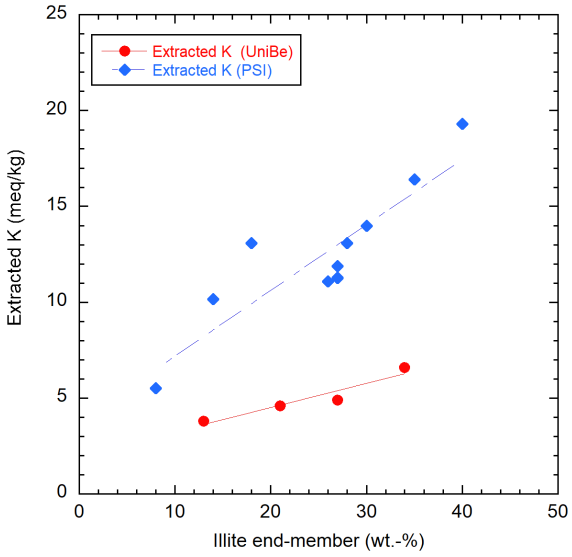

Fig. 5.6-8: Content of the illite end-member vs. extracted K

Extracted anions

The amounts of Cl and SO_4 extracted are consistent between the two data sets of PSI and University of Bern (but note the higher amount of Cl extracted from sample 812.24-AD by University of Bern, see discussion above) (Fig. 5.6-9). The Cl data suggest an increasing trend with decreasing depth within the Opalinus Clay, followed by a decreasing trend within the «Brauner Dogger». Sulphate exhibits more constant levels in these two units but seems to increase with depth in the underlying Staffelegg Formation.

Total inorganic carbon (TIC) measured in the PSI extracts is 10 – 20 mmol/$kg_{dry\ rock}$ (not shown). This is higher than expected for University of Bern extracts. The latter were not measured but calculated to be below 1 mmol/$kg_{dry\ rock}$ based on the assumption of calcite equilibrium (data not shown). The higher TIC in the PSI extracts is explained by the lower S/L ratio which induces a higher proportion of dissolved carbonate from carbonate minerals.

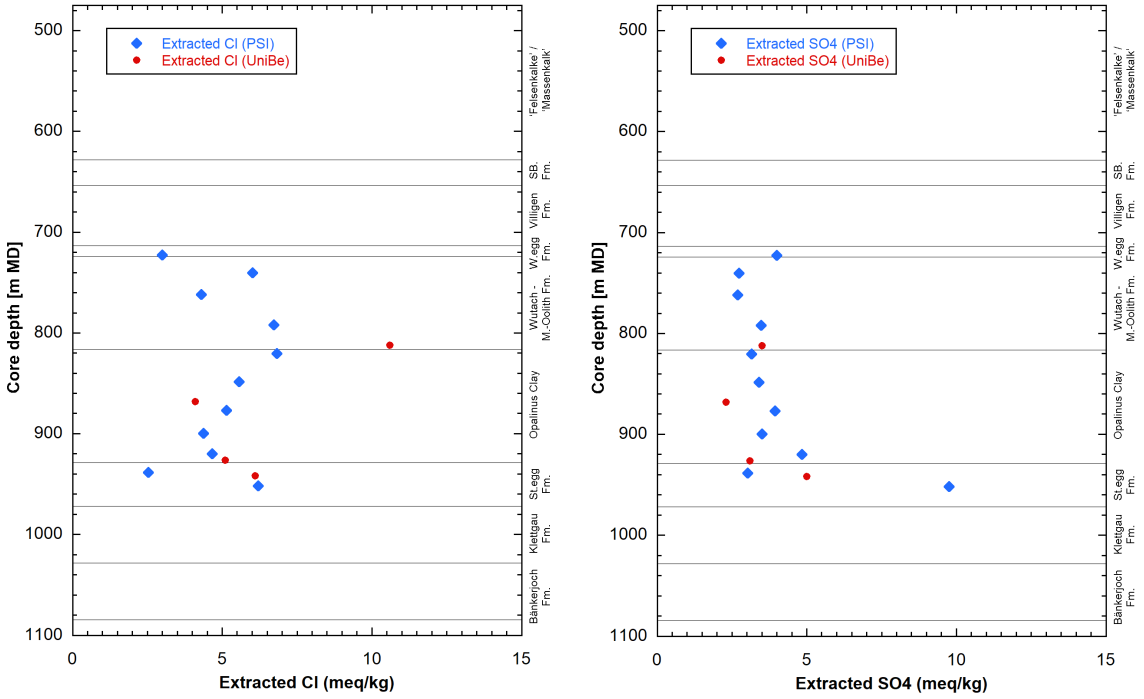

Fig. 5.6-9: Extracted Cl (left) and SO_4 (right) according to University of Bern and PSI data

5.7 Stable water isotopes

H. Niklaus Waber & Lukas Aschwanden

5.7.1 Comparison between different laboratories and methods for the determination of stable porewater isotope compositions

5.7.1.1 Different laboratories

The isotope diffusive-exchange technique was used by Hydroisotop GmbH and – on a smaller set of samples – by RWI, University of Bern to derive porewater $\delta^{18}O$- and $\delta^{2}H$-values. Good agreement within the propagated uncertainty is obtained between the two data sets for all lithologies when applying the same post-processing to the experimental and analytical data (*cf.* Section 4.8).

5.7.1.2 Different methods

The porewater oxygen and hydrogen isotope compositions were approached by three different methods including the isotope diffusive-exchange (Section 4.8), advective displacement (Section 4.7) and high-pressure squeezing (Section 4.6) techniques. Data of the three techniques are available for the section from about 750 – 960 m depth where clay-rich rocks dominate, and all methods can be applied. For the clay-poor rocks of the Malm, Keuper and Muschelkalk only data produced by the isotope diffusive-exchange technique are available. For the advective displacement technique, the average of the first two displaced solution aliquots is considered as being most representative for the in situ porewater. For the squeezed water, the one obtained at a squeezing pressure of 200 MPa is considered as being most representative for the in situ porewater. Water squeezed at higher pressures becomes increasingly depleted in ^{18}O and ^{2}H although the differences in $\delta^{18}O$ and $\delta^{2}H$ are less than 1 ‰ for sample 748.54, the only sample with solutions obtained at squeezing pressures of 200 to 400 MPa.

The porewater $\delta^{18}O$- and $\delta^{2}H$-values obtained by these three techniques are shown in Fig. 5.7-1 as a function of sample depth. Note that the error bars given in this figure describe the propagated experimental and analytical uncertainty for the isotope-diffusive exchange technique but only the analytical error for the advective displacement and high-pressure squeezing techniques. Porewater $\delta^{18}O$- and $\delta^{2}H$-values agree well within the uncertainty between the isotope diffusive-exchange and the advective displacement techniques. Porewater $\delta^{2}H$-values of the squeezing technique also generally agree within the uncertainty with the two other methods. However, some squeezed waters obtained at pressures above 200 MPa display a slightly larger difference towards more negative values outside the propagated uncertainty. Such depletion in ^{18}O and ^{2}H in squeezed water with increasing pressure has also been observed in the less consolidated Opalinus Clay and surrounding formations at the Mont Terri URL (Mazurek et al. 2017, Waber & Rufer 2017). Apart from this, the consistency between the three methods is good.

5.7.2 Comparison with groundwater data and depth profiles

Porewater $\delta^{18}O$- and $\delta^{2}H$-values describe well-defined, curved profiles between the groundwater in the Malm aquifer and the Keuper aquifer. Somewhat less well-defined profiles are also observed between the Keuper aquifer and Muschelkalk aquifer based on larger sampling intervals. In the Malm and Keuper the isotope composition of porewater in core samples from the water-conducting zones («Felsenkalke» + «Massenkalk» and Seebi Member, respectively) essentially overlaps with that of the groundwater collected from these zones (Fig. 5.7-1). The difference in

$\delta^{18}O$ between porewater and groundwater in the Keuper can be associated to contamination of this porewater sample with drilling fluid (*cf.* Section 4.4). The drilling fluid is enriched in ^{18}O and less so in ^{2}H compared to the in situ porewater and thus had a greater impact on the $\delta^{18}O$-value in the isotope diffusive-exchange experiment. No porewater sample is available from the water-conducting zone in the Stamberg Member (Schinznach Formation) of the Muschelkalk, but the porewater $\delta^{18}O$- and $\delta^{2}H$-values approach the very negative values obtained for the groundwater in this zone (Fig. 5.7-1). The agreement between the $\delta^{18}O$- and $\delta^{2}H$-values of groundwater and porewater in samples from the water-conducting zones is a strong argument for the accuracy of the porewater isotope composition derived by the isotope diffusive-exchange techniques.

From the Malm aquifer to the base of the Villigen Formation the curvature of the isotope concentration profiles is different for oxygen and hydrogen (Fig. 5.7-1). Porewater isotope compositions of samples from 587.55 m and 599.79 m of depth are identical to that of the groundwater sample for which fluid logging data indicate the major inflow zone at 591.9 – 593.9 m (Dossier VII). With increasing depth, the $\delta^{18}O$-values evolve towards lower values until reaching a relative minimum at about 660 – 680 m before they increase again towards the base of the Villigen Formation. In contrast, the $\delta^{2}H$-values display a more regular increase across this depth interval. The excursion in $\delta^{18}O$ is, however, also imitated by the porewater Cl concentrations (*cf.* Section 5.2) suggesting that these tracers indeed record an event of the geological past. Possible explanations of such an event are given in Chapter 5.8.

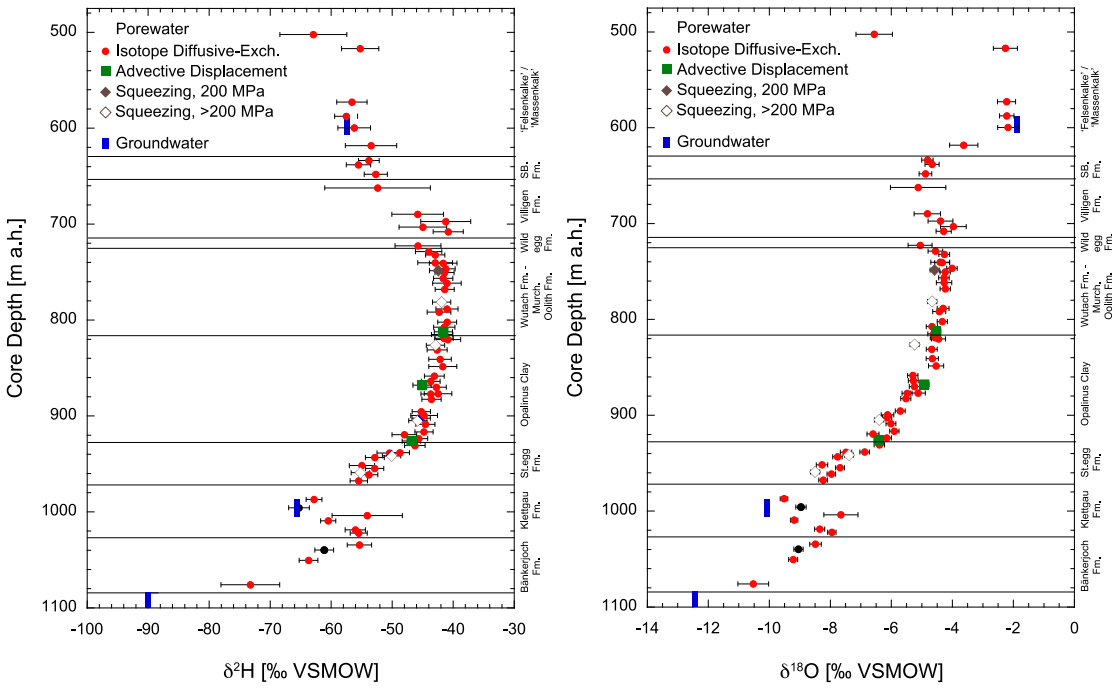

Fig. 5.7-1: Depth trends of $\delta^{18}O$ and $\delta^{2}H$ in groundwater and porewater derived by all techniques

Bars indicate propagated analytical errors (diffusive exchange) or simple analytical errors (squeezing, advective displacement). Groundwater data are from Lorenz (2020). Less reliable data are shown in black.

From the base of the Wildegg Formation down to the Keuper groundwater, porewater $\delta^{18}O$- and $\delta^{2}H$-values show the same (complex) profile shape. The differently steep gradients across the «Brauner Dogger», the lower part of the Opalinus Clay and the Staffelegg Formation are well defined by the data of all different techniques (Fig. 5.7-1).

Between the groundwater in the Seebi Member of the Klettgau Formation and that in the Stamberg Member of the Schinznach Formation no porewater isotope data exist from advective displacement and squeezing tests. The isotope diffusive-exchange data describe an asymmetric profile that approaches along a steep gradient across the Bänkerjoch Formation the very negative $\delta^{18}O$- and $\delta^{2}H$-values of the Muschelkalk groundwater in the Stamberg Member (Fig. 5.7-1).

5.7.3 $\delta^{18}O$ versus $\delta^{2}H$ and comparison with Global Meteoric Water Line (GMWL)

In the $\delta^{18}O$ – $\delta^{2}H$ space the porewater isotope compositions display distinct groups with respect to the Global Meteoric Water Line (GMWL, Fig. 5.7-2), which are also expressed in the distribution of the D-Excess versus depth (Fig. 5.7-3).

Porewater in rocks of the «Felsenkalke» + «Massenkalk» down to the top of the Villigen Formation are enriched in ^{18}O and ^{2}H and plot to the right of the GMWL. The strongest enrichment is displayed by the porewater samples within the water-conducting zone in the «Felsenkalke» + «Massenkalk» that overlap with the isotope composition of the Malm groundwater. Porewater samples between about 502 and 660 m depth in the Malm («Felsenkalke» + «Massenkalk» to top Villigen Formation) have similar or less negative $\delta^{18}O$-values but more negative $\delta^{2}H$-values compared to the samples at greater depth from the centre of the Villigen Formation to the base of the Opalinus Clay (Fig. 5.7-2). Their position in the $\delta^{18}O$ – $\delta^{2}H$ space results in the most negative D-Excess of less than −10 ‰ what clearly distinguishes them from the samples at greater depth (Fig. 5.7-3). The $\delta^{18}O$ – $\delta^{2}H$ signature of porewater in the «Felsenkalke» + «Massenkalk» down to the top of the Villigen Formation thus indicates a different origin and evolution of the main water component compared to that in porewater further down. The pronounced deviation of the $\delta^{18}O$ – $\delta^{2}H$ signatures of porewater and groundwater from the seawater dilution line further indicates complex, long-lasting processes of water – rock interaction and exchange with different water bodies over geological time scales. In fact, these observations corroborate the record of a past geological event in the Villigen Formation as the $\delta^{18}O$ – $\delta^{2}H$ signatures of porewater in the «Felsenkalke» + «Massenkalk» (here including the groundwater) down to the base of the Villigen Formation cannot be explained by exchange with porewater from underlying rock formation alone (*cf.* Section 5.8).

A different case arises for the depth section from about 680 m in the Villigen Formation to the water-conducting zone in the Seebi Member of the Klettgau Formation. Here the porewater $\delta^{18}O$ – $\delta^{2}H$ signatures display a continuous evolution from enriched $\delta^{18}O$- and $\delta^{2}H$-values towards more negative values that fall on the GMWL below a depth of around 938 m in the Staffelegg Formation (Fig. 5.7-2). Along this section the D-Excess mimics the behaviour as described for the $\delta^{18}O$- and $\delta^{2}H$-values in that it remains almost constant across the «Brauner Dogger» lithologies down to about 877 m in the Opalinus Clay (Fig. 5.7-3). Then the D-Excess starts to increase (with an increasing gradient) across the lower part of the Opalinus Clay and the Staffelegg Formation and approaches that of the groundwater (d = 15 ‰) in the Seebi Member (Fig. 5.7-3). The main water mass in the porewater system in this section appears to be of different origin and evolution compared to the system in the «Felsenkalke» + «Massenkalk» limestones. Here, the evolution of the $\delta^{18}O$ – $\delta^{2}H$ signatures seems to be dominated by long-lasting exchange

with the underlying groundwater in the Keuper aquifer. The pronounced deviation of the $\delta^{18}O - \delta^{2}H$ signatures from the GMWL at the top of the section in the Villigen Formation again gives evidence for a long residence time of this porewater in the underground.

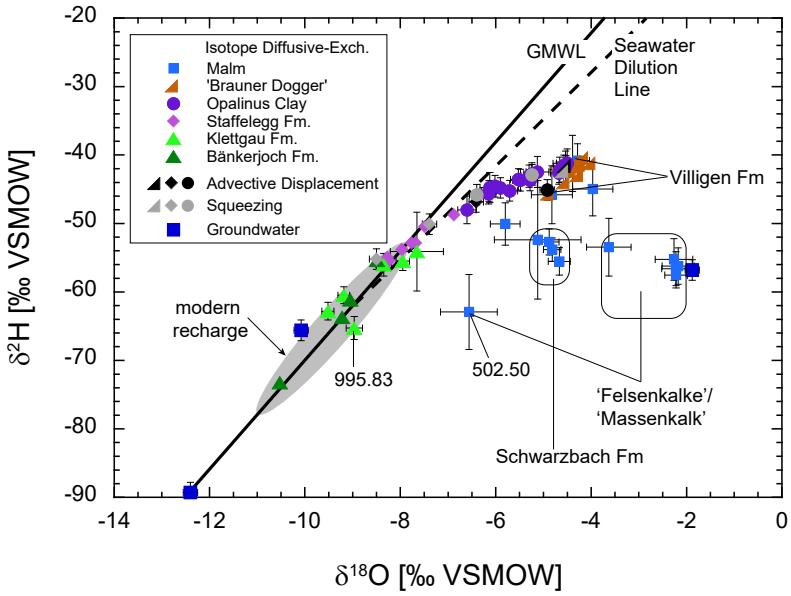

Fig. 5.7-2: $\delta^{18}O$ vs. $\delta^{2}H$ for groundwater and porewater derived by all techniques

Bars indicate propagated analytical errors (diffusive exchange) or simple analytical errors (squeezing, advective displacement). Symbols for advective displacement and squeezing indicate different formations. Groundwater data are from Lorenz (2020). GMWL = Global Meteoric Water Line). Range of modern recharge from Kullin & Schmassmann (1991).

Between the Keuper and Muschelkalk aquifers, porewater $\delta^{18}O - \delta^{2}H$ signatures plot on the GMWL (Fig. 5.7-2) and have a D-Excess of around 10 ‰ equal to that of the Muschelkalk groundwater ($d = 9.9$ ‰; Fig. 5.7-3). This suggests that the porewater – groundwater exchange in this interval is more advanced as a consequence of the significantly shorter distance between the two aquifers (ca. 100 m).

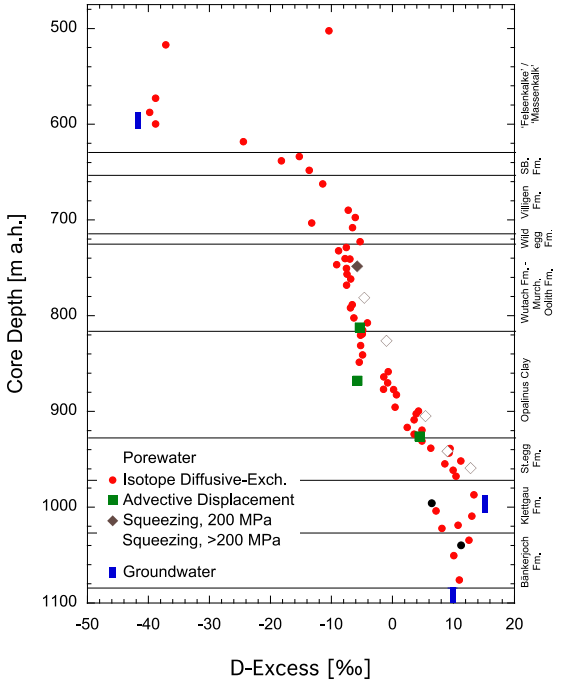

Fig. 5.7-3: Deuterium-Excess in groundwater and porewater derived by all techniques

Deuterium excess is +10 ‰ for a sample that lies on the GMWL. Note that the D-Excess of porewater has no implication on the paleo-climatic conditions during infiltration. Less reliable data are shown in black.

5.8 A closer look at tracer profiles in the Malm section

The shapes of both the Cl and $\delta^{18}O$ (but not $\delta^{2}H$) profiles show some complexity in the Malm section (Figs. 5.2-1, 5.7-1). Both profiles show a relative maximum near 593 m, at the level of a permeable fault from which a groundwater sample was taken. The Cl and $\delta^{18}O$ data of the groundwater fit well with adjacent porewater values. With increasing depth, both tracers evolve towards lower values until reaching relative minima at about 640 – 660 m (Cl) and 660 – 680 m ($\delta^{18}O$), respectively. Below these minima, Cl contents increase markedly, whereas the increase of $\delta^{18}O$ is only marginal. Note that $\delta^{2}H$ shows a regular increase with depth throughout the Malm.

The observed tracer profiles can be explained by two alternative hypotheses:

1) *The relative minimum at 640 – 680 m is due to the interaction with mobile groundwater located in this depth interval.* This groundwater must have a lower salinity and a slightly more negative $\delta^{18}O$ signature compared to the regions above and below. However, there are some arguments against this hypothesis:

- According to structural core logging (Dossier V), the section 640 – 680 m is essentially devoid of open structures that could potentially be attributed to a water-conducting zone. The only noticeable structure is a section with broken core found in the interval 677.17 – 678.47 m, classified as a fault zone by the structural geologists (see Tab. 2-3). However, this structure finds no expression in acoustic borehole-wall images (Dossier V). Moreover, it originates from a zone with drilling problems – the core could not be retrieved at first attempt, and the section had to be overcored, resulting in core damage and a core loss of 46%. Also note that this section is located distinctly deeper than the observed minimum for Cl.
- Fluid logging was performed in the interval 491 – 712 m (Dossier VII). A major inflow was identified at 591 – 594 m, and a minor one at 531 – 537 m. No indications of water inflows were identified at deeper levels.

2) *The tracer profiles showed Cl and $\delta^{18}O$ trends regularly decreasing upwards before the exchange with the groundwater currently residing at the 593 m level was initiated.* This hypothesis implies a change in the groundwater composition towards higher salinity and $\delta^{18}O$ in the «Felsenkalke» + «Massenkalk», leading to a local maximum of Cl and $\delta^{18}O$ in the adjacent porewater. The fact that $\delta^{2}H$ shows no excursion can be taken as an indication that the original signal in the porewaters was similar to that of the new groundwater at 593 m.

It is remarkable that both the $\delta^{18}O$ and the $\delta^{2}H$ data of the 4 porewater samples in the interval 517.13 – 599.79 m and those of the groundwater at 593 m are identical within error, and the $\delta^{18}O$ data decrease on both sides beyond this interval. This could be explained by the presence of an interconnected fracture network in the «Felsenkalke» + «Massenkalk», leading to a rapid spreading of the groundwater signal in these massive limestones. Indeed, 2 fault zones (Tab. 2-3) and a number of steeply dipping fault planes, joints and tension gashes were identified in this section (Dossier V; examples in Fig. 5.8-1) and could constitute the building blocks of such a network. The Cl concentrations tend to show a limited upward decrease but would still be consistent with a flat profile within error.

At the current stage of knowledge, both hypotheses presented here are possible in principle. However, from the discussion above, in particular regarding the integration of structural and fluid-logging data, hypothesis 2) is considered to be more plausible.

Fig. 5.8-1: Core photographs of fractures in the «Felsenkalke» + «Massenkalk»
Width of drill core is 10 cm.

6 Final remarks and main conclusions

RWI team

For reasons of quality assurance and optimisation of data production time, three different laboratories were involved in rock and porewater characterisation of core materials obtained from the TRU1-1 borehole. These are Hydroisotop GmbH, the French Geological Survey (BRGM) and the Rock-Water Interaction Group (RWI) of the University of Bern. The data sets produced by the different laboratories are broadly consistent, however, a part of the samples analysed for petrophysical parameters at BRGM suffered from partial desaturation during sample preparation. For low-porosity (i.e. clay-poor) samples this effect is substantial. Consequently, all quantities that refer to the wet mass are somewhat biased compared to a saturated sample and thus, the recalculation of ion concentrations in aqueous extracts to concentrations in bulk porewater had to be done via the pycnometer porosity.

The average clay-mineral content of the Opalinus Clay is 56 ± 5 wt.-%, a typical value when compared with other locations. Given the unprecedented dense sample spacing (typically 3 m), specific depth trends of various parameters within the formation were identified, presumably correlating with depositional cycles. Boundaries of sub-units within the Opalinus Clay as defined by lithostratigraphic core logging generally correlate with discontinuities or trend reversals, best seen for water content and the ratio quartz/clay minerals. Systematic depth trends can also be seen in the Staffelegg Formation. Contrastingly, in the «Brauner Dogger», less systematic depth trends in mineralogy or water content are observed. The composition of the clay-mineral fraction within the Opalinus Clay is remarkably constant. In the overlying «Brauner Dogger» the ratio kaolinite / illite sharply decreases and then increases towards the top of the unit.

Porosity of all rock units increases with clay-mineral content, but a break in slope is identified at about 30 – 40 wt.-% clay minerals, where the increase becomes weaker. This break could be related to the transition from a grain-supported to a matrix-supported fabric. However, the correlation is far from perfect, meaning that parameters other than clay-mineral content also affect the porosity of a rock sample. In particular, a number of highly porous samples with low clay-mineral contents are found in dolomite-rich lithologies. These were affected by dolomitisation and diagenetic dissolution to some degree. Thus, their porosity is not the result of compaction and cementation alone.

The external surface area (BET, N_2 adsorption) correlates well with water and clay-mineral contents except in a dolomite-rich sample of the Klettgau Formation. The average diameter of external pores derived from N_2 adsorption (ignoring interlayer water) is around 3 – 4 nm in clay-rich lithologies, whereas it is slightly larger (4 – 6 nm) in limestones. The latter rocks show bimodal pore-size distributions, with peaks at diameters < 10 nm and ~ 100 nm. The more clay-rich the lithology, the more dominant the < 10 nm peaks become.

A detailed inspection of aqueous-extract data indicated that a high-porosity dolomite sample from the Klettgau Formation was strongly contaminated by drilling fluid, in spite of the fact that only the central parts of the core were used for extraction. This sample is affected by diagenetic mineral dissolution, leading to friable fabrics dominated by large pores. In addition, contamination by drilling fluid is also indicated for the aqueous extracts of clay-rich Dogger samples used for advective displacement experiments. However, in this case, the contamination results from sample preparation during which not enough of rim material was removed from the drill core samples. The extract compositions for these contaminated samples do not relate to in situ signatures.

Across the section «Felsenkalke» + «Massenkalk» – Villigen Formation the depth profile for δ^2H-values of the porewater show a rather smooth trend towards less negative values with depth. In contrast, δ^{18}O-values show a curved profile shape with a maximum in the «Felsenkalke» + «Massenkalk», in line with the Malm groundwater and relatively steep gradients towards lighter values up- and downwards. Throughout the units of the «Brauner Dogger» both δ^{18}O- and δ^2H-values of the porewater remain rather constant, whereas in the Opalinus Clay they increasingly become more negative while approaching the values of the groundwater in the Klettgau Formation. In the δ^{18}O – δ^2H-diagram the isotope composition of porewater in these formations shows a remarkably consistent trend with depth. Porewaters in the Villigen Formation plot distinctly to the right of the Global Meteoric Water Line and then steadily evolve towards values that plot on the Meteoric Water Line in the Staffelegg Formation indicating a strong meteoric component in these porewaters.

Anion-accessible porosities have been derived from squeezed and advectively displaced porewaters, as well as from through-diffusion tests performed at PSI. The derived values of the Cl-accessible porosity fraction (f_{Cl}) are consistent for the three different methods. They vary around a value of ~ 0.45 at clay-mineral contents of approximately > 40 wt.-% and indicate an increasing trend towards lower clay-mineral contents. The onset of this increasing trend is not obvious in view of the limited number of data at low clay-mineral contents, the scatter of the data and their large uncertainties. Even for clay-mineral contents of > 40 wt.-%, f_{Cl} scatters in a wide range of 0.37 – 0.54. Considering the mean value of 0.45, this reflects an uncertainty of about 20% $_{rel}$.

The Cl profile between the Malm und the Keuper aquifers displays a curved shape, with the highest free-water Cl concentrations in the Opalinus Clay and the «Brauner Dogger» of ~ 10 g/L, decreasing towards the upper and lower aquifer, respectively. As for the oxygen isotopes, a local maximum is observed in the «Felsenkalke» + «Massenkalk» at around 590 m depth where the groundwater sample was collected. The interpretation of the Cl profile is less straightforward than that of water isotopes because assumptions need to be made about anion accessibility in the pore space of rocks with widely variable mineralogical compositions and microfabrics. The error associated with these assumptions is substantial (see error bars in Fig. 5.2-1), and much of the observed variability is within the error. It needs to be emphasised that from an analytical perspective, the Cl data are final and will not change, whereas future improvements in the understanding of anion accessibility in different lithologies and geological formations may lead to updates in the recalculation procedure to concentrations per anion-accessible porosity. This means that the Cl and Br depth profiles, which are the basis for modelling diffusive solute transport in the low-permeability sequence, may be subject to revisions in the future.

The depth profile of the Br/Cl ratio is better defined than that of Cl or Br, due to the fact that no assumptions on anion accessibility need to be made and the uncertainty regarding recalculation to the rock porosity cancels out. Data from aqueous extraction, advective displacement and squeezing are consistent and show Br/Cl ratios scattering around the value of modern seawater in the Malm, a sudden drop at the base of the Villigen Formation to values distinctly below that of modern seawater and then they remain remarkably constant across the interval «Brauner Dogger» – Klettgau Formation.

Sulphate data obtained from squeezing and advective displacement, which cover the «Brauner Dogger», Opalinus Clay and Staffelegg Formation, are approximately consistent. On the other hand, aqueous extraction data systematically exhibit higher and more variable values when recalculated to total or anion-accessible porosity. The same discrepancy has been found in the BUL1-1 borehole, the Schlattingen-1 borehole and at the Mont Terri Rock Laboratory. In the lower part of the profile, i.e. in the Keuper units, aqueous extraction data are clearly affected by

anhydrite dissolution. Across the «Brauner Dogger» and most of the Opalinus Clay the SO_4/Cl ratios from squeezing/advective displacement are similar to that of modern seawater. However, at the base of the Opalinus Clay they start to deviate towards higher values and further increase across the Staffelegg Formation.

The cation exchange capacity is correlated with the clay-mineral content. The main exchangeable cations are Na and Ca, followed by Mg and K. In the argillaceous Staffelegg Formation, Opalinus Clay and Wedelsandstein Formation, the exchanger composition (cation occupancies) is relatively constant. Comparing cation exchange data with those obtained at PSI reveals broadly consistent data sets in spite of the different methodologies employed. The differences in cation occupancies are largely explained by the higher amounts of K extracted by the Cs extraction method used by PSI. It appears that with that method more strongly bound K is mobilised during the extraction process.

Even though an in-depth comparison of the findings obtained from core and borehole studies at TRU1-1 with pre-existing data is beyond the scope of this report, a few points can nevertheless be made:

- The mean f_{Cl} value of 0.45 at clay-mineral contents of > 40 wt.-% is slightly lower than the corresponding mean f_{Cl} values that were derived for the Schlattingen-1 borehole (0.52) or the Bülach-1-1 borehole (0.52). Increasing f_{Cl} values towards lower clay-mineral contents were also derived for the latter borehole but only for clay-poor samples with clay-mineral contents of < 20 wt.-%. These slight differences in the relationship between clay-mineral content and f_{Cl} at BUL1-1 and TRU1-1 should not be over-emphasised at this stage, given the fact that the number of data points is limited, in particular on the clay-poor side.
- The tracer profiles for $\delta^{18}O$, $\delta^{2}H$, Cl and Br reveal remarkable similarity with those of nearby deep boreholes at Benken and Schlattingen-1. In particular, the $\delta^{2}H$ values are very similar to those at Benken in the Opalinus Clay and the confining units, with somewhat more negative values at Schlattingen-1. The corresponding $\delta^{18}O$ values are highest at TRU1-1 followed by those at Benken and Schlattingen-1. Regarding the Cl profile, the porewater concentrations are somewhat higher at TRU1-1, reaching maximum values of ~ 10 g/L in the Opalinus Clay. At the other two sites maximum concentrations are about 7 g/L.
- Porewater samples obtained by advective displacement and squeezing in the section «Brauner Dogger» – Opalinus Clay – Staffelegg Formation are generally near saturation with respect to celestite as was also observed in porewaters from other sites (Bülach-1-1, Schlattingen-1, Mont Terri Rock Laboratory). Except for two samples, porewaters are undersaturated with respect to gypsum, which is in line with results from Schlattingen-1 and Mont Terri but not with Bülach-1-1 where most porewaters are close to equilibrium with gypsum.
- The porewaters in the clay-rich section are of the Na-Cl type, which is in line with findings at other sites.

7 References

Allison, J.D., Brown, D.S. & Novo-Gradac, K.J. (1991): MINTEQA2/PRODEFA2, a geochemical assessment model for environmental systems: Version 3.0 user's manual. Environmental Research Laboratory, Office of Research and Development, U.S. Environmental Protection Agency, 106 p.

Aschwanden, L. & Wersin, P. (2020): Experimental study of sulphate in the Opalinus Clay: Results from extraction tests. Nagra Arbeitsbericht NAB 20-17.

Bradbury, M.H. & Baeyens, B. (1998): A physicochemical characterisation and geochemical modelling approach for determining porewater chemistries in argillaceous rocks. Geochim. Cosmochim. Acta 62, 783-795.

Cappa, C.D., Hendricks, M.B., DePaolo, D.J. & Cohen, R.C. (2003): Isotopic fractionation of water during evaporation. Journal of Geophysical Research 108/D16.

Charpentier, D., Tessier, D. & Cathelineau, M. (2003): Shale microstructure evolution due to tunnel excavation after 100 years and impact of tectonic paleo-fracturing. Case of Tournemire, France. Engineering Geology 70, 55-69.

Debure, M. & Gailhanou, H. (2019): GD experiment: Experimental study of sulphate in Opalinus Clay. Unpubl. Mont Terri Technical Note. Mont Terri Project, Switzerland.

Gaboreau, S., Prêt, D., Tinseau, E., Claret, F., Pellegrini, D. & Stammose, D. (2011): 15 years of in situ cement–argillite interaction from Tournemire URL: Characterisation of the multiscale spatial heterogeneities of pore space evolution. Appl. Geochem. 26, 2159-2171.

Gimmi, T. & Alt-Epping, P. (2018): Simulating Donnan equilibria based on the Nernst-Planck equation. Geochim. Cosmochim. Acta 232, 1-13.

Gimmi, T. & Waber, H.N. (2004): Modelling of tracer profiles in porewater of argillaceous rock in the Benken borehole: Stable water isotopes, chloride and chlorine isotopes. Nagra Technical Report NTB 04-05.

Hadi, J., Wersin, P., Mazurek, M., Waber, H.N., Marques Fernandes, M., Baeyens, B., Honty, M., De Craen, M., Frederickx, L., Dohrmann, R. & Fernandez, A.M. (2019): Intercomparison of CEC method within the GD project. Mont Terri Technical Report TR 2017-06. Mont Terri Project, Switzerland.

Isler, A., Pasquier, F. & Huber, M. (1984): Geologische Karte der zentralen Nordschweiz 1:100'000. Herausgegeben von der Nagra und der Schweiz. Geol. Komm.

Jenni, A., Aschwanden, L., Lanari, P., de Haller, A. & Wersin, P. (2019): Spectroscopic investigation of sulphur-containing minerals in Opalinus Clay. Nagra Arbeitsbericht NAB 19-23.

Kullin, M. & Schmassmann, H. (1991): Isotopic composition of modern recharge. *In:* Pearson F.J., Balderer, W., Loosli, H.H., Lehmann, B.E., Matter, A., Peters, Tj., Schmassmann, H.-J. & Gautschi, A. (1991): Applied Isotope Hydrogeology – A Case Study in Northern Switzerland. Studies in Environmental Science 43, Elsevier, Amsterdam, 65-89.

Lorenz, G.D. (2020): Borehole TRU1-1 (Trüllikon): Fluid sampling and analytical hydrochemical data report. Unpubl. Nagra Interner Bericht.

Mäder, U. (2018): Advective displacement method for the characterisation of porewater chemistry and transport properties in claystone. Geofluids 2018, Article ID 8198762, doi.org/10.1155/2018/8198762

Mäder, U. & Waber, H.N. (2017): Results of advective displacement / multi-component transport experiments from claystone samples of the Schlattingen borehole. Nagra Arbeitsbericht NAB 17-16.

Marques Fernandes, M. & Baeyens. B. (*in prep.*): Sorption measurements of Cs, Ni, Eu, Th and U on rock samples of Opalinus Clay and confining geological units from deep boreholes at the potential siting regions for a deep geological repository for radioactive waste in Switzerland: Jura Ost, Nördlich Lägern and Zürich Nordost. Nagra Technical Report NTB 22-02.

Mazurek, M. (2017): Gesteinsparameter-Datenbank Nordschweiz – Version 2. Nagra Arbeitsbericht NAB 17-56.

Mazurek, M. & Aschwanden, L. (2020): Multi-scale petrographic and structural characterisation of the Opalinus Clay. Nagra Arbeitsbericht NAB 19-44.

Mazurek, M., Oyama, T., Wersin, P. & Alt-Epping, P. (2015): Pore-water squeezing from indurated shales. Chemical Geology 400, 106-121.

Mazurek, M., Al, T., Celejewski, M., Clark, I.D., Fernández, A.M., Kennell-Morrison, L., Matray, J.M., Murseli, S., Oyama, T., Qiu, S., Rufer, D., St-Jean, G., Waber, H.N. & Yu, C. (2017): Mont Terri Project: Mont Terri DB-A Experiment: Comparison of pore-water investigations conducted by several research groups on core materials from the BDB-1 borehole. Technical Report for the Nuclear Waste Management Organization, NWMO-TR-2017-09. (also published as Mont Terri TR 2017-01).

Mazurek, M., Aschwanden, L., Camesi, L., Gimmi, T., Jenni, A., Kiczka, M., Mäder, U., Rufer, D., Waber, H.N., Wanner, P., Wersin, P. & Traber, D. (2021): TBO Bülach-1-1: Data Report – Dossier VIII: Rock properties, porewater characterisation and natural tracer profiles. Nagra Arbeitsbericht NAB 20-08.

Monnier, G., Stengel, P.T. & Fies, J. (1973): Une méthode de mesure de la densité apparente de petits agglomérats terreux – Application à l'analyse des systèmes de porosité du sol. Ann. Agron. 24.

Naef, H., Büchi, M., Bläsi, H.R., Deplazes, G. & Gysi, M. (2019): Lithology Manual – Lithological description of drill cores and cuttings in Northern Switzerland. Nagra Arbeitsbericht NAB 19-11.

Nagra (2008): Vorschlag geologischer Standortgebiete für das SMA- und das HAA-Lager. Geologische Grundlagen. Nagra Technischer Bericht NTB 08-04.

Nagra (2014): SGT Etappe 2: Vorschlag weiter zu untersuchender geologischer Standortgebiete mit zugehörigen Standortarealen für die Oberflächenanlage. Geologische Grundlagen. Dossier II: Sedimentologische und tektonische Verhältnisse. Nagra Technischer Bericht NTB 14-02.

Parkhurst, D.L. & Appelo, C.A.J. (2013): Description of input and examples for PHREEQC Version 3: A computer program for speciation, batch-reaction, one-dimensional transport, and inverse geochemical calculations. No. 6-A43. US Geological Survey.

Pearson, F.J., Arcos, D., Bath, A., Boisson, J.Y., Fernandez, A.M., Gäbler, H.E., Gaucher, E., Gautschi, A., Griffault, L., Hernan, P. & Waber, H.N. (2003): Mont Terri project – geochemistry of water in the Opalinus Clay formation at the Mont Terri rock laboratory. Federal Office for Water and Geology Rep. 5, Bern, Switzerland.

Pietsch, J. & Jordan, P. (2014): Digitales Höhenmodell Basis Quartär der Nordschweiz – Version 2013 (SGT E2) und ausgewählte Auswertungen. Nagra Arbeitsbericht NAB 14-02.

Rufer, D. (2019): Field Manual: Drillcore sampling for analytical purposes. Nagra Arbeitsbericht NAB 19-13.

Rufer, D. & Mazurek, M. (2018): Pore-water extraction and characterization: Benchmarking of the squeezing and adapted isotope diffusive exchange methods. NWMO Technical Report NWMO-TR-2018-14. Nuclear Waste Management Organization, Toronto, Canada.

Thoenen, T., Hummel, W., Berner, U. & Curti, E. (2014): The PSI/Nagra Chemical Thermodynamic Database 12/07. PSI Bericht Nr. 14-04, Paul Scherrer Institut, Villigen, Switzerland.

Tournassat, C., Vinsot, A., Gaucher, E.C. & Altmann, S. (2015): Chemical conditions in clayrocks. *In:* Tournassat, C., Steefel, C.I., Bourg, I.C. & Berrgaya, F. (eds.): Natural and engineered clay barriers. Developments in Clay Science 6, Chapter 3, 71-100. Elsevier.

Van Loon, L. (2014): Effective diffusion coefficients and porosity values for argillaceous rocks and bentonite: Measured and estimated values for the provisional safety analyses for SGT-E2. Nagra Technical Report NTB 12-03.

Van Loon, L.R. & Glaus, M. A. (*in prep.*): Diffusion measurements of HTO, $^{36}Cl^-$ and $^{22}Na^+$ on rock samples of Opalinus Clay and confining geological units from deep boreholes at the potential siting regions for a deep geological repository for radioactive waste in Switzerland: Jura Ost, Nördlich Lägern and Zürich Nordost. Nagra Technical Report NTB 22-01.

Waber, H.N. & Rufer, D. (2017): Porewater geochemistry, method comparison and Opalinus Clay – Passwang Formation interface study at the Mont Terri URL. Technical Report for the Nuclear Waste Management Organization, NWMO-TR-2017-10. (also published as Mont Terri TR 2017-02).

Waber, H.N. (ed.) (2020): SGT-E3 deep drilling campaign (TBO): Experiment procedures and analytical methods at RWI, University of Bern (Version 1.0, April 2020). Nagra Arbeitsbericht NAB 20-13.

Wersin, P., Mazurek, M., Waber, H.N., Mäder, U.K., Gimmi, T., Rufer, D. & de Haller, A. (2013): Rock and porewater characterisation on drillcores from the Schlattingen borehole. Nagra Arbeitsbericht NAB 12-54.

Wersin, P., Mazurek, M., Mäder, U.K., Gimmi, T., Rufer, D., Lerouge, C. & Traber, D. (2016): Constraining porewater chemistry in a 250 m thick argillaceous rock sequence. Chemical Geology 434, 43-61.

Wersin, P., Pekala, M., Mazurek, M., Gimmi, T., Mäder, U.K., Jenni, A., Rufer, D. & Aschwanden, L. (2021): Porewater chemistry of Opalinus Clay: Methods, modelling & buffering capacity. Nagra Technical Report NTB 18-01.

Wigger, C. & Van Loon, L.R. (2017): Importance of interlayer equivalent pores for anion diffusion in clay-rich sedimentary rocks. Environmental Science & Technology 51, 1998-2006.